Affinity and activity profiling of agrochemical-metabolising enzymes



Maria Font Farre

Somerville College

Department of Plant Sciences

University of Oxford

Supervised by Professor Renier A.L. van der Hoorn

Thesis submitted for the degree of *Doctor of Philosophy*

Trinity 2021

Affinity and activity profiling of agrochemical-metabolising enzymes

Maria Font Farre

Somerville College

Department of Plant Sciences

University of Oxford

Supervised by Professor Renier A.L. van der Hoorn

Thesis submitted for the degree of *Doctor of Philosophy*

Trinity 2021

Abstract

Agrochemical detoxification involves the consecutive action of several families of detoxifying enzymes. Cytochrome P450s (CYP450s) and Glutathione transferases (GSTs) are two large and diverse superfamilies of enzymes that play important roles in xenobiotic detoxification in many living organisms. Many efforts have been taken in order to identify the selectivity of these enzymes and understand their biological function. However, just a few specific CYP450s and GSTs have been identified as the actual cause of agrochemical modifications and little is known about the specific role and mechanisms by which these enzymes contribute to response to abiotic and biotic stress.

In this research we aim to establish and use activity-based protein profiling (ABPP) to monitor, identify and characterise the activity of CYP450 and GST enzymes in plants and fungi. To do so, we present a first chapter describing the relevance of agrochemical metabolising enzymes in agriculture and their importance for crop protection and food safety. Second, we studied the labelling of mouse and plant (Arabidopsis, maize and *Nicotiana benthamiana*) CYP450s by a set of CYP450 activity-based probes, identifying key aspects between mammal and plant CYP450 profiling. CYP450 probes label many CYP450s in mouse liver microsomes in a NADPH-dependent manner; however, the relatively low abundance and reactivity of CYP450s in plant tissues limit their activity-based profiling in plant extracts. Third, we identified the main targets of CYP450 activity-based probes in the fungal plant pathogen *Zymoseptoria tritici* and described the specific blockage of *Zt*CYP5080H1 labelling by the fungicide cyprodinil. Fourth, we validated the use of the glutathione-based photoaffinity probe, GST-G, to target GSTs in several plant species. We demonstrated the potential use of GST-G photoaffinity profiling to study the activation of GST upon safener application in wheat and identified the activation of several members of GSTU and GSTF classes upon the BION treatment of Arabidopsis plants. Overall, these innovative tools have great potential to support the development of more effective agrochemicals and identify new enzymes involved in the metabolism of pesticides.

Acknowledgements

The accomplishment of this thesis would not have been possible without the help and encouragement of many people. Here I would like to thank all those people who have accompanied me through these years.

I would like to particularly thank Prof. Renier van der Hoorn. Thank you for your guidance and precious feedback during the duration of my whole PhD. Thank you for giving me the opportunity to do my PhD in such a dynamic and enthusiastic group with a great cluster of international researchers. I am grateful for our scientific discussions and friendly chats, for your sincere feedback and endless patience.

Thanks to Daniel Brown and Johnathan Burton for our fruitful discussions and project collaboration. I learn so much chemistry during this collaboration. Thanks to Samantha Hall, Richard Dale, John Sinclair and Mel Morris for the helpful and rich discussions during our industrial CASE partnership meetings. Also, thanks to Urvashi, for her help and support during the last part of the *Zymoseptoria tritici* project. Many thanks to all people at Syngenta who made my placement there a memorable experience, I spent such an amazing time there!

Many thanks to all Plant Chemetics Laboratory, former and current lab members. Thanks for sharing your knowledge as well as your passion for Plant Science research. Thank you for the coffees and lunch we spent together, great talks and science discussions. Many thanks to Kyoko, Jiorgos, Judy, Daniela, Friederike, Shivani, Pierre, Emma, Tee, Daniel Krahn and Marcel for their warm welcome when I joined the lab. Thanks to Philippe, Mariana, Laura, Felix, Alice and Issy for the hardworking but also fun time spent together in the lab. Thanks also to all the students that have been involved in my project: Cameron, Salih and Maurice. Thank you for helping with the lab work during my PhD and to continue to grow as a scientist. I would also like to thank Sarah, Urszula and Caroline for their excellent technical support, all members from Gail Preston group for our scientific meetings on Wednesday and the support from the Department of Plant Sciences at University of Oxford.

I would also like to thank Somerville College, BBSRC and DTP for their kind sponsorship and Somerville College for their academic and financial support.

Special thanks to Tee and Emma, my fellow PhDs. Thanks for all the time shared in the lab and office (that was a lot!). It has been great to have shared all the PhD experience with you; all the stressful and difficult moments we went through, but also the happy and exciting ones. Special thanks also to Laura. Thank you for being always there. You have been a central support inside and outside the lab, being

always there to cheer me up when needed. I am sure this friendship will last for more than our Oxford time.

I would also like to thank my family and friends for all the support and love:

- To my amazing mum and dad. Gràcies per haver estat sempre al meu costat tot i estar lluny. Gràcies pel vostre suport constant en totes les decisions que he pres durant aquests últims 30 anys i per tots els vostres sacrificis.

- To my favourite brothers, Xexu i Lolo. Gràcies per haver estat amb mi sempre que us he necessitat, per motivar-me sense saber-ho. Mil gràcies també a la Judit i la Mònica.

- To my partner and best friend, Jose Antonio. Gracias por tu motivación constante y tu apoyo diario. Gracias por haber sabido animarme en los días malos, por haber sabido desconectar mi mente del trabajo con paseos, dando pedales o con una pinta o copa de vino. Mil gracias también a Jose Antonio (padre), Puri, Paz y Andoni por sus constantes mensajes de apoyo.

- To my best friends: Clara, Anna i Elisenda. Gràcies pel vostre suport i amor des que vam començar la carrera, que no entén de fronteres, ni de països, ni de continents.

Many thanks to you all,

Maria

Abbreviations

1-ABT	1-Aminobenzotriazole
2EN	2-ethynylnaphthalene
ABC	ATP-binding cassette
ABPP	Activity-based protein profiling
ACCase	Acetyl-CoA carboxylase
AP	Anilino-pyrimidine
β-met	β-mercaptoethanol
B	BION
BSA	Bovine serum albumin
BTH	Benzothiadiazole
CA	2-chloroacetamide
CAN	Acetonitrile
CAR	Constitutive androstane receptor
CC	Click control
cDNA	complementary DNA
CDNB	1-Chloro-2,4-dinitrobenzene
CFU	Colony-forming unit
CO	Carbon monoxide
CPR	Cytochrome P450 reductase
CuSO4	Copper(II) sulfate
CYP450	Cytochrome P450
DHAR	Dehydroascorbate reductase
DMI	De-methylation inhibitor
DMSO	Dimethyl sulfoxide
dpi	days post-infiltration
EA	Ethacrynic acid
EDTA	Ethylenediaminetetraacetic acid
EF1Bγ	Elongation factor 1B- γ subunit
ER	Endoplasmic reticulum
EV	Empty vector
FDR	False discovery rate
FLS3	Flagellin-sensing 3
FP	Fluorophosphonate

GHR	Glutathionyl hydroquinone reductase
GSH	Glutathione
G-site	Glutathione-binding site
GST	Glutathione transferase
GST-G	Glutathione-based probe targeting glutathione transferases
H-site	Substrate-binding site
IA	Iodoacetamide
IPG	Immobilised pH gradient
LB	Lysogeny broth
LC-MS	Liquid chromatography-mass spectrometry
LC-MS/MS	Liquid chromatography-tandem mass spectrometry
Lys-C	Lysyl endopeptidase
MAPEG	Membrane-associated proteins in eicosanoid and glutathione metabolism
MAR	Missing at random
MBC	Methyl benzimidazole carbamate
MDR	Multiple disease resistance
MFS	Major facilitator superfamily
MNAR	Missing not at random
mPGES-2	Microsomal prostaglandin E-synthase type 2
MS	Mass spectrometry
MW	Molecular weight
NADPH	Nicotinamide adenine dinucleotide phosphate
NPC	No probe control
NTSR	Non-target site resistance
OD_{600}	Optical density at 600 nm
PBS	Phosphate-buffered saline
PCA	Principal component analysis
pI	isoelectric point
ppm	part per million
PR-2	Pathogenesis-related protein 2
PVPP	Polyvinylpolypyrrolidone
PXR	Pregnane X receptor
QoI	Quinone outside inhibitor
ROS	Reactive oxygen species

RT	Room temperature
SA	Salicylic acid
SBI	Sterol biosynthesis inhibiting
Sd	Standard desviation
Sdh	Succinate dehydrogenase
SDHI	Succinate dehydrogenase inhibitor
SDS	Sodium dodecyl sulfate
SHG	S-hexylglutathione
STB	*Septoria tritici* blotch
TBTA	Tris((1-benzyl-1H-1,2,3-triazol-4-yl) methyl)amine
TCEP	Tris(2-carboxyethyl)phosphine hydrochloride
TCHQD	Tetrachloro-phydroquinone dehydrogenase
TEAB	Triethylammonium bicarbonate
TFA	Trifluoroacetic acid
THPTA	Tris-hydroxypropyltriazolylmethylamine
TSR	Target site resistance
UGT	UDP-glycosyltranferase
W	Water

Table of Contents

Abstract..... i

Acknowledgments..... iii

Abbreviations..... v

Table of Contents..... ix

Chapter 1: General Introduction..... 1

Overview..... 1

Pesticide resistance: a major problem in agriculture..... 1

Metabolic resistance..... 3

Cytochrome P450s..... 4

Glutathione transferases..... 7

Chemical proteomics as a discovery tool to study agrochemical-metabolising enzymes in plants and fungi..... 9

Aim of the thesis..... 13

Chapter 2: Profiling Cytochrome P450 activities in plants..... 15

Abstract..... 16

Introduction..... 17

Results..... 20

Chemical probes label CYP450s in mouse liver microsomes but not in Arabidopsis leaf microsomes..... 20

MS analysis shows differences in abundance and number of CYP450s between mouse liver and Arabidopsis microsomes..... 24

MS analysis is insufficient to detect CYP450 labelling in Arabidopsis leaf microsomes..... 26

CYP450 probes label transiently expressed mouse cytochrome P450s in NADPH-dependent manner, but not Arabidopsis cytochrome P450s..... 29

Maize CYP81A9 is targeted by several CYP450 chemical probes..... 32

Labelling of CYP81A9 and several *N. benthamiana* CYP450s can be detected by mass spectrometry CYP450 labelling pull-downs..... 34

Most abundant CYP450 in CYP81A9 overexpressing *N. benthamiana* microsomes correlate to the main labelled CYP450s..... 38

Discussion..... 40

Importance of microsomal isolation when labelling endogenous and overexpressed CYP450s..... 40

Transiently expression of CYP450s using *N. benthamiana* plants..... 40

Labelling and abundance of plant CYP450s: Arabidopsis, maize and *N. benthamiana*..... 41

Differences between CYP450 labelling by click chemistry and biotinylated probes..... 42

Materials and Methods 43
Chemical probes and chemicals 43
Biologic materials and growth conditions 43
Cloning 43
Agroinfiltration 44
CYP81A9 and CYP81A2 expression in yeast and microsome preparation 44
Protein extraction and microsomal fraction isolation from plant tissues 45
Carbon monoxide (CO) displacement assay 46
Activity-based protein profiling and click chemistry 46
CYP81A9 and CYP81A2 activity assay with bentazon 46
In-gel fluorescence scanning and Western Blot 47
Filter-aided sample preparation for Mass spectrometry 47
Large-scale labelling, affinity purification 48
On-bead trypsin and Lys-C digestion 48
LC-MS/MS and peptide identification using MaxQuant 48
Supplemental data 50
Chapter 3: CYP450 profiling: a new tool to study fungicide metabolism in the wheat pathogen *Zymoseptoria tritici* 57
Abstract 58
Introduction 59
Results 62
Activity-based CYP450 probes target several CYP450s from *Zymoseptoria tritici* 62
Zymoseptoria tritici CYP450s have distinct labelling characteristics 68
CYP5080H1 may contribute to the detoxification of cyprodinil in *Zymoseptoria tritici* 70
Phylogenetic analysis of CYP450s in plant pathogens 75
Discussion 77
Challenges of CYP450 labelling in *Zymoseptoria tritici* 77
Selective CYP450 labelling 78
The use of competitive CYP450 labelling to study fungicide metabolism 80
Materials and Methods 81
Chemical probes and chemicals 81
Biologic materials and growth conditions 81
Cloning 81
Agroinfiltration 82
Protein extraction and microsomal fraction isolation preparation 82
Activity-based protein profiling and click chemistry 83

In-gel fluorescence scanning and Western Blot 83
Filter-aided sample preparation for Mass spectrometry 84
Large-scale labelling, affinity purification 84
On-bead trypsin and Lys-C digestion 85
LC-MS/MS and peptide identification 85
Image quantification and statistical analysis 87
Bioinformatics 87
Supplemental data 87
Chapter 4: Photoaffinity profiling of Glutathione transferases in plants 91
Abstract 92
Introduction 93
Results 97
Glutathione transferases are the main target of GST-G in Arabidopsis 97
GST-G has different affinities within GST classes 102
GST profiling can be applied to other plant species 104
Profiling of GSTs in the context of agrochemical detoxification 106
Profiling of GSTs in the context of plant immunity 108
Role of GSTU10, GSTF2 and GSTF6 in plant defence against biotrophic and hemibiotrophic plant pathogens 114
Discussion 117
GST-G labelling: targets and selectivity 117
Glutathione transferases inducibility after agrochemical treatment 118
Glutathione transferases inducibility after BION treatment 119
Materials and Methods 120
Chemical probes, inhibitors and agrochemicals 120
Plant materials, growth conditions and agrochemical treatments 120
Cloning 121
Agroinfiltrations 121
Heterologous expression in *E. coli* 122
Protein extraction 122
Activity-based protein profiling and click chemistry 122
CDNB assay 123
IEF 2D SDS-PAGE 123
In-gel fluorescence scanning and Western Blot 124
Large-scale labelling, affinity purification 124
On-bead trypsin and Lys-C digestion 125

LC-MS/MS and peptide identification using MaxQuant 125
*Pto*DC3000 and *P. infestans* infections 126
Image quantification and statistical analysis 127
Bioinformatics 127
Supplemental data 128
Chapter 5: General Discussion and Conclusion 133
CYP450 probes: current status and future perspectives 133
Limitations and recommendations when using CYP50 activity profiling in plants and fungi 133
Next step of CYP450 profiling in plants and fungi 134
GST-G photoaffinity profiling: current status and future perspectives 136
ABPP beyond classical detoxification enzymes families 137
The unstudied role of sulfotransferases in xenobiotic detoxification in plants 137
ABPP for the discovery of safener receptors in cereal crops 138
Conclusion 139
References 141
Appendix 156

Chapter 1: General Introduction

Overview

The increasing weed resistance to herbicides and more regular outbreaks of plant pests and diseases are negatively affecting global food production, leading to huge problems in agriculture (Liu, 2017; Peters and Strek, 2017). Herbicides and fungicides help to grow crops in weed- and pathogen-free fields, respectively, improving crop performance and increasing yield production. Nevertheless, the repeated use of agrochemicals with similar modes of actions has led to a rapid increase of herbicide and fungicide resistance in weeds and plant pathogens (Lucas *et al.*, 2015; Peters and Strek, 2017; Powles and Yu, 2010). Agrochemicals remain an essential and economically attractive chemical tool for farmers, together with other physical, biological and cultural control practices, due to their relatively low-cost and simple application. Therefore, investing in the discovery of agrochemicals with new modes of action and understanding the molecular mechanisms underlaying agrochemical resistance is essential for the future of chemical control and general crop protection.

Pesticide resistance: a major problem in agriculture

There are two main mechanisms through which organisms can evolve resistance to pesticides: target site resistance (TSR) and non-target site resistance (NTSR) (Figure 1) (Gaines *et al.*, 2020; Lucas *et al.*, 2015; Yuan *et al.*, 2007). TSR occurs when there are changes in the agrochemical target enzyme that decrease the binding of the active molecule at the site of action. Gene mutations that cause amino acid changes in the target enzyme or increased expression levels of the target enzyme are the two best known TSR mechanisms (Délye *et al.*, 2013; Powles and Yu, 2010). NTSR occurs when the amount of agrochemical reaching the target site is decreased. The limitation of the arrival of pesticide to the target site can be due to a reduced pesticide uptake and translocation and/or an increased rate of pesticide metabolism, also known as metabolic resistance (Hu and Chen, 2021; Powles and Yu, 2010). The different biology and ecology of crop pests (e.g. weeds, insects and pathogens) together with pesticides doses and application times, significantly influences the evolution of evolved resistance mechanisms.

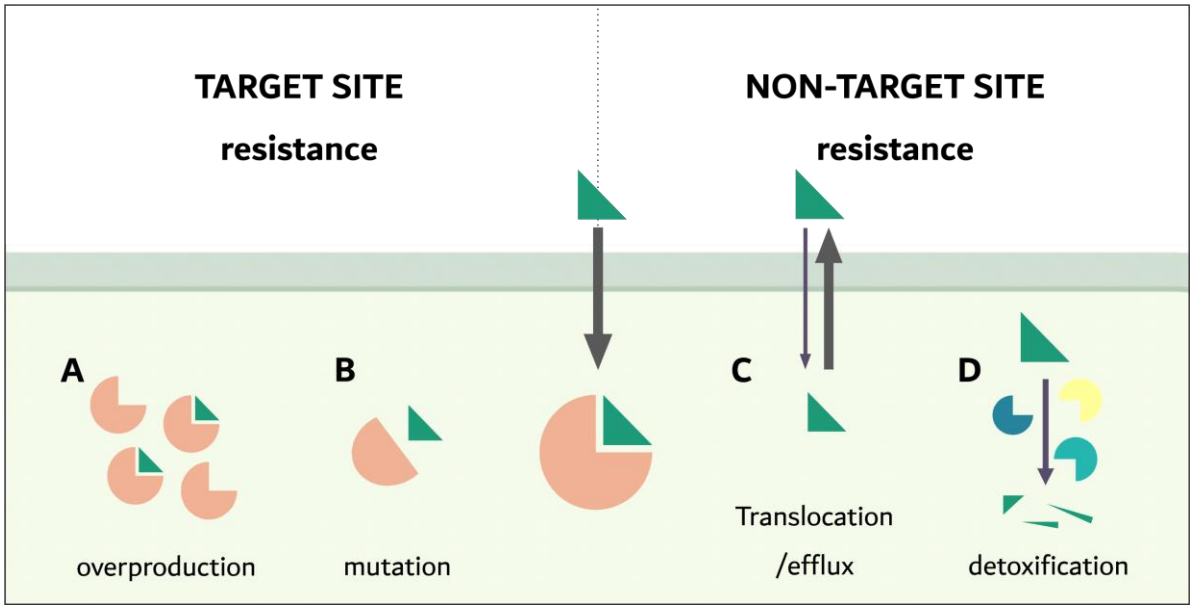


Figure 1. Main molecular mechanisms of herbicide and fungicide resistance. A and B) Target site resistance due to the overproduction of the target enzyme or the spontaneous mutation of the target enzyme, respectively. C and D) Non-target site resistance caused by the increased translocation/efflux of the agrochemical out from the cells or the break down of agrochemicals by detoxification enzymes. Figure adapted from (Lucas *et al.*, 2015).

In plants, the herbicide rate used in the field is known to be a key factor influencing the type of herbicide resistance mechanism selected in weeds (Yu and Powles, 2014). On one hand, when herbicides are applied in higher doses and high weed mortality occurs, herbicide resistance is usually associated with target-site gene mutations, presenting TSR. On the other hand, when lower herbicide doses are applied and lower weed mortality occurs, the surviving weeds can be selected for higher herbicide metabolization capacities, conferring NTSR. NTSR is the principal cause of resistance to several of the main herbicide groups used worldwide, such as synthetic auxin inhibitors and acetyl-CoA carboxylase (ACCase) inhibitors, and usually confers indiscriminate resistance to agrochemicals with different modes of actions and even to new potential herbicides (Délye, 2013; Todd *et al.*, 2020). Thus, NTSR is a major problem in agriculture and crop protection as it usually confers resistance to multiple herbicides and it involves the action of multiple genes (Yuan *et al.*, 2007).

In fungi, the most prevalent type of resistance is the occurrence of point mutations in the fungicide-target enzymes (Beckie *et al.*, 2021). Although several point mutations can occur in the target enzymes, not all target site resistance mutations provide the same level of fungicide resistance and sometimes they impose a fitness cost (Avenot and Michailides, 2010; Mikaberidze and McDonald, 2015). Nonetheless, NTSR has also been reported as a cause of fungicide resistance in many fungal species. Fungicide efflux through major facilitator superfamily (MFS) and ATP-binding cassette (ABC) transporters is the main cause of NTSR found in fungi. Efflux transporters are able to translocate

fungicides outside the fungal cell, therefore preventing the accumulation of toxic compounds (Hu and Chen, 2021). However, the metabolization of fungicides through detoxification enzymes is a much less studied mechanism of resistance, compared to the well-studied detoxification of drugs, herbicides and insecticides.

Metabolic resistance

Metabolic resistance is caused by an increased activity of detoxifying enzymes and usually involves the consecutive action of several enzyme families. Foreign compound (xenobiotic) detoxification is divided in four different phases based on the nature of the reactions and the modifications made (Figure 2). Cytochrome P450s (CYP450s) are phase I enzymes which typically oxidise xenobiotics, introducing or creating chemically active groups which can later on be modified. In phase II, already activated or not, xenobiotic molecules are conjugated to hydrophilic groups such as sugars or glutathione. The two most important phase II enzymes are glutathione transferases (GSTs) and UDP-glycosyltranferases (UGTs). Next, in phase III, the end products of phase II are recognized and sequestrated by ABC transporters and the conjugated xenobiotics are transported into the vacuole or the extracellular space. Finally, in phase IV, compartmentalized xenobiotics are degraded or incorporated into the cell wall (Dalazen *et al.*, 2016; Iyanagi, 2007; Xu *et al.*, 2005; Yuan *et al.*, 2007).

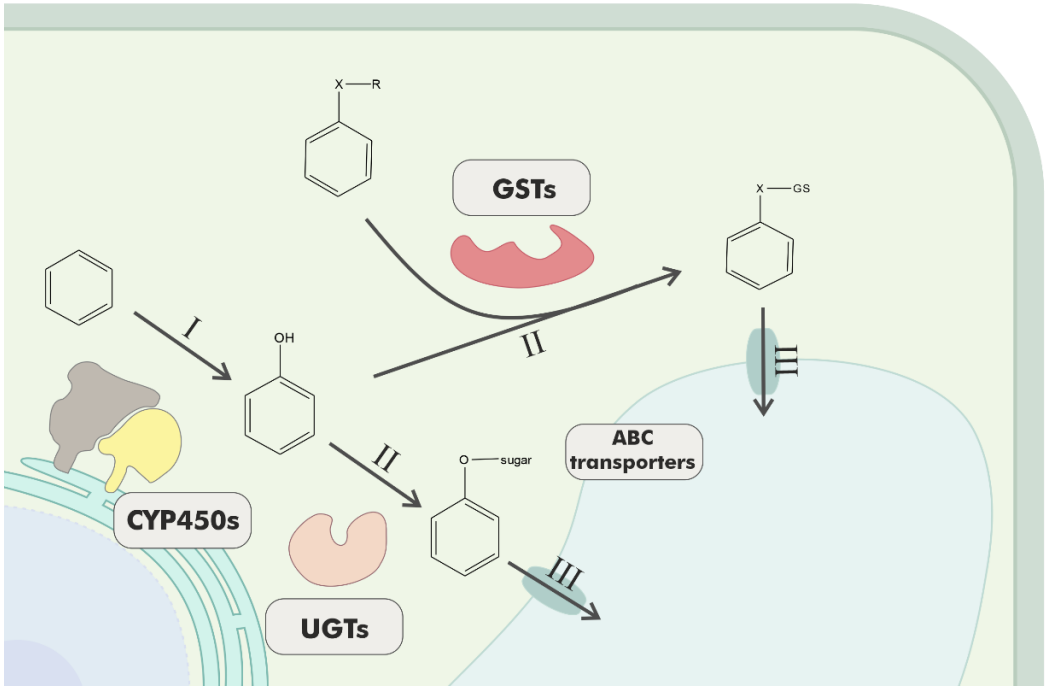


Figure 2. Schematic representation of the main enzyme superfamilies involved in herbicide detoxification. Cytochrome P450s (P450s), phase I detoxification enzymes, create chemically active groups that can be modified by phase II detoxification enzymes, glutathione transferases (GSTs) and UDP-glycosyltranferases (UGTs). The end products of phase II metabolism can then be recognized and sequestrated by ABC transporters, phase III detoxification enzymes, which can transport the conjugated compounds into the vacuole. Figure adapted from (Yu and Powles, 2014).

Cytochrome P450s

CYP450s are haem-containing monooxygenases present in all kingdoms of life (Bernhardt, 2006). CYP450s are known for their versatility in oxidising a wide range of chemical compounds through diverse reactions, including hydroxylation, dealkylation and epoxidation (Bernhardt, 2006; Guengerich, 2007). Most CYP450s require a redox partner for the supply of one or more electrons from NADPH/NADH. Depending on the type of protein partners associated in the electron transfer, CYP450 systems are classified in ten different classes (Hannemann *et al.*, 2007; Omura, 2010). In eukaryotes, the majority of CYP450 systems are microsomal (class II) and are formed by two membrane-anchored components: a CYP450 monooxygenase and a NADPH-dependent CYP450 reductase (CPR) (Schuler *et al.*, 2006; Šrejber *et al.*, 2018). By contrast, in prokaryotes, the most common CYP450 system is class I, composed of three soluble components: a CYP450 monooxygenase, a ferredoxin and a ferredoxin reductase. Other CYP450 systems are the class VII and VIII found in bacteria and fungi where CYP450 proteins are self-sufficient in electron transfer as they are directly fused to the reductase domain.

CYP450s are classified by structural homology and phylogeny and not by reaction type (Hannemann *et al.*, 2007). CYP450s are grouped into multigene families, following the general CYP nomenclature where CYP450s belonging to the same family and subfamily must share at least 40% and 55% protein sequence identity, respectively ((Bak *et al.*, 2011). At present, plant CYP450s are assigned to CYP71-CYP99, CYP701-CYP99 and CYP7001-CYP9999 families and grouped into 10 clans, containing four multiple-family clans (clan 71, clan 72, clan 85 and clan 86) and six single-family clans (clan 51, clan 74, clan 97, clan 710, clan 711 and clan 727) (Nelson *et al.*, 2004, Nelson 2009) (Figure 3). Fungal CYP450s are being assigned to CYP51-CYP69, CYP501-CYP699 and CYP5001-CYP6999 families and grouped into 15 clades based on their phylogenetic relationship (Chen *et al.*, 2014, Nelson 2009) (Figure 4). In all cases, following the family number, subfamilies are indicated by a capital letter and gene isoforms by a number. Nonetheless, despite the generally low amino acid identity between CYP450 families, all CYP450s have a conserved three-dimensional structure and a distinctive catalytic site containing a universally conserved cysteine that acts as heme binding site (Bak *et al.*, 2011; Lamb and Waterman, 2013; Schuler and Werck-Reichhart, 2003).

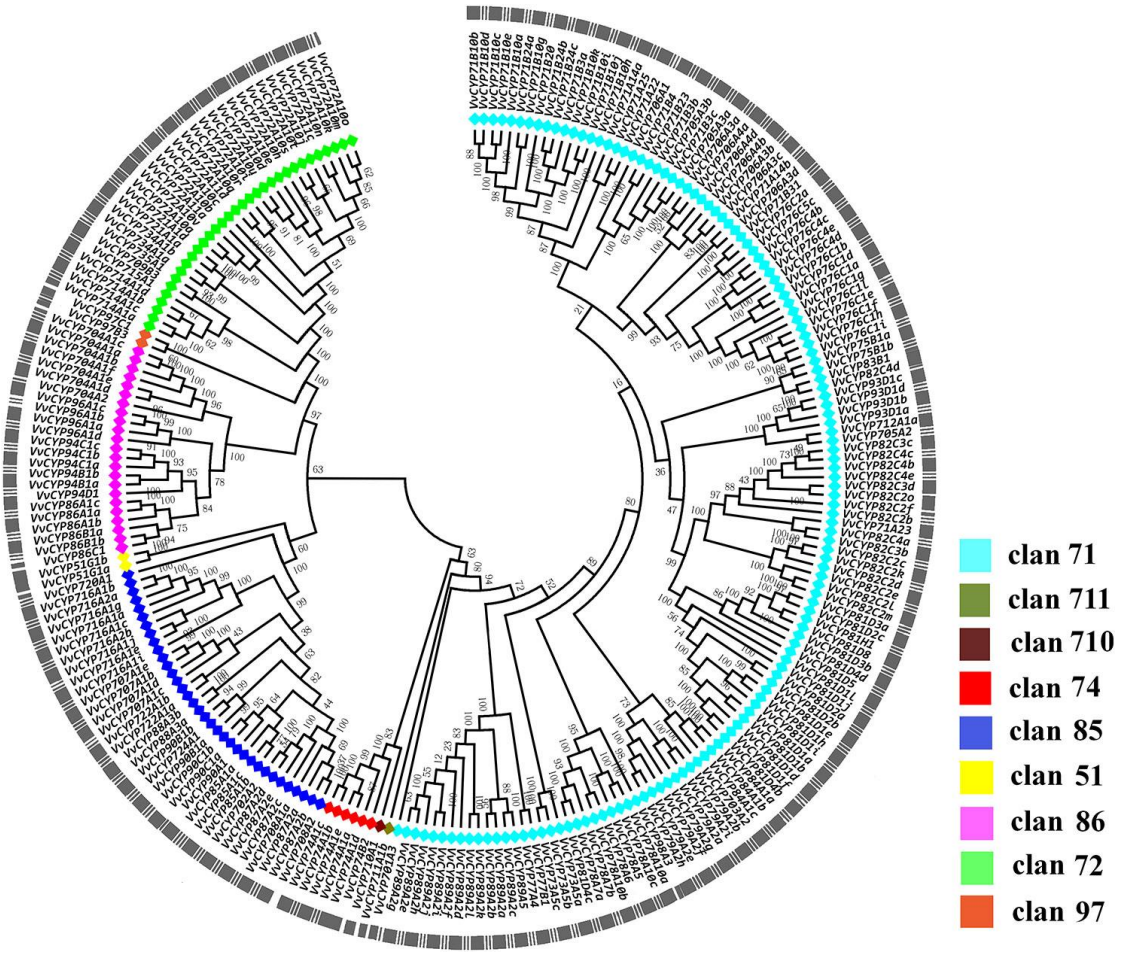


Figure 3. Phylogenetic analysis of CYP450 proteins in grapevine showing the division of CYP450s into clans. The colour of the inner circle indicates the corresponding CYP clans. Figure from Jiu *et al.,* 2020.

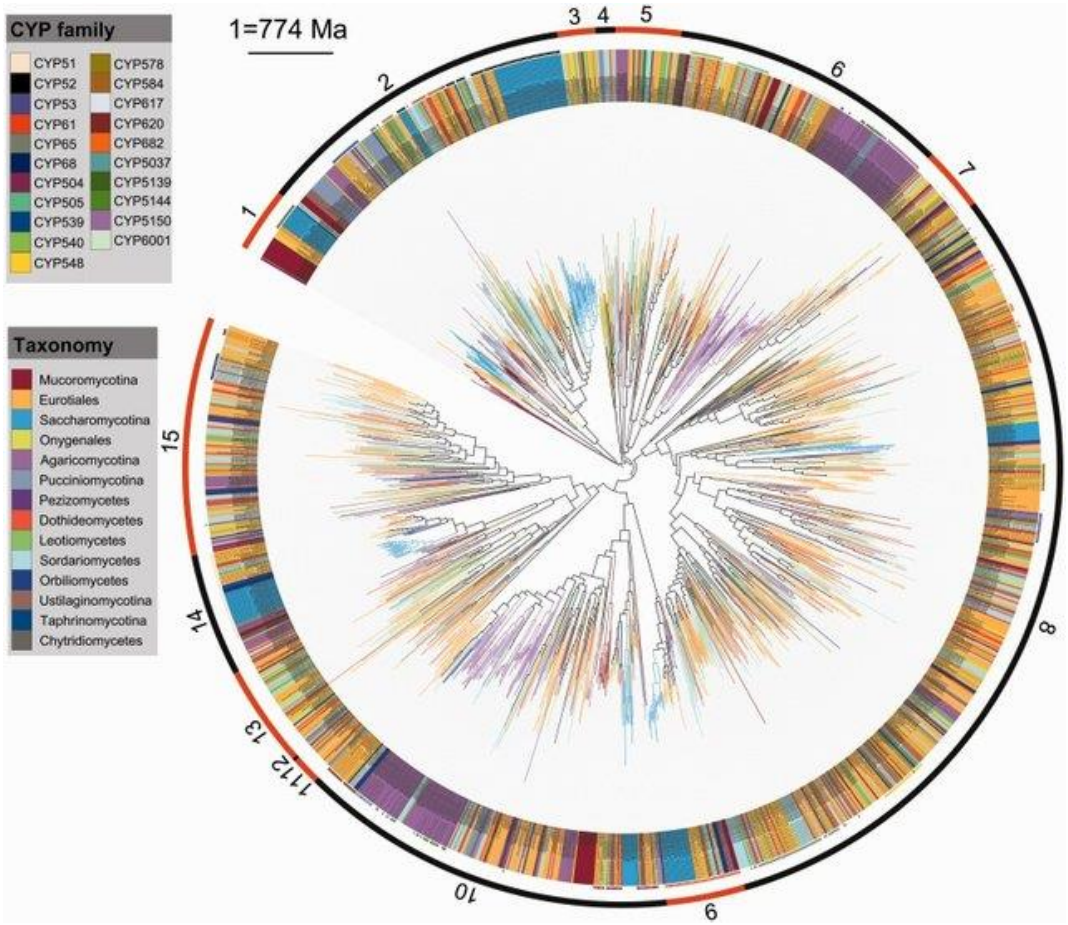


Figure 4. Phylogenetic analysis of fungal CYP450 proteins showing their division into clades. The colour of the branches and inner circle indicate the taxonomic groups. The middle circle indicates the corresponding CYP family. The outer circle indicates the 15 clades. Figure from Chen *et al.*, 2014.

The first CYP450 structure resolved was the bacterial P450cam (CYP101A1) in 1987 by Poulos and co-workers. Since then, many other CYP450 crystal structures from organisms from all kingdoms have been resolved. CYP74A1 was the first plant P450 for which a crystal structure was available (Lee *et al.*, 2008). Although many CYP450 structures have been resolved from bacteria (587 NCBI structure entries), fungi (84 NCBI structure entries) and human (266 NCBI structure entries), crystallised structures from plant CYP450s are rare, being Arabidopsis CYP74A1 and CYP90B1 the only ones (Fujiyama *et al.*, 2019; Lee *et al.*, 2008).

CYP450s are also important metabolising enzymes of a wide variety of endogenous and exogenous substrates. CYP450s play crucial roles in the synthesis of primary and secondary metabolites such as steroids, sterols, auxin, gibberellins and brassinosteroids (Ačimovič *et al.*, 2016; Mnguni *et al.*, 2020; Xu *et al.*, 2015; Zhang *et al.*, 2019). CYP450s have also been extensively studied in the context of xenobiotic and drug detoxification (Rettie and Thummel, 2014; Zanger *et al.*, 2008). Furthermore, another

important application of CYP450s is their use for biomedical and biotechnology applications due to their ability to catalyse different types of oxidations and ability to synthesises complex secondary metabolite structures (Li *et al.*, 2020; Urlacher and Girhard, 2019).

CYP450s have also been linked to the metabolism of pesticides in plants and fungi. Higher expression levels of CYP450s are commonly associated with herbicide and fungicide resistance in weeds and fungi, and many CYP450s been identified to confer herbicide resistance in different crop species (Gaines *et al.*, 2014; Iwakami *et al.*, 2014; Liu *et al.*, 2018; Sang and Hulvey, 2018). The combination of CYP450 inhibitors (e.g. piperonyl butoxide, 1-aminobenzotriazole, malathion) together with herbicides have been recurrently used in research studies to identify CYP450s involved in metabolism-based resistance to herbicide and fungicides (Elmore *et al.*, 2015; Jugulam and Shyam, 2019; Yanniccari *et al.*, 2020). Although the combination of CYP450 inhibitors together with insecticides is a more common practice in insects for increasing the efficacy of these agrochemicals by blocking their metabolization by CYP450s, this is a less common strategy in the application of herbicides and fungicides in crop protection (Feyereisen, 2015; Özdemir *et al.*, 2021). In plants, the most common way to protect cereal crops against weeds is by using safeners. Safeners are bioactive compounds that protect crops by selectively inducing the detoxification of herbicide in crops but not in weeds (Elmore *et al.*, 2015; Hatzios and Burgos, 2004; Persans *et al.*, 2001). Although safener selective protection is well known, the actual molecular mechanisms by which this specific response is activated and the main players of this protective effect is still unknown (Hu *et al.*, 2021).

Glutathione transferases

Glutathione (γGlu-Cys-Gly) is a key redox metabolite that has protective roles in cells as it reacts with electrophilic compounds and protects cells from oxidative stress (Forman *et al.*, 2009). Although the reaction of glutathione can occur spontaneously, GSTs are able to accelerate this reaction and conjugate the tripeptide glutathione to the electrophilic centre of a broad range of substrates (Sylvestre-Gonon *et al.*, 2019). Apart from conjugation capabilities, certain GSTs are also known to have isomerase, peroxidase and reductase activities (Deponte, 2013; Edwards, 2000).

GSTs are divided into three main families: cytosolic, mitochondrial and membrane-associated proteins in eicosanoid and glutathione metabolism (MAPEG). In humans, there are seven main cytosolic GST classes: alpha (GSTA), mu (GSTM), pi (GSTP), theta (GSTT), zeta (GSTZ), omega (GSTO) and sigma (GSTS) (Wu and Dong, 2012). In plants, the seven best known classes of cytosolic GSTs in plants are: phi (GSTF), tau (GSTU), theta (GSTT), zeta (GSTZ), lambda (GSTL), dehydroascorbate reductase (DHAR) and tetrachloro-phydroquinone dehydrogenase-related (TCHQD) (Dixon *et al.*, 2002a) (Figure 5). The majority of cytosolic GSTs form dimers and each subunit have two conserved pockets in the

active site: a glutathione-binding site (G-site) and a substrate-binding site (H-site) (Ding *et al.*, 2017; Edwards and Dixon, 2005; Wu and Dong, 2012). Usually, cytosolic GSTs dimerise with identical class members (homodimers) but heterodimers of different members from the same class have also been observed, incrementing the diversity of soluble GSTs found *in vivo* (Allocati *et al.*, 2018). In some cases, as is the case of the plant-specific phi and tau classes, only homodimer forms have been described (Dixon *et al.*, 2002a). More recently, new types of proteins having GST-like structure and biochemistry have been discovered in animals and plants, resulting in 14 GST classes described in plants (Lallement *et al.*, 2014; Oakley, 2011). For example, in Arabidopsis, four new GST classes were added: the membrane associated proteins in eicosanoid and glutathione metabolism (MAPEG), the glutathionyl hydroquinone reductase (GHR), the microsomal prostaglandin E-synthase type 2 (mPGES-2) and the eukaryotic translation elongation factor 1B- γ subunit (EF1Bγ) (Figure 5).

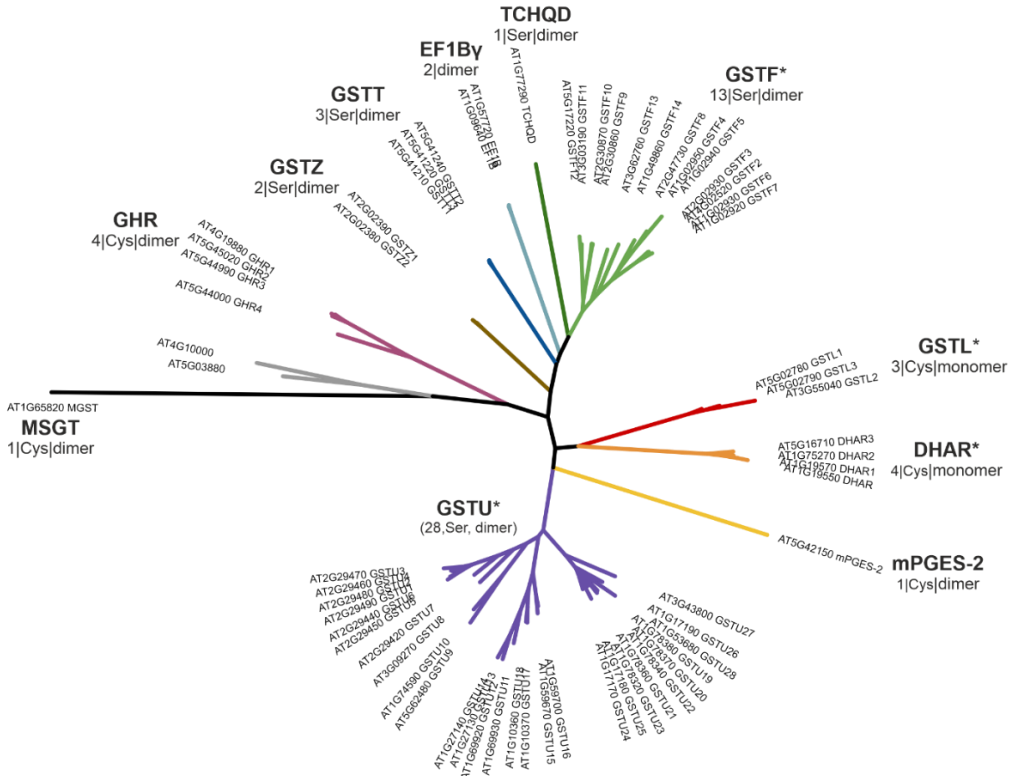


Figure 5. Classification of Arabidopsis glutathione transferases (GSTs) based on amino acid sequence identity. The sequences used were retrieved from Arabidopsis TAIR10 and aligned using PROMAL3D. The unrooted phylogenetic tree was constructed using the Maximum Likelihood method (1000 bootstraps) and edited with iTOL. GST classes are indicated in bold. Plant-specific GST classes are indicated with an asterisk (*). For each class, the number of Arabidopsis GSTs, the conservation of a serine or a cysteine in their catalytic site (Ser|Cys) and their monomeric or dimeric composition are indicated (monomer|dimer).

GSTs are redox enzymes involved in the detoxification of electrophilic compounds harmful for the cells, including xenobiotics (e.g. drugs, pesticides) and reactive oxidative stress products (Wu and Dong, 2012). In humans, GSTs have received special attention due to their involvement in cancer development and interference with anticancer drug treatments. GSTs are overexpressed in tumor cells and have been identified as key enzymes in metabolising procarcinogens or activating/inhibiting anticancer drugs (Singh and Reindl, 2021). In plants, GSTs play important roles in biosynthetic pathways, agrochemical detoxification, plant defence and oxidative stress (Basantani and Srivastava, 2007; Hernández Estévez and Rodríguez Hernández, 2020). For example, GSTs catalyse the reduction of organic hydroperoxides, lipid peroxides or hydrogen peroxide (derivate products of oxidative stress) into non-toxic molecules (Hossain *et al.*, 2017). Furthermore, one of the most studied roles of GSTs is also their involvement in metabolising agrochemicals, including herbicide and safeners (Cummins *et al.*, 2011). So far, all existing safeners are used to protect cereal (monocotyledonous) crops against dicotyledonous and monocotyledonous weed competitors. Although safeners do not protect dicotyledonous weeds against the lethal effects of herbicides, some dicotyledonous species like the model plant *Arabidopsis thaliana*, do respond against safener treatments by up-regulating xenobiotic detoxification enzymes. Therefore, there is still a lot more to study in the molecular mechanisms after herbicide metabolising enzyme activation in plants and whether the same classes of GSTs are induced from different herbicide and agrochemical chemistries in monocotyledonous and dicotyledonous plants. Furthermore, diverse transcriptomic studies have associated GSTs with herbicide resistance as they have been found to be constitutively up-regulated in resistant weed strains or highly overexpressed after herbicide and safener treatments (Cummins *et al.*, 2013; Deridder *et al.*, 2002; Evans *et al.*, 2017; Skipsey *et al.*, 2011; Smith *et al.*, 2004). However, GSTs can either have a direct involvement in the detoxification or are part of the overall stress response (and oxidative stress detoxification). In addition, GSTs are induced after pathogen infections and provide pathogen resistance in multiple plant species, as well as abiotic stresses such as salt and metal stress (Csiszár *et al.*, 2014; Gullner *et al.*, 2018; Kumar and Trivedi, 2018; Nianiou-Obeidat *et al.*, 2017; Smith *et al.*, 2004).

Chemical proteomics as a discovery tool to study agrochemical-metabolising enzymes in plants and fungi

Although quantitative proteomics and genetic-functional approaches have been crucial techniques for the association of CYP450s and GSTs in xenobiotic detoxification, protein studies are crucial for the determination of the direct metabolism of agrochemicals by the candidate genes.

Chemical proteomics methods enable the deep analysis of proteomes through the combinatory use of small molecule-based methods and the high sensitivity of mass spectrometry analysis. Activity-based

protein profiling (ABPP) is based on the use small chemical probes to detect, monitor and identify specific enzyme activities within complex proteome samples. ABPP has been extensively used in many research fields for: 1) the identification of cellular targets of small molecules (including drugs, agrochemicals and natural products), 2) the understanding of the reaction mechanisms of small molecules, 3) the study of relevant enzymes in diseases and other stresses (e.g. proteases, galactosidases, and 4) the discovery of new selective inhibitors (Benns *et al.*, 2021; Moellering and Cravatt, 2012; Morimoto and van der Hoorn, 2016; Wright, 2018; Wright and Sieber, 2016).

Independent of their application, all chemical probes must contain a warhead group, responsible for the irreversible attachment of the probe to their targeted enzymes, and a reporter tag (e.g. affinity tag, fluorophore, radioactive or chemical minitag), used for the purification and detection of the labelled proteins (Morimoto and van der Hoorn, 2016). Depending on the mechanism of the warhead activation, chemical probes can be classified into four categories: 1) Mechanism-based inhibitor probes, based on the covalent attachment of substrates, 2) Suicide substrate probes, based on substrates that upon enzyme activation become hyper-reactive and bind to a nearby amino acid, 3) Affinity-based probes, based on reversible inhibitors or substrates that incorporate a photoreactive group to enable its covalent attachment, and 4) Unbiased reactivity probes, based on hyperreactive amino acid residues (e.g. cysteine, tyrosine, lysine) (Morimoto and van der Hoorn, 2016). In all cases, functionalisation of the small molecule always requires the introduction of functional groups to facilitate covalent attachment or detection. Therefore, a rational design is required for the successful modification of bioactive molecules to retain their biological activity. Furthermore, extra considerations have to be taken depending on the chemical probes use; for example, *in vivo* studies usually require cell permeable chemical probes and usually carry a chemical (e.g. azide or alkyne) minitag as they are small and are less likely to affect the molecule bioactivity and permeability. By contrast, chemical probes used for *in vitro* studies can be already attached to bigger reporter tags such as affinity and fluorophore tags.

Previous studies have implemented chemical proteomics to study CYP450s and GSTs. Wright and co-workers designed a set of nine activity-based probes based on three different mechanisms of inactivation of mammal CYP450s (Wright *et al.*, 2009; Wright and Cravatt, 2007). CYP450 probes successfully labelled mammalian CYP450s in a NADPH-dependent manner and showed their different specificity against several mouse and human CYP450s. Furthermore, CYP450 probes enabled the identification of mouse CYP450s activated and inhibited upon drugs treatment and the monitoring response of CYP450s when using aromatase inhibitors, currently used for breast cancer treatments. In all cases CYP450 probes were suicide substrate probes where a suicide inhibitor, or a modification of it, were activated by CYP450-mediated substrate monooxygenation, resulting in reactive intermediate that covalently attaches the probe to the closest nucleophile site, usually within the binding pocket of

CYP450s (Figure 6). Additionally, a further two studies have also used chemical probes targeting CYP450s (Bennett *et al.*, 2016; Ismail *et al.*, 2013).

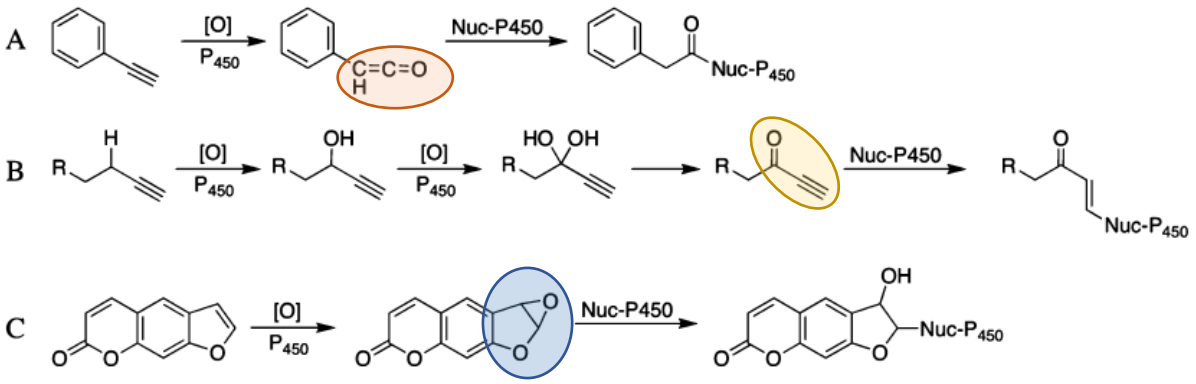


Figure 6. Reactivity of mechanism-based CYP450 probes. A) Aryl alkyne-based probes are activated by CYP450-mediated oxidation and form an electrophilic ketene intermediate (orange). B) Propynyl-based probes are activated by CYP450-mediated oxidation and form a reactive Michael acceptor intermediate (yellow). C) Furanocoumarine-based probes are activated by CYP450-mediated oxidation and form a reactive furan epoxide intermediate (blue). All reactive intermediates subsequently react with the the closest nucleophile site and form a covalent attachemnt to CYP450 proteins. Adapted from (Wright *et al.*, 2009).

Stoddard and co-workers designed a glutathione-based probe designed to target the G-site of GSTs, therefore named GSTABP-G (Stoddard *et al.*, 2017). GSTABP-G relied on the reactivity of a UV-dependent photoreactive group for its covalent label of GSTs, therefore classified as an affinity-based probe (Figure 7). Furthermore, GSTABP-G contains an alkyne tag as a reporter group, that is small and is used to detect the labelled protein by its chemical conjugation to a reporter molecule. GSTABP-G successfully several GSTs from mouse liver and lung cytosolic extracts and was applied for studying the differential activation of GSTs in diet induced obese mice (Stoddard *et al.*, 2017). Photoaffinity profiling has been routinely and successfully used for the identification of new enzymes involved in biotransformations or to study other enzyme families such as kinases and histone deacetylases (Korovesis *et al.*, 2021; Wang *et al.*, 2019; Wong *et al.*, 2020; Zheng *et al.*, 2017). Furthermore, affinity profiling is commonly used for the target identification of many drug compounds (Burton *et al.*, 2021; Smith and Collins, 2015).

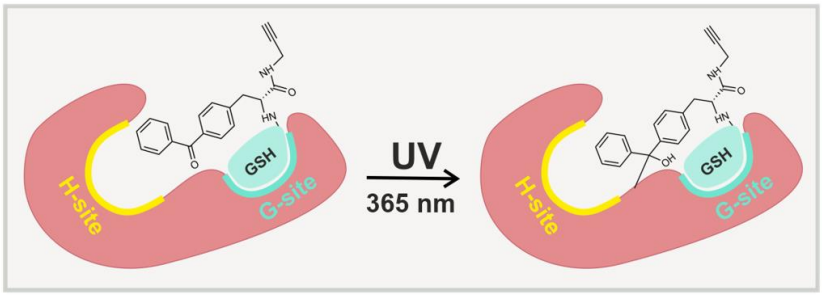


Figure 7. Reactivity of affinity-based GST probe. The tripeptide glutathione (GSH) directs and binds to the G-site of GSTs. Formation of covalent probe - GST conjugates accur after exposure of the photoreactive benzophenone to UV light (365 nm).

Click chemistry is commonly used to couple reporter groups to alkyne-derivatised probes. The most common used click chemistry reaction is the copper-catalysed azide–alkyne cycloaddition reaction, which catalyses the reaction between a terminal alkyne and an azide group (Martell and Weerapana, 2014). All CYP450 and GST-targeting probes described above, have a terminal alkyne that when incubated with an azide-containing reporter group (e.g. fluorophore-azide or biotin-azide) in the presence of copper, can quickly and selectively react (Figure 8). Doing so, the probe labelled enzymes can be visualised by in-gel fluorescence scanning or identified by streptavidin enrichment prior to mass spectrometry analysis, when using a fluorophore or a biotin reporter tag, respectively.

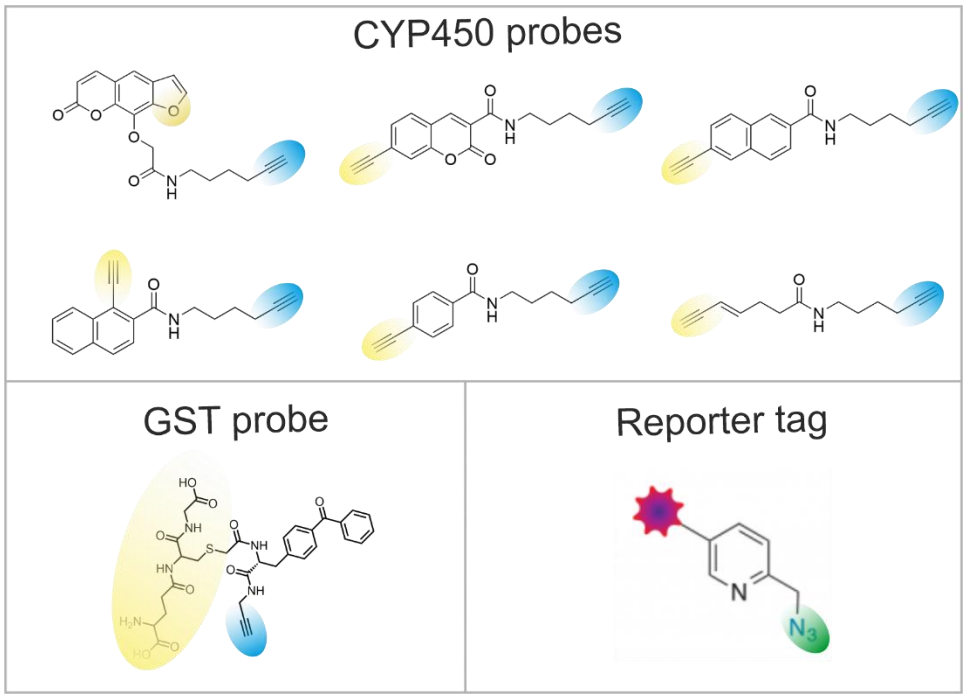


Figure 8. Chemical structure of probes and reporter tag. All probes (CYP450/GST) contain a warhead group (yellow) for the irreversible attachment of the probe to their targeted enzymes, and an alkyne tag (blue) for click chemistry coupling to a reporter tag. The reporter tag (fluorophore or biotin) contains an azide group (green) needed for the click chemistry reaction.

Aim of the thesis

CYP450s and GSTs are two very attractive families for the agrochemical industry due to their direct implication in metabolism-based resistance of pesticides in weeds, insects and pathogens. Furthermore, CYP450s and GSTs have also been described to play a role in biotic stresses. Due to their expanded families and substrate promiscuity, CYP450s and GSTs are difficult classes of enzymes to study. The application of activity-based protein profiling of CYP450s and GSTs in plants and fungi would be of relevance for discovering new functional enzymes directly involved in agrochemical detoxification or plant defence. The aim of this thesis is to:

Chapter 1: Our first objective aims to establish and validate CYP450 labelling in plants using click-chemistry and biotinylated CYP450 probes. This chapter includes the efforts made on understanding the main differences between the labelling of mammalian and plant CYP450s using mouse liver microsomes (well-stablished system for CYP450 labelling) and Arabidopsis microsomes (model plant organism). We discovered that click chemistry CYP450 probes label several *N. benthamiana* CYP450s and the herbicide-detoxifying CYP81A9 and recognised differences in CYP450 labelling by click chemistry and biotinylated probes.

Chapter 2. Our second objective aims to establish CYP450 labelling in the fungi *Zymoseptoria tritici* and use the CYP450 probes as a tool to study fungicide metabolism selectivity. First, we identified the target spectrum of the CYP450 probes in *Z. tritici*, identifying the top CYP450 candidates labelled in *Z. tritici* microsomes by LC-MS/MS. We confirmed the labelling of *Zt*P450 candidates by transiently overexpressing them in *N. benthamiana* and described the specific blockage of *Zt*CYP5080H1 labelling by the fungicide cyprodinil.

Chapter 3: Our third objective aims to use GST-G, a glutathione-based probe designed to target the G-site of GSTs, to monitor and identify the GSTs involved in agrochemical and plant-pathogen stress responses. First, we optimised the probe profiling by adjusting important parameters such are probe concentration, incubation time and optimal labelling pH. We identified the main classes of Arabidopsis GSTs targeted by the probe and confirmed labelling of GSTs by competing GST-G labelling by known GST inhibitors. We implemented photoaffinity profiling of GSTs to study the activation of GSTs upon safener and BION treatment of wheat seedlings and Arabidopsis plants, respectively.

Chapter 2: Profiling Cytochrome P450 activities in plants

Maria Font Farre[1], Daniel Brown[2], Melissa Brazier-Hicks[3], John Sinclair[3], Richard Dale[3], Samantha Hall[3], Melloney Morris[3], Aaron Wright[4], Jonathan Burton[2] and Renier A.L. van der Hoorn[1]

[1] The Plant Chemetics Laboratory, Department of Plant Sciences, University of Oxford, Oxford, UK.

[2] The Burton Group, Department of Chemistry, University of Oxford, Oxford, UK.

[3] Bioscience, Syngenta, Jealotts Hill International Research Centre, Bracknell, UK.

[4] Chemical Biology & Exposure Sciences, Pacific Northwest National Laboratory, Richland WA USA; The Gene and Linda Voiland College of Chemical Engineering and Bioengineering, Washington State University, Pullman WA USA.

Abstract

Cytochrome CYP450s (CYP450s) are linked to the metabolism of agrochemicals and various stress responses in plants. Many efforts have been taken in order to understand the specific function and selectivity of this diverse enzyme family. However, their complex regulation and versatile chemical reactions have made their characterisation challenging. Here, using chemical probes that have previously been confirmed to target CYP450s in mammals, we show the applicability of activity-based protein profiling to study plant CYP450s. CYP450 probes can be used to monitor the activity of many CYP450s in mouse liver microsomes in a NADPH-dependent manner. By contrast, the low CYP450 concentrations in plant tissues limits activity-based profiling of CYP450s in plant extracts. When overexpressed *in planta*, we can label several plant CYP450s, but not all, suggesting that plant CYP450s have different probe requirements. Among these, alkyne-tagged CYP450 probes label CYP81A9, a CYP450 from maize involved in xenobiotic detoxification, suggesting that CYP450 activity-based probes are functional and powerful tools to study xenobiotic detoxification enzymes in plants.

Introduction

Non-target site resistance (NTSR) is the principal cause of resistance to several of the main herbicide groups used worldwide, such as synthetic auxin inhibitors and Acetyl-CoA carboxylase (ACCase) inhibitors. NTSR usually confers indiscriminate and unpredictable resistance to agrochemicals with different modes of actions, and even to new potential herbicides (Délye, 2013). Metabolic resistance is a type of NTSR that occurs when there is a limitation in the amount of herbicide reaching the target site due to an increased rate of herbicide metabolism (Powles and Yu, 2010; Yu and Powles, 2014). Metabolic resistance is caused by an increased activity of detoxifying enzymes and involves the consecutive action of several enzyme families such as cytochrome P450s (CYP450s), glutathione transferases (GSTs), UDP-glycosyltranferases (UGTs) and ATP-binding cassette (ABC) transporters (Dalazen *et al.*, 2016; Yuan *et al.*, 2007). This pool of enzymes that allow plants to defend themselves against herbicides and other foreign compounds (xenobiotics) is commonly known as the xenome, and has the ability to metabolise a broad array of chemicals, from allelochemicals such as microbial toxins to agrochemicals and pollutants (Brazier-Hicks *et al.*, 2018; Edwards *et al.*, 2005). We focused on CYP450s as they are the largest family of enzymes found to have xenobiotic metabolising activities in all kingdoms of life (Nelson and Nebert, 2018).

CYP450s are thiolate-ligated haem monooxygenases able to oxidise a broad range of substrates by transferring an oxygen atom into them. The vast majority of eukaryotic CYP450s are membrane bound proteins, mainly integrated in the endoplasmic reticulum (ER) facing the cytosol, but these enzymes can also be found in subcellular compartments such as mitochondria and chloroplasts (Schuler *et al.*, 2006; Šrejber *et al.*, 2018). In contrast, all studied prokaryotic CYP450s are soluble and located in the cytosol (Omura, 2010). With few exceptions, CYP450s need the help of reductases as redox partners and nicotinamide adenine dinucleotides (NADH/NADPH) as cofactors. Cytochrome P450 reductase (CPR) is the common redox partner in microsomal CYP450 systems and contains FAD- and FMN-binding sites, responsible for the transfer of reducing equivalents from NADPH to CYP450s (Hannemann *et al.*, 2007; Hrycay and Bandiera, 2015).

In mammals, CYP450s have been extensively studied in the context of xenobiotic and drug detoxification (Rettie and Thummel, 2014; Zanger *et al.*, 2008). Furthermore, mammal CYP450s have also been associated with carcinogenesis and many monogenic and polygenic diseases, increasing CYP450s as novel therapeutic targets (McFadyen *et al.*, 2004; Nebert *et al.*, 2013; Pikuleva and Waterman, 2013; W. Wang *et al.*, 2019). Analysis of CYP450s involved in drug and xenobiotic detoxification in mammals have revealed that although there is a large and diverse number of CYP450s, CYP450s associated with xenobiotic detoxification generally belong to specific CYP450 families. In humans, CYP450s belonging to CYP1, 2, 3 and 4 families are primarily associated with the detoxification of drugs

and xenobiotics, ten of which are the main CYP450s responsible for drug oxidation: CYP3A4/5, CYP2D6, CYP2C9, CYP1A2, CYP2B6, CYP2C19, CYP2C8, CYP2A6, CYP2E1 and CYP2J2 (Nelson and Nebert, 2018; Tanaka, 1998; Zanger and Schwab, 2013). Although bacterial genomes are known to contain smaller numbers of CYP450s, microbial CYP450s are of great interest due to their high stability and efficiency in biotechnology and synthetic biology applications (Girvan and Munro, 2016; Kelly and Kelly, 2013; Kumar, 2010). For instance, BM3 (CYP102A1 from *Bacillus megaterium*) is a natural fusion of a CYP450 and a CPR and is useful as biocatalyst due to its self-sufficiency, great solubility and highest oxidation activity known for a CYP450 monooxygenase (Jeffreys *et al.*, 2019; Yun *et al.*, 2007). In fungi, the number of CYP450s vary a bit more between species. While *Saccharomyces cerevisiae* (baker's yeast) has just three functional CYP450 sequences, human and plant fungal pathogens usually contain larger numbers of CYP450s. For instance, *Aspergillus fumigatus* and *Fusarium oxysporum* have 77 and 169 CYP450s, respectively (Chen *et al.*, 2014; Durairaj *et al.*, 2016). Fungal CYP450s are of special interest as drug targets considering their essential role in primary metabolism (Parker *et al.*, 2014). In insects, CYP450s have been associated with the detoxification of multiple insecticides and allelochemicals and play a role in the production of defence compounds (Jensen *et al.*, 2011; Li *et al.*, 2004; Shi *et al.*, 2018; Yin *et al.*, 2019). For example, CYP450s from the CYP4G subfamily play a role in the synthesis of cuticular hydrocarbons, protecting insects from desiccation and also preventing insecticide penetration (Wu *et al.*, 2020).

Plant genomes have high numbers of CYP450 genes (e.g. 245 in Arabidopsis, 326 in rice and 769 in Eucalyptus) in comparison to animals, fungi and bacteria (e.g. 57 in humans, 102 in mouse) (Nelson, 2004; Nelson and Nebert, 2018; Wei and Chen, 2018). This high number and expansion of CYP450s in plants contributed to the evolution of their specialised and complex metabolism and the multitude of active compounds they produce. CYP450s are the largest family of enzymes supporting plant metabolic pathways (Nelson and Werck-Reichhart, 2011). In plants, CYP450s are linked to the detoxification of agrochemicals and various stress responses. Although many plant CYP450s are associated with herbicide-metabolism, the actual origin of detoxifying plant CYP450s and whether there are main CYP450 families responsible for the metabolism of xenobiotics is not clear. The capacity of CYP450 to metabolise agrochemicals could be a consequence of the casual fit of agrochemicals to the active site of certain CYP450s that play other roles in secondary metabolism or the specific evolution of CYP450 for "natural" xenobiotic detoxification such as allelochemicals (Dimaano and Iwakami, 2020). Higher expression levels of CYP450s are commonly associated with herbicide resistance in weeds and many CYP450s confer herbicide resistance in different crop species. For example, whole-transcriptome sequencing of diclofop-resistant populations of *Lolium sp.* showed to have high constitutive expression of CYP450s from CYP72A, CYP716A and CYP81B1 families (Duhoux *et al.*, 2015; Gaines *et al.*, 2014).

The up-regulation of four members of the CYP81A subfamily in *Echinochloa phyllopogon*, an important weed in rice fields, was responsible for its resistance to different herbicide classes (Guo *et al.*, 2019; Iwakami *et al.*, 2014). In rice, genetic studies indicated the involvement of CYP81A6 and CYP72A31 in the detoxification of bispyribac sodium and bensulfuron-methyl, respectively (Liu *et al.*, 2012; Pan *et al.*, 2006; Saika *et al.*, 2014). Furthermore, CYP450s associate with safener protection of cereal crops due to the capacity of these safeners to induce the expression of specific CYP450s in cereal crops but not in weeds (Elmore *et al.*, 2015; Hatzios and Burgos, 2004; Persans *et al.*, 2001). Recent studies in cyprosulfamide safener selectivity determined the role of CYP81A9 as the principal CYP450 responsible for the selective protection of maize, but not wheat, from injury by ALS-inhibiting herbicide thiencarbazone-methyl (Giannakopoulos *et al.*, 2020).

Although functional genomics have identified the role of many CYP450s involved in plant metabolism and xenobiotic detoxification, the extended functional diversity, distinct substrate specificity and large family size have made the study of CYP450s a big challenge. More general and comprehensive approaches that consider the study of CYP450s in crude extracts and living systems are needed to fully understand the specific function and selectivity of this highly diverse enzyme family. Activity-based protein profiling (ABPP) is a powerful chemical proteomic tool used in various biological systems to monitor, identify and characterise the activity of different enzymes within complex proteomes (Kovács and van der Hoorn, 2016). ABPP aims to selectively label the active site of enzymes using bifunctional chemical probes. On one side, chemical probes have a reactive group, known as warhead, which is responsible for the irreversible attachment of the probe to their targeted enzymes. On the other side, activity-based probes carry a reporter tag (e.g. biotin or fluorescent dye), or a ligation handle that can be coupled to a reporter tag via 'click chemistry', which is used for the purification and detection of the labelled proteins (Morimoto and van der Hoorn, 2016).

Previously, chemical probes targeting CYP450s were used to monitor drug induction and inhibition of CYP450 activities and to identify their inhibition by drugs (Wright *et al.*, 2009; Wright and Cravatt, 2007). Two other studies have used ABPP probes to characterise ammonia monooxygenases and pyrethroid-metabolising CYP450s in bacteria and insects, respectively (Bennett *et al.*, 2016; Ismail *et al.*, 2013). In all cases, CYP450 activity-based probes are based on alkyne-based warheads that become reactive upon mono-oxygenation and subsequently react with nucleophiles in the substrate binding pocket of CYP450s.

Results

Chemical probes label CYP450s in mouse liver microsomes but not in Arabidopsis leaf microsomes

Wright and co-workers designed a set of nine activity-based probes based on three different mechanisms of inactivation of mammal CYP450s. CYP450 probes successfully labelled mammalian CYP450s in a NADPH-dependent manner and showed their different specificity against several mouse and human CYP450s, altogether providing a new and functional tool to study *in vivo* and *in vitro* CYP450 activities (Wright *et al.*, 2009; Wright and Cravatt, 2007). To study the chemical reactivity of these probes in plants, we selected the best six CYP450 probes from Wright and co-workers and tested them for labelling in Arabidopsis leaf microsomes, and compared these to CYP450 labelling in mouse liver microsomes. All CYP450 probes consist of two parts: (1) a reactive group that reacts with the target protein and binds covalently. Most probes carry an aryl alkyne-based reactive group (yellow), except from DB080 and DB143, which contain a furan (purple) and an enyne (orange), respectively; and (2) an alkyne tag that allows the coupling of the probe to a fluorescent or affinity tag (Figure 1).

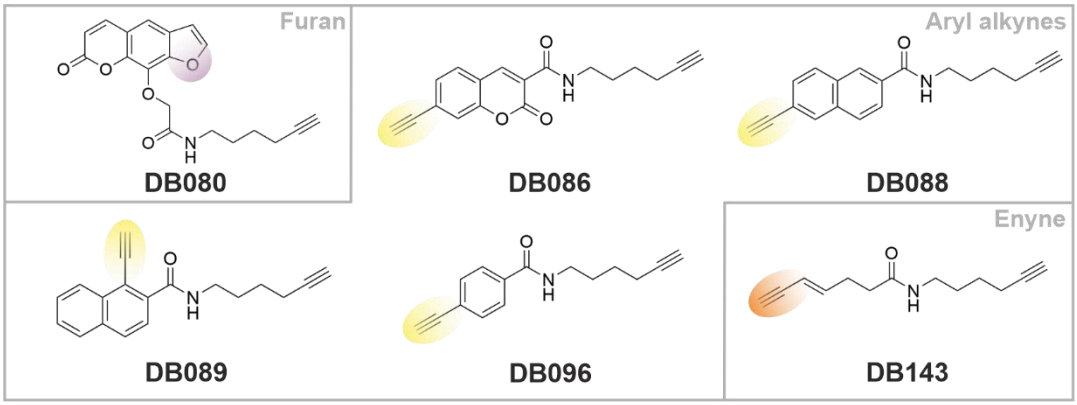


Figure 1. Chemical structures of CYP450 probes. Most probes carry an aryl alkyne-based reactive group (yellow), except from DB080 and DB143, which contain a furan (purple) and an enyne (orange), respectively. All probes contain an alkyne tag (right), for click chemistry coupling to fluorophores and/or biotin.

To confirm CYP450 labelling with these probes, mouse liver microsomes (GIBCO™ Mouse (CD-1) Microsomes) and isolated microsomes from Arabidopsis leaves were incubated with 10 μM probes in the presence or absence of NADPH. After an hour incubation, labelled proteins were coupled to a fluorophore via click chemistry and visualised by in-gel fluorescence scanning. All six CYP450 probes caused NADPH-dependent signals at approximately 55 kDa in mouse liver microsomes, which indicates selective activity-based labelling of mouse CYP450s (Figure 2A). However, no NADPH-dependent signal was detected when labelling Arabidopsis leaf microsomes, apart from a persistent NADPH-independent background signal at approximately 55 kDa, which corresponds to rubisco, the most abundant protein in leaf proteomes (Figure 2B, asterisk).

Due to the possible masking of the NADPH-dependent CYP450 signals by the rubisco background, we next performed CYP450 labelling in microsomes isolated from Arabidopsis and maize cell cultures grown in the dark (etiolated). Unfortunately, no NADPH-dependent labelling was observed in any of these two experiments (Figure 3A and 3B). Iodoacetamide (IA), a cysteine-reactive probe, and fluorophosphonate (FP), a serine hydrolases probe, containing alkyne tags were included as positive control for the click chemistry reaction.

Plant CYP450s are known to be upregulated after safener and herbicide treatments (Brazier-Hicks *et al.*, 2018; Didierjean *et al.*, 2002; Skipsey *et al.*, 2011). Therefore, in order to maximise the CYP450 presence in our microsomes fraction, we treated an Arabidopsis cell culture with the safener benoxacor and the herbicide chlorsulfuron and we labelled the isolated microsomes with CYP450 probes. Unfortunately, no NADPH-dependent labelling was observed in any of the chemical-treated microsomes (Figure 3C). Labelling with FP was successful, demonstrating the success of the labelling procedure via click chemistry.

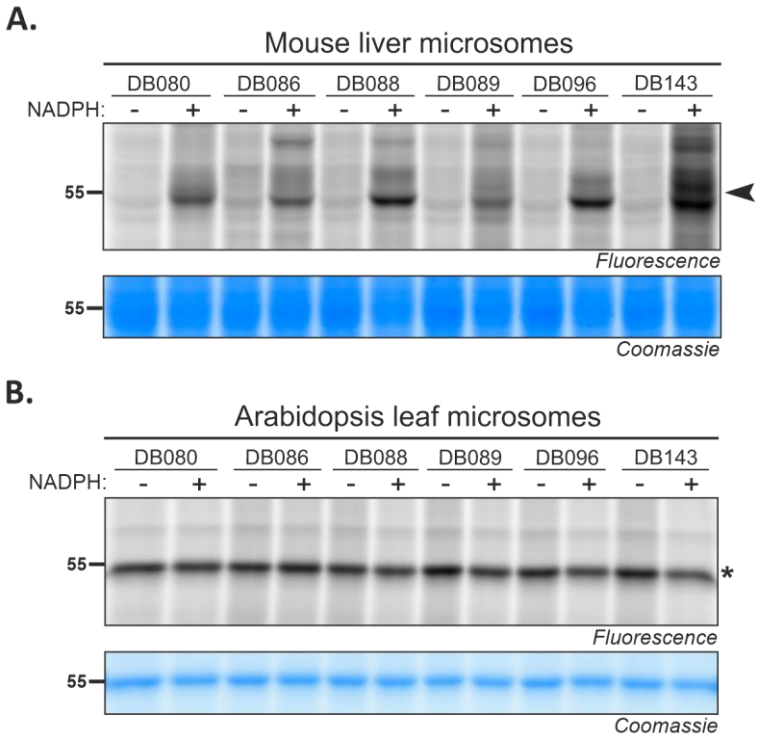


Figure 2. CYP450 probes label Cytochrome P450s in mouse liver microsomes but not in Arabidopsis leaf microsomes. **A**, NADPH-dependent labelling of mouse CYP450s. Mouse liver microsomes were labelled for 1 hour with 10 μM probe with or without 1 mM NADPH. Labelled proteins were coupled to picolyl azide fluorophore via click chemistry, separated on SDS-PAGE gels and visualised by in-gel fluorescence scanning. Coomassie staining is shown as loading control. Similar results were obtained in two replicate experiments. B, No detectable NADPH-dependent labelling of Arabidopsis CYP450s. Arabidopsis leaf microsomes were isolated via ultracentrifugation and resuspended microsomes were labelled with 10 μM probe with or without NADPH. Labelled proteins were processed and detected as described above. Coomassie staining is shown as loading control. Similar results were obtained in two replicate experiments.

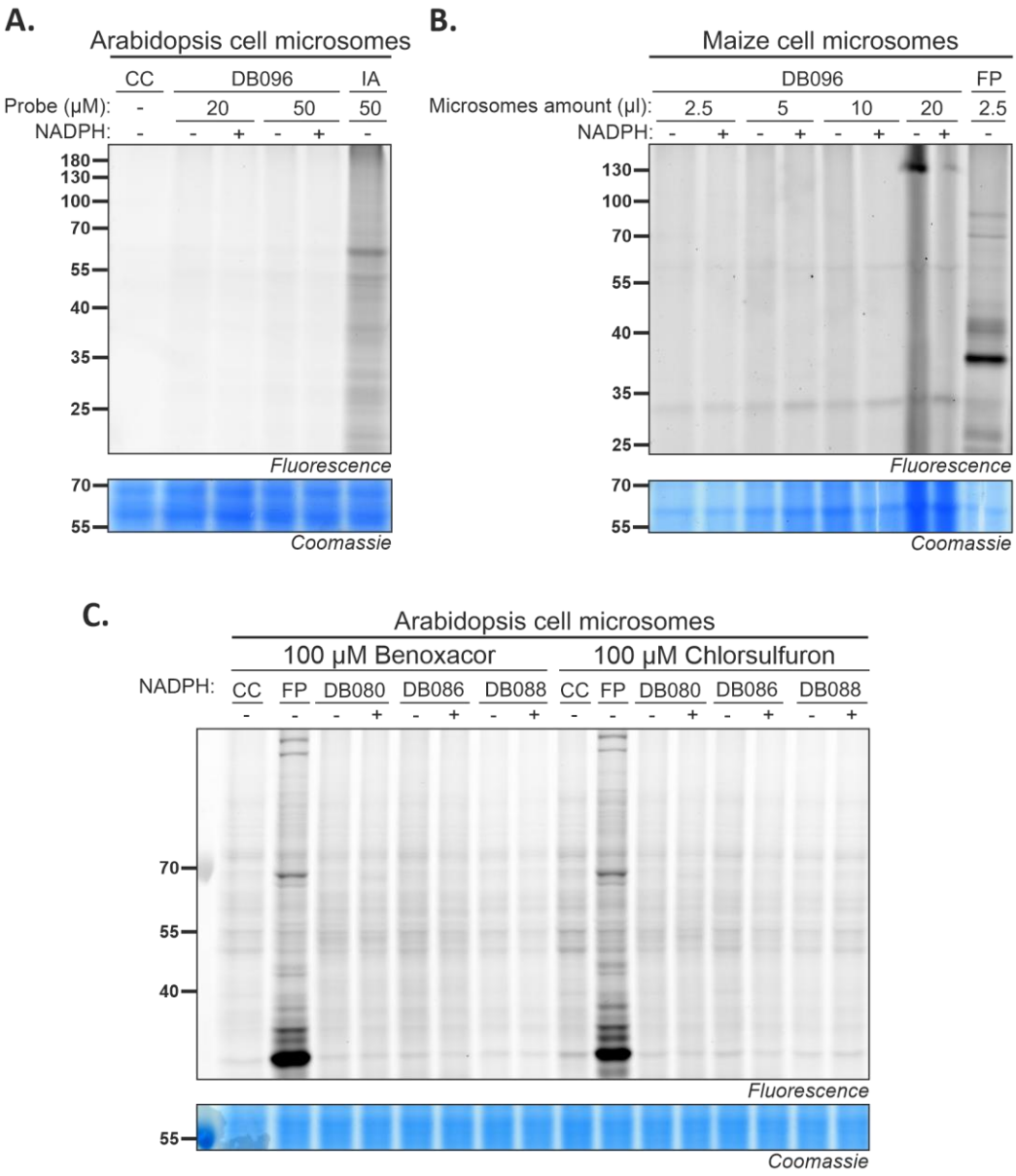


Figure 3. CYP450 probes do not label CYP450s in microsomes of cell cultures of Arabidopsis or maize cell. **A**, No detectable NADPH-dependent labelling in microsomes of Arabidopsis cell culture. Arabidopsis cell culture microsomes were labelled with different DB096 probe concentrations (20 and 50 μM) with the presence or absence of 1 mM NADPH. Click chemistry control containing the fluorophore-azide (CC) and iodoacetamide-alkyne (IA) were used as a negative and a positive control for labelling, respectively. Labelled proteins were processed and detected as described in Figure 2. **B**, No detectable NADPH-dependent labelling in maize microsomes. Different amount of maize microsomes were labelled with 5 μM DB096 with or without 1 mM NADPH. Fluorophosphonate-alkyne (FP) was used as a positive control for labelling. Labelled proteins were processed and detected as described in Figure 2. **C**, No detectable NADPH-dependent labelling in agrochemical-treated Arabidopsis cell cultures. Arabidopsis cell cultures were treated with 100 μM Benoxacor (safener) and Chlorsulfuron (herbicide) for 8h. Microsomes were isolated and labelled with 10 μM DB080, DB086 and DB088 probes with the presence or absence of 1mM NADPH. Click chemistry control containing the fluorophore-azide (CC) and fluorophosphonate-alkyne (FP) were used as a negative and a positive control for labelling, respectively. Labelled proteins were processed and detected as described in Figure 2.

To independently assess CYP450 activity, we used the classic carbon monoxide (CO) displacement assay for qualifying the activity of CYP450s. When CYP450s bind CO, their absorbance shifts from 420 nm to 450 nm, which is characteristic of and eponymous to CYP450 proteins (Guengerich *et al.*, 2009). Microsomes to be tested were diluted and reduced using sodium dithionite crystals. Next, the same microsomes were bubbled with CO and their absorbance was measured. As positive control, mouse liver microsomes showed the typical absorbance peak at 450 nm, indicating the presence of active CYP450s in mouse liver microsomes (Figure 4A). However, there was no peak at 450 nm for Arabidopsis leaf microsomes, Arabidopsis cell culture microsomes and maize cell culture microsomes, indicating that not enough CYP450s were present or inactive in the plant microsomes (Figure 4B, 4C and 4D).

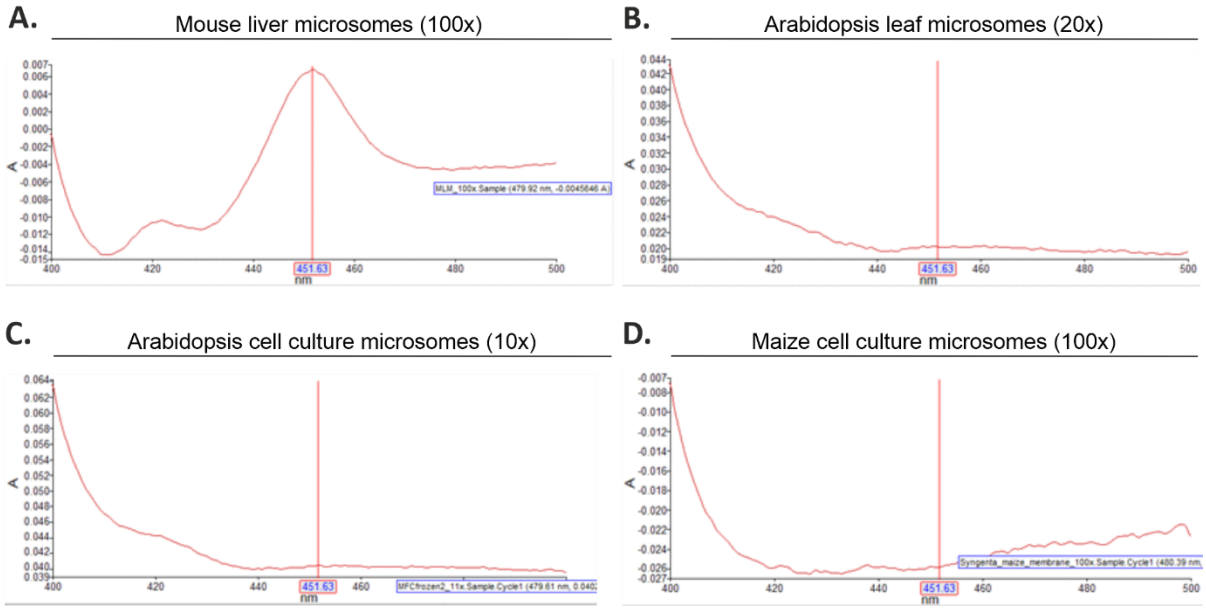
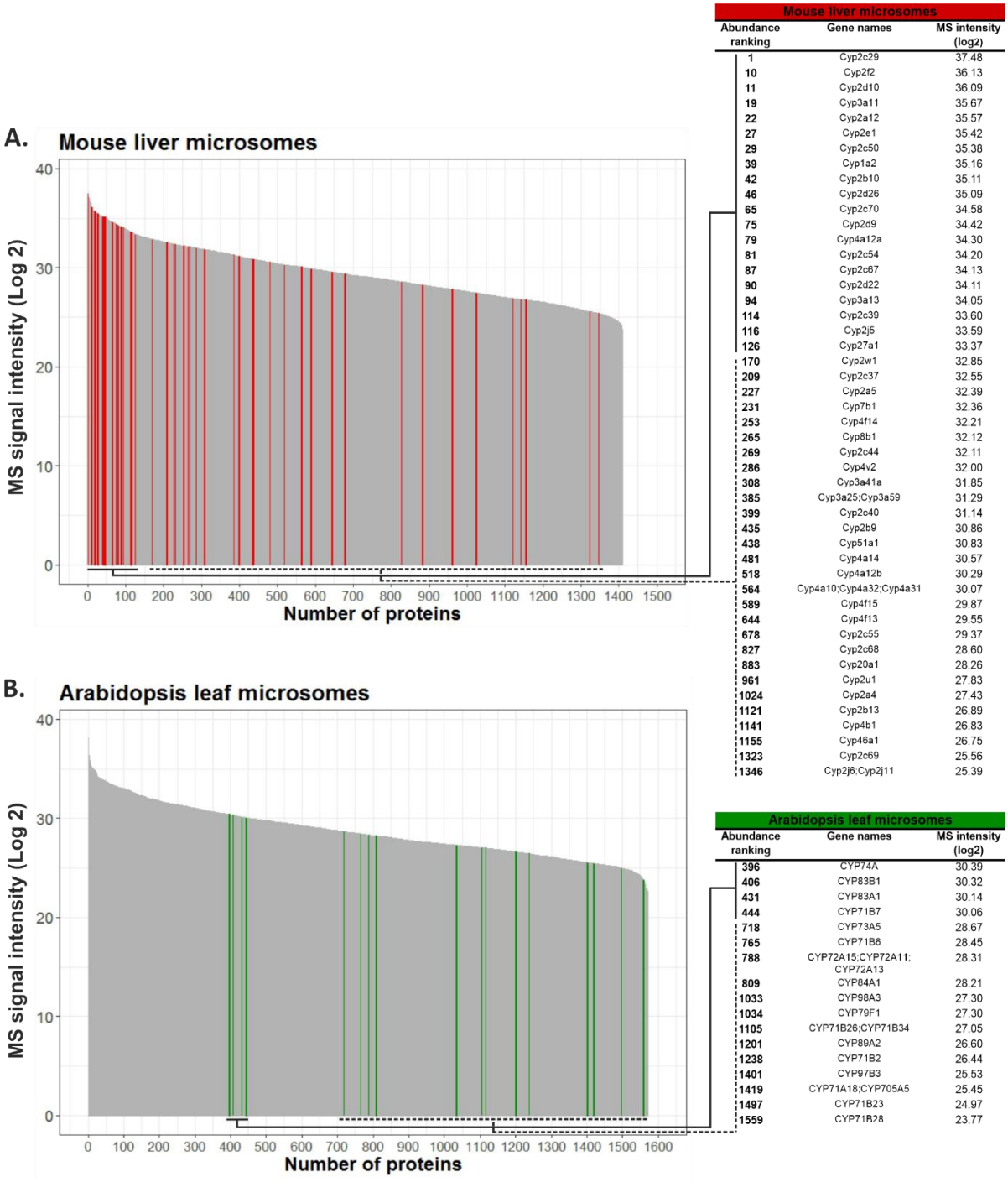


Figure 4. Absorbance spectrum of mouse liver, Arabidopsis and maize microsomes upon CO exposure. In parenthesis, the dilution it was used for the assay (100x, a hundred times diluted; 20x, twenty times diluted; 10x, ten times diluted). **A**, Mouse liver microsomes. **B**, Arabidopsis leaf microsomes. **C**, Arabidopsis cell culture microsomes. **D**, Maize cell culture microsomes.

MS analysis shows differences in abundance and number of CYP450s between mouse liver and Arabidopsis microsomes

To compare the presence and abundance differences between Arabidopsis and mouse CYP450s, we performed a mass spectrometry (MS)-based global proteomic analysis of mouse liver microsomes and Arabidopsis leaf microsomes. Microsomes were digested with Lys-C and trypsin and peptides were analysed by liquid chromatography-tandem mass spectrometry (LC-MS/MS). Proteins were ranked by their spectral intensity. A total of 48 CYP450s were detected amongst 1410 proteins in the proteome of mouse liver microsomes (Figure 5A). We detected 20 CYP450s having an intensity higher than 1.0E+10 (log_2 MS intensity > 33) within the top 150 most abundant proteins, positioning CYP450s as the most abundant class of proteins found in mouse liver microsomes. Cyp2c29 was the most abundant protein in mouse liver microsomes (log_2 MS intensity of 37.48). In contrast, just 17 CYP450s were detected amongst 1571 proteins in the Arabidopsis leaf microsomes (Figure 5B). The large chain of Rubsico (rbcL) was the most abundant protein in Arabidopsis leaf microsomes (log_2 MS intensity of 38.10) and CYP74A was the first CYP450, found at position 396 (log_2 MS intensity of 30.39), indicating that CYP450s in Arabidopsis leaf microsomes are present at two orders of magnitude less abundant than in mouse liver microsomes. In addition, we confirmed that microsomal fraction isolation is a crucial step for CYP450 enrichment as we could just detect two CYP450s (CYP97B3, log_2 MS intensity of 25.81 and CYP74A, log_2 MS intensity of 25. 17), in Arabidopsis total extract with MS analysis (Figure 6).



Mouse liver microsomes

Abundance ranking	Gene names	MS intensity (log2)
1	Cyp2c29	37.48
10	Cyp2f2	36.13
11	Cyp2d10	36.09
19	Cyp3a11	35.67
22	Cyp2a12	35.57
27	Cyp2e1	35.42
29	Cyp2c50	35.38
39	Cyp1a2	35.16
42	Cyp2b10	35.11
46	Cyp2d26	35.09
65	Cyp2c70	34.58
75	Cyp2d9	34.42
79	Cyp4a12a	34.30
81	Cyp2c54	34.20
87	Cyp2c67	34.13
90	Cyp2d22	34.11
94	Cyp3a13	34.05
114	Cyp2c39	33.60
116	Cyp2j5	33.59
126	Cyp27a1	33.37
170	Cyp2w1	32.85
209	Cyp2c37	32.55
227	Cyp2a5	32.39
231	Cyp7b1	32.36
253	Cyp4f14	32.21
265	Cyp8b1	32.12
269	Cyp2c44	32.11
286	Cyp4v2	32.00
308	Cyp3a41a	31.85
385	Cyp3a25;Cyp3a59	31.29
399	Cyp2c40	31.14
435	Cyp2b9	30.86
438	Cyp51a1	30.83
481	Cyp4a14	30.57
518	Cyp4a12b	30.29
564	Cyp4a10;Cyp4a32;Cyp4a31	30.07
589	Cyp4f15	29.87
644	Cyp4f13	29.55
678	Cyp2c55	29.37
827	Cyp2c68	28.60
883	Cyp20a1	28.26
961	Cyp2u1	27.83
1024	Cyp2a4	27.43
1121	Cyp2b13	26.89
1141	Cyp4b1	26.83
1155	Cyp46a1	26.75
1323	Cyp2c69	25.56
1346	Cyp2j6;Cyp2j11	25.39

Arabidopsis leaf microsomes

Abundance ranking	Gene names	MS intensity (log2)
396	CYP74A	30.39
406	CYP83B1	30.32
431	CYP83A1	30.14
444	CYP71B7	30.06
718	CYP73A5	28.67
765	CYP71B6	28.45
788	CYP72A15;CYP72A11; CYP72A13	28.31
809	CYP84A1	28.21
1033	CYP98A3	27.30
1034	CYP79F1	27.30
1105	CYP71B26;CYP71B34	27.05
1201	CYP89A2	26.60
1238	CYP71B2	26.44
1401	CYP97B3	25.53
1419	CYP71A18;CYP705A5	25.45
1497	CYP71B23	24.97
1559	CYP71B28	23.77

Figure 5. Cytochrome P450s are highly abundant in mouse liver microsomes but not in Arabidopsis leaf microsomes. Comparison of the presence and abundance of Cytochrome P450s found in mouse liver microsomes (**A**) and Arabidopsis leaf microsomes (**B**). Mouse liver microsomes and Arabidopsis leaf microsomes were digested with Lys-C and trypsin and free peptides were analysed by LC-MS/MS. Identified proteins were ranked by their spectral intensity (MS signal intensity) and plotted against their MS signal intensity (log2). List of CYP450s found in the global proteomic analysis is on the right. The abundance ranking number reflects the abundance of CYP450s in the microsomal proteome ranked on their spectral intensities (MS intensity (log2)).

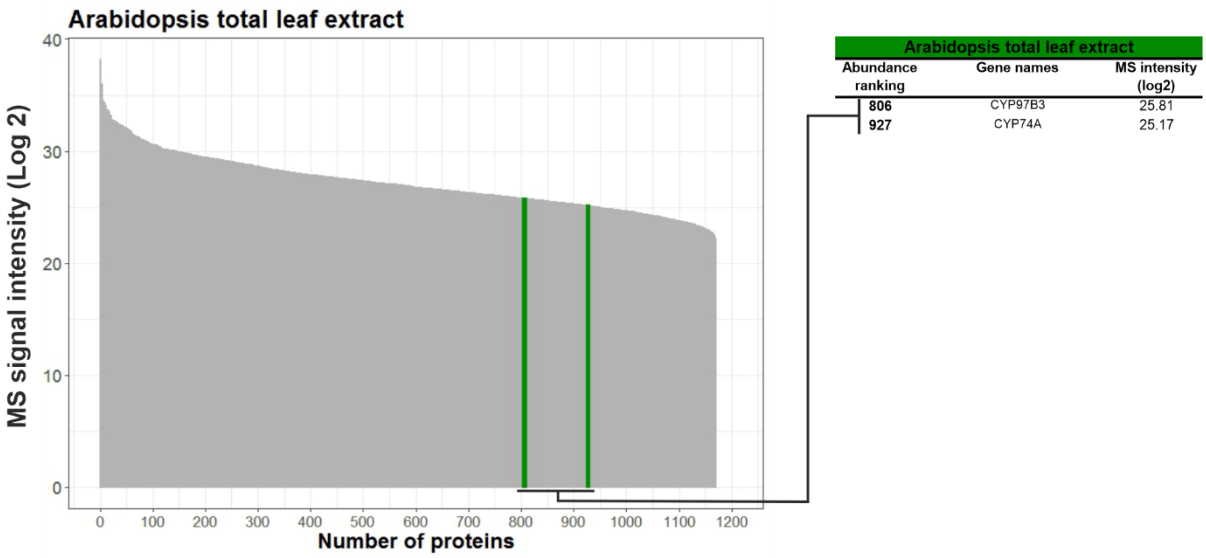


Figure 6. Cytochrome P450s are barely detected in total leaf extract of Arabidopsis. Representation of the Arabidopsis proteins detected in the global proteomic analysis of total leaf extract. Arabidopsis leaf extract was digested with Lys-C and trypsin and free peptides were analysed by LC-MS/MS. On the left, identified proteins were ranked by their spectral intensity (MS signal intensity) and plotted against their MS signal intensity (log2). On the right, list of CYP450s found in the global proteomic analysis of Arabidopsis total leaf extract. The abundance ranking number reflects the abundance of CYP450s in the microsomal proteome ranked on their spectral intensities (MS signal intensity (log2)).

MS analysis is insufficient to detect CYP450 labelling in Arabidopsis leaf microsomes

We next evaluated CYP450 labelling of mouse liver microsomes and Arabidopsis leaf microsomes by performing pull-downs of labelled proteins. We performed a quick test of DB096 pull-down using one labelling replicate for each microsome sample. DB096-labelled proteins were coupled to a biotin-azide affinity tag, purified on streptavidin beads and on-bead digested with Lys-C and trypsin. A total of 40 CYP450s were enriched from mouse liver extracts in the DB096 labelled sample, in the presence of NADPH (Figure 7B). Although we could not calculate the significance of these enrichment due to the lack of replicates, this experiment allowed us to identify Cyp2c29 and Cyp1a2 as top mouse CYP450 candidates labelled by DB096. In contrast, no CYP450s were detected in the DB096 labelled sample from Arabidopsis leaf microsomes (Figure 7C). The majority of the proteins detected in the pull-down were unchanged between the DB096 and CC and included endogenously biotinylated proteins such as MCCA as well as abundant photosynthetic proteins such as RBCL and RBSC-1A (Figure 7C, top signals)

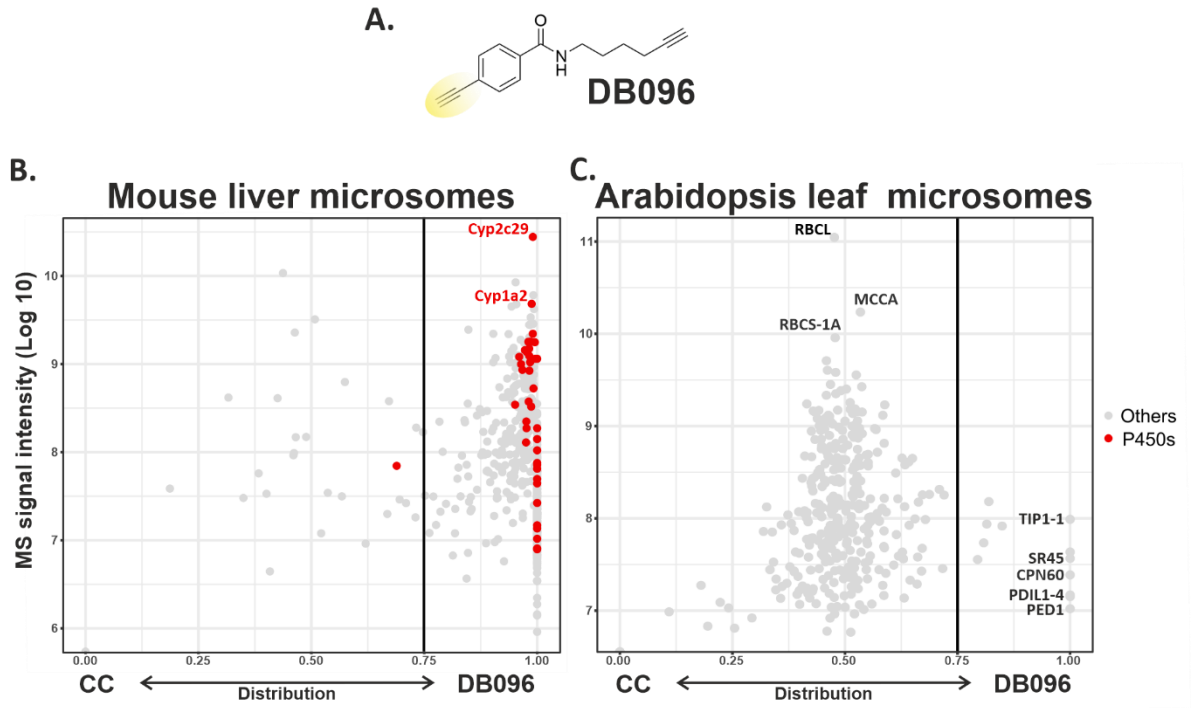


Figure 7. NADPH-dependent labelling of CYP450s by DB096 in mouse liver microsomes and Arabidopsis leaf microsomes. **A**, Chemical structure of DB096 containing an aryl-alkyne reactive group (yellow) and an alkyne tag (right) used to couple the probe to a biotin affinity tag via click chemistry. **B**, NADPH-dependent labelling of CYP450s in mouse liver microsomes by DB096. **C**, NADPH-dependent labelling of CYP450s in Arabidopsis leaf microsomes by DB096. Distribution of the LC-MS/MS spectral intensity values (MS signal intensity) of the identified proteins against the ratio of the probe enriched sample. Enrichment was calculated as the ratio between the spectral intensities of the DB096 enriched sample divided by sum of DB096 and Click Control (DB096/ [DB096+CC]). Mouse liver microsomes were incubated with 30 μM probe or an equal volume of DMSO in the presence of NADPH. In red: all CYP450s detected in the probe and control samples. Red dots > 0.75 in the DB096 ratio are CYP450s considered to be enriched in the probe sample.

Two-step labelling of active enzymes has some limitations due to the partial inefficiency of the chemical reaction. Also, in this case, the presence of NADPH may activate a CYP450 able to oxidase the alkyne mini tag, thereby hampering the purification of labelled proteins. We therefore synthesised a biotinylated probe based on DB096, JB001. JB001 was made by coupling of DB096 to an azide-biotin, resulting in a mix of two possible probes structures (Figure 8A). In mouse liver microsomes, a total of 24 CYP450s were enriched in the JB001 sample in a NADPH-dependent manner (Figure 8B). Cyp2c29 and Cyp1a2 were also identified as top targets of JB001. However, after performing labelling of Arabidopsis leaf microsomes with JB001 no CYP450s were enriched in the probe containing samples (Figure 8C).

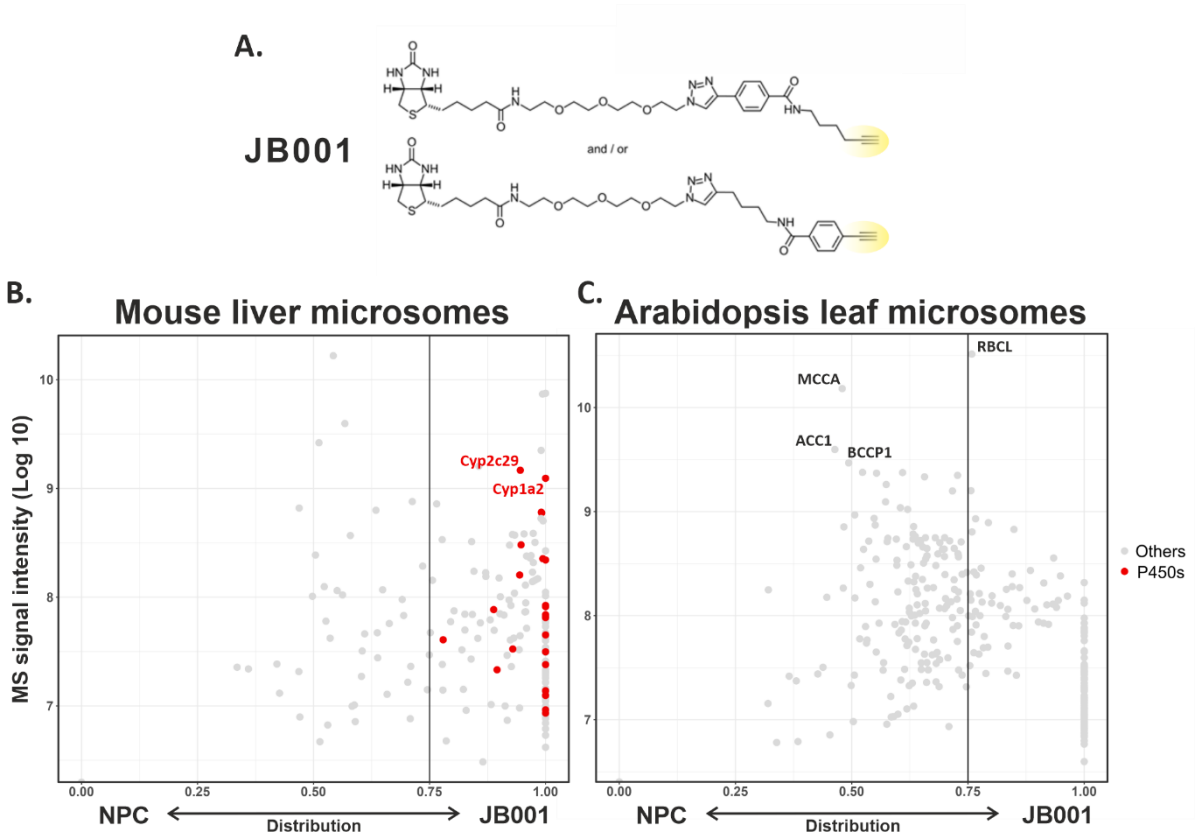


Figure 8. NADPH-dependent labelling of CYP450s by JB001 in mouse liver and Arabidopsis leaf microsomes. **A**, Chemical structure of JB001, a mix of two CYP450 chemical probes. JB001 contains alkyne-based reactive group (yellow) and a biotin tag (left). **B**, NADPH-dependent labelling of CYP450s in mouse liver and Arabidopsis leaf microsomes by JB001. **C**, NADPH-dependent labelling of CYP450s in Arabidopsis leaf microsomes by JB001. Distribution of the LC-MS/MS spectral intensity values (MS signal intensity) of the identified proteins against the ratio of the probe enriched sample. Enrichment was calculated as the ratio between the spectral intensities of the JB001 enriched sample divided by sum of JB001 and No Probe Control (JB001/ [JB001+NPC]). Microsomes were incubated with 30 μM probe or an equal volume of DMSO in the presence of NADPH. In red: all CYP450s detected in the probe and DMSO samples. Red dots > 0.75 in the JB001 ratio are P450s considered to be enriched in the probe sample.

CYP450 probes label transiently expressed mouse cytochrome P450s in NADPH-dependent manner, but not Arabidopsis cytochrome P450s

We first wanted to know whether *in planta* expression of mouse CYP450s was a compatible system for the overexpression and labelling of CYP450s. We cloned and expressed two of the mouse CYP450s, Cyp1a2 and Cyp2c29, identified as top targets of 2-ethynylnaphthalene (2EN)-ABP probe (Wright and Cravatt, 2007) and found be enriched in the MS proteomic pull-down of DB096 and JB001 in mouse liver microsomes (Figure 7 and 8). Cyp1a2 and Cyp2c29 coding sequence were synthesised with optimised codons for *in planta* expression. CYP450s were cloned into a golden gate binary vector (pJK268c) such that they were fused C-terminally to His tag to ensure their detection by western blotting. CYP450s carried their endogenous signal peptide and the coding sequence was flanked by a 35S promoter and terminator and the T-DNA also encodes the silencing suppressor P19.

We tested CYP450 probes with microsomal fractions from agroinfiltrated *N. benthamiana* leaves isolated at four days post infiltration (dpi). Microsomes were incubated with 5 μM of probe with or without NADPH for an hour. Labelled proteins were coupled to a fluorophore and detected as described before. Firstly, we tested three CYP450 probes in the His-tagged overexpressed mouse Cyp1a2 and Cyp2c29 constructs. While Cyp1a2 was robustly labelled in an NADPH-dependent manner with DB080, DB086 and DB088, Cyp2c29 only just showed a clear NADPH-dependent labelling with DB086 (Figure 9A, arrow). However, in both cases we detected a strong background signal at around 55 kDa that did not allow us to clearly distinguish CYP450 labelling (Figure 9A, asterisk). Therefore, we decided to C-terminally tag Cyp1a2 to GFP (27 kDa) to shift the CYP450 signals above the rubisco background signal and detect its accumulation using anti-GFP western blot. Cyp1a2-GFP was robustly labelled in and NADPH-dependent manner with DB080, DB086, DB088 and DB096 (Figure 9B, arrow). DB088 labelled Cyp1a2 more strongly, followed by DB086 and DB096 with the second greatest signal intensity. As a consequence of the GFP fusion, Cyp1a2-GFP was detected at a molecular weight between 70 and 100 kDa, instead of the 55 kDa observed before.

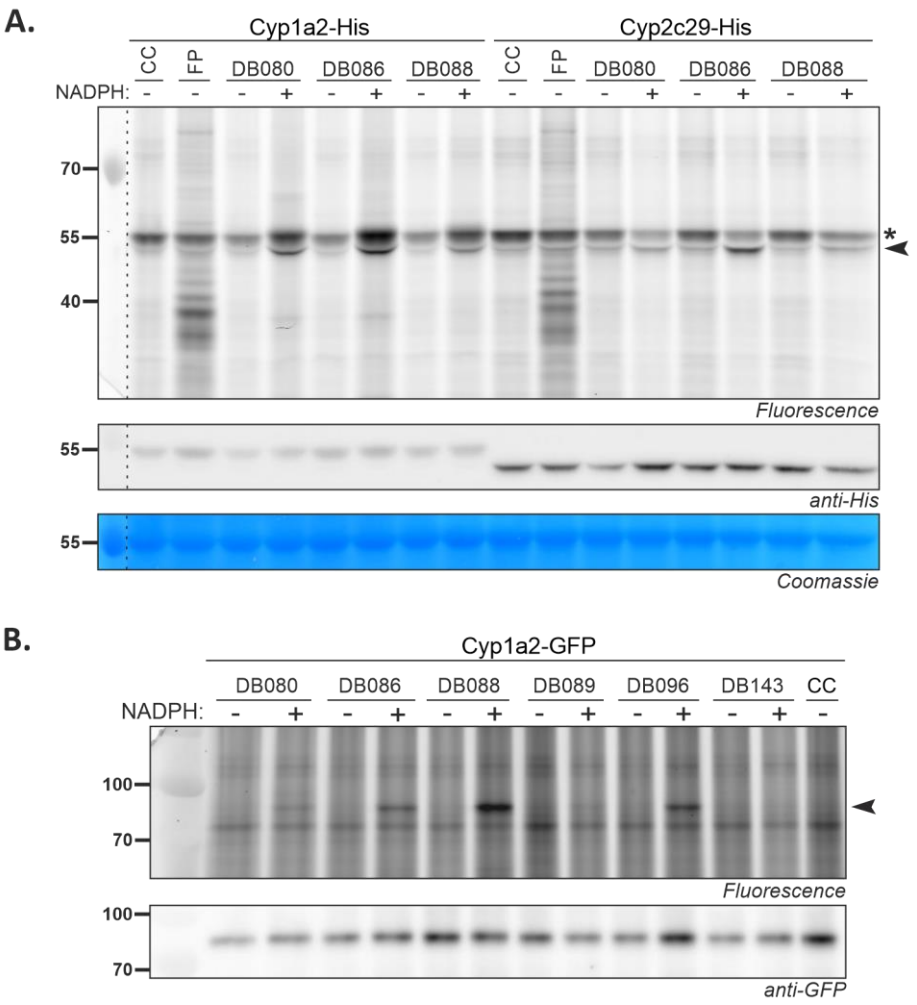


Figure 9. Labelling of transiently expressed mouse Cyp1a2 and Cyp2c29 in *N. benthamiana* microsomes. **A**, Labelling of His-tagged mouse Cyp1a2 and Cyp2c29. **B**, Labelling of GFP-tagged Cyp1a2. Agroinfiltrated *N. benthamiana* leaf microsomes were isolated via ultracentrifugation and resuspended microsomes were labelled with 5 μM probe concentration in the absence or presence of NADPH. Labelled proteins were coupled to picolyl-azide fluorophore via click chemistry and visualised by in-gel fluorescence scanning. Anti-GFP western blot is shown as protein expression and loading control. Coomassie staining is shown as loading control. Similar results were obtained in another independent replicate.

Given the low presence and abundance of CYP450 in Arabidopsis leaf microsomes, we used *Agrobacterium tumefaciens*-mediated transient transformations (agroinfiltrations) to increase the amount of CYP450s in plant tissue. We selected four Arabidopsis CYP450 candidates: CYP73A5 and CYP79F1, which are both detected in the global proteomic analysis of Arabidopsis leaf microsomes; and CYP81D8 and CYP82C2, which have herbicide metabolising activities according to the literature (Das *et al.*, 2010; Rajniak *et al.*, 2015; Skipsey *et al.*, 2011).

The four selected Arabidopsis CYP450 candidates were amplified from Arabidopsis cDNA. As before, Arabidopsis CYP450s were cloned into a golden gate binary vector (pJK268c) such that they were fused C-terminally to GFP to ensure detection using anti-GFP antibodies and shift the CYP450 signals above the background rubisco signal. Arabidopsis CYP450s carried their endogenous signal peptide and the

coding sequence was flanked by a 35S promoter and terminator and the T-DNA also encodes the silencing suppressor P19.

To continue, we used two of the best probes for the labelling of overexpressed Arabidopsis CYP450s. Consistent with previous results, Cyp1a2-GFP was successfully labelled in a NADPH-dependent manner when transiently expressed *in planta*. However, no NADPH-dependent labelling of Arabidopsis CYP450s was detected. We detected weak signals at the expected molecular weight, but they were also present in the click chemistry control and were not NADPH-dependent (Figure 10, arrow). We could confirm expression of all proteins by anti-GFP western blot at the predicted 85 kDa.

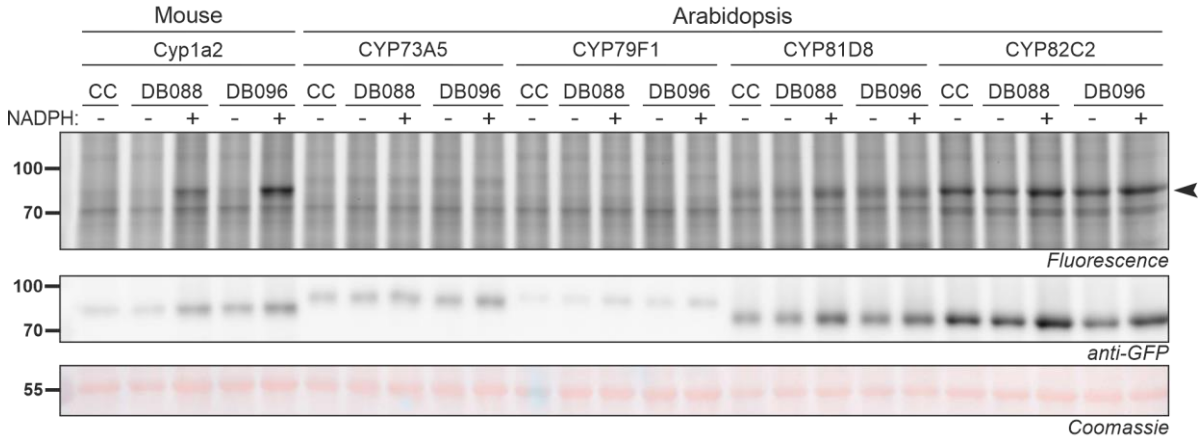


Figure 10. Labelling of transiently expressed mouse Cyp1a2 but not Arabidopsis CYP450s. NADPH-dependent labelling of transiently expressed CYP450s from mouse and Arabidopsis. Agroinfiltrated *N. benthamiana* leaf microsomes were isolated via ultracentrifugation and resuspended microsomes were labelled with 5 μM probe concentration in the absence or presence of NADPH. Labelled proteins were coupled to picolyl-azide fluorophore via click chemistry and visualised by in-gel fluorescence scanning. Anti-GFP western blot is shown as protein expression and loading control. Coomassie staining is shown as loading control. Similar results were obtained in two more experimental replicates.

To confirm the importance of microsome isolation for the labelling, we overexpressed CYP450s in *N. benthamiana* and extracted them in total leaf extract or by microsomal isolation. We detected a strong labelling signal of Cyp1a2 labelling in microsomes but not in total extract from agroinfiltrated *N. benthamiana* leaves (Figure 11, Fluorescence). As expected, a more enriched isolation of all expressed CYP450s in microsomes samples in comparison to total extract samples was detected by anti-GFP western blot, indicating the successful enrichment of CYP450s by ultra-centrifugation (Figure 11, anti-GFP). As observed before, Arabidopsis CYP450s were properly expressed in *N. benthamiana* microsomes but we could not detect NADPH-dependent labelling by DB096 in extracts. Surprisingly, we observed an overall intense fluorescence signal in the microsomes samples in comparison to the total extract samples, suggesting that plant microsomes cause a higher click chemistry background.

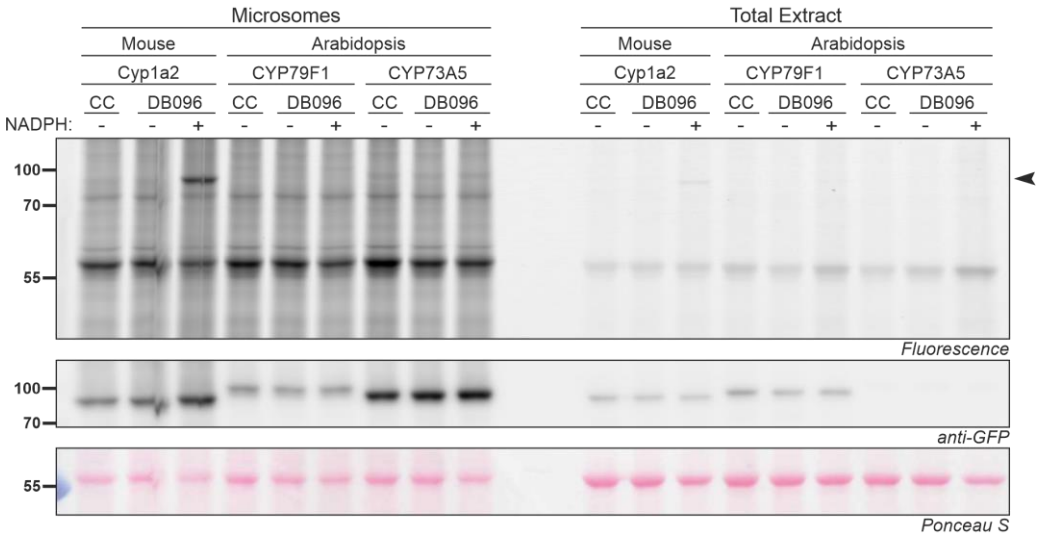


Figure 11. Microsomal fraction isolation is crucial for the labelling of transiently expressed CYP450s. NADPH-dependent labelling of transiently expressed CYP450s from mouse and Arabidopsis. Agroinfiltrated *N. benthamiana* leaf microsomes were isolated via ultracentrifugation and resuspended microsomes were labelled with 5 μM DB096 in the absence or presence of NADPH. Labelled proteins were coupled to picolyl-azide fluorophore via click chemistry and visualised by in-gel fluorescence scanning. Anti-GFP western blot is shown as protein expression and loading control. Ponceau staining (Ponceau S) is shown as loading control. Similar results were obtained in another biological replicate.

Maize CYP81A9 is targeted by several CYP450 chemical probes

To test if the probes can inhibit a plant CYP450, we tested CYP450 81A9 (CYP81A9), which is an important herbicide-metabolising enzyme responsible for the modification of several herbicides with unrelated modes of action (Li *et al.*, 2013; Liu *et al.*, 2019; Pataky *et al.*, 2008). CYP81A9 was produced in yeast (WAT11 *S. cerevisiae* strain) and CYP81A9 microsomes were isolated via ultracentrifugation. To detect CYP81A9 activity, enzymatic conversion of the herbicide bentazon to its hydroxylated product hydroxybentazon was analysed via liquid chromatography-mass spectrometry (LC-MS). CYP81A9 microsomes hydroxylated bentazon effectively in a NADPH-dependent manner (Figure 12B).

Having established this CYP81A9 activity assay, we next tested if the probes can inhibit this activity. 1-Aminobenzotriazole (1-ABT) is a well-known mechanism-based inhibitor of CYP450s and was included as a positive control for inhibition (Montellano, 2018). HPLC analysis revealed that at 300 μM, all CYP450 probes could inhibit the activity of CYP81A9 (Figure 12B). Similarly, we studied the activity of a different maize CYP450 also involved in herbicide-detoxification, CYP81A2, and observed a lower, but still considerable, inhibition of maize CYP81A2 by CYP450 probes (Figure 12C).

To confirm that CYP450 probes label maize CYP81A9 in an activity-dependent manner, we transiently overexpressed GFP-tagged CYP81A9 in *N. benthamiana*. Microsomal fractions from agroinfiltrated *N. benthamiana* leaves were isolated and incubated with 5 μM of all six CYP450 probes in the presence or

absence of NADPH for an hour. Labelled proteins were processed and detected as described in Figure 2. CYP81A9 was robustly labelled with DB088 and less well with the other probes (Figure 12D).

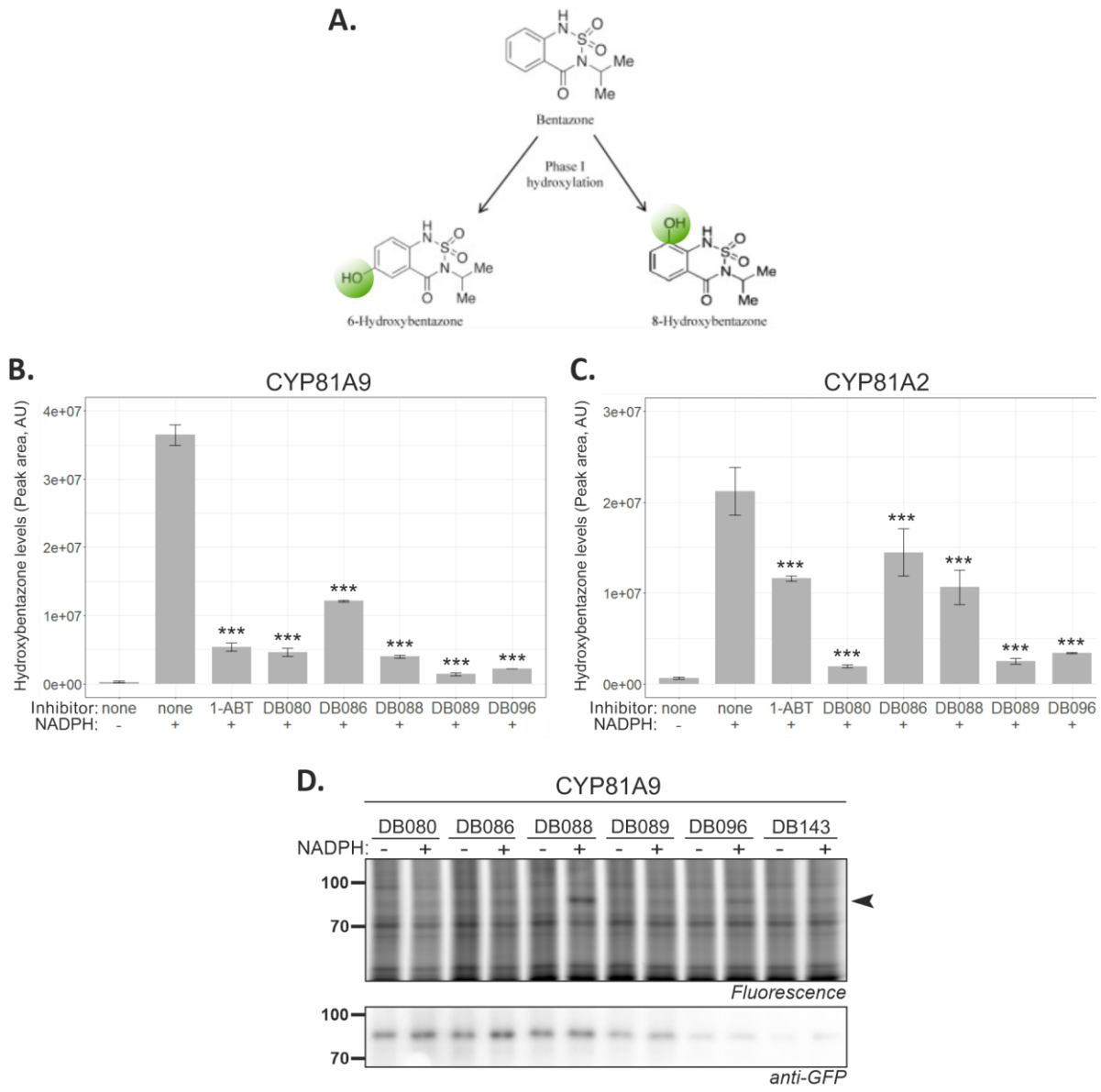


Figure 12. Maize CYP81A9 and CYP81A2 are targeted by CYP450 probes. A, Chemical structure of bentazon and its two known hydroxylated forms (modified from Cho *et al.*, 2017). CYP450 probes inhibit bentazon hydroxylation by CYP81A9 (**B**) and CYP81A2 (**C).** CYP81A9 and CYP81A2 microsomes isolated from *S. cerevisiae* (WAT11 strain) were incubated with 300 μM inhibitor probes plus 1 mM NADPH before the incubation of the microsomes with bentazon. Metabolites were extracted with acetonitrile and analysed via LC-MS. Data is expressed in amount of hydroxylated bentazon detected (Peak area, AU) in the incubated microsomes. Represented are the means of three replicates ± S.D. Inhibition P values were calculated when compared to the none + control (***, P < 0.001). **D**, NADPH-dependent labelling of transiently expressed maize CYP81A9. Agroinfiltrated *N. benthamiana* leaf microsomes were isolated via ultracentrifugation and resuspended microsomes were labelled with 5 μM probe concentration in the absence or presence of NADPH. Labelled proteins were coupled to picolyl-azide fluorophore via click chemistry and visualised by in-gel fluorescence scanning. Anti-GFP western blot is shown as protein expression and loading control. This experiment was performed another time with similar results.

To confirm that CYP81A9 is labelled in an activity-based manner, we substituted the catalytic cysteine (C) into alanine (C457A) or serine (C457S) and tested for labelling with DB086, DB088 and DB096. In both C457A and C457S mutants, the 85 kDa signal was absent upon labelling with DB086, DB088, and DB096. However, both C457 mutants accumulated less compared to wild-type CYP81A9, suggesting that the C457A and C457S mutants are unstable in agroinfiltrated tissues (Figure 13B).

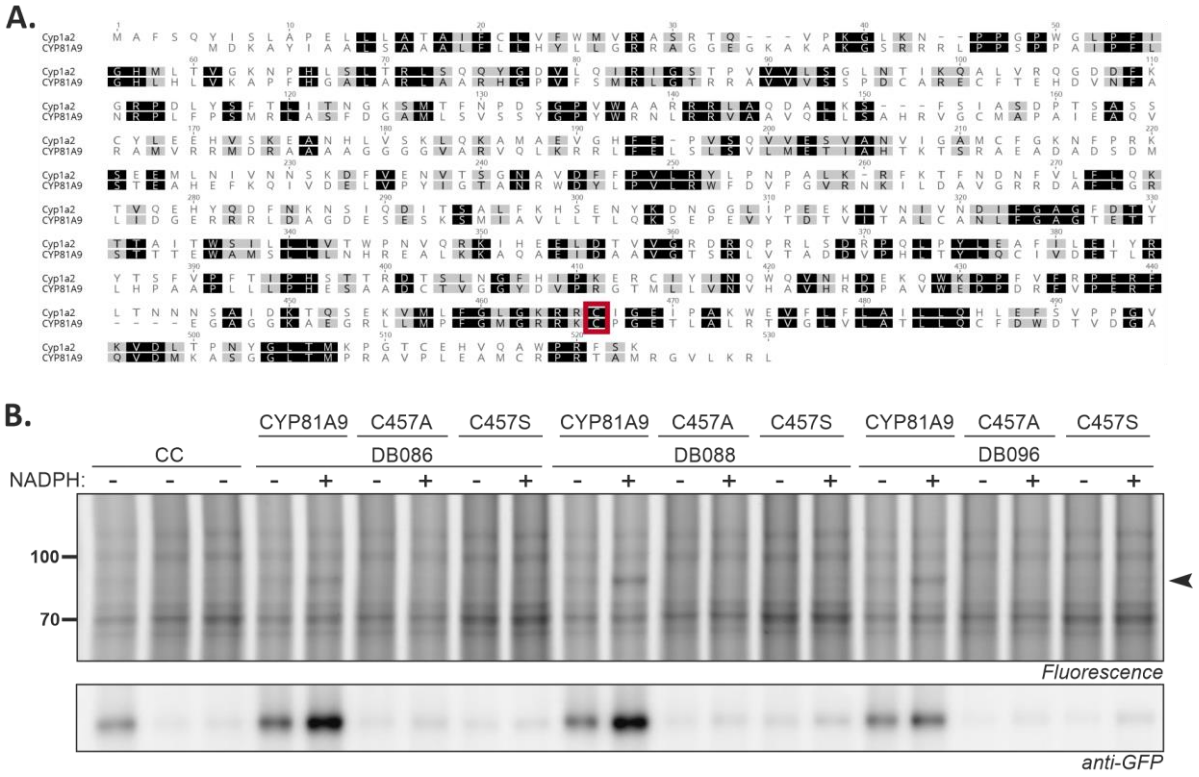


Figure 13. CYP81A9 labelling might be dependent on the conserved cysteine in its catalytic centre. **A**, Alignment of mouse Cyp1a2 and CYP81A9. Identical residues are shaded in black, similar residues are shaded in grey. The cysteine in the catalytic centre of P450s is marked with a red box. **B**, NADPH-dependent labelling of transiently expressed maize CYP81A9, CYP81A9^{C457A} and CYP81A9^{C457S}. Agroinfiltrated *N. benthamiana* leaf microsomes were isolated prepared and labelled as described in section B. Similar results were obtained from repetition experiments.

Labelling of CYP81A9 and several *N. benthamiana* CYP450s can be detected by mass spectrometry CYP450 labelling pull-downs

We next confirmed CYP81A9 labelling by performing pull-downs of labelled proteins. Due to the low abundance of CYP450s in plants, we specifically synthesised a biotinylated probe based on DB096, called DB569 (Figure 14A). DB569 is a one-step labelling probe by which we can directly enrich probe targets by streptavidin pull-downs, without the need of performing a click chemistry reaction; contrarily to DB096, which needs a second step for biotin attachment via click chemistry.

We compared the biotinylation of DB569 with two click chemistry probes, DB096 and DB088, which from previous results are known to label CYP81A9. The alkyne-labelled proteins were biotinylated with azide-biotin via click chemistry. Strikingly, when labelling CYP81A9 overexpressing *N. benthamiana* microsomes we observed a clear biotinylation of CYP81A9 by DB096 and DB088, but not by DB569 (Figure 14B, arrow). As a control, we confirmed the presence of CYP81A9 at the predicted molecular weight by anti-GFP western blot (Figure 14B, anti-GFP). Interestingly, we observed a labelling signal at around 55 kDa on DB569 labelling in comparison to its no probe control (NPC) (Figure 14B, asterisk). However, we could not observe a similar 55 kDa labelling signal for DB096 and DB088 due to the high rubisco background, also present in the click control (CC) labelling sample.

We next wanted to confirm these results by LC-MS/MS analysis of purified biotinylated proteins. When using DB569, we detected an enrichment of four *N. benthamiana* CYP450s, including two 98A2-like, an 71A1-like and an 83F1-like CYP450s (Figure 14C, green diamonds). Consistent with the previous blot results, the overexpressed CYP81A9 was found among the four detected but not enriched CYP450s (Figure 14C, grey diamonds). The 152 enriched proteins included two protein disulfide isomerase-like proteins and a xylose isomerase-like (Figure 14C, $\log_2 FC > 4$), which have a molecular weight of approximately 55 kDa (Table S1).

When labelling with DB096, we detected the enrichment of the same four *N. benthamiana* CYP450s, together with the maize CYP81A9 and an NADPH-CYP450 reductase (Figure 14D). In this case, a total of 20 proteins were enriched by DB096 labelling, including the same xylose isomerase and CYP81A9 being the main enriched CYP450 (Table S2).

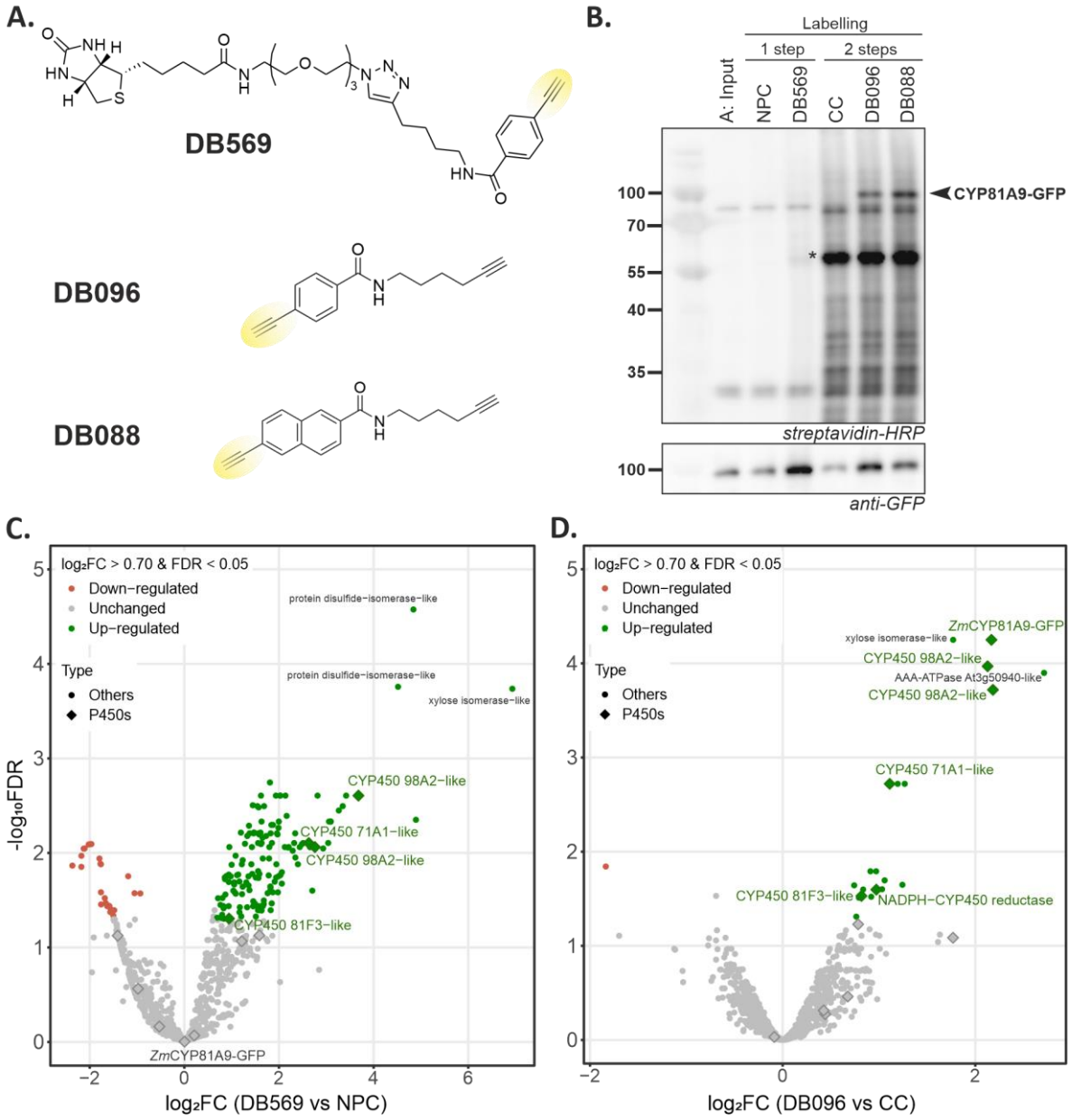


Figure 14. Mass spectrometry confirms the targeting of CYP81A9 and *N. benthamiana* CYP450s by CYP450activity-based probes. **A**, Chemical structures of DB569, DB096 and DB088. **B**, Labelling comparison of one step, DB569, and two steps, DB096 and DB088, CYP450 labelling by protein blot. NPC corresponds to the no probe control of DB569. CC corresponds to the click chemistry control of DB096. **C and D**, Volcano plots highlighting proteins depleted and enriched by DB569 and DB096 labelling of CYP81A9 overexpressing *N. benthamiana* microsomes. Microsomes were incubated with 5 μM of DB569 and DB096, or an equal volume of DMSO, in the presence of 1 mM NADPH. DB096-labelled proteins were subjected to click chemistry for biotin attachment and, DB569-labelled and DB096-labelled proteins were enriched via streptavidin pull-down, enzymatically digested and subjected to LC-MS/MS analysis. Enrichment is represented by volcano plots where the $\log_2$FC (CYP450 probe/control) against the significance ($-\log_{10}$FDR) between the control and each CYP450 probe, DB569 or DB096, using four or three independent biological replicates, respectively. The colour of the dots means whether proteins (dots) were enriched (green), unchanged (grey) or depleted (red) in the CYP450 probe containing sample.

Similar results were obtained when performing CYP450 labelling by DB088 in microsomes isolated from CYP81A9-overexpressing leaves (Figure 15). In this case the maize CYP81A9 was also found as the top CYP450 enriched, followed by the same two CYP450 98A2-like, all detected with a log_2FC of around 2. Among the 98 enriched proteins, we also detected the previous enriched CYP450 71A1-like, CYP450 81F3-like and a NADPH-CYP450 reductase, together with a CYP450 71A15-like and another NADPH-CYP450 reductase (Table S3).

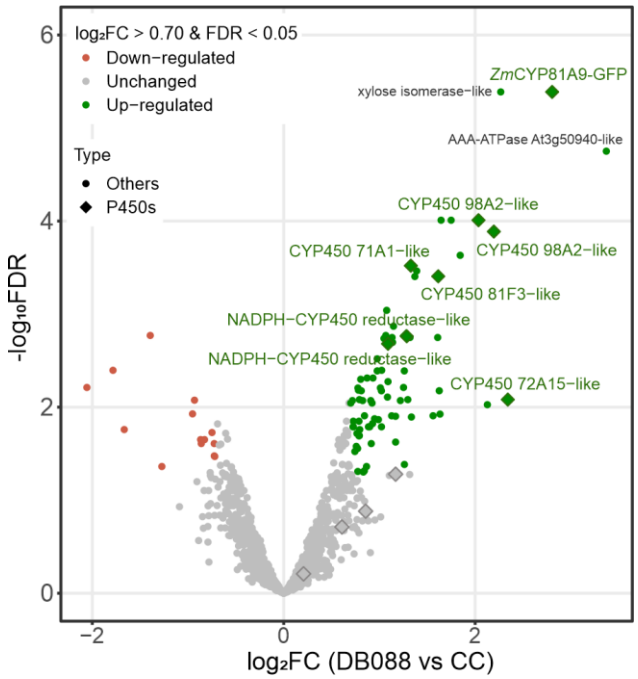


Figure 15. DB088 also labels CYP81A9 and *N. benthamiana* CYP450s. Volcano plot highlighting proteins depleted and enriched by DB088 labelling of CYP81A9 overexpressing *N. benthamiana* microsomes. Microsomes were incubated with 5 μM DB088, or an equal volume of DMSO, in the presence of 1 mM NADPH. DB088-labelled proteins were subjected to click chemistry for biotin attachment, enriched via streptavidin pull-down, enzymatically digested and subjected to LC-MS/MS analysis. Enrichment is represented by volcano plots where the log_2FC (DB088/CC) against the significance ($-log_{10}FDR$) between the control and DB088, using three independent biological replicates. The colour of the dots means whether proteins (dots) were enriched (green), unchanged (grey) or depleted (red) in the CYP450 probe containing sample.

To further compare the labelling differences between DB569 and its click chemistry derivative DB096, we performed labelling of mouse liver microsomes. Although DB569 and DB096 probes caused labelling of proteins at around 55 kDa, the signal intensity was much stronger with DB096 (Figure 16). In this experiment, we also observed the striking differences between the controls. As observed for the labelling of *N. benthamiana* microsomes, just a few bands of endogenous biotinylated proteins are detected in the no probe control (NPC). However, when performing biotin attachment with click chemistry, we observed a prominent background in the click control (CC) sample.

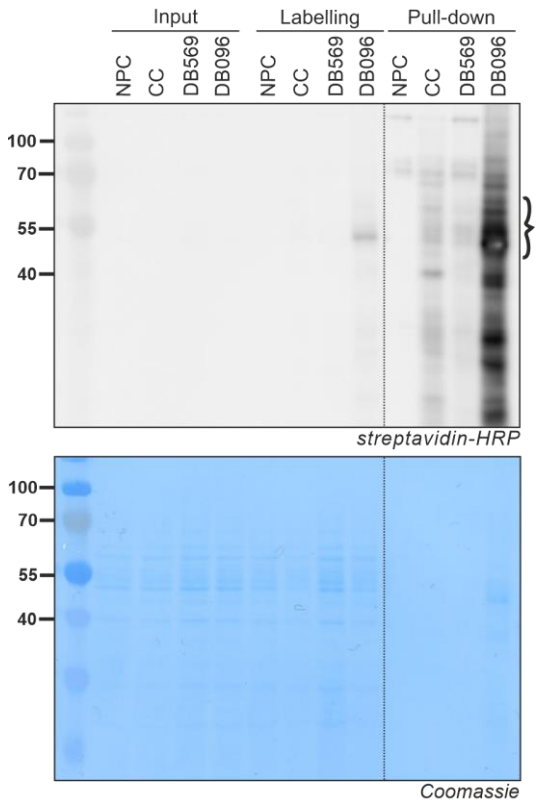
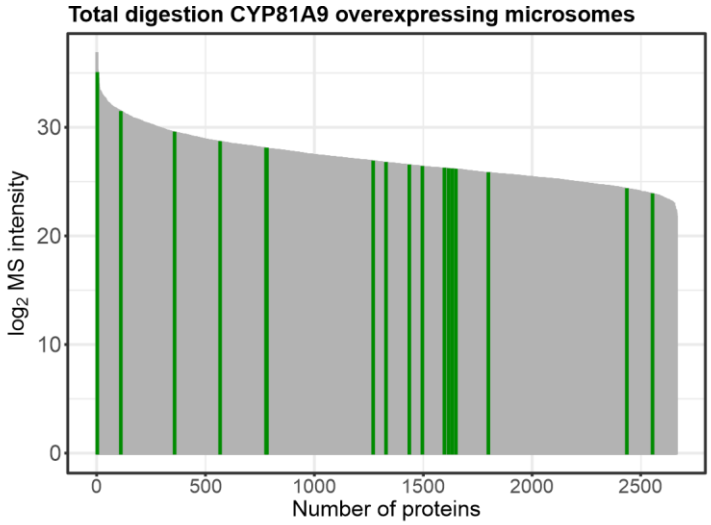


Figure 16. Differences in labelling by DB569 and DB096 probes in mouse liver microsomes. Labelling comparison of one step, DB569, and two steps, DB096, CYP450 labelling by western blot. Mouse liver microsomes were incubated with 5 μM of DB569 and DB096, or an equal volume of DMSO, in the presence of 1 mM NADPH. DB096-labelled proteins were subjected to click chemistry for biotin attachment and biotinylated proteins were purified via streptavidin pull-down. NPC corresponds to the no probe control of DB569. CC corresponds to the click chemistry control of DB096. Enriched proteins (Pull-down) together with the input samples (Input) and the labelling check before pull-down (Labelling) were loaded in an SDS-PAGE gel and visualised by streptavidin-HRP protein blot. Coomassie staining is shown as protein abundance control.

Most abundant CYP450 in CYP81A9 overexpressing *N. benthamiana* microsomes correlate to the main labelled CYP450s

Lastly, we wanted to investigate whether the CYP450s we found enriched in our chemical proteomic analyses corresponded with the most abundant CYP450s in CYP81A9-overexpressing *N. benthamiana* microsomes. We therefore performed a MS-based global proteomic analysis of microsomes isolated from CYP81A9-overexpressing plants. A total of 15 CYP450s and two NADPH-CYP450 reductases were detected in the total microsomal fraction, which consisted of a total of 2662 proteins (Figure 17). The overexpressed maize CYP81A9 was detected as the third most abundant protein in the microsomal fraction. The other CYP450s detected were from *N. benthamiana* and were distributed all along the proteome, finding a total of three *Nb*CYP450s (81F3-like, 72A15-like and 71A1-like) among the top 25% most abundant proteins. Interestingly, all the CYP450s significantly enriched by CYP450 probes were found within the most abundant CYP450 detected in the global proteomic analysis. DB569, however, seems to label only a subset of the abundant CYP450s.



CYP450s abundance in *N. benthamiana* microsomes overexpressing CYP81A9

Abundance ranking	Majority protein IDs	Fasta headers	MS intensity (log2)	DB569	DB096	DB088
3	Zm00001d013230	Zm_CYP81A9|C-term GFP tag	34.95		**2**	**1**
111	NbD039121.1	cytochrome P450 81F3-like (XP_016503274.1)	31.37	**4**	**5**	**5**
358	NbD049629.1	cytochrome P450 72A15-like (XP_016491347.1)	29.47			**2**
567	NbE03057724.1	cytochrome P450 71A1-like (XP_016505274.1)	28.60	**3**	**4**	**6**
778	NbD021663.1	NADPH--cytochrome P450 reductase (XP_009786522.1)	27.99			
782	NbD000964.1	cytochrome P450 98A2-like (XP_019261854.1)	27.99	**2**	**1**	**3**
1270	NbE05063946.1; NbD045366.1	NADPH--cytochrome P450 reductase-like (XP_019252798.1, XP_009786522.1)	26.81			
1329	NbE05065515.1	cytochrome P450 98A2-like (XP_019241025.1)	26.68	**1**	**3**	**4**
1436	NbD041770.1	cytochrome P450 84A1-like (XP_019239417.1)	26.44			
1496	NbD007620.1	cytochrome P450 CYP736A12-like (XP_009615258.1)	26.31			
1597	NbD047028.1	cytochrome P450 CYP72A219-like (XP_016476160.1)	26.15			
1616	NbD024028.1	NADPH--cytochrome P450 reductase (XP_009786522.1)	26.11			
1633	NbD047029.1	cytochrome P450 CYP72A219-like (XP_019265382.1)	26.08			
1650	NbE05066496.1; NbD012321.1; NbE44071443.1	cytochrome P450 97B2, chloroplastic isoform (XP_009784850.1, XP_009784851.1, XP_016484256.1)	26.05			
1799	NbD050055.1; NbE44074016.1; NbD043035.1	cytochrome P450 89A2-like (XP_019234830.1, XP_016510483.1, XP_016510483.1)	25.74			
2435	NbD034063.1	cytochrome P450 77A1-like (XP_019228509.1)	24.26			
2553	NbD023242.1; NbE44070573.1	cytochrome P450 76A1-like (XP_019250803.1, XP_019250803.1)	23.79			

Figure 17. CYP450 activity-based probe mainly label top abundant CYP450s in CYP81A9-overexpressing *N. benthamiana* microsomes. CYP81A9-overexpressing *N. benthamiana* microsomes were digested with Lys-C and trypsin and digested peptides were analysed by LC-MS/MS. All proteins identified were ranked by their mass spectrometry (MS) signal intensity and plotted against the $\log_2$ MS intensity. The list of all CYP450s detected and ranked is showed as a table. DB569, DB096 and DB088 columns show the CYP450s ranked by $\log_2$FC (dark grey) and NADPH-CYP450 reductases (light grey) significantly enriched in the proteomic pull-down presented on Figure 14 and Figure 15. The abundance ranking number reflects the abundance of CYP450s in the microsomal proteome ranked on their spectral intensities (MS signal intensity).

Discussion

In this chapter, the application of activity-based protein profiling to study plant CYP450s was demonstrated. Click chemistry CYP450 probes were find to label several *N. benthamiana* CYP450s and the herbicide-detoxifying CYP81A9, but not Arabidopsis CYP450s. Furthermore, the importance of microsomal fraction isolation for the enrichment and labelling of CYP450s and the recognised differences in CYP450 labelling by click chemistry and biotinylated probes were identified.

Importance of microsomal isolation when labelling endogenous and overexpressed CYP450s

Microsomes isolation is typically used to study eukaryotic CYP450 activities as they are membrane bound proteins. We showed the importance of microsomal isolation for the enrichment and labelling of endogenous and overexpressed CYP450s. Firstly, we increased the detection from two CYP450s in total leaf extracts to 17 CYP450s in microsomal fractions (Figure 5 and 6). CYP74A, for example, was detected with a $\log_2$ MS intensity of 25.17 in total leaf extracts and a $\log_2$ MS intensity of 30.39 in leaf microsomes. Secondly, fluorescent labelling of Cyp1a2 was much stronger when using leaf microsomes than total leaf extract, indicating the relevance of microsomes isolation for the labelling of endogenous and overexpressed CYP450s.

Transiently expression of CYP450s using *N. benthamiana* plants

We successfully used the *Agrobacterium- N. benthamiana* overexpression system to overexpress and label animal and plant CYP450s. This is remarkable because all eukaryotic CYP450s require a reductase partner for electron supply (Hannemann *et al.*, 2007; Hrycay and Bandiera, 2015). Although each organism has its own reductases, we conclude that mouse Cyp1a2 and Cyp2c29, and maize CYP81A9 can successfully interact with the endogenous NADPH-CYP450 reductases from *N. benthamiana* to activate the CYP450 probes. From previous studies of fungal and mammalian CYP450s, it is known that CYP450 catalytic efficiency and specificity depends on the partner reductase (Agrawal *et al.*, 2010; Durairaj *et al.*, 2016). Future experiments should aim to target the two main *N. benthamiana* NADPH-CYP450 reductases (XP_009786522.1 and XP_019252798.1) identified by MS-based global proteomic analysis (Figure 17) and silence their expression by virus-induced gene silencing (VIGS), to confirm their role in CYP450 activity. Furthermore, it will be interesting to co-express CYP450s with their natural reductase and check whether they have similar probe specificity than when interacting with the endogenous *N. benthamiana* reductase.

When comparing the labelling of overexpressed CYP450s in microsomes and total extract samples, we observed a much higher click chemistry background when labelling CYP450s using microsomes (Figure 11). Furthermore, the high abundance of rubisco in the microsomal fraction caused high click chemistry fluorescent background signal at around 55 kDa in all plant leaf extracts (Figure 2B and 9A),

pointing to the limitation of two step labelling of CYP450 in plant tissues as the majority of plant CYP450s also have a molecular weight between 50-62 kDa. In order to reduce the click chemistry background, we observed that Arabidopsis and maize cell culture had much less background labelling in fluorescence gels at 55 kDa (Figure 3). Therefore, the use of plant cell cultures or etiolated plant tissue is a great alternative to avoid the main rubisco background signal. However, the use of cell cultures instead of whole plants can not represent all active CYP450s that participate in plant physiology. Furthermore, this solution is not possible when using the *N. benthamiana* overexpression system. We therefore propose to reduce the click chemistry background by optimising the click chemistry protocol, either by testing reducing amounts of the click chemistry reagents used, substituting the copper-chelating agent TBTA for other alternatives or using a new generation of azide reporter tags named as 'Azide Plus Reagents' (https://clickchemistrytools.com/next-generation-azide-plus-reagents/). Meanwhile, we recommend the use of C-terminally GFP tag on CYP450s to shift them above the rubisco band in protein gels.

Labelling and abundance of plant CYP450s: Arabidopsis, maize and *N. benthamiana*.

We did not detect labelling of endogenous or overexpressed Arabidopsis CYP450s by fluorescence labelling nor mass spectrometry (Figure 2, 3, 7 and 8). First, we thought that the main reason for the lack of Arabidopsis CYP450 labelling was the low CYP450 concentrations found in Arabidopsis leaf microsomes. However, a low number of CYP450s were detected when we isolated microsomes from *N. benthamiana* plants, and we could indeed observe the labelling of *N. benthamiana* CYP450s by mass spectrometry analysis (Figure 14 and 15). Surprisingly, we observed that plant microsomes contain much less CYP450s and at a lower abundance in comparison to mouse liver microsomes, which explains the lack of fluorescent CYP450 labelling and carbon monoxide displacement spectrum in plant leaf microsomes (Figure 2, 3 and 4). But this is not the only reason, as we could also not detect the labelling of overexpressed Arabidopsis CYP73A5 and CYP79F1, which were detected with higher MS intensities than the majority of *N. benthamiana* CYP450s. This indicates that the lack of CYP450 labelling in Arabidopsis leaf microsomes is also due to the lack of reactivity to the probes. Overall, we attribute the lack of labelling of Arabidopsis CYP450s to a combination of: i) low CYP450 concentrations, ii) low CYP450 reactivity towards the probes, and iii) high click chemistry background.

The first evidence we obtained that the probes may target plant CYP450s was when we detected that CYP450 probes inhibit bentazon hydroxylation by maize CYP81A9 and CYP81A2 (Figure 12). We further confirmed that these probes label CYP81A9 by fluorescence and mass spectrometry (Figure 12, 13 and 14). We believe that the reason why all CYP450 probes inhibited bentazon hydroxylation by maize CYP81A9 but could not label it when visualised by in-gel fluorescence scanning could be due to

some non-specific inhibition caused by the high concentration of bentazone used in the inhibition assay. So far, we detected the activity-dependent labelling of CYP81A9 by *N. benthamiana* overexpression, but we could not detect fluorescent labelling of CYP450s in maize cell culture microsomes. This indicates that the low abundance of CYP450s is a limiting factor when using fluorescence as a read-out. Now that we know that CYP450 probes target at least one maize CYP450, it will be interesting to use CYP450-activity labelling to detect the activity of CYP450 in maize cell culture microsomes or etiolated maize seedlings. Firstly, it will be interesting to perform a global proteomic analysis to understand the number and abundance of CYP450 in maize microsomes. Secondly, mass spectrometry is the best read-out to detect labelled plant CYP450s.

We consistently detected the significant enrichment of several *N. benthamiana* CYP450s, in addition to overexpressed maize CYP81A9, including two CYP450 98A2-like, a CYP450 71A1-like, a CYP450 81F3-like and a CYP450 71A15-like (Figure 14 and 15). In order to validate *Nb*CYP450s as probe targets, it will be interesting to clone and overexpress these five top *N. benthamiana* CYP450 candidates as we did previously with the mouse and maize CYP450s. Furthermore, due to the nature of the pull-down protocol, we find the majority of the *Nb*CYP450s also in our no-probe samples; however, the presence of these CYP450s is still significantly higher in the probe containing samples. Although all five *Nb*CYP450s were enriched (Table S1, S2, S3), the pull-down protocol could be improved further by increasing the washing stringency. Nevertheless, these results are an exciting starting point for the use of CYP450 activity-based protein profiling to discover CYP450 activated upon biotic or abiotic stresses.

Differences between CYP450 labelling by click chemistry and biotinylated probes

Although DB569 and DB096 share the same reactive warhead, we noticed differences in the probe labelling profiles of mouse liver microsomes and CYP81A9 overexpressing *N. benthamiana* microsomes (Figure 14B and 16). DB569 and DB096 caused distinct CYP450 labelling intensities when used in mouse liver microsomes, DB569 being the probe that enriched fewer mouse CYP450s (Figure 16). We also observed the labelling limitation of DB569 when labelling CYP81A9 in *N. benthamiana* microsomes, as we could not detect its enrichment by protein blot nor mass spectrometry (Figure 14B and 14C). Interestingly, DB569 and DB096 equally labelled and enriched the same *N. benthamiana* CYP450s, showing the potential use of both biotinylated and click chemistry probes, for the labelling of CYP450s in *N. benthamiana* microsomes. We hypothesise that the differences between the labelling of these two probes are a consequence of the bulkiness of the biotin moiety that causes an impediment to access the active site of specific CYP450s. To comprehensively understand the differences between DB569 and DB09 labelling, it will be interesting to model the docking of the two different probes in a CYP81A9 3D model and see if we could explain the labelling differences because of the presence of the biotin moiety

in DB569. However, we cannot exclude that the differences are due to a technical error when diluting the probes. Therefore, we need to confirm these results by repeating this experiment using a different batch of probes.

Materials and Methods

Chemical probes and chemicals

The synthesis and chemical characterisation of the CYP450 probes will be reported in the D. Phil Thesis of Daniel Brown (DB). CYP450 probes DB080, DB086, DB088, DB089, DB096 and DB143 were resynthesised by Daniel Brown with some modifications (Wright *et al.*, 2009; Wright and Cravatt, 2007). JB001 and DB569 are newly designed CYP450 probes designed and synthesised by Daniel Brown.

The CYP450 inhibitor 1-ABT (A3940-50MG) and agrochemicals benoxacor (46001-50MG) and chlorsulfuron (34322-100MG) were purchased from Sigma-Aldrich. NADPH was purchased from MELFORD (N20140-0.1).

Biologic materials and growth conditions

Arabidopsis (*Arabidopsis thaliana*) ecotype Columbia plants were grown on soil at 25 °C under short day conditions (8/16 h light/dark regime) in a growth room. *N. benthamiana* (*Nicotiana benthamiana*) plants were grown on soil at 21 °C under long day conditions (16/8 h light/dark regime) in a greenhouse. Arabidopsis cell suspension cultures (ecotype Landsberg erecta) were grown and weekly subcultured in MS culture media (4.41 g/L MS-Basal medium including nitsch vitamins (Duchefa M0256), 30 g/L sucrose, 5.4 μM α -naphthyleneacetic acid, 0.23 μM kinetin, adjusted to pH 5.6). Maize cell culture microsomes were obtained from Syngenta. Mouse CD-1 microsomes were purchased from ThermoFisher Scientific (MSMCPL).

Cloning

Golden Gate Modular Cloning kit (Weber *et al.*, 2011) and Golden Gate Modular Cloning Toolbox for plants (Engler *et al.*, 2014) were used for cloning. Used and generated plasmids are summarised in Table S4. The primers used for sequence amplification are summarised in Table S5. The binary vector pJK268c containing the P19 silencing inhibitor (pL1V2-P19-F2) was used as binary vector.

The sequences encoding Arabidopsis CYP450s (CYP71B7, CYP73A5, CYP81D8 and CYP82C2) were amplified from Arabidopsis complementary DNA (cDNA) using the forward and reverse primer pairs summarised in Table S5. The sequence encoding the mouse Cyp1a2, Cyp2c29 and the maize CYP81A9 were codon-optimised for *in planta* expression (Table S6) and synthetized as a GeneString (GeneArt, ThermoFisher Scientific). When using BsaI restriction sites, PCR products were combined with GG1-

55, GG1-57, GG1-70 or GG1-78 to assemble the corresponding expression plasmids. When using BpiI restriction sites, PCR products were first cloned into the level 0 module GG1-01 and later transferred to pJK268c together with GG1-55, GG1-57, GG1-70 or GG1-78 in a BsaI ligation reaction. To generate CYP81A9^{C457A} and CYP81A9^{C457S}, we designed a set of primers introducing a single nucleotide mutation to generate C to A or C to S codon changes in the catalytic cysteine region (Table S2), using the CYP81A9-GFP expression plasmid (pMF325) as template. PCR products were assembled into pJK268c together with fragments of GG1-55, GG1-57 and GG1-78.

Generated expression plasmids were transformed into *E. coli* for their amplification and sequencing. Afterwards, plasmids were transformed into *Agrobacterium* (*Agrobacterium tumefaciens*) strain GV3101, carrying the pMP90 helper plasmid. *Agrobacterium* transformants were selected on LB plates (10 g/L NaCl, 10 g/L Tryptone, 5 g/L yeast extract, 15 g/L agar) containing 50 μM gentamycin, 25 μM rifampicin and 50 μM kanamycin. Single colonies were picked and grown in liquid LB (10 g/L NaCl, 10 g/L Tryptone, 5 g/L yeast extract) containing the same antibiotic used before. Glycerol stocks of the selected transformants were prepared mixing *Agrobacterium* cultures with 50% sterile glycerol in a 1:1 ratio.

Agroinfiltration

N. benthamiana plants were grown on soil at greenhouse conditions described before. *Agrobacterium* GV3101-pMP90 carrying a plasmid encoding the silence inhibitor P19 (pJK268c, empty vector (EV) containing P19) or *Agrobacterium* GV3101-pMP90 carrying the CYP450-encoding plasmids (pJK268c, plasmid containing a CYP450 sequence plus P19) were grown overnight (approximately 18 h) at 28 °C with agitation in LB media containing 50 μM gentamycin, 25 μM rifampicin and 50 μM kanamycin. Bacteria cells were collected by centrifugation at 1000 g for 10 min at room temperature (RT), washed with infiltration buffer (10 mM MES, 10 mM $MgCl_2$, pH 5.6 and 100 μM acetosyringone) to OD_{600}= 0.5. *Agrobacterium* were incubated at 28 °C for 2 h and afterwards, the two new fully-expanded leaves of *N. benthamiana* plants (4-5 weeks old) were hand-infiltrated with the *Agrobacterium* suspensions with the help of a needle-less 10 ml syringe.

CYP81A9 and CYP81A2 expression in yeast and microsome preparation

Saccharomyces cerevisiae WAT11 strain transformed with pYES3:CYP81A9 and pYES3:CYP81A2 were provided by Syngenta. For yeast cultivation, yeast glycerols were grown in selective agar media containing adenine (6.7 g/L yeast nitrogen base without aminoacids (Sigma Y0626), 0.64 g/L complete supplement mixture minus tryptophan (CMS-Trp), 20 g/L glucose (Sigma G8270), 20 g/L bacto agar (BD Difco, 214050), 0.04 g/L adenine sulphate (Sigma A-9126)) at 30 °C for 48 h. A single yeast colony was inoculated in 25 ml of selective liquid media (6.7 g/L yeast nitrogen base without aminoacids

(Sigma Y0626), 0.64 g/L complete supplement mixture minus tryptophan (CMS-Trp), 20 g/L glucose (Sigma G8270), 0.04 g/L adenine sulphate (Sigma A-9126)) and grown at 30 °C, 180 rpm, for 24 h. Following, 300 ml of YPGE + adenine media (10 g/L yeast extract (Sigma 92144), 10 g/L peptone (Melford P20P240), 30 ml/L ethanol, 20 g/L glucose and 0.04 g/L adenine sulphate (Sigma A-9126)) were inoculated with 6 ml of the selective culture and incubated with agitation (180 rpm) at 30 °C for 30 h. To induce protein expression, yeast cells were washed with water in sterile conditions, resuspended in 300 ml of YPLE + adenine media (10 g/L yeast extract (Sigma 92144), 10 g/L peptone (Melford P20P240), 30 ml/L ethanol, 20 g/L D-galactose, 0.04 g/L adenine sulphate (Sigma A-9126)) and incubated with agitation (180 rpm) at 30 °C for 16 h. Yeast cells were harvest by centrifugation and used for microsomal isolation.

Yeast microsomes were prepared by washing the harvested yeast cells in TEK buffer (50 mM Tris-HCL pH 7.5, 1 mM EDTA, 100 mM KCl). Yeast cells were resuspended in ice-cold TESB + DTT buffer (50 mM Tris-HCL pH 7.5, 1 mM EDTA, 600 mM D-Sorbitol, 30 mM DTT) and incubated for 10 min at RT. Afterwards, yeast cells were centrifuged at 5,000 g, resuspended in ice-cold TESB (50 mM Tris-HCL pH 7.5, 600 mM D-Sorbitol) and grinded using 0.5 mm glass beads and a bead mill homogenizer (BioSpec BeadBeater 1107900-105). Cell extract was filtered through a nylon cloth and centrifuged at 16,000 g for 10 min. Supernatant containing soluble proteins were ultra-centrifuged at 100,000 g for 1h. Pellet containing the microsomal membranes were resuspended in TEG buffer (50 mM Tris-HCL pH 7.5, 1 mM EDTA, 20% glycerol) and protein concentration was adjusted to 2 mg/ml by Bradford protein assay. Microsomes were kept at -80 °C until used.

Protein extraction and microsomal fraction isolation from plant tissues

Arabidopsis leaf tissue was collected from 5-week-old Arabidopsis. Agroinfiltrated *N. benthamiana* leaf tissue was collected at 4 days post-infiltration (dpi). Leaf tissue was frozen in liquid nitrogen and ground to fine powder with a mortar and pestle. Total proteins were extracted in cold homogenization buffer (100 mM potassium phosphate buffer pH 7.5, 400 mM sucrose, 1% (w/v) polyvinylpolypyrrolidone (PVPP) and 4 mM β-mercaptoethanol). The extracts were left for 20 min rotating at 4 °C for complete homogenization and centrifuged at 5,000 g for 20 min at 4 °C. Supernatants containing soluble proteins were filtered through a layer of miracloth filter and ultra-centrifuged at 100,000 g for 1h. Pellets containing the microsomal membranes were resuspended in resuspension buffer (100 mM potassium phosphate buffer pH 7.5 containing 20% glycerol). Total protein concentration was determined by DC protein assay Kit (Bio-Rad) with bovine serum albumin standards, protein concentration was adjusted to 0.75 mg/ml for each sample and the resulting samples were used for labelling without freeze thawing.

Carbon monoxide (CO) displacement assay

Microsomes to be tested were diluted (100x, a hundred times; 20x, twenty times; 10x, ten times) in a cuvette and reduced using sodium dithionite crystals. Next, microsomes were bubbled with CO for 30 sec and absorbance between 400 and 500 nm was measured.

Activity-based protein profiling and click chemistry

All probes were prepared at 0.5–2 mM stock solutions in dimethyl sulfoxide (DMSO). Protein preparation samples of 50 μl were incubated with or without the indicated probes in the presence or absence of NADPH for 1h at the indicated probe concentration (usually 5-10 μM). For inhibition experiments, 50 μl extracts were pre-incubated with the corresponding amount of 1-ABT (1-500 μM) for 10 min before labelling with 5 μM DB088. Labelling reactions were stopped by adding 1:4 (v/v) cold acetone and precipitated by 3 min centrifugation at maximum speed using a benchtop centrifuge. Protein pellets were resuspended in 44.5 μl of PBS-SDS buffer (phosphate-buffered saline (PBS) pH 7.4 with 1% (w/v) sodium dodecyl sulfate (SDS)) and heated for 5 min at 90 °C.

For click chemistry, 44.5 μl of labelled proteins were treated with 2 μM Cy5 Picolyl Azide (Click Chemistry Tools, 50 μM stock in DMSO) or Fluorescein Picolyl Azide (Click Chemistry Tools, 50 μM stock in DMSO) and a premixture of 100 μM tris((1-benzyl-1H-1,2,3-triazol-4-yl) methyl)amine (TBTA; 3.4 mM stock in DMSO:*t*-butanol 1:4), 2 mM tris(2-carboxyethyl)phosphine hydrochloride (TCEP; 100 mM stock in water) and 1 mM copper(II) sulfate ($CuSO_4$; 50 mM stock in water). Samples were incubated for 1 h at RT in the dark and quenched by acetone precipitation. Protein pellets were resuspended in 50 μl of 2x gel loading buffer (100 mM Tris-HCl pH 6.8, 200 mM dithiotreitol, 4% SDS, 20% glycerol and 0.02% bromophenol blue) and heated for 5 min at 90 °C.

CYP81A9 and CYP81A2 activity assay with bentazon

Seventeen microliters of yeast microsomes expressing CYP81A9 and CYP81A2 (2 mg/ml) were incubated with 200 μM bentazon in the presence or absence of 1 mM NADPH and a final volume of 100 μl of 50 mM Tris-HCl pH 7.5 buffer, at 28 °C for 2 h. For inhibition experiments, yeast microsomes were pre-incubated with 300 μM CYP450 probes or 1-ABT for 10 min in the prescence of 1 mM NADPH before the addition of 200 μM bentazon. Reactions were stopped by adding 100 μl of acetonitrile: HCl (99:1) and proteins were precipitated by 3 min centrifugation at maximum speed using a benchtop centrifuge. Supernatants were diluted by adding 1:5 (v/v) acetonitrile in glass vials. LC-MS samples were run and analysed by Melissa Brazier-Hicks (Syngenta) using the electrospray ionization interface (ESI) in negative mode. The presecence of bentazon and hydroxybentazon was monitored at retention

time of 1.57 and 1.49, respectively. Data is expressed in amount of hydroxylated bentazon detected (Peak area, AU) in the incubated microsomes.

In-gel fluorescence scanning and Western Blot

Labelled proteins were loaded and separated on 10-12% SDS-PAGE acrylamide gels at 150V. Fluorescence scanning of acrylamide gels was performed on an Amersham Typhoon 5 scanner (GE Healthcare Life Sciences). Scanned gels were stained with Coomassie Brilliant Blue G-250. Image J was used for the quantification of the detected labelled proteins.

For Western Blot, proteins separated in SDS-PAGE gels were transferred to a PVDF membrane using Trans-Blot Turbo Transfer System (Bio-Rad). Membranes were blocked in 5% (w/v) milk in TBS-T (50 mM Tris-HCl pH 7.6, 150 mM NaCl and 0.1% Tween-20) overnight at 4 °C, incubated in 1:5,000 anti-GFP-HRP (Abcam, ab6663) or anti-HIS-HRP (ThermoFisher, R931-25) for 1.5 h at RT and washed in TBS-T for 5 times for 5 min and in TBS for the last wash. Clarity Western ECL substrate (Bio-Rad) was used for chemiluminescent protein detection. When performing streptavidin-HRP protein blots, samples were processed the same way except that membranes were blocked in 1% (w/v) BSA in TBS-T and incubated in 1:1,000 streptavidin-HRP (Sigma, S2438).

Filter-aided sample preparation for Mass spectrometry

Arabidopsis leaf and mouse liver microsomes were diluted to 1 mg/ml protein concentration. YM-10 microcon centrifugal filters (Millipore) were prewashed by adding 200 μl of 0.1% trifluoroacetic acid (TFA) in 50% acetonitrile (ACN) and centrifuged at 15,000 g for 15min at RT. Filters were pre-equilibrated with 200 μl of 8 M urea in 100 mM triethylammonium bicarbonate (TEAB) pH 8.5 and centrifuged at 15,000 g for 15 min at RT. Afterwards, an equivalent of 200 μg total protein were mixed with 200 μl of 8 M urea in 100 mM TEAB, pH 8.5 in the pre-treated filters. Filters were centrifuged at 15,000 g for 40 min at RT and retained proteins were washed with 200 μl of 8 M urea in 100 mM TEAB a total of 4 times. Protein reduction and alkylation were achieved by sequential incubation of the concentrates in 200 μl of 8 M urea in 100 mM TEAB containing tris(2-carboxyethyl) phosphine hydrochloride (TCEP; 10 mM final concentration, 30 min incubation at RT) and 2-chloroacetamide (CA, 50 mM final concentration, 30 min incubation at RT in the dark) followed by centrifugation. The concentrates were washed with 6 M urea in 50 mM TEAB a total of 2 times and subjected to proteolytic digestion with 2.5 μg of lysyl endopeptidase (Lys-C from FUJIFILM Wako, in 50 mM Tris-HCL pH 8, 4 hours incubation at 37 °C) and 5 μg of trypsin (Trypsin Gold from Promega, in 50 mM TEAB pH 8.5, overnight incubation at 37 °C). Digested peptides were collected by centrifugation, and the filters were washed with 150 μl 0.1% TFA and 150 μl 0.1% TFA in 50% ACN. The combined filtrates were dried by vacuum centrifugation and submitted for MS analysis.

Large-scale labelling, affinity purification

1.5 ml of microsomal fraction extracts (0.75 mg/ml protein concentration) were incubated with or without the indicated probes (20 μM) in the presence or absence of NADPH for 1 h. Labelling reactions were stopped by methanol/chloroform precipitation (addition of 4 volumes of ice-cold methanol, 1 volume of ice-cold chloroform and 3 volumes of water) and precipitated by 40 min centrifugation at 4,000 g at 4 °C. Protein pellets were resuspended in 1ml of PBS-SDS buffer by bath sonication and heated at 90 °C for 10 min. Labelled proteins were biotinylated with 30 μM Azide-PEG3-biotin (Sigma-Aldrich, 2 mM stock in DMSO) using click chemistry as described in "Activity-based protein profiling and click chemistry". Samples were incubated for 1 h at RT in the dark, quenched by the addition of 10 mM ethylenediaminetetraacetic acid (EDTA) and precipitated via the methanol/chloroform method. Protein pellets were resuspended in 1.5 ml of 1.2% (w/v) SDS dissolved in PBS by bath sonication and diluted by adding 7.5 ml of PBS. The resulting solution was incubated with 100 μl of pre-equilibrated Pierce High Capacity Streptavidin Agarose beads (Thermo Fisher Scientific) for 2h at RT. Agarose beads containing the labelled proteins were collected by centrifugation at 1,000 g for 5 min at RT. Agarose beads were washed successively three times with 10ml of PBS-SDS buffer, three times with PBS and a final wash with 10 ml of water.

On-bead trypsin and Lys-C digestion

For on-bead digestion, the captured agarose beads containing the labelled proteins were treated with 500 μl 6 M urea dissolved in PBS and 10mM TCEP (200 mM stock in water) for 15 min at 65 °C. A final concentration of 20 mM CA (400 mM stock in water) was added and left incubated for 30 min at 35 °C in the dark. Reaction was diluted by the addition of 950 μl of PBS and the supernatant was removed by centrifuging the beads at 500 g for 2 min. 100 μl of Lys-C digestion solution (Walko, 5 μg of Lys-C were reconstituted in 200 μl 1 M urea/ 50 mM Tris-HCl buffer pH 8) was added to the beads and left incubating at 37 °C for 3 h. 100 μl of trypsin digestion solution (Promega, 5 μl of reconstituted trypsin were dissolved in 100 μl 50 mM Tris-HCl buffer pH 8) was added to the beads and left incubating at 37 °C overnight. The supernatant containing the digested peptides was dried by vacuum centrifugation and submitted for MS analysis.

LC-MS/MS and peptide identification using MaxQuant

MS samples were analysed as described in Morimoto et. al., 2019. Briefly, the acidified tryptic peptides were desalted using C18 Tips (Thermo Fisher Scientific, 10 μL bed, 87782) and peptide samples were resuspended in 0.1% FA solution and analysed on an Orbitrap Elite instrument (ThermoFisher Scientific) (Michalski *et al.*, 2012) attached to an EASY-nLC 1000 liquid chromatography system (Thermo Fisher Scientific). Samples were separated on an analytical column based on a fused silica

capillary with an integrated PicoFrit emitter (New Objective) with Reprosil-Pur 120 C18-AQ 1.9 μm resin. Peptides were next separated using 140 min gradient of solvent and analysed with Orbitrap analyser (using Fourier Transform MS) at a resolution of 60,000 with the internal lock-mass option switched on (Olsen *et al.*, 2005).

RAW spectra were submitted to an Andromeda search in MaxQuant (version 1.5.3.30) using the default settings (Cox *et al.*, 2011; Cox and Mann, 2008). Label-free quantification and match between-runs were activated (Cox *et al.*, 2014). The MS/MS spectra data were searched against the UniProt *Mus musculus* reference database (55,412 entries) and the UniProt *Arabidopsis thaliana* reference database (39,359 entries). All searches included a contaminants database (as implemented in MaxQuant, 245 entries). Enzyme specificity was set to 'Trypsin/P' and the MS/MS match tolerance was set to ±0.5 Da. The peptide spectrum match FDR and the protein FDR were set to 0.01 (based on target-decoy approach) and the minimum peptide length was seven amino acids. For protein quantification, unique and razor peptides were allowed. Modified peptides were allowed for quantification with a minimum score of 40. Relative quantification of proteins between different MS runs is based exclusively on the label-free quantifications as calculated by the software MaxQuant, using the "MaxLFQ" algorithm (Cox *et al.*, 2014). Filtering of results was done in Perseus version 1.6.13.0 (Tyanova *et al.*, 2016). Briefly, data was filtered against contaminants and only those proteins found in at least one group in all two/three replicates were considered. Further analysis and graphs were performed using the Qfeatures and ggplot R packages (Gatto, 2021). Imputed values were generated using a missing not at random (MNAR) and missing at random (MAR) mixed imputation over the whole matrix, and the fold change and adjusted P values (adj. P Val) were calculated using the fdr method over the three biological replicates. The correct clustering of the biological replicates by categorical groups was evaluated using principal component analysis (PCA) plots.

Supplemental data

Table S1. Description of the top 40 proteins ranked by log_2FC differentially up-regulated in DB569 labelling pull-down. Table includes: Protein IDs, Fasta headers, log_2 Fold Change (log_2FC), log_2 MS intensity (MS intensity), adjusted P. value (adj.P.Val), Molecular weight (MW [kDa]), FDR significance (FDR) and Significance.

	Protein IDs	Fasta headers	Log_2 FC	MS intensity	adj.P.Val	MW [kDa]	FDR
1	NbE03055681.1	xylose isomerase-like (XP_016435649.1)	6.93	23.84	0.0002	53.77	FDR 0.001
2	NbD000822.1;NbD036094.1	malate dehydrogenase, chloroplastic isoform X1 (XP_019230288.1);malate dehydrogenase, chloroplastic isoform X2 (XP_019230290.1)	4.89	22.82	0.0045	47.62	FDR 0.01
3	NbE03057670.1;NbD046213.1	protein disulfide-isomerase-like (XP_019231449.1);protein disulfide-isomerase-like (XP_019231449.1)	4.84	25.03	0.0000	55.11	FDR 0.001
4	NbE05063564.1;NbD046180.1; NbE05063563.1;NbD029787.1	protein disulfide-isomerase-like (XP_018631719.1);protein disulfide-isomerase-like (XP_018631719.1);protein disulfide-isomerase-like (XP_019229837.1)	4.52	25.07	0.0002	55.46	FDR 0.001
5	NbE05065515.1	cytochrome P450 98A2-like (XP_019241025.1)	3.68	22.22	0.0025	58.12	FDR 0.01
6	NbE05065421.1;NbD033181.1; NbD020814.1	protein disulfide isomerase-like 1-3 (XP_019245617.1);protein disulfide isomerase-like 1-3 (XP_019245617.1)	3.42	23.98	0.0025	63.90	FDR 0.01
7	NbD031373.1	delta(24)-sterol reductase (XP_009624736.1)	3.35	22.05	0.0032	66.11	FDR 0.01
8	NbE03060735.1;NbD037232.1; NbD011138.1;NbD013322.1	molybdate-anion transporter-like (XP_016455278.1);molybdate-anion transporter-like (XP_016455278.1);molybdate-anion transporter-like (XP_016455278.1)	3.26	22.01	0.0036	50.50	FDR 0.01
9	NbD016046.1	60S ribosomal protein L5-like (XP_016438102.1)	3.09	21.92	0.0047	34.57	FDR 0.01
10	NbD045303.1;NbD031955.1	30S ribosomal protein S13, chloroplastic-like (XP_016493236.1);30S ribosomal protein S13, chloroplastic-like (XP_016493236.1)	3.09	21.92	0.0047	18.80	FDR 0.01
11	NbD013330.1	60S ribosomal protein L3-2 (XP_009598742.1)	3.06	21.91	0.0047	44.48	FDR 0.01
12	NbE05063379.1	gamma carbonic anhydrase 1, mitochondrial-like (XP_009612501.1)	3.04	22.70	0.0078	29.62	FDR 0.01
13	NbD011866.1;NbD048851.1;N bD033132.1	catalase (ACL27272.1)	2.93	22.67	0.0090	56.82	FDR 0.01
14	NbD036727.1;NbD051534.1;N bD049521.1;NbE03061008.1	dynamin-2A-like (XP_016447760.1)	2.82	22.83	0.0025	99.07	FDR 0.01
15	NbD000964.1;NbD000959.1;N bE05068087.1;NbE03055005.1; NbD022764.1;NbD008309.1	cytochrome P450 98A2-like (XP_019261854.1)	2.76	24.10	0.0087	57.95	FDR 0.01
16	NbD009282.1	mitochondrial-processing peptidase subunit alpha-like (XP_019245878.1)	2.70	22.46	0.0251	54.61	FDR 0.05
17	NbD004407.1	probable protein disulfide-isomerase A6 (XP_016486857.1)	2.66	22.37	0.0087	39.56	FDR 0.01
18	NbE05065398.1;NbD046197.1; NbD019649.1;NbD017004.1;N bD026193.1	40S ribosomal protein S21-2-like (XP_016478008.1);40S ribosomal protein S21-like (XP_019223972.1);40S ribosomal protein S21-like (XP_019223972.1)	2.66	21.70	0.0087	8.85	FDR 0.01
19	NbE03057724.1;NbD040562.1	cytochrome P450 71A1-like (XP_016505274.1)	2.63	21.69	0.0079	58.07	FDR 0.01
20	NbD005288.1	phosphoinositide phosphatase SAC6-like (XP_016481383.1)	2.51	21.63	0.0079	67.83	FDR 0.01
21	NbD047267.1;NbE03058179.1	phototropin-2-like (XP_016471108.1);phototropin-2-like (XP_016471108.1)	2.49	21.62	0.0081	107.21	FDR 0.01
22	NbD044079.1	protein disulfide isomerase-like 1-4 (XP_019255435.1)	2.44	21.60	0.0087	64.77	FDR 0.01
23	NbE05066551.1;NbD005386.1	tripeptidyl-peptidase 2 isoform X1 (XP_009796711.1);tripeptidyl-peptidase 2 isoform X1 (XP_009796711.1)	2.40	22.14	0.0132	149.43	FDR 0.05
24	NbD016339.1	aminomethyltransferase, mitochondrial (XP_019252116.1)	2.35	21.55	0.0112	44.24	FDR 0.05
25	NbD030668.1	9-divinyl ether synthase (XP_016478324.1)	2.34	21.73	0.0062	54.02	FDR 0.01
26	NbE44072655.1	L-galactono-1,4-lactone dehydrogenase, mitochondrial (XP_019254343.1)	2.32	22.08	0.0079	66.91	FDR 0.01
27	NbD044669.1	ras-related protein RABE1c-like (XP_016441463.1)	2.29	21.52	0.0095	23.99	FDR 0.01
28	NbD014644.1;NbD045772.1	cell division cycle protein 48 homolog (XP_016498748.1);cell division cycle protein 48 homolog (XP_016498748.1)	2.20	22.58	0.0087	88.06	FDR 0.01
29	NbD046136.1;NbE03054704.1	dynamin-related protein 1E (XP_019260331.1);dynamin-related protein 1E (XP_019260331.1)	2.19	22.42	0.0088	68.78	FDR 0.01

30	NbD019576.1;NbD027010.1	QM (ACT65738.1)	2.16	26.77	0.0041	24.78	FDR 0.01
31	NbD001331.1	60S ribosomal protein L3-2-like (XP_016443425.1)	2.14	24.66	0.0025	44.40	FDR 0.01
32	NbD037633.1	40S ribosomal protein S11 (XP_019254927.1)	2.12	26.56	0.0087	17.69	FDR 0.01
33	NbD007127.1	60S ribosomal protein L8-like (XP_019250372.1)	2.06	25.92	0.0160	28.20	FDR 0.05
34	NbD001471.1	ferritin-1, chloroplastic (XP_019231012.1)	2.06	21.41	0.0211	27.87	FDR 0.05
35	NbD030018.1;NbD024768.1;NbE03061739.1;NbD047769.1;NbE03059409.1;NbD002858.1;NbE03056049.1;NbD018777.1	S-adenosylmethionine synthase 3 (XP_019250722.1);S-adenosylmethionine synthetase (BAR72289.1);S-adenosylmethionine synthase 3 (XP_019250722.1);S-adenosylmethionine synthase 2 (XP_019233687.1);S-adenosylmethionine synthase 2-like (XP_019229012.1);S-ade	2.03	21.39	0.0172	42.62	FDR 0.05
36	NbD019734.1;NbD044430.1;NbD019732.1	40S ribosomal protein S2-3-like (XP_019250704.1);40S ribosomal protein S2-3-like (XP_019250704.1);40S ribosomal protein S2-3-like (XP_019250704.1)	2.03	26.65	0.0025	30.24	FDR 0.01
37	NbD031906.1	40S ribosomal protein S3a (XP_019247516.1)	2.02	26.60	0.0025	29.73	FDR 0.01
38	NbD045171.1	patellin-3-like (XP_009617344.1)	2.00	22.23	0.0047	68.14	FDR 0.01
39	NbD030400.1;NbD033288.1;NbE03054978.1;NbD036656.1	acetoacetyl-coenzyme A thiolase (BAR94039.1);acetyl-CoA acetyltransferase, cytosolic 1-like (XP_016500617.1)	2.00	21.37	0.0176	41.30	FDR 0.05
40	NbD052049.1	V-type proton ATPase catalytic subunit A-like (XP_016489565.1)	1.99	26.01	0.0054	68.62	FDR 0.01

Table S2. Description of all proteins differentially up-regulated in DB096 labelling pull-down. Table includes: Protein IDs, Fasta headers, log_2 Fold Change (log_2FC), log_2 MS intensity (MS intensity), adjusted P. value (adj.P.Val), Molecular weight (MW [kDa]), FDR significance (FDR) and Significance.

	Protein IDs	Fasta headers	log_2 FC	MS intensity	adj.P.Val	MW [kDa]	FDR
1	NbD025066.1;NbD039780.1;NbD014018.1;NbD021111.1;NbD027296.1;NbD010669.1;NbD021113.1;NbE03055230.1;NbD001435.1	AAA-ATPase At3g50940-like (XP_016452706.1)	2.71	26.72	0.00013	57.42	FDR 0.001
2	NbD000964.1;NbD000959.1;NbE05068087.1;NbE03055005.1;NbD022764.1;NbD008309.1	cytochrome P450 98A2-like (XP_019261854.1)	2.18	23.80	0.00019	57.95	FDR 0.001
3	Zm_CYP81A9|C-term;CON__Q9U6Y5	Zm_CYP81A9|C-term GFP tag	2.17	30.30	0.00006	84.03	FDR 0.001
4	NbE05065515.1	cytochrome P450 98A2-like (XP_019241025.1)	2.13	22.84	0.00011	58.12	FDR 0.001
5	NbE03055681.1	xylose isomerase-like (XP_016435649.1)	1.77	25.41	0.00006	53.77	FDR 0.001
6	NbE03056327.1;NbD008897.1	trans-cinnamate 4-monooxygenase-like (XP_016493546.1);trans-cinnamate 4-monooxygenase-like (XP_016493546.1)	1.27	23.75	0.00190	58.54	FDR 0.01
7	NbE03054909.1	LOW QUALITY PROTEIN: 5-epiaristolochene 1,3-dihydroxylase-like (XP_009801864.1)	1.24	22.00	0.02248	57.11	FDR 0.05
8	NbD002635.1;NbD038528.1;NbD002618.1;NbE05064480.1	trans-cinnamate 4-monooxygenase (XP_016509005.1)	1.19	21.54	0.00190	58.08	FDR 0.01
9	NbE03057724.1;NbD040562.1	cytochrome P450 71A1-like (XP_016505274.1)	1.11	22.99	0.00190	58.07	FDR 0.01
10	NbD030408.1;NbD008963.1;NbD020511.1	long chain acyl-CoA synthetase 8 (XP_019249337.1)	1.06	23.03	0.02016	79.22	FDR 0.05
11	NbD013867.1	apolipoprotein A-I-like (XP_019227464.1)	1.03	22.47	0.02506	51.22	FDR 0.05
12	NbD039121.1	cytochrome P450 81F3-like (XP_016503274.1)	0.97	25.87	0.02531	59.04	FDR 0.05
13	NbE03054662.1;NbD017803.1;NbD021263.1;NbD010507.1;NbD016401.1;NbE05063015.1	protein ROOT HAIR DEFECTIVE 3-like isoform X1 (XP_016515249.1);protein ROOT HAIR DEFECTIVE 3-like isoform X1 (XP_016515249.1)	0.97	22.75	0.01616	91.07	FDR 0.05
14	NbD011866.1;NbD048851.1;NbD033132.1	catalase (ACL27272.1)	0.92	24.76	0.03013	56.82	FDR 0.05
15	NbD039178.1	microsomal glutathione S-transferase 3-like (XP_016468433.1)	0.91	22.65	0.01616	16.48	FDR 0.05
16	NbE44071593.1;NbD020002.1	long chain base biosynthesis protein 2a (XP_016488956.1);long chain base biosynthesis protein 2a (XP_016488956.1)	0.84	21.43	0.02523	54.04	FDR 0.05
17	NbD021663.1;NbE05067503.1	NADPH--cytochrome P450 reductase (XP_009786522.1)	0.82	22.91	0.02952	76.05	FDR 0.05

18	NbE03053580.1;NbD049457.1	uncharacterized protein LOC104230414 (XP_009781515.1);uncharacterized protein LOC104230414 (XP_009781515.1)	0.79	23.27	0.03084	63.72	FDR 0.05
19	NbD018366.1	calcium-transporting ATPase 4, endoplasmic reticulum-type-like (XP_019224158.1)	0.76	23.30	0.04901	116.18	FDR 0.05
20	NbD022993.1;NbE03057138.1;NbD039670.1	dolichyl-diphosphooligosaccharide--protein glycosyltransferase subunit STT3B (XP_019254124.1);dolichyl-diphosphooligosaccharide--protein glycosyltransferase subunit STT3B (XP_019254124.1)	0.74	21.03	0.02278	82.45	FDR 0.05

Table S3. Description of the top 40 proteins ranked by log_2FC differentially up-regulated in DB088 labelling pull-down. Table includes: Protein IDs, Fasta headers, log_2 Fold Change (log_2FC), log_2 MS intensity (MS intensity), adjusted P. value (adj.P.Val), Molecular weight (MW [kDa]), FDR significance (FDR) and Significance.

	Protein IDs	Fasta headers	log_2 FC	MS intensity	adj.P.Val	MW [kDa]	FDR
1	NbD025066.1;NbD039780.1;NbD014018.1;NbD021111.1;NbD027296.1;NbD010669.1;NbD021113.1;NbE03055230.1;NbD001435.1	AAA-ATPase At3g50940-like (XP_016452706.1)	3.37	26.72	0.000018	57.42	FDR 0.001
2	Zm_CYP81A9|C-term;CON__Q9U6Y5	Zm_CYP81A9|C-term GFP tag	2.80	30.30	0.000004	84.03	FDR 0.001
3	NbD049629.1;NbE03060085.1;NbD031292.1	cytochrome P450 72A15-like (XP_016491347.1)	2.34	22.36	0.008416	59.79	FDR 0.01
4	NbE03055681.1	xylose isomerase-like (XP_016435649.1)	2.27	25.41	0.000004	53.77	FDR 0.001
5	NbD000964.1;NbD000959.1;NbE05068087.1;NbE03055005.1;NbD022764.1;NbD008309.1	cytochrome P450 98A2-like (XP_019261854.1)	2.20	23.80	0.000130	57.95	FDR 0.001
6	NbD017236.1	LOW QUALITY PROTEIN: calcium-transporting ATPase 2, plasma membrane-type-like (XP_009787048.1)	2.13	21.17	0.009407	110.89	FDR 0.01
7	NbE05065515.1	cytochrome P450 98A2-like (XP_019241025.1)	2.04	22.84	0.000098	58.12	FDR 0.001
8	NbD013867.1	apolipoprotein A-I-like (XP_019227464.1)	1.84	22.47	0.000233	51.22	FDR 0.001
9	NbE03056327.1;NbD008897.1	trans-cinnamate 4-monooxygenase-like (XP_016493546.1);trans-cinnamate 4-monooxygenase-like (XP_016493546.1)	1.75	23.75	0.000098	58.54	FDR 0.001
10	NbD002635.1;NbD038528.1;NbD002618.1;NbE05064480.1	trans-cinnamate 4-monooxygenase (XP_016509005.1)	1.64	21.54	0.000098	58.08	FDR 0.001
11	NbD002561.1;NbD001937.1;NbE03057294.1;NbD024076.1	uncharacterized protein LOC107817229 isoform X1 (XP_016498506.1);uncharacterized protein LOC107817229 isoform X1 (XP_016498506.1);uncharacterized protein LOC109211713 isoform X1 (XP_019230826.1);uncharacterized protein LOC107817229 isoform X1 (XP_01649	1.63	19.43	0.011875	47.04	FDR 0.05
12	NbD045132.1;NbE44071908.1;NbD051359.1	AAA-ATPase At3g50940-like (XP_016468477.1);AAA-ATPase At3g50940-like (XP_016468477.1)	1.62	21.67	0.006664	56.41	FDR 0.01
13	NbD039121.1	cytochrome P450 81F3-like (XP_016503274.1)	1.62	25.87	0.000394	59.04	FDR 0.001
14	NbE03054909.1	LOW QUALITY PROTEIN: 5-epiaristolochene 1,3-dihydroxylase-like (XP_009801864.1)	1.61	22.00	0.001784	57.11	FDR 0.01
15	NbD021231.1;NbE44069489.1	probable manganese-transporting ATPase PDR2 (XP_016463581.1);probable manganese-transporting ATPase PDR2 (XP_016463581.1)	1.56	20.73	0.012372	131.23	FDR 0.05
16	NbD039178.1	microsomal glutathione S-transferase 3-like (XP_016468433.1)	1.39	22.65	0.000343	16.48	FDR 0.001
17	NbE44071593.1;NbD020002.1	long chain base biosynthesis protein 2a (XP_016488956.1);long chain base biosynthesis protein 2a (XP_016488956.1)	1.37	21.43	0.000394	54.04	FDR 0.001
18	NbD036805.1	calcium-transporting ATPase 1, chloroplastic-like (XP_009796868.1)	1.33	19.84	0.012764	110.60	FDR 0.05
19	NbE03057724.1;NbD040562.1	cytochrome P450 71A1-like (XP_016505274.1)	1.33	22.99	0.000302	58.07	FDR 0.001
20	NbD030408.1;NbD008963.1;NbD020511.1	long chain acyl-CoA synthetase 8 (XP_019249337.1)	1.32	23.03	0.001784	79.22	FDR 0.01
21	NbD013687.1	reticulon-like protein B5 (XP_016442312.1)	1.30	22.33	0.008298	30.11	FDR 0.01
22	NbE05063946.1;NbD045366.1	NADPH--cytochrome P450 reductase-like (XP_019252798.1);NADPH--cytochrome P450 reductase (XP_009786522.1)	1.28	19.97	0.001696	78.44	FDR 0.01
23	NbD046570.1	dehydrogenase/reductase SDR family member 7 isoform X1 (XP_019228894.1)	1.26	20.53	0.041292	34.99	FDR 0.05

24	NbD044289.1;NbD015934.1	choline/ethanolaminephosphotransferase 1 (XP_019232078.1);choline/ethanolaminephosphotransferase 1 (XP_019232078.1)	1.26	21.10	0.004076	43.51	FDR 0.01
25	NbD028822.1	5-epiaristolochene 1,3-dihydroxylase (XP_009625417.1)	1.25	19.46	0.006141	56.72	FDR 0.01
26	NbD011007.1;NbE05066686.1	dnaJ protein ERDJ2A-like (XP_019234489.1);dnaJ protein ERDJ2A-like (XP_019234489.1)	1.22	21.04	0.008496	75.16	FDR 0.01
27	NbE03057974.1;NbD006156.1	eukaryotic translation initiation factor 3 subunit A isoform X1 (XP_019250286.1);eukaryotic translation initiation factor 3 subunit A isoform X1 (XP_019250286.1)	1.17	19.96	0.023739	111.58	FDR 0.05
28	NbD012201.1;NbD012200.1	Partial, 11-oxo-beta-amyrin 30-oxidase-like (XP_019261687.1);11-oxo-beta-amyrin 30-oxidase-like (XP_019261687.1)	1.17	20.28	0.012539	45.77	FDR 0.05
29	NbD031906.1	40S ribosomal protein S3a (XP_019247516.1)	1.15	26.83	0.001350	29.73	FDR 0.01
30	NbE03054662.1;NbD017803.1;NbD021263.1;NbD010507.1;NbD016401.1;NbE05063015.1	protein ROOT HAIR DEFECTIVE 3-like isoform X1 (XP_016515249.1);protein ROOT HAIR DEFECTIVE 3-like isoform X1 (XP_016515249.1)	1.14	22.75	0.002009	91.07	FDR 0.01
31	NbD024270.1	very-long-chain 3-oxoacyl-CoA reductase 1 (XP_009590833.1)	1.13	21.70	0.001784	35.94	FDR 0.01
32	NbD038998.1;NbD033652.1;NbD004035.1	AAA-ATPase At3g28580-like (XP_019247198.1)	1.13	22.56	0.012390	62.00	FDR 0.05
33	NbD021663.1;NbE05067503.1	NADPH--cytochrome P450 reductase (XP_009786522.1)	1.09	22.91	0.002092	76.05	FDR 0.01
34	NbE05068424.1;NbD015392.1	TSC13 protein (AAY17262.1);TSC13 protein (AAY17262.1)	1.09	21.44	0.005317	36.27	FDR 0.01
35	NbD021980.1	7-dehydrocholesterol reductase-like (XP_016480318.1)	1.08	22.07	0.007800	49.74	FDR 0.01
36	NbD022993.1;NbE03057138.1;NbD039670.1	dolichyl-diphosphooligosaccharide--protein glycosyltransferase subunit STT3B (XP_019254124.1);dolichyl-diphosphooligosaccharide--protein glycosyltransferase subunit STT3B (XP_019254124.1)	1.08	21.03	0.000911	82.45	FDR 0.001
37	NbD045262.1	reticulon-like protein B4 (XP_016513127.1)	1.07	22.47	0.001696	30.09	FDR 0.01
38	NbD019576.1;NbD027010.1	QM (ACT65738.1)	1.05	26.11	0.001825	24.78	FDR 0.01
39	NbD018366.1	calcium-transporting ATPase 4, endoplasmic reticulum-type-like (XP_019224158.1)	1.02	23.30	0.004016	116.18	FDR 0.01
40	NbD036075.1	calcium-transporting ATPase 4, endoplasmic reticulum-type-like (XP_019224158.1)	1.02	20.92	0.016264	116.20	FDR 0.05

Table S4. Plasmids

Golden Gate Modules	
Lab number	**Description**
pJK268c	pL1V2-P19-F2, Binary vector.
GG1-01	pL0V-SC1-15456, Level 0 Cloning vector, Golden Gate original vector, EC15456.
GG1-55	pL0M-T-35S-1-41414, Level 0 Module, 35S terminator, Golden Gate plant kit, pICH41414.
GG1-57	pL0M-PU-35S-TMV-3-51288, Level 0 Module, 2 x 35S promoter + TMV Ω (0.8 kb), Golden Gate plant kit, pICH51288.
GG1-70	pL0M-C2-6xHis-15259, Level 0 Module, His for C terminal fusion, EC15259. ENSA consortium https://www.ensa.ac.uk/
GG1-78	pL0M-C2-eGFP-15095, Level 0 Module, eGFP for C terminal fusion. EC15095. ENSA consortium https://www.ensa.ac.uk/
Golden Gate binary vectors in *Agrobacterium tumefaciens* GV3101	
Lab number	**Description**
pMF70	pL2M-P19-kan-2x35S::CYP71B7-GFP
pMF65	pL2M-P19-kan-2x35S::CYP73A5-GFP
pMF41	pL2M-P19-kan-2x35S::CYP81D8-GFP
pMF42	pL2M-P19-kan-2x35S::CYP82C2-GFP
pMF63	pL2M-P19-kan-2x35S::ATR1-HIS
pMF261	pL2M-P19-kan
pMF115	pL2M-P19-kan-2x35S::Cyp1a2-GFP
pMF325	pL2M-P19-kan-2x35S::ZmCYP81A9-GFP
pMF326	pL2M-P19-kan-2x35S::ZmCYP81A9(CtoA)-GFP
pMF328	pL2M-P19-kan-2x35S::ZmCYP81A9(CtoS)-GFP

Table S5. Nucleotide sequences of the primers used for cloning and mutagenesis. The BsaI restriction sites for Golden Gate cloning are underlined. The BpiI restriction sites are marked in bold.

Lab number	**Name**	**Sequence**
oMF0033	FW_CYP71B7	TTGGTCTCAAATGTCAATCTTGCTCTGTTTCC
oMF0034	RV_CYP71B7	TTGGTCTCACACCATGATGAACAAGTGG
oMF0021	FW_CYP73A5	TTGGTCTCAAATGGACCTCCTCTTGC
oMF0022	RV_CYP73A5	TTGGTCTCACACCACAGTTCCTTGGTTTC
oMF0009	FW_CYP81D8	**TTGAAGACAA**AATGGAAACCAAAACCCTAATTTTC
oMF0010	RV_CYP81D8	**TTGAAGACAA**CACCAACGGACTCGTTGAAG
oMF0011	FW_CYP82C2	**TTGAAGACAA**AATGGATACTTCCCTCTTTTC
oMF0012	RV_CYP82C2	**TTGAAGACAA**CACCCACATAAAGCCCTTC
oMF0013	FW_ATR1	TTGGTCTCAAATGACTTCTGCTTTGTATGC
oMF0014	RV_ATR1	TTGGTCTCACACCCCAGACATCTCTGAG
oMF0224	FW1_CYP81A9	TTGGTCTCAAATGGACAAGGCTTACATTGCTGCTC
oMF0225	RV1_CYP81A9_CtoA	TTGGTCTCAAGCCTTACGTCTGCCCATGCC
oMF0226	RV1_CYP81A9_CtoS	TTGGTCTCAAGACTTACGTCTGCCCATGCC
oMF0227	RV2_CYP81A9	TTGGTCTCACACCCAGCCTCTTAAGCACACCCCTC
oMF0228	FW2_CYP81A9_CtoA	TTGGTCTCAGGCTCCTGGTGAAACTCTTGCTC
oMF0229	FW2_CYP81A9_CtoS	TTGGTCTCAGTCTCCTGGTGAAACTCTTGCTCTTAGG

*FW, forward; RV, reverse

Table S6. Codon-optimised nucleotide sequences for *in planta* expression. The BpiI restriction sites for Golden Gate cloning are marked in bold and underlined.

Cyp1a2	**TTGAAGACAA**AAATGGCGTTCTCCCAGTACATCTCCTTAGCCCCAGAGCTGCTACTGGCCACTGCCATCTTCTGTTTAGTGTTCTGGATGGTCAGAGCCTCAAGGACCCAGGTTCCCAAAGG CCTGAAGAATCCACCCGGACCCTGGGCTTGCCCTTCATTGGGCACATGCTGACTGTGGGGAAGAACCCACACCTGTCACTGACACGGCTGAGTCAGCAGTATGGGGACGTGCTGCAGA TCCGCATCGGCTCCACTCCTGTGGTGCTGAGCGGCCTGAACACCATCAAGCAGGCCCTGGTGAGGCAGGGAGATGACTTCAAGGGCCGACCAGACCTCTACAGCTTCACACTTATCA CTAACGGCAAGAGCATGACTTCAACCCAGACTCTGGACCCGTGTGGGCTGCCCGCCGGCGCCTGGCCCAGGATGCCCTGAAGAGCTTCTCCATAGCCTCGGACCCGACGTCAGCATCCT CTTGCTATTTGGAGGACACGTGAGCAAGGAGGCTAACCATCTCGTCAGCAAGCTTCAGAAGGCGATGGCAGAGGTTGGCCACTTCGAACCAGTCAGCCAGGTGGTGGAATCGGTGGCT AACGTCATTGGTGCCATGTGCTTTGGGAAGAACTTCCCCCGGAAGAGCGAGGAGATGCTCGAACATCGTGAATAACAGCAAGGACTTTGTGGAGAATGTCACCTCAGGGAATGCAGTGGA CTTCTTCCCGGTCCTGCCGCTACCTGCCCCAACCCGGCCCTCAAGAGGTTTAAGACCTTCAATGATAAACTTCGTGCTGTTTCTGCCAGAAAACTGTCCAGGAGCACTACCAAGACTTCAACAAG AACAGTATCCAAGACATCACAAGTGCCCTGTTCAAGCACAGCGAGAACTACAAAGACAATGGCGGACTCATCCCCGAGGAGAAGATTGTCAACATTGTCAATGACATCTTTGGAGCTGG CTTTGACACAGTCACCACAGCCATTTTGCTACTTGTGACATGGCCTAACGTGCAGAGGAAGATCCATGAGGAGCTGGCGTTGGTTGGCACGGGATCGGCAACCAC GGCTTTCTGACCGTCCCCAGCTGCCATATCTAGAGGCCTTCATCCTGGAGATCTACCGATACACATCCTTTGTCCCCTTCACCATCCCCCACAGCACAACGAGGACACCTCACTGAATGG CTTCCACATTCCCAAGGAGCGCTGTATCTACATAAACCAGTGGCAGGTCAACCATGATGAGAAGCAGTGGAAACACCCTTTGTGTTCCGCCCAGCAGCGGTTTCTTACCAATAACAACTC GGCCATCGACAAGACCCAGAGCGAAAGGTGATGCTCTTCGGCTTGGGAAAGCGCCCGGTGCATTGCGGGAAGTATTCCTCTTCTTAGCCATCCTCGCTGCAGC ATCTGGAGTTTAGTGTGCCACCGGGTGTGAAGGTGGACCTGACACCCAACTATGGGTTGACCATGAAGCCCGGGACCTGTGAACACGTCCAGGCATGGCCATCGCCAGGCTTTTCCAAGGGTGTT**GC** **TCTTCAA**
Cyp2d29	**TTGAAGACAA**AAATGGACCTCGTGGTGTTCCTTGCTCTTACCCTGTCTTGCCTTATCCTGCTGTCTCTTTGGAGGCAGTCATCTGGTAGAGGTAAGCTTCCTCCTGGTCCTACTCCCTTCCTA TTATCGGTAACTTCCTGCAGATCGAACGTGAAGAACATCAGCCAGAGCTTCACCAACTTCAGCAAGGCTTACGGTCCTGTGTTCACCCTTTACCTGGGTTCTAAGCCTACCGTGATTCTGCAT GGTTACGAGGCTGTGAAAGAGGCTCTTATCGATAGGGGTGAAGAGTTTGCTGGTAGGGGCTCTTTTCCGATGCCGAAAGATCATCAAAGGCTTCGGTGTTCAGCAACGGCAAT AGATGGAAAGAGATGCGGAGGTTCACCCTGATGACCTTAGGAATCTTGGCATGGGCAAGCGTAACATCGAGGATAGGGTTCAAGAAGAGGCTCAGTGCCTTGTGGAAGAGTTGAGAA AGACCAAGGGCTCTCCTTGCGATCCTACTTTATTCTGTCTTGCGCTCCGTGCAACGTGATCTGCTCTATCATTTTCCAGAACAGGTTCGACTACAAGGACAAAGAATTCCTGATCCTGATG GACAAGATCAACGAGAACGTGAAGATCCTGTCCTCCATGGCTTCAGGTGTGCAACTCTTTCCCTTCTCGATCGAATTACTGCCCTGGCTCTCACCACAAGATTGTGAAGAACTTCAACT ACCTGAAGTCCTACCTGCTCGAGAAGATCAAAGAGCACAAAGAAAGCCTGGACGTGACTTCATTGACTACTACCTGATCAAGCAGAAGCAGGTCAACCACATCGA GCAGTCTGAGTTCAGCCTTGAGAACCTGGCTAGCACCATCAACGATTTCGTTCGGTGCTGGTACTGAGACTACCTCTACTACTCTTAGGTACGCTCGTCCTGCTGCTTGAAGTACCCTGATG TTACTGCTAAGGTGCAAGAAGAGATCGACCGAGTTGTTGGTAGGCATAGGTCACCTTGCATGCAGGATAGGTCACACACATGCCTTACATGAGGTGCAGCGGTTCA TTGATCTGCTGCCTACTTCTTTGCCTCACGCTGTGACCTGCGACATCAAGTTTCGGAAGTACTTGATCCCTAAGGGCACAACCGTGATCAACCAGCCTTTCTTCAGTGCTGCACGACAGCAAA GAGTTCCCGAATCCTGAGATGTTCGATCCTGGTCACTTCCTGAACGGTAACGGCAACTTCAAGAAAAGCGACTACTTCATGCCGTTCTCCACCGGTAAGAGAATTTGTGCTGGTGAGGGTC TTGCCCGGATGGAACTTTTCCTTATTCTGACCACCATCCTGCAGAATTTCAAGCTGAAGTCTCTGGTGCACCCCAAAGAGATTGATATCACCCCTGTGATGAACGGATTT**GTCTTCAA** **TTGTCTTCAA**
CYP81A9	**TTGAAGACAA**AAATGGACAAGGCTTACATTGCTGCTCTGTCTGCTGCTCTTTTCCTTCTCACTACCTGCTTGGTAGACGTGCTGGTGGTGAAGGTAAGGCTAAAGCTAAGGGCTCTAG AAGAAGGCTGCCTCCTTCACCTCCTGCTATTCCTTTCTTGGGTCACCTCCATTCCATGGTGCTCTTTGCTAGACTTGCTGCTAGGCCATGGTCCTGTGTTCTCTATGAG ACTTGGAACTCGGAGGGCTGTCGTGGTTTCTTCACCTGAATTGTGCTAGGGAATGCTTCACCGAGCACGATGTGAATTTCGCTAACAGCCTCTGTTCCCGTCTATGAGGCTTGCTTCTTTCG ATGGCGCCTATGCTGAGCGTGTCAAGCTATGGTCCTTATTGGAGGAACCTTAGGCGTGTTGCTGCTGTGCAACTTCTTTCAGCTCATAGAGTGGGTTGCATGCCTCCAGCTATTGAAGCTCAG GTGAGAGCTATGGTGAGAAGGATGGATAGAGCTGCTGCAGCTGGTGGCGGTGGTGTTGCTAGAGTTCAACTTAAGAGAAGGCTGTTCGAGCTGAGCTGTCTGTGCTGATGGAAACTATT GCTCACACCAAGACCAGCAGAGCTGAGGCTGATGCTGATAGCGATATGTCTACTGAGGCCCACGAGTTCAAGCAGATTGTGGATGAGCTTCCTTGCCTTCACATCGGCACTGCTAACAGGTGG GATTACCTTCCTGTGCTGAGATGGTTCGATGTGTTCGGTGTGAGGAACAAGATCCTGGATGCTGTTGGTAGAAGGGATGCTTTCCTTGGCAGGCTTATCGATGGTGAGAGAAGGCGTCTTG ATGCTGGTGATGAGAGCGAGAGCAAGTCAATGATTGCTGTGCTTCTGACCCTGCAGAAGTCTGAGCCTGAGGTTTACACCGATACCGTGATTACTGCTCTGTGCGCTAACCTTTTCGGTGC TGGTACTGAGACTACTTCTACTACTACCGAGTGGGCCATGAGCCCTGTTTTGAATCATAGAGAAGGCCCAGGCTGAAATTGATGCTGCTGTTGGAACATCTAGGCTGGT GACTCGCTGATGATGTGCCTCACCTTACTTACCTGCAGTGCATCGTGGATGAGACTCTTAGGCTTCCTCATCGCTCCTCTGCTTTTGCCTCATGAATCTGCAGCTGATTGCACCGTTGGTGG TTACGATGTTCCTAGGGGTACTATGCTGTTGTGAATGTGCATGCTGTGTGTGGGAAGATCCTGATAGATTCGTTCCCGAGAGGTTCGAAGGTGCTGGCGGTAAG GCTGAAGGTAGACTTCTTATGCCTTTCGGCATGGGCAGACGTAAGTGTCCTGGTGAAACTCTTGCTCTTAGGACCGTGGGTCTTGTGCTTCAGTGCTTCGATTGGGATACC GTGGATGGTGCTCAAGTGGACATGAAGGCTTCAGGTGGTCTTACTATGCCTAGGCTATGTGCAGACCTAGAACTGCTATGAGCGGGTGTGCTTAAGAGGCCTGGGTG**TT** **GTCTTCAA**

Chapter 3: CYP450 profiling: a new tool to study fungicide metabolism in the wheat pathogen *Zymoseptoria tritici*

Maria Font Farre[1], Daniel Brown[2], John Sinclair[3], Urvashi Thacker[3], Sian Deller[3], Ian Southworth[3], Samantha Hall[3], Richard Dale[3], Melloney Morris[3], Aaron Wright[4], Jonathan Burton[2] and Renier A.L. van der Hoorn[1]

[1] The Plant Chemetics Laboratory, Department of Plant Sciences, University of Oxford, Oxford, UK.

[2] The Burton Group, Department of Chemistry, University of Oxford, Oxford, UK.

[3] Bioscience, Syngenta, Jealotts Hill International Research Centre, Bracknell, UK.

[4] Chemical Biology & Exposure Sciences, Pacific Northwest National Laboratory, Richland WA USA; The Gene and Linda Voiland College of Chemical Engineering and Bioengineering, Washington State University, Pullman WA USA.

Abstract

Among the detoxifying enzymes, CYP450s are the largest and most versatile family of enzymes having xenobiotic metabolising activities in all kingdoms of life. Although CYP450s are well characterised detoxifying enzymes in animals and plants, little is known about the role of this large family of enzymes in fungicide detoxification. Fungicides are a key player in maintaining crop production in wheat fields by controlling *Septoria tritici* blotch (STB) caused by *Zymoseptoria tritici* infections. However, the development of multiple fungicide resistance and cross-resistance is a threat to the future of disease control in agriculture. Here, we show the use activity-based probes to study the role of CYP450s in fungicide detoxification in the plant pathogen, *Zymoseptoria tritici*. Using chemical proteomic analysis, we report the enrichment of *Z. tritici* CYP450s by three independent CYP450 probes and we confirm CYP450 labelling of *Zt*CYP450s upon transient expression in *N. benthamiana*. Furthermore, using competitive activity-based protein profiling, we support the role for cyprodinil detoxification capacity of *Z. tritici* CYP5080H1. Thus, the use of CYP450 activity-based probes in the wheat pathogen *Z. tritici* provides important new insights into the involvement of CYP450s in fungicide detoxification, establishing a powerful tool to study xenobiotic detoxification in fungal plant pathogens.

Introduction

Zymoseptoria tritici (*Zt*, formerly *Septoria tritici*, *Mycosphaerella graminicola* (telomorph)) is a hemibiotrophic plant fungi that causes the *Septoria tritici* blotch (STB) in wheat. *Z. tritici* is considered one of the top 10 most important fungal plant pathogens, being the most economically damaging disease of wheat in Europe (Dean *et al.*, 2012; Kettles and Kanyuka, 2016). Disease management is mainly achieved by the use of fungicides together with resistant cultivars, together with several cultural practices such as delayed planting and crop rotation (Fones and Gurr, 2015; Ponomarenko *et al.*, 2011).

Fungicides are a key player in maintaining crop production in wheat fields. In Europe, nearly 70% of the total of fungicides used on cereals is applied to control STB (Ponomarenko *et al.*, 2011). In consequence of this intensive antifungal application, *Z. tritici* populations have developed different degrees of resistance to the four major single-site fungicide classes used to control STB (Hayes *et al.*, 2016; McDonald *et al.*, 2019). While it is known that *Z. tritici* populations have acquired full resistance against methyl benzimidazole carbamates (MBCs) and quinone outside inhibitors (QoIs) in the field, effectiveness of demethylation inhibitors (DMIs or azoles) has been substantially decreased (Fedoryshchak *et al.*, 2020; McDonald *et al.*, 2019). Furthermore, field monitoring studies have already reported cases of *Z. tritici* with decreased sensitivity to the newest fungicide class introduced to control STB, the succinate dehydrogenase inhibitors (SDHIs) (Dooley *et al.*, 2016; Rehfus *et al.*, 2018). Therefore, the current most effective way to control STB in the field is by using fungicide mixtures to delay *Z. tritici* sensitivity shifts and resistance development (Garnault *et al.*, 2019; Torriani *et al.*, 2015).

Fungicide resistance can be achieved by different mechanisms. In *Z. tritici*, the most common resistance mechanism for single-site fungicides is the modification of the target site (Mullins *et al.*, 2011). In the case of QoIs, a single glycine to alanine (G143A) mutation in the mitochondrial cytochrome *b* enzyme explains the majority of QoI resistance found in field isolates (Cheval *et al.*, 2017; Sierotzki and Scalliet, 2013). Since it first discovery in the United Kingdom in 2001, QoI-resistant *Z. tritici* isolates have been detected across Europe and have also been reported in over 30 other plant fungal pathogens (Fraaije *et al.*, 2005). Similarly, *Z. tritici* resistance to SDHI fungicides has been primarily attributed to several mutations at the three subunits (SdhB, SdhC and SdhD) of the succinate dehydrogenase (Sdh) enzyme (Dooley *et al.*, 2016; Rehfus *et al.*, 2018). So far, Sdh mutations is the only mechanism reported for SDHI resistance in the field, with more than 27 different mutations being identified in field isolates of different plant pathogens (Sierotzki and Scalliet, 2013).

Another mechanism of fungicide resistance is via the action of metabolising enzymes and efflux transporters, also known as xenobiotic detoxification (Sang and Hulvey, 2018). Xenobiotic detoxification plays a key role on the detoxification of drugs, pesticides and herbicides in animals and

plants (Li *et al.*, 2007; Siminszky, 2006; Yin *et al.*, 2019; Zanger and Schwab, 2013). The reduced sensitivity of fungal field isolates to different fungicide classes is usually attributed to multiple mechanisms of resistance. For instance, the decreased sensitivity of *Z. tritici* is a polygenic trait (Cools and Fraaije, 2013). The main cause of azole resistance is the accumulation of multiple point mutations in their target protein, the sterol 14-α-demethylase (CYP51), followed by the overexpression of CYP51 and the increased azole efflux by membrane transporters (Cools and Fraaije, 2013; Heick *et al.*, 2017).

Most fungicide detoxification studies have focused their attention on the role of phase III secretion systems, such as ATP-binding cassette (ABC) and the major facilitator superfamily (MFS) efflux transporter families, that can actively secrete cytotoxic compounds outside the fungal cell (Deising *et al.*, 2008). In *Z. tritici*, two transporter families confer multidrug resistance (Omrane *et al.*, 2015, 2017; Roohparvar *et al.*, 2007; Zwiers *et al.*, 2003). However, the involvement of metabolising enzymes, such as cytochrome P450s (CYP450s) and glutathione transferases (GSTs), in the detoxification of fungicides have been reported in only a few plant pathogenic fungi. Among the detoxifying enzymes, CYP450s are the largest and more versatile family of enzymes having xenobiotic metabolising activities in all kingdoms of life (Nelson and Nebert, 2018; Zanger and Schwab, 2013).

CYP450s are key enzymes in a wide range of important metabolic processes in fungi (eg. biosynthesis of strutural components, toxin production or xenobiotic detoxification) (Shin *et al.*, 2018). Generally, filamentous fungi have a higher number of CYPs than animals but a lower number than plants (Chen *et al.*, 2014). In fungal plant pathogens, the expansion and functional diversification of CYP450s has been associated with the evolution of their phytopathogenicity (Soanes *et al.*, 2008). Fungal CYP450s are classified into multigene families, following the general CYP450 nomenclature where CYP450s having 40% or greater amino acid identity are classified in the same family, and CYP450s having 55% or greater amino acid identity are classified in the same subfamily (Chen *et al.*, 2014). At present, fungal CYP450s are being assigned into CYP51-CYP69, CYP501-CYP699 and CYP5001-CYP6999 families and grouped in 15 clades based on their phylogenetic relationship (Chen *et al.*, 2014). Following the family number, subfamilies are indicated by a capital letter and gene isoforms by a number.

Although CYP450s are well characterised detoxifying enzymes in animals and plants, little is known about the role of this large family of enzymes in fungicide detoxification in phytopathogens. To date, the detoxification of fungicides through CYP450 metabolising activity has only been reported in the fungal plant pathogens *Botrytis cinerea*, *Magnaporthe oryzae* and *Sclerotinia homoecarpa* (Billard *et al.*, 2011; Sang and Hulvey, 2018; Wang *et al.*, 2018; C. Zhang *et al.*, 2020). First evidence of CYP450-based detoxification of fungicides was in Botrytis species, when the deletion of CYP684 in *B. pseudocinerea* (*Δcyp684)* caused loss of its naturally resistant phenotype against fenhexamid (Billard *et al.*, 2011). In

M. oryzae, RNA-seq analyses uncovered the upregulation of three CYP450s (MGG_01353, MGG_02239 and MGG_09920) in a SYP-34773-resistant field isolate (C. Zhang *et al.*, 2020). Furthermore, overexpression of three CYP450s (CYP561, CYP65 and CYP68) in a drug-sensitive *S. homoecarpa* strain resulted in an increased fungicide resistance against several classes of fungicides (Sang and Hulvey, 2018). Likewise, CYP561 and CYP65 overexpression in *S. homoecarpa* caused faster metabolization of the fungicide chlorothalonil (Green *et al.*, 2018).

The development of multiple fungicide resistance and cross-resistance is a threat to the future of disease control in agriculture. Therefore, identifying the main players involved in multidrug resistance pathways is crucial. Chemical proteomic technologies can be used to monitor protein activities and identify small-molecule target proteins. Activity-based protein profiling (ABPP) relies on the derivatization of reactive molecules with a reporter tags (e.g. fluorescent tags, affinity tags, or chemical tags such as azide or alkyne) for the selective detection, enrichment and identification of specific enzyme families (Kovács and van der Hoorn, 2016). CYP450 activity-based probes were first designed and used to detect the activity of CYP450s in mammalian systems (Wright *et al.*, 2009; Wright and Cravatt, 2007). Cravatt and co-workers derivatised known CYP450 mechanism-based inhibitors such as the suicide inhibitor 2-ethynylnaphthalene (2EN) and successfully labelled and identify mouse and human CYP450s targeted by the chemical probes. Furthermore, CYP450 probes enabled the identification of mouse CYP450s activated and inhibited upon drug treatment and the monitoring response of CYP450s when using aromatase inhibitors, currently used for breast cancer treatments. In Chapter 2, we also successfully used a set of these CYP450 probes to label and detect the activity of plant CYP450s, including the well-studied herbicide-detoxing CYP81A9 from maize and several *Nicotiana benthamiana* CYP450s. Here, we applied the use of chemical CYP450 probes to study the role of CYP450s in fungicide metabolism of *Z. tritici*.

Results

Activity-based CYP450 probes target several CYP450s from *Zymoseptoria tritici*

To check the potential use of CYP450 probes to study fungi CYP450s, we selected a set of six CYP450 probes to be tested on *Z. tritici* (Figure 1A). *Z. tritici* was grown in liquid cell cultures and microsomes were isolated via ultracentrifugation. The obtained microsomal fraction was incubated with 5 μM DB088 probe in the presence or absence of NADPH. After one-hour incubation, labelled proteins were coupled to a fluorophore reporter tag via click chemistry and visualised by in-gel fluorescence scanning. As the majority of *Z. tritici* CYP450s have a predicted molecular weight of 50-65 kDa, we expected to observe NADPH-dependent signals at the height of the 55 kDa marker band. Unfortunately, no NADPH-dependent signal was detected around 55 kDa when labelling *Z. tritici* microsomes with DB088, apart from the click chemistry background (Figure 1B).

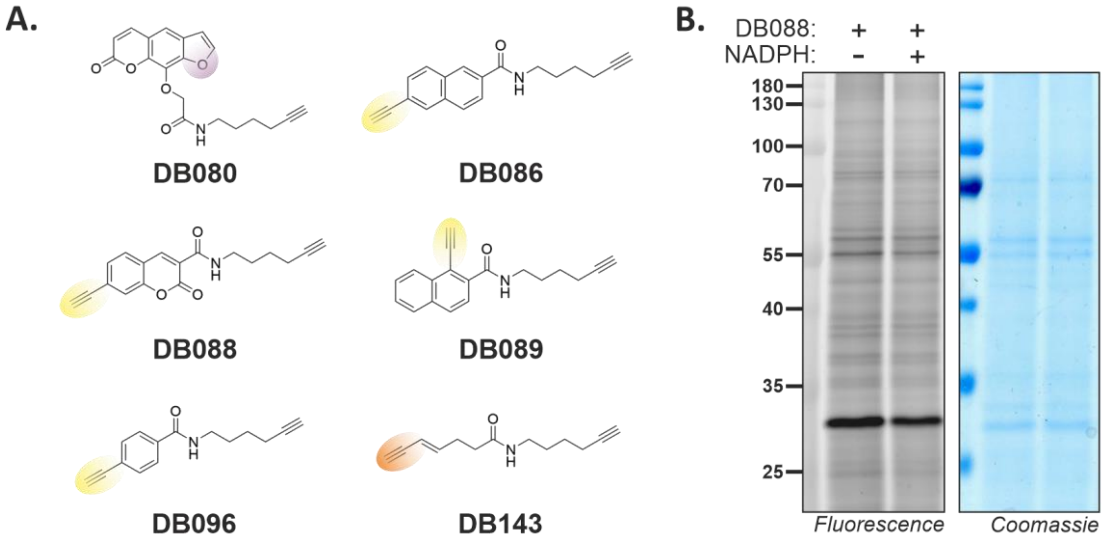


Figure 1. No detectable activity-based profiling of *Zymoseptoria tritici* Cytochrome P450s by in-gel fluorescence. **A**, Chemical structures of CYP450 activity-based probes used in this study. Reactive groups are coloured: in yellow, alkyne-based reactive group; in purple, furan-based reactive group; in orange, enyne reactive group. All probes carry an alkyne tag (right) for reporter tag (fluorophore/biotin) coupling via click chemistry. **B**, No detectable NADPH-dependent labelling of *Z. tritici* microsomes. *Z. tritici* was grown in liquid culture and microsomes were isolated via ultracentrifugation. Microsomes were incubated with 5 μM DB088 in the presence or not of NAPDH for 1h. Labelled proteins were coupled to a fluorophore via click chemistry, separated in an SDS-PAGE gel and visualised by in-gel fluorescence scanning. Coomassie staining is shown as loading control. Similar results were obtained in an additional independent replicate.

We next performed a large-scale CYP450 labelling followed by streptavidin enrichment pull-down to maximise the CYP450 signal detection by target enrichment. CYP450 labelling was performed as before with the difference that labelled proteins were coupled via click chemistry to a biotin reporter tag and enriched via streptavidin bead pull-down. First, we compared the labelling enrichment between the

click control (CC) sample and the probe-containing samples (DB080/DB086/DB096) by protein blot with streptavidin-HRP (Figure 2, first panel). Unfortunately, no clear CYP450 labelling or pull-down enrichment was observed for any of the three CYP450 probes used. For DB080 and DB096, we observed a signal at around 49 kDa but this band was also observed it in the click control sample (CC), suggesting that the band was caused by click chemistry background. When using DB086, we detected increased signal intensity of the whole labelling profile so we could not attribute the increased signal intensity in the 49 kDa zone to specific CYP450 labelling. When using mouse liver microsomes, we did observe the labelling difference between the click control and the three CYP450 probes (Figure 2, second panel). While the click control sample did not show any signal at approximately 49 kDa, we detected specific signals at the correspondent molecular weight of CYP450s for all the three used probes.

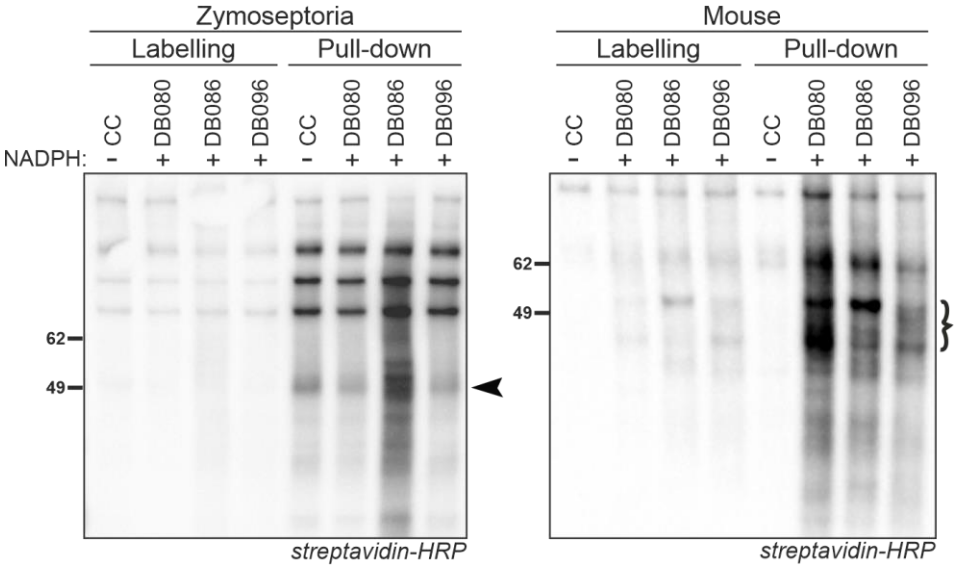


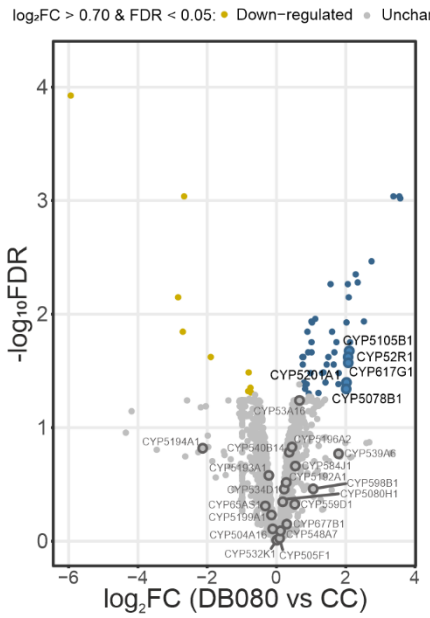
Figure 2. Protein blot analyses of the CYP450 labelling and enrichment pull-downs of CYP450 probes (DB080, DB086 and DB096) in *Zymoseptoria tritici* and mouse liver microsomes. Microsomes from *Z. tritici* cell cultures and mouse liver microsomes were incubated with 30 μM CYP450 probe (DB080, DB086 and DB096) or an equal volume of DMSO in the presence of 1 mM NADPH for 1h. Labelled proteins were subjected to click chemistry for biotin attachment and enriched via streptavidin pull-down. Labelled samples (Labelling) together with enriched labelled samples (Pull-down) were loaded in an SDS-PAGE gel and visualised by streptavidin-HRP protein blot. Coomassie staining is shown as protein abundance control. CC corresponds to the click chemistry control., Protein blot analyses of the CYP450 labelling and enrichment pull-downs of CYP450 probes (DB080, DB086 and DB096) and the click chemistry control (CC) in *Z. tritici* microsomes.

To have a more sensitive read-out we combined *Z. tritici* CYP450 labelling and enrichment with mass-spectrometry analysis. DB080, DB086 and DB096-labelled proteins were coupled to a biotin affinity tag, enriched by streptavidin pull-down, on-bead digested with Lys-C and trypsin and further analysed by liquid chromatography-tandem mass spectrometry (LC-MS/MS). DB080 pull-down enriched a total of 45 proteins, of which 5 where identify as annotated *Zt*CYP450s (Figure 3, first panel). DB086 pull-down enriched a total of 404 proteins, of which 18 where identify as annotated *Zt*CYP450s (Figure 3, second panel). A total of 43 proteins were enriched with DB096, of which 12 were identified as annotated

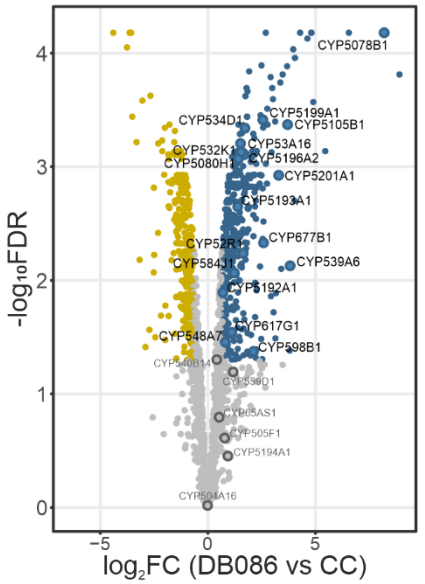
*Zt*CYP450s (Figure 3, third panel). Among all probes, when comparing the enrichment of proteins between the click chemistry control and probe containing samples, the top enriched protein was CYP5078B1 with a log_2FC enrichment of 9.4 upon DB096 labelling. The other CYP450s enriched by DB096 were all enriched by fold changes between 1.3 and 4.8. CYP5078B1 was also detected as top CYP450 labelled by DB086 with a fold change enrichment of 8.2. A large number of proteins were found to be enriched upon DB086 labelling, indicating a more promiscuous labelling of DB086 in *Z. tritici* microsomes. This mass spectrometry data corresponds with the overall higher intensity profile of DB086 labelling observed by western blotting analysis. We observed a weaker enrichment of *Zt*CYP450s by DB080 as all enriched CYP450s were detected with a lower fold change enrichment (log_2FC of approximately 2), suggesting that the same *Zt*CYP450s react with the furan reactive group but in a weaker manner.

To further validate *Zt*CYP450 labelling by CYP450 probes, we independently repeated DB096 proteomic labelling using three independent biological replicates of *Z. tritici* microsomes. This time, five out the seven enriched proteins in DB096 samples were identified as CYP450s (Figure 4, blue dots). As detected before, most of the detected proteins were not different between DB096 and CC (Figure 4, grey dots). Likewise, CYP5078B1 was the top CYP450 labelled by DB096 with a log_2FC of 7.11 (Figure 4, table).

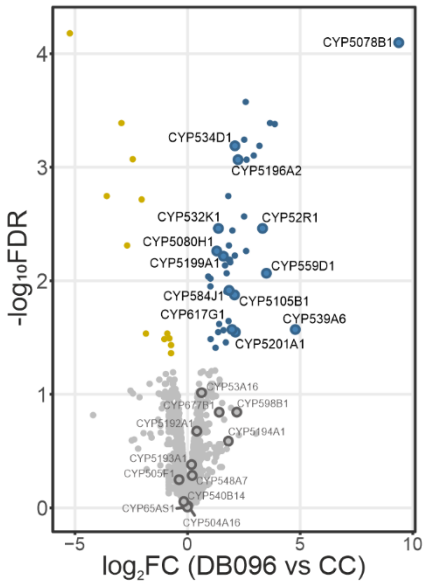
To confirm *Z. tritici* CYP450 labelling by CYP450 probes we cloned and overexpressed *Zt*CYP450s by agroinfiltration in *N. benthamiana*. We selected four *Z. tritici* candidates: three CYP450s that were consistently and significantly enriched in the two DB096 proteomic analyses (CYP5078B1, CYP539A6 and CYP52R1) and CYP5080H1, which is enriched but not always significantly in DB096 pull-downs. All four CYP450s were amplified from *Z. tritici* cDNA, cloned into the golden gate binary vector pJK268c and *in planta* expressed by agroinfiltration. *Zt*CYP450s were fused C-terminally to GFP to ensure its detection by western blotting and shift its labelling signal above the rubisco background signal in in-gel fluorescence scans (Chapter 2). *N. benthamiana* plants were agroinfiltrated with the *Zt*CYP450 constructs and leaf tissue was harvested four days after. Microsomes were isolated via ultracentrifugation and incubated with 5 μM probes in the presence or absence of NADPH for an hour. Labelled proteins were coupled to a fluorophore via click chemistry and detected by in-gel fluorescence scanning. Interestingly, all four GFP-tagged *Zt*CYP450s showed specific labelling against the different CYP450 probes and were robustly labelled by at least three of the six CYP450 probes (Figure 5). While DB086 labelled CYP5078B1 most strongly, DB088 labelled CYP52R1 and CYP5080H1 most strongly. Although all *Zt*CYP450s were detected to be enriched in the DB096 proteomic analysis, DB096 labelling was one of the weakest signals for all the overexpressed *Z. tritici* CYP450s. Overall, DB086 and DB088 were identified as best probes for labelling transiently overexpressed *Zt*CYP450s in *N.benthamiana*.



	Up-regulated				
	Name	UniProtKB	log_2FC	MS int.	FDR
1	CYP5105B1	F9WYQ3	2.10	23.36	0.05
2	CYP617G1	F9X140	2.07	26.91	0.05
3	CYP52R1	F9XML6	2.07	26.17	0.05
4	CYP5201A1	F9XIL1	2.02	25.11	0.05
5	CYP5078B1	F9X0K1	2.01	25.67	0.05
	Unchanged				
6	CYP539A6	F9XDL6	1.79	24.94	ns
7	CYP598B1	F9XJ19	1.06	23.69	ns
8	CYP53A16	F9X127	0.66	26.36	ns
9	CYP584J1	F9X9F0	0.54	24.71	ns
10	CYP559D1	F9X4J0	0.53	24.67	ns
11	CYP5196A2	F9XHE6	0.45	27.08	ns
12	CYP5193A1	F9WXK9	0.40	22.85	ns
13	CYP540B14	F9X9B9	0.37	26.28	ns
14	CYP677B1	F9X3L5	0.30	24.03	ns
15	CYP5192A1	F9WYJ8	0.28	26.06	ns
16	CYP534D1	F9XDA4	0.22	26.60	ns
17	CYP5080H1	F9X6Z0	0.18	27.52	ns
18	CYP548A7	F9XQ69	0.12	26.60	ns
19	CYP505F1	F9X5V5	0.09	23.02	ns
20	CYP532K1	F9XNX8	0.01	26.45	ns
21	CYP504A16	F9X1J4	-0.11	27.61	ns
22	CYP5199A1	F9XFL7	-0.14	25.59	ns
23	NA	F9XJP5	-0.22	28.29	ns
24	CYP65AS1	F9WWF0	-0.32	23.45	ns
25	NA	F9XBQ2	-0.97	24.51	ns
26	CYP5194A1	F9XH77	-2.13	22.68	ns

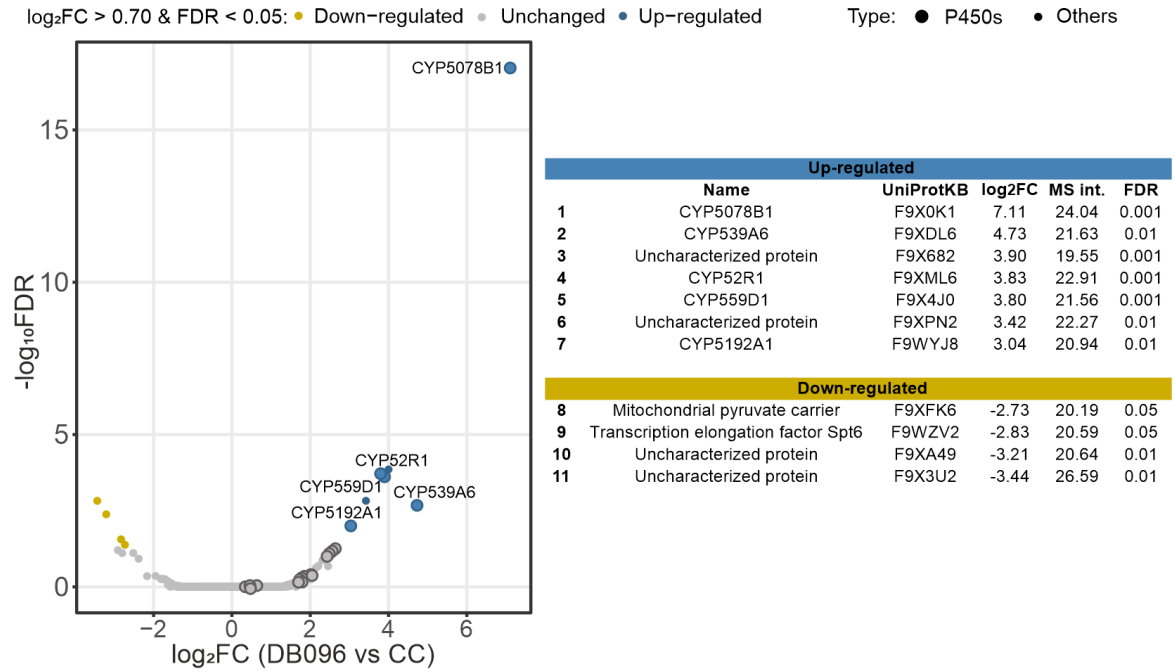


	Up-regulated				
	Name	UniProtKB	log_2FC	MS int.	FDR
1	CYP5078B1	F9X0K1	8.19	25.67	0.001
2	CYP539A6	F9XDL6	3.82	24.94	0.01
3	CYP5105B1	F9WYQ3	3.70	23.36	0.001
4	CYP5201A1	F9XIL1	3.29	25.11	0.01
5	CYP677B1	F9X3L5	2.59	24.03	0.01
6	CYP5199A1	F9XFL7	2.56	25.59	0.001
7	CYP598B1	F9XJ19	2.12	23.69	0.05
8	CYP534D1	F9XDA4	1.73	26.60	0.001
9	CYP5196A2	F9XHE6	1.69	27.08	0.001
10	CYP52R1	F9XML6	1.64	26.17	0.01
11	CYP53A16	F9X127	1.56	26.36	0.001
12	CYP532K1	F9XNX8	1.52	26.45	0.001
13	CYP5080H1	F9X6Z0	1.42	27.52	0.001
14	CYP5193A1	F9WXK9	1.39	22.85	0.01
15	CYP584J1	F9X9F0	1.23	24.71	0.01
16	CYP617G1	F9X140	1.11	26.91	0.05
17	CYP548A7	F9XQ69	0.81	26.60	0.05
18	CYP5192A1	F9WYJ8	0.70	26.06	0.05
	Unchanged				
19	CYP559D1	F9X4J0	1.18	24.67	ns
20	CYP5194A1	F9XH77	0.93	22.68	ns
23	CYP505F1	F9X5V5	0.78	23.02	ns
22	CYP65AS1	F9WWF0	0.52	23.45	ns
24	NA	F9XBQ2	0.48	24.51	ns
19	CYP540B14	F9X9B9	0.42	26.28	ns
26	CYP504A16	F9X1J4	-0.01	27.61	ns
20	NA	F9XJP5	-0.31	28.29	ns



	Up-regulated				
	Name	UniProtKB	log2FC	MS int.	FDR
1	CYP5078B1	F9X0K1	9.38	25.67	0.001
2	CYP539A6	F9XDL6	4.78	24.94	0.05
3	CYP559D1	F9X4J0	3.50	24.67	0.01
4	CYP52R1	F9XML6	3.33	26.17	0.01
5	CYP5196A2	F9XHE6	2.24	27.08	0.001
6	CYP5201A1	F9XIL1	2.12	25.11	0.05
7	CYP534D1	F9XDA4	2.10	26.60	0.001
8	CYP5105B1	F9WYQ3	2.08	23.36	0.05
9	CYP617G1	F9X140	1.97	26.91	0.05
10	CYP584J1	F9X9F0	1.84	24.71	0.05
11	CYP5199A1	F9XFL7	1.59	25.59	0.01
12	CYP532K1	F9XNX8	1.37	26.45	0.01
13	CYP5080H1	F9X6Z0	1.29	27.52	0.01
	Unchanged				
14	CYP598B1	F9XJ19	2.18	23.69	ns
15	CYP5194A1	F9XH77	1.81	22.68	ns
16	CYP677B1	F9X3L5	1.40	24.03	ns
17	CYP53A16	F9X127	0.62	26.36	ns
18	CYP5192A1	F9WYJ8	0.41	26.06	ns
19	CYP5193A1	F9WXK9	0.20	22.85	ns
20	NA	F9XJP5	0.17	28.29	ns
21	CYP548A7	F9XQ69	0.15	26.60	ns
22	CYP540B14	F9X9B9	0.03	26.28	ns
23	CYP504A16	F9X1J4	0.02	27.61	ns
24	CYP65AS1	F9WWF0	-0.01	23.45	ns
25	CYP505F1	F9X5V5	-0.17	23.02	ns
26	NA	F9XBQ2	-0.38	24.51	ns

Figure 3. Enrichment of *Zymoseptoria tritici* CYP450s enrichment by three CYP450 activity-based probes. Microsomes isolated from *Z. tritici* cell cultures were incubated with 30 μM CYP450 probe (DB080, DB086 and DB096) or an equal volume of DMSO in the presence of 1 mM NADPH for 1h. Labelled proteins were subjected to click chemistry for biotin attachment, enriched via streptavidin pull-down and analysed by LC-MS/MS. Volcano plots highlighting significant proteins depleted and enriched by DB080, DB086 and DB096 labelling of *Z. tritici* microsomes labelling. Enrichment is represented by the log_2FC (CYP450 probe/CC) against the significance ($-log_{10}FDR$) between the CC and each CYP450 probe (DB080, DB086 and DB096) using two technical replicates. The dots colour means whether proteins (dots) were enriched (blue), unchanged (grey) or depleted (yellow) in the CYP450 probe containing sample.



Up-regulated

	Name	UniProtKB	log2FC	MS int.	FDR
1	CYP5078B1	F9X0K1	7.11	24.04	0.001
2	CYP539A6	F9XDL6	4.73	21.63	0.01
3	Uncharacterized protein	F9X682	3.90	19.55	0.001
4	CYP52R1	F9XML6	3.83	22.91	0.001
5	CYP559D1	F9X4J0	3.80	21.56	0.001
6	Uncharacterized protein	F9XPN2	3.42	22.27	0.01
7	CYP5192A1	F9WYJ8	3.04	20.94	0.01

Down-regulated

8	Mitochondrial pyruvate carrier	F9XFK6	-2.73	20.19	0.05
9	Transcription elongation factor Spt6	F9WZV2	-2.83	20.59	0.05
10	Uncharacterized protein	F9XA49	-3.21	20.64	0.01
11	Uncharacterized protein	F9X3U2	-3.44	26.59	0.01

Figure 4. Mass spectrometry consistently identifies *Z. tritici CYP*450 as probe targets of DB096. Microsomes isolated from *Z. tritici* cell cultures were incubated with 30 μM DB096 or an equal volume of DMSO in the presence of 1 mM NADPH. Labelled proteins were subjected to click chemistry for biotin attachment, enriched via streptavidin pull-down and analysed by LC-MS/MS. Enrichment is represented by the log2FC (DB096/CC) against the significance (-log10FDR) between the CC and DB096 samples using n=3 biological replicates. The dots colour means whether proteins (dots) were enriched (blue), unchanged (grey) or depleted (yellow) in the DB096 sample.

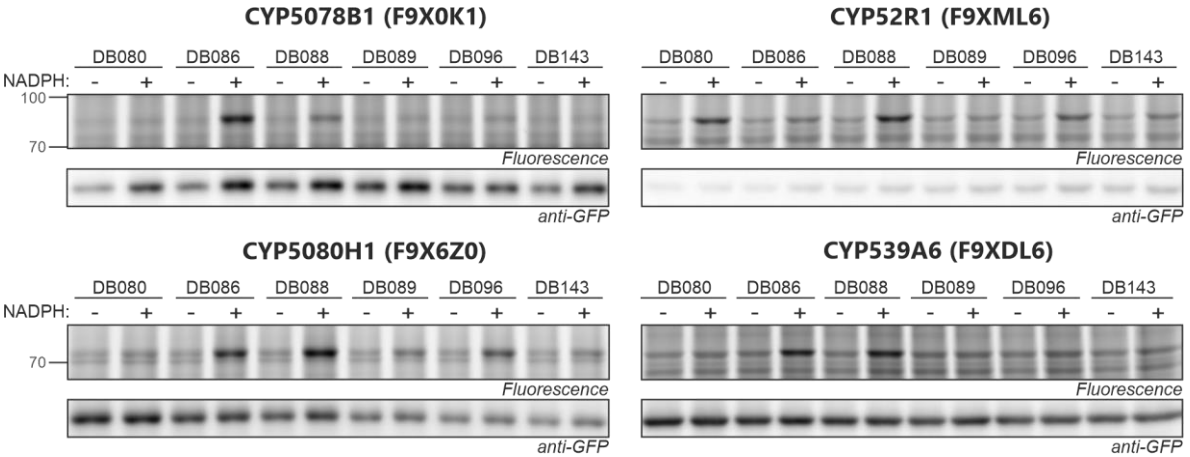
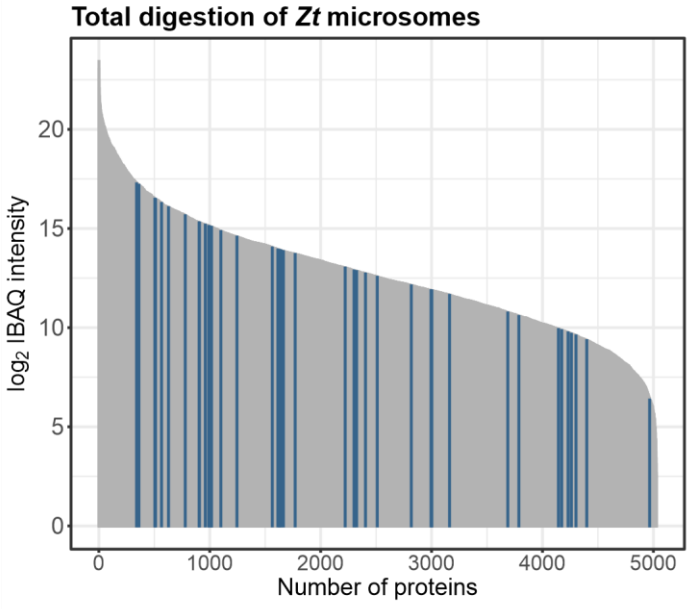


Figure 5. Validation of *Zymoseptoria tritici* CYP450s as main targets of CYP450 activity-based probes. NADPH-dependent labelling of four *Z. tritici* CYP450s transiently overexpressed in *N. benthamiana*. Agroinfiltrated *N. benthamiana* leaf microsomes were isolated via ultracentrifugation and resuspended microsomes were labelled with 5 μM probe concentration in the absence or presence of 1 mM NADPH for 1h. Labelled proteins were coupled to a fluorophore via click chemistry and visualised by in-gel fluorescence scanning. Anti-GFP western blot is shown as protein expression and loading control. Same results were obtained in two additional independent replicates.

Next, we investigated whether the *Zt*CYP450s we found enriched in our chemical proteomic analyses corresponded to the most abundant CYP450s in *Z. tritici* microsomes or whether probes have different selectivity. Microsomes from isolated from cell cultures were digested with Lys-C and trypsin and generated peptides were analysed by LC-MS/MS. IBAQ values were obtained by dividing protein intensities by the number of theoretically observable tryptic peptides, and is on average highly correlated with protein abundance. Forty CYP450s were detected in the microsomal proteome of *Z. tritici*, which consisted of a total of around 5000 proteins (Figure 6). These *Zt*CYP450s were distributed all along the proteome, including two CYP450s (CYP504A16 and CYP61A1) in the top 10% most abundant proteins. Interestingly, the top CYP5078B1 always found significantly enriched by CYP450 probes ranked at position 2995, suggesting that probes are selective for specific CYP450s, and abundance in microsomes is not a limitation when using CYP450 probes.



CYP450s abundance in *Zt* microsomes					
Abundance ranking	Protein name	log_2 IBAQ	MS1 DB080	MS1 DB096	MS2 DB096
340	CYP504A16	17.25			
361	CYP61A1	17.18			
505	CYP534D1	16.48		7	
511	CYP53A16	16.46			
565	CYP51F1	16.26			
628	CYP5196A2	16.05		5	
779	CYP540B14	15.64			
904	CYP584J1	15.28		10	
907	CYP5080H1	15.28		13	
960	CYP559D1	15.17		3	4
991	CYP5201A1	15.10	4	6	
995	CYP548A7	15.10			
1014	CYP52R1	15.06	3	4	3
1015	CYP532K1	15.06		12	
1100	CYP5192A1	14.85			5
1245	CYP617G1	14.57	2	9	
1564	CYP548N1	14.02			
1614	CYP539A6	13.92		2	2
1629	CYP5194A1	13.90			
1642	CYP5193A1	13.87			
1664	CYP677B1	13.84			
1770	CYP65AM2	13.69			
2221	CYP598B1	13.01			
2301	CYP5199A1	12.86		11	
2324	CYP65AS1	12.83			
2404	CYP505F1	12.71			
2510	CYP5105B1	12.54	1	8	
2817	CYP598B2	12.11			
2995	CYP5078B1	11.86	5	1	1
3002	CYP578G1	11.86			
3162	CYP503D1	11.63			
3687	CYP5080G1	10.75			
3787	CYP596C1	10.57			
4144	CYP5128D1	9.91			
4173	CYP5196A1	9.85			
4231	CYP5191A1	9.74			
4260	CYP528A5	9.67			
4302	CYP584E9	9.59			
4399	CYP577A6	9.35			
4966	CYP543B1	6.35			

Figure 6. Cytochrome P450s are abundant and well-detected proteins in *Zymoseptoria tritici* microsomes. *Z. tritici* microsomes were digested with Lys-C and trypsin and digested peptides were analysed by LC-MS/MS. All proteins identified were ranked by their IBAQ spectral intensity and plotted against the log_2IBAQ intensity. The list of all P450s ranked by their log_2IBAQ intensity is on the right. MS1, CYP450s enriched, and ranked by log_2FC, in DB080 and DB096 proteomic pull-down presented on Figure 3. MS2, CYP450s enriched, and ranked by log_2FC, in DB096 proteomic pull-down presented on Figure 4.

Taken together, this data confirms that *Z. tritici* CYP450s are able to activate and become labelled by different CYP450 probes. *Zt*CYP450s have different reactivity towards CYP450 probes as we could detect differences in fluorescent probe labelling when we overexpressed four selected *Z. tritici* CYP450s by agroinfiltrations. This data indicates the selective activity-based labelling of *Z. tritici* CYP450s by several CYP450 probes.

Zymoseptoria tritici **CYP450s have distinct labelling characteristics**

The labelling experiments presented so far suggest that *Z. tritici* CYP450 might have different specificities and reactivities to the different CYP450 probes. Consequently, we tested the distinct labelling by the two best identified probes of CYP5078B1 and CYP5080H1 produced by agroinfiltration. First, we tested the optimal probe concentration required for CYP5078B1 and CYP5080H1 labelling (Figure 7A). CYP5078B1 labelling was saturated with 1 μM DB088 concentration and with 5 μM DB086 concentration. DB086 labelling was stronger than DB088 labelling as DB086 signal intensities doubled DB088 signal intensities at higher probe concentrations (Figure 7B, first panel). Contrarily, CYP5080H1 labelling was saturated at 5 μM for both DB086 and DB088. Both probes labelled CYP5080H1 to similar fluorescence signal intensities at around 5 μM probe concentration (Figure 7B, second panel).

Second, we generated a time course of labelling by DB086 and DB088 labelling using 5 μM concentration of probes (Figure 8A). CYP5078B1 was labelled within minutes when using DB086 and reached a maximum labelling intensity with longer time incubations, around 90-120 min (Figure 8B, first panel). By contrast, DB088 labelling of CYP5078B1 was slower and less intense than DB086 labelling. Oppositely, CYP5080H1 was labelled with DB088 within minutes and reached its maximum intensity (Figure 8B, second panel). CYP5080H1 labelling by DB086 reached similar intensity level than DB088 labelling, but reached a maximum labelling intensity with longer time incubations, around 90-120 min.

In conclusion, CYP5078B1 and CYP5080H1 seem to react differently to DB086 and DB088. CYP5078B1 is labelled faster and more intensely by DB086 than DB088 and CYP5080H1 has a higher turnover rate and faster labelling with DB088.

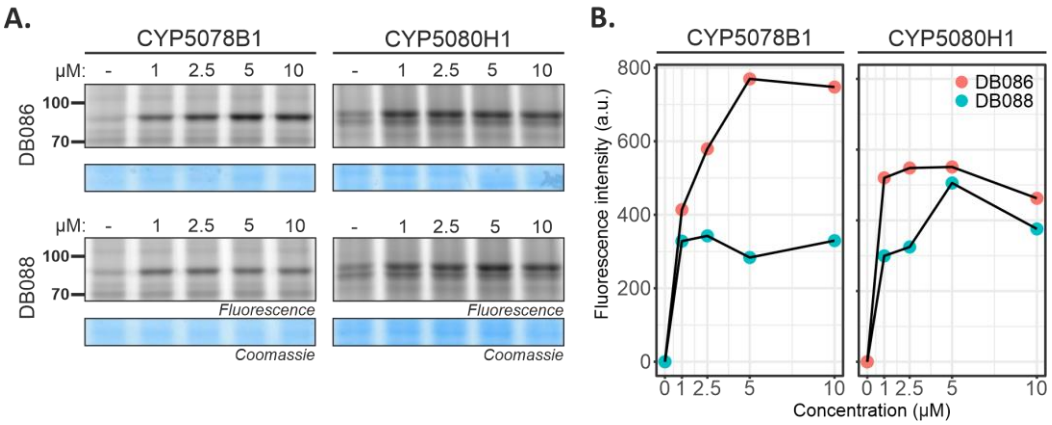


Figure 7. Probe concentration of DB086 and DB088 labelling of CYP5078B1 and CYP5080H1. A, *In planta* overexpressed CYP5078B1 and CYP5080H1 were labelled with different DB086 and DB088 probe concentration in the presence of 1 mM NADPH for 1h. Labelled proteins were coupled to a fluorophore via click chemistry, separated in an SDS-PAGE gel and visualised by in-gel fluorescence scanning. Coomassie staining is shown as loading control. Similar results were obtained in an additional independent replicate. **B**, Signal intensity quantification of DB086 and DB088 concentration course labelling of CYP5078B1 and CYP5080H1. Quantified signal intensities from section A.

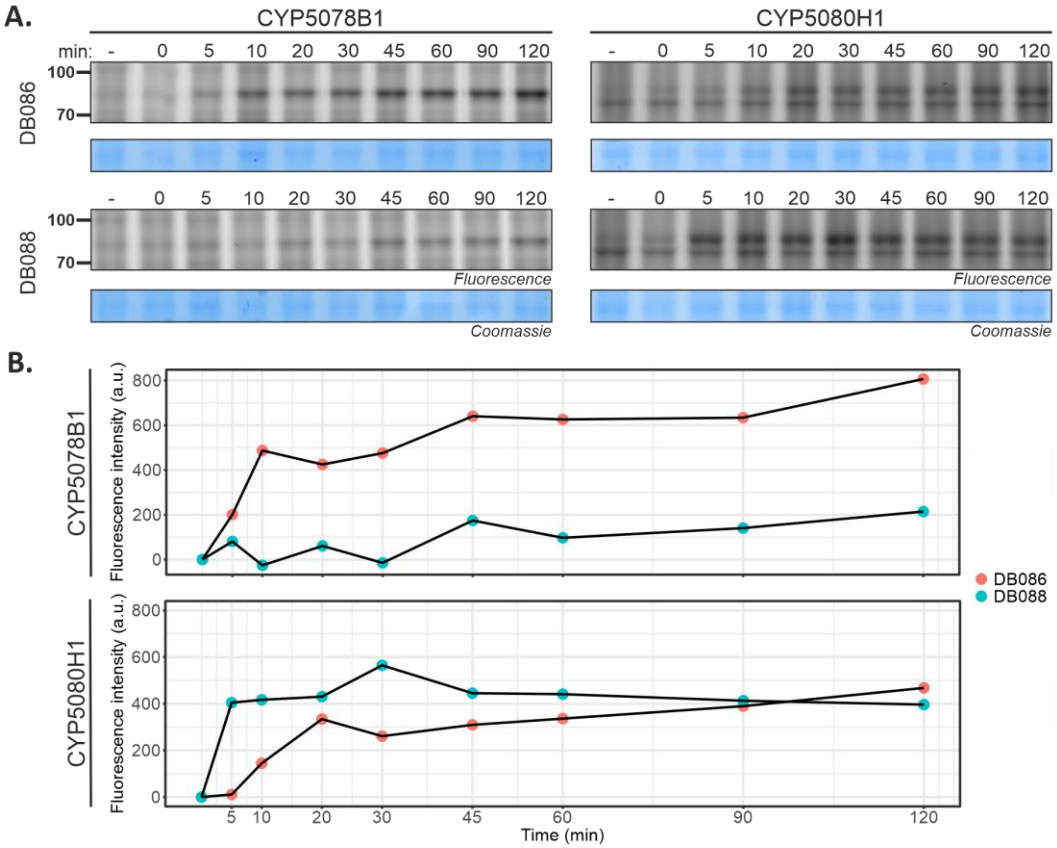


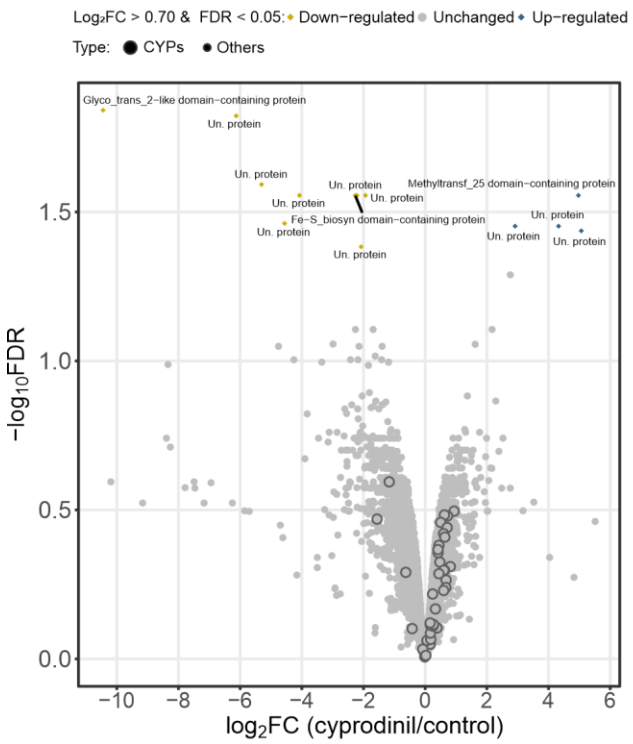
Figure 8. Time dependency of DB086 and DB088 labelling of CYP5078B1 and CYP5080H1. A, *In planta* overexpressed CYP5078B1 and CYP5080H1 were labelled with 5 µM DB086 and DB088 in the presence of 1 mM NADPH for different amount of time. Labelled proteins were coupled to a fluorophore via click chemistry, separated in an SDS-PAGE gel and visualised by in-gel fluorescence scanning. Coomassie staining is shown as loading control. Similar results were obtained in an additional independent replicate. **B**, Signal intensity quantification of DB086 and DB088 time course labelling of CYP5078B1 and CYP5080H1. Quantified signal intensities from section A.

CYP5080H1 may contribute to the detoxification of cyprodinil in *Zymoseptoria tritici*

CYP450s are important xenobiotic detoxifying enzymes in mammals, insects and plants (Lu *et al.*, 2021; Siminszky, 2006; Zanger and Schwab, 2013). Although the most well-known CYP450 in fungi is CYP51, an essential catabolism enzyme target of the main de-methylation inhibitors (DMI) fungicides, other fungal CYP450s have gained attention due to their significant up-regulation during fungicide treatments and fungicide resistance (Green *et al.*, 2018; Lepesheva *et al.*, 2018; T. Zhang *et al.*, 2020). Anilino-pyrimidine (AP) fungicides have been hypothesised to act by inhibiting methionine biosynthesis in fungal cells and are commonly used for the control of many plant pathogens in the field (Mosbach *et al.*, 2017). Previous data from Syngenta suggested the possible involvement of *Z. tritici* CYP5080H1 in AP fungicide detoxification as CYP5080H1 was the main CYP450 transcriptionally up-regulated upon cyprodinil and mepanipyrim treatments of *Z. tritici* liquid cell cultures (Figure S1). By contrast, CYP5080H1 was not up-regulated when *Z. tritici* cells were treated with fenpropimorph and fenpropidin, which belong to the sterol biosynthesis inhibiting (SBI) fungicide class.

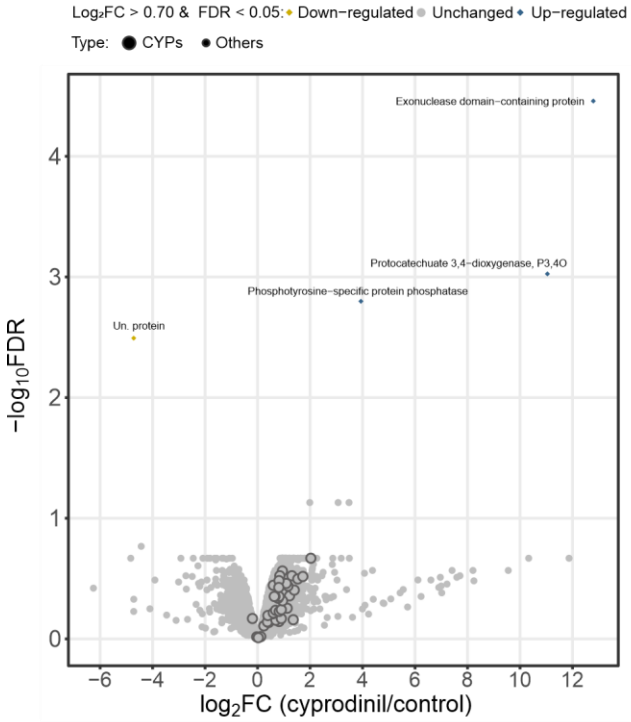
We next tested whether we could detect this same cyprodinil-dependent CYP450 activation in *Z. tritici* cell cultures using two LC-MS/MS methods: a global proteome digestion analysis and DB088 pull-down analysis. *Z. tritici* cell cultures were treated with or without 1 part per million (ppm) cyprodinil, or an equal amount of DMSO, for four hours, before cell collection and microsome isolation. In the global proteome of *Z. tritici* cyprodinil-treated and untreated microsomes we detected a total of four up-regulated and nine down-regulated proteins in the cyprodinil-treated samples, none of these being CYP450s (Figure 9). The majority of the differentially accumulating proteins were annotated as unknown proteins besides one upregulated methyltransferase (F9X961) and a downregulated glycotransferase (F9WW89) and Fe-S containing protein (F9X2J1).

In the DB088 labelling and enrichment dataset, no CYP450s were enriched (Figure 10). However, many CYP450s were detected in both samples but none of them were found increased in abundance in response to the cyprodinil treatment. Among these, CYP5080H1 with a $\log_2$FC of 1.72 and MS intensity of 19.56.



	Unchanged				
	Name	UniProtKB	log_2FC	MS int.	adj.P.Val
1	CYP596C1	F9XFD5	0.94	13.91	0.32
2	CYP5078B1	F9X0K1	0.82	13.79	0.49
3	CYP53A16	F9X127	0.72	18.38	0.33
4	CYP503D1	F9WWF4	0.71	13.48	0.36
5	CYP617G1	F9X140	0.68	16.50	0.54
6	CYP5191A1	F9WWG0	0.67	11.90	0.58
7	CYP5199A1	F9XFL7	0.64	14.40	0.39
8	CYP584J1	F9X9F0	0.63	16.51	0.50
9	CYP539A6	F9XDL6	0.62	16.73	0.33
10	CYP598B2	F9XHT9	0.62	14.40	0.36
11	CYP577A6	F9XIV4	0.60	14.14	0.50
12	CYP677B1	F9X3L5	0.60	15.95	0.59
13	CYP65AM2	F9WZB7	0.60	16.35	0.38
14	CYP61A1	F9X4J7	0.54	19.12	0.36
15	CYP505F1	F9X5V5	0.52	15.67	0.36
16	CYP532K1	F9XNX8	0.50	17.94	0.35
17	CYP598B1	F9XJ19	0.48	14.83	0.47
18	CYP559D1	F9X4J0	0.45	17.22	0.41
19	CYP51F1	F9XG32	0.45	17.23	0.52
20	CYP548N1	F9XKM2	0.44	16.39	0.43
21	CYP534D1	F9XDA4	0.42	19.03	0.44
22	CYP5080H1	F9X6Z0	0.39	17.76	0.79
23	CYP5192A1	F9WYJ8	0.33	17.01	0.68
24	CYP5105B1	F9WYQ3	0.27	13.69	0.77
25	CYP65AS1	F9WWF0	0.25	14.41	0.78
26	CYP578G1	F9X6B4	0.24	13.74	0.61
27	CYP5194A1	F9XH77	0.18	16.53	0.86
28	CYP52R1	F9XML6	0.17	16.59	0.77
29	CYP5201A1	F9XIL1	0.17	17.30	0.82
30	CYP548A7	F9XQ69	0.16	18.87	0.89
31	CYP5193A1	F9WXK9	0.16	15.36	0.76
32	CYP540B14	F9X9B9	0.06	18.59	0.87
33	CYP528A5	F9XFS5	0.02	13.24	0.97
34	CYP5196A2	F9XHE6	-0.01	17.73	0.98
35	CYP504A16	F9X1J4	-0.08	19.35	0.93
36	CYP584E9	F9XPH9	-0.42	13.65	0.79
37	CYP5128D1	F9XF18	-0.63	13.66	0.51
38	CYP5196A1	F9XNG2	-1.17	14.27	0.25
39	CYP543B1	F9X9M1	-1.56	14.44	0.34

Figure 9. Comparative proteomic analysis of *Zymoseptoria tritici* cell cultures treated or not with the fungicide cyprodinil. *Z. tritici* cell cultures were treated with 1 part per million (ppm) cyprodinil, or an equal amount of DMSO, for 4 hours previous to cell collection and microsome isolation. *Z. tritici* microsomes (n= 3) were digested with Lys-C and trypsin and digested peptides were analysed by LC-MS/MS. Enrichment is represented by volcano plots where the log_2FC (cyprodinil/control) is plotted against their significance ($-log_{10}FDR$) using three biological replicates. The colour of the dots means whether proteins (dots) were enriched (blue), unchanged (grey) or depleted (yellow) in the CYP450 containing sample. Differentially regulated proteins are named in the graph where no-annotated proteins are marked as unknown proteins.



	Unchanged				
	Name	UniProtKB	log_2FC	MS int.	adj.P.Val
1	CYP5128D1	F9XF18	2.03	10.92	0.21
2	CYP5080H1	F9X6Z0	1.72	19.56	0.30
3	CYP548A7	F9XQ69	1.53	19.23	0.32
4	CYP617G1	F9X140	1.40	17.67	0.39
5	CYP5078B1	F9X0K1	1.36	17.67	0.69
6	CYP5191A1	F9WWG0	1.31	13.40	0.30
7	CYP677B1	F9X3L5	1.22	16.31	0.44
8	CYP548N1	F9XKM2	1.16	16.99	0.36
9	CYP5192A1	F9WYJ8	1.13	17.55	0.56
10	CYP584J1	F9X9F0	1.11	17.91	0.58
11	CYP5196A1	F9XNG2	1.09	13.95	0.35
12	CYP503D1	F9WWF4	1.08	14.53	0.35
13	CYP5201A1	F9XIL1	0.95	18.55	0.48
14	CYP5080G1	F9X1Q3	0.95	14.69	0.27
15	CYP52R1	F9XML6	0.91	18.50	0.68
16	CYP5194A1	F9XH77	0.90	17.47	0.57
17	CYP65AS1	F9WWF0	0.90	15.03	0.32
18	CYP53A16	F9X127	0.90	18.52	0.37
19	CYP504A16	F9X1J4	0.85	20.41	0.30
20	CYP5196A2	F9XHE6	0.82	19.10	0.59
21	CYP598B2	F9XHT9	0.82	15.62	0.44
22	CYP539A6	F9XDL6	0.82	18.18	0.72
23	CYP577A6	F9XIV4	0.81	14.98	0.37
24	CYP578G1	F9X6B4	0.78	14.86	0.46
25	CYP559D1	F9X4J0	0.70	18.33	0.70
26	CYP5199A1	F9XFL7	0.69	14.16	0.58
27	CYP5193A1	F9WXK9	0.66	15.98	0.44
28	CYP65AM2	F9WZB7	0.64	17.25	0.44
29	CYP584E9	F9XPH9	0.60	14.75	0.61
30	NA	F9XJP5	0.60	20.57	0.36
31	CYP534D1	F9XDA4	0.58	19.03	0.62
32	CYP532K1	F9XNX8	0.42	17.97	0.73
33	CYP5105B1	F9WYQ3	0.39	15.35	0.64
34	CYP5085B1	F9X214	0.37	14.94	0.72
35	CYP598B1	F9XJ19	0.24	15.68	0.79
36	CYP505F1	F9X5V5	0.24	16.42	0.78
37	CYP596C1	F9XFD5	0.12	14.62	0.96
38	NA	F9XBQ2	0.03	16.81	0.98
39	CYP528A5	F9XFS5	-0.03	14.16	0.96
40	CYP540B14	F9X9B9	-0.20	18.80	0.68

Figure 10. DB088 differential labelling of *Z. tritici* microsomes isolated from cell cultures treated or not with cyprodinil. *Z. tritici* cell cultures were treated with 1 part per million (ppm) cyprodinil, or an equal amount of DMSO, for 4 hours previous to cell collection and microsome isolation. Microsomes isolated from cyprodinil-treated and untreated *Z. tritici* cell cultures were incubated with 5 μM of DB088 or an equal volume of DMSO in the presence of 1 mM NADPH for 1h. Labelled proteins were subjected to click chemistry for biotin attachemnt and enriched via streptavidin pull-down. Enrichment is represented by volcano plots where the log_2FC (cyprodinil/control) is plotted against their significance ($-log_{10}FDR$) using three biological replicates. The colour of the dots means whether proteins (dots) were enriched (blue), unchanged (grey) or depleted (yellow) in the CYP450 containing sample. Differentially regulated proteins are named in the graph where no-annotated proteins are marked as unknown proteins.

As previous data suggested that CYP5080H1 transcripts were the highest upregulated of the CYP450s upon cyprodinil treatment of *Z. tritici* cell cultures, next we wanted to investigate whether cyprodinil can suppress labelling of CYP5080H1 using competitive ABPP. Our in-gel fluorescence analysis of CYP5080H1 labelling identified DB088 as the best probe for a faster and reliable labelling CYP5080H1. Therefore, we pre-incubated microsomes of CYP5080H1 overexpressing leaves with increasing concentrations of three AP fungicides (cyprodinil, C; mepanipyrim, M; pyrimethanil, P) and an SBI fungicide (fenpropimorph, F) as an unrelated fungicide (Figure 11A). Fungicides were pre-incubated with microsomes for 10 min prior to a 5 min DB088 labelling of CYP5080H1. We observed a strong concentration-dependent suppression of CYP5080H1 labelling by cyprodinil and a slightly decrease in fluorescent labelling by mepanipyrim and pyrimethanil. Pre-incubation of CYP5080H1 microsomes with fenpropimorph did not affect the labelling of CYP5080H1 (Figure 11B). The strongest inhibition of CYP5080H1 occurred with cyprodinil concentrations of 50 μM and above. Thus, when tested at 100 μM, cyprodinil is the best suppressor of CYP5080H1 labelling (Figure 11C). Signal intensity quantification and statistical analysis confirmed the significant inhibition of CYP5080H1 labelling by cyprodinil but not by mepanipyrim, pyrimethanil and fenpropimorph. This data is in line with metabolism data from Syngenta where they reported an increased metabolization of cyprodinil in transgenic *Z. tritici* overexpressing CYP5080H1 and a decreased metabolization of cyprodinil in CYP5080H1 knock-out lines (Figure S2A). Furthermore, it was observed that CYP5080H1 deletion strain had a different metabolite a (+16) profile in comparison to the wild type and knockout *Z. tritici* strains, indicating the different cyprodinil metabolization by the knockout strain (Figure S2B).

Taken together, these data demonstrate that competitive ABPP and CYP450 probes can be used as a tool to identify possible fungicide substrates of fungal CYP450s. However, we could not demonstrate the use proteomic approaches as a discovery tool to identify CYP450 activated or repressed by fungicide treatments.

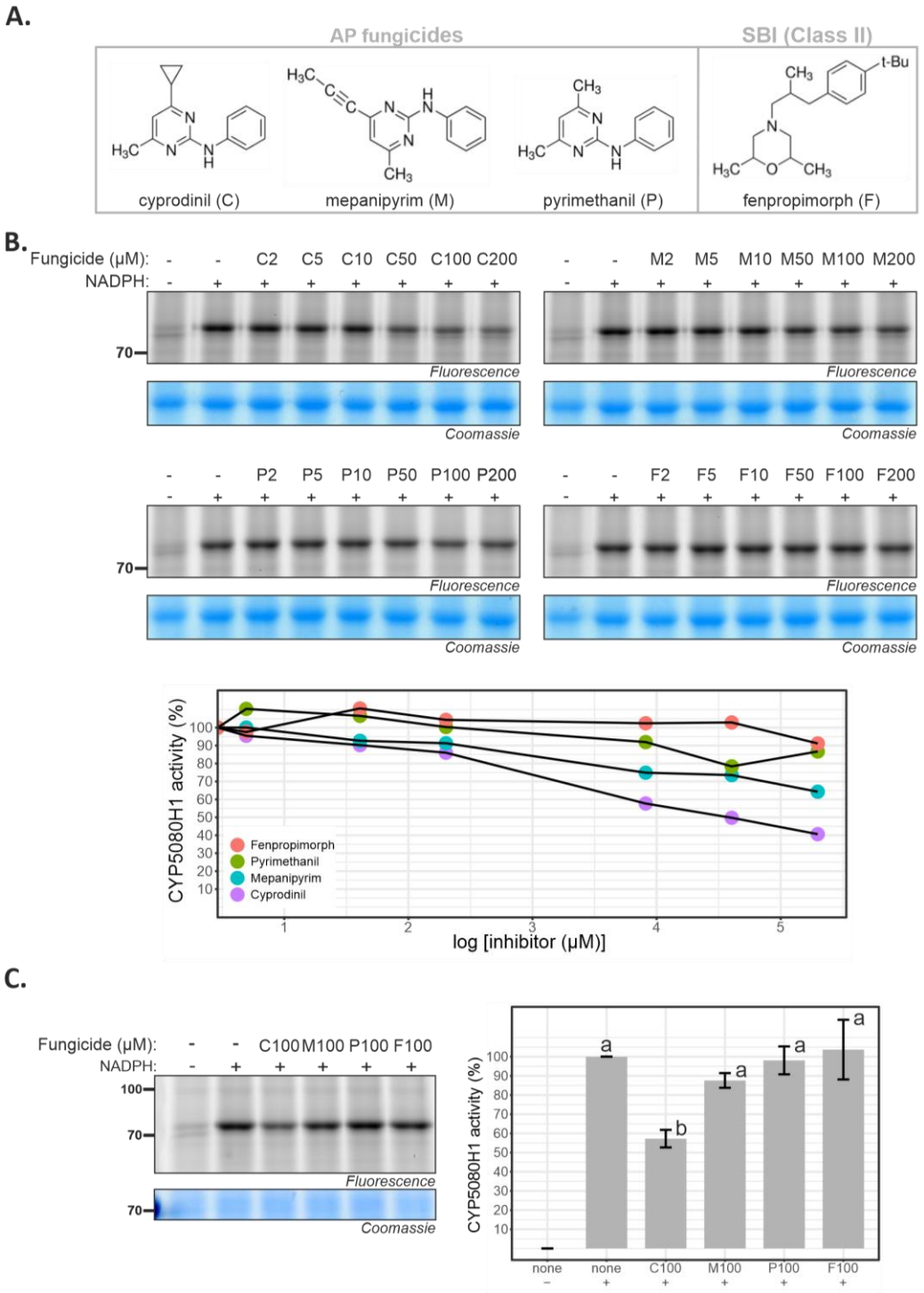


Figure 11. Strong blockage of CYP5080H1 labelling by the fungicide cyprodinil. **A**, Chemical structures of anilino-pyrimidine (AP) fungicides (cyprodinil, C; mepanipyrim, M; pyrimethanil, P) and a sterol biosynthesis inhibiting (SBI) fungicide (fenpropimorph, F). **B**, Inhibition course of DB088 labelling of CYP5080H1 by fungicides. Labelling conditions: microsomes protein concentration, 0.7 mg/ml; DB088, 5 µM probe concentration and 5 min labelling time. Quantified signal intensities from section B are represented by CYP5080H1 activity (%) and calculated by comparing the signal intensity of the fungicide-sample to the no-fungicide-control set to 100%. Similar results were obtained in an independent replicate. **C**, Competitive labelling of CYP5080H1 labelling by four fungicides at 100 µM concentration. CYP5080H1 activity (%) was calculated when comparing the signal intensity of the 100 µM inhibition fungicide-samples to the no-fungicide-control set to 100% CYP5080H1 labelling. Data represents the average ± standard deviation of n=3 independent inhibition experiments. ANOVA test (a, not significant; b, $P < 0.05$).

Phylogenetic analysis of CYP450s in plant pathogens

Cyprodinil is a common fungicide used to control many fungal plant pathogens in cereals, vegetables and fruit crops (Karadag and Ozhan, 2015). Therefore, we wanted to investigate the closest orthologs of CYP5080H1 in other economical-important fungal plant pathogen species. The evolutionary relationship of CYP450 from fungal plant pathogens was predicted by comparing their full amino acid sequences. A total number of 495 CYP450s from five fungal species – 79 from *Zymoseptoria tritici* (*Zt*), 132 from *Botrytis cinerea* (*Bc*), 134 from *Magnaporthe oryzae* (*Mo*), 115 from *Fusarium graminearum* (*Fg*), 17 from *Puccinia graminis (Pg)* and 20 from *Ustilago maydis* (*Um*) - were used to construct an unrooted phylogenetic tree using MEGA Maximum-likelihood method with 500 bootstraps. We observed that all labelled *Z. tritici* CYP450s were scattered across the phylogenetic tree (Figure 12A, blue highlights). Furthermore, CYP450s labelled by DB080 and DB096 do not represent a specific clade of CYP450s as we detected probe targets in seven of 12 clades represented (Figure 12A, blue dots). The tree clearly suggested a good alignment and clustering as the well-annotated *Zt*CYP51F1 clustered well with the other species CYP51 enzymes (Figure 12C). *Zt*CYP5080H1 closely clusters with one *B. cinerea* (Bcin02g01260), two *F. graminearum* (FGRAMPH1 01G12445 and FGRAMPH1 01G08807), one *U. maydis* (KIS69663) and one *M. oryzae* (MGG 05235) CYP450s, indicating that these CYP450 could also be involved in cyprodinil detoxification response in other fungal plant pathogens (Figure 12B).

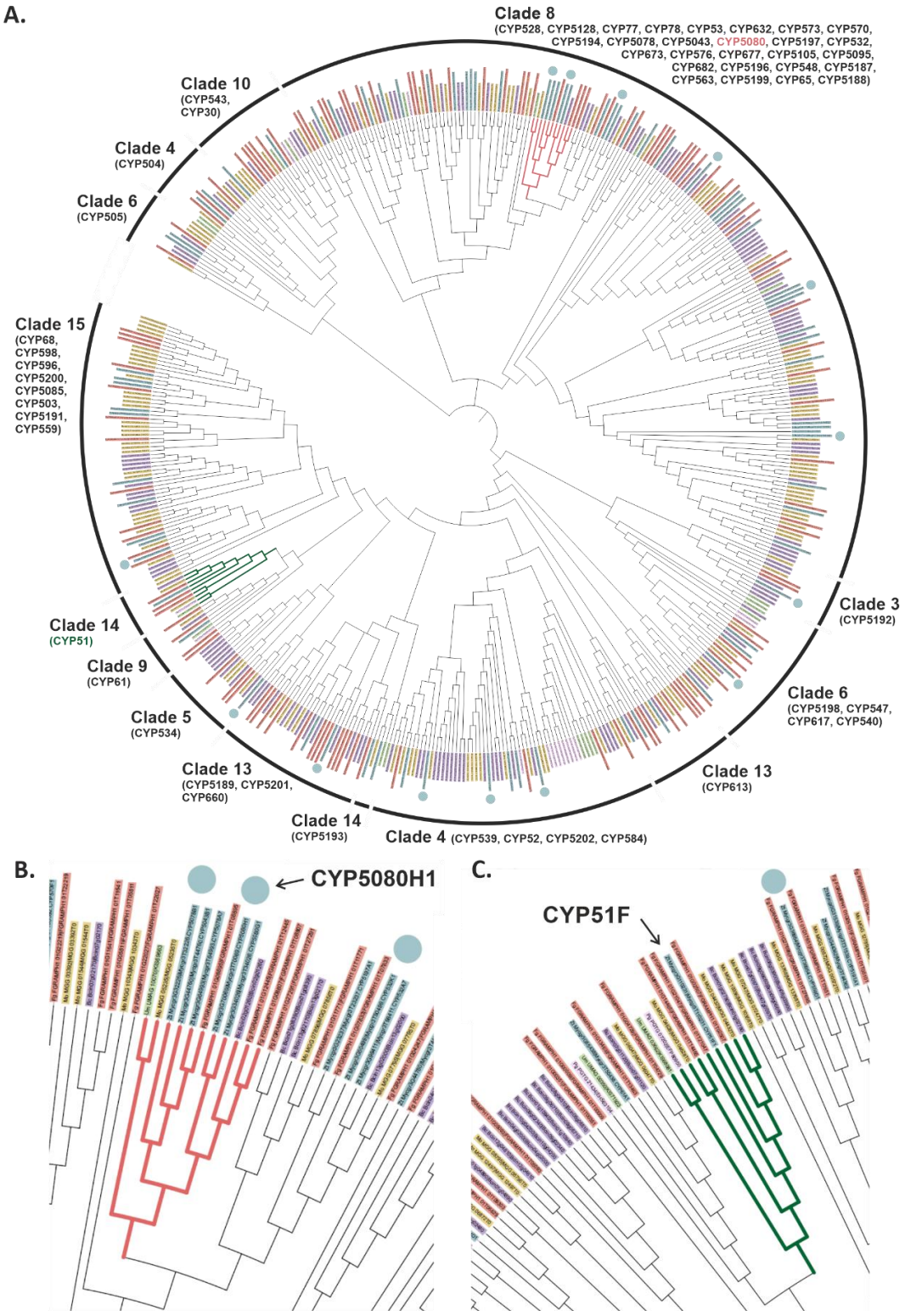


Figure 12. Phylogenetic analysis of cytochrome P450 proteins. CYP450s from six species of plant fungal pathogens – in blue, *Zymoseptoria tritici* (*Zt*); in purple, *Botrytis cinerea* (*Bc*); in yellow, *Magnaporthe oryzae* (*Mo*); in red, *Fusarium graminearum* (*Fg*); in pink, *Puccinia graminis* (*Pg*) and in green, *Ustilago maydis* (*Um*) - were used to construct an unrooted phylogenetic tree using MEGA Maximum-likelihood method with 500 bootstraps. All *Z. tritici* CYP450s are highlighted in blue and CYP450s detected by DB080 and DB096 pull-downs marked with a blue dot. The CYP51 class formed a distinct clade, highlighted in purple, where *Zt*CYP51 is the one highlighted in dark purple. CYP5080H1 closest orthologs are highlighted in red, where *Zt*CYP5080H1 is highlighted in dark red.

Discussion

We applied ABPP to study CYP450s in the important plant pathogen *Zymoseptoria tritici*. Using CYP450 probes we identified several *Z. tritici* CYP450s labelled and enriched in proteomic analyses. We also confirmed the labelling of *Zt*CYP450 with protein overexpression and fluorescence labelling scanning. Further work revealed the specific involvement of CYP5080H1 in cyprodinil metabolism as we identified the blockage of CYP5080H1 labelling by cyprodinil using competitive *in vitro* ABPP studies.

Challenges of CYP450 labelling in *Zymoseptoria tritici*

ABPP is a distinct and powerful tool used in many biological systems to monitor, identify and characterise the activity of different enzymes within complex proteomes (Kovács and van der Hoorn, 2016). Although transcriptomics studies have been a dominant approach to discover players of detoxification of agrochemicals and to unravel its complex function and regulation, conventional transcriptomic analyses do not necessarily directly correlate to protein activities (Willems *et al.*, 2014).

When using ABPP, usually the banding pattern of labelled samples strongly differs from the no probe control, indicating the specific labelling of specific subset family of enzymes (Morimoto and van der Hoorn, 2016). In our experiments, CYP450 probes had a strong labelling profile at around 50 kDa when using mouse liver but not in *Z. tritici* microsomes (Figure 2). Unfortunately, none of the CYP450 probes have specific labelling profile at around 50-65 kDa, molecular size of the majority of *Z. tritici* CYP450s, when checking labelling by fluorescent scanning or protein blotting (Figure 1B and 2). Similar data were reported by Mooij 2018, where they could not report evidence of CYP450 labelling in *Z. tritici* microsomes using the already described CYP450 probe DB086 and four other new developed di-alkyne CYP450 probes (Mooij, 2018). When performing click chemistry for the reporter tag coupling after CYP450 labelling, we found that same click protocol gave much less background in mouse liver microsomes than in *Z. tritici* microsomes (Figure 2). We hypothesise that it could be the intrinsic nature of *Z. tritici* microsomes, the lower reactivity of fungal CYP450s towards chemical probes or the lower abundance of CYP450s in *Z. tritici* microsomes causing this problem. We mainly attribute that the lack of signals is due to the high click chemistry background signal we find at approximately 49 kDa. In addition, lower reactivity and abundance of *Z. tritici* CYP450s in comparison to mouse CYP450s may also reduce signals of *Zt*CYP450s, as observed in previous chapter 2 where CYP450 abundance was a problem when labelling plant microsomes. Furthermore, as seen in our global proteomic analysis, not all CYP450s present in the proteome are reactive to CYP450 probes and can be targeted and enriched. Therefore, we hypothesise that specific CYP450 signals we aimed to detect at around the molecular size of CYP450s might be too weak to detect.

To further improve CYP450 labelling detection, we decided to combine CYP450 labelling with streptavidin bead enrichment and LC-MS/MS analysis. In our first probe screen, we used DB080, DB086 and DB096 for CYP450 labelling using two technical replicates for the pull-down and we identified 5, 18 and 12 *Zt*CYP450s, respectively (Figure 3). We identified DB096 as the most promising labelling probe as the top CYP450 enriched, CYP5078B1, was enriched with a higher log_2FC and we enriched fewer other proteins. We further confirm *Z. tritici* CYP450 enrichment by performing a second DB096 enrichment pull-down using three independent biological *Z. tritici* microsomes. Numbers of CYP450 detected in this second pull-down were lower, 5, but the proportion of other proteins was also reduced (Figure 4). We also believe that the same problems mentioned before are preventing observation of a specific CYP450 enrichment in mass spectrometry analyses as we also enriched for other promiscuous click chemistry targets.

Overall, we managed to detect enriched CYP450 in *Z. tritici* microsomes, but only using mass spectrometry analysis. To better enrich and label CYP450s, we suggest two approaches: (1) improve the click chemistry protocol and (2) use biotinylated CYP450 probes. The click chemistry reaction could be improved by either trying to reduce the amount of click chemistry reagents, substituting the copper-chelating agent TBTA for other alternatives such as tris-hydroxypropyltriazolylmethylamine (THPTA) or using the new generation of azide reporter tags named as 'Azide Plus Reagents' which have an enhanced reactivity towards alkyne moieties in comparison to the picolyl-azide reporter tags (https://clickchemistrytools.com/next-generation-azide-plus-reagents/). Furthermore, we suggest the use of biotinylated CYP450 probes to avoid the click chemistry background. Using one-step labelling ABPP did not gave us much background in the no probe control of plant microsomes, and we detected the enrichment of several *N. benthamiana* CYP450s (Chapter 2). It will be interesting to synthesise trifunctional CYP450 probes containing both: a fluorophore, for in-gel target detection, and a biotin moiety, for target enrichment and identification. However, the biotin or fluorophore moiety could reduce the probe reactivity to CYP450 as we detected for the maize CYP81A9 (Chapter 2).

Selective CYP450 labelling

To further validate CYP450 labelling we cloned and overexpressed four top CYP450 probe targets identified by chemical proteomic pull-down analysis. All cloned *Zt*CYP450s were properly expressed and detected in *N. benthamiana* leaf microsomes, showing a high utility of agroinfiltration for the study of fungal CYP450s (Figure 5). Although DB096 was the more specific and reliable probe for chemical proteomic analysis, we did not observe a strong fluorescent signal when using DB096 for in-gel fluorescence scanning. By contrast, DB086 and DB088 were the strongest probes to label *in planta* overexpressed CYP450s. DB086 was not a good probe for *Z. tritici* chemical proteomic experiments as

it displayed significant off target activity. We also detected different labelling characteristic of two *Zt*CYP50s: CYP5078B1 and CYP5080H1. Although these two CYP450 cluster close together in the CYP450 phylogenetic tree, they have a remarkably different reactivity against DB086 and DB088. Therefore, depending on their application, each CYP450 probe should be chosen taking into consideration their reactivity and off-target probability.

We identified a total of 79 CYP450s in the *Z. tritici* genome and used the annotation proposed by Kelly and co-workers for their identification (Newsome *et al.*, 2013). However, just 40 were detected in the global proteomic analysis of *Z. tritici* microsomes, and a total of 14 were enriched upon labelling with DB080 and DB096 (Figure 6). The low abundance of CYP450 is not a limiting factor as the top labelled CYP450, CYP5078B1, was ranked at the bottom of the abundance ranking of *Z. tritici* microsomes. Furthermore, CYP450 probes do not target a specific subclass of CYP450s as detected CYP450s are all around the phylogenetic tree (Figure 12). Therefore, we hypothesise that CYP450 labelling might be more dependent on individual CYP450 selectivity and reactivity towards the different probes.

Intriguingly, we observed that the top studied CYP450 in fungi, the azole fungicide target CYP51, was not labelled by any of the CYP450 probes although we found it among the five top most abundant CYP450s in *Z. tritici* microsomes. It will be interesting to clone and overexpress *Zt*CYP51F1 and check if it can be labelled with CYP450 probes, along with the most abundant CYP450 detected in the global proteomic analysis, CYP504A16 and CYP61A1, which are also not labelled. CYP61A1 is described as a sterol C-22 desaturase involved in the in the pathway of ergosterol biosynthesis (Hu *et al.*, 2017; Kelly *et al.*, 1995; Lah *et al.*, 2011; Ohk *et al.*, 2015). It is possible that more conserved CYP450s involved in conserved metabolic pathways have a strict specificity towards their substrates and are not targeted by CYP450 probes. Regarding CYP504A16, we could not find any references regarding its involvement in any biosynthesis pathway (Newsome *et al.*, 2013). We hypothesis that specific metabolic CYP450s may require other probes designs and that some CYP450s can have more promiscuous substrates than others and those are the ones more likely to metabolise and activate the chemical probes.

Altogether, this data illustrates the use of activity-based CYP450 profiling to monitor and identify active CYP450s in fungal proteomes. First, we recommend testing the whole set of CYP450 probes on fungal microsomes to identify the most suitable CYP450 probe depending on the labelling read-out. Next, we recommend using protein overexpression to validate CYP450 probe candidates. On one hand, in order to maximise number of *Z. tritici* CYP450s labelled we propose the use of a mixture of probes (probe cocktail). In order to label and detect new *Zt*CYP450s we propose to grow *Z. tritici* in different media or chose a different fungal developmental stage to stimulate the expression and abundance of other CYP450s.

The use of competitive CYP450 labelling to study fungicide metabolism

Several CYP450s are upregulated in plant pathogens after fungicide exposure (Sang and Hulvey, 2018; Wang *et al.*, 2018; C. Zhang *et al.*, 2020). However, the direct implication and biochemical characterisation of these potential CYP450s in fungicide detoxification has just been demonstrated for a fungicide-CYP450 pair (Green *et al.*, 2018).

Previous data from Syngenta suggested the possible involvement of *Z. tritici* CYP5080H1 in AP cyprodinil detoxification as CYP5080H1 was the main CYP450 transcriptionally up-regulated upon cyprodinil treatment of *Z. tritici* liquid cell cultures. Furthermore, transgenic *Z. tritici* overexpressing CYP5080H1 and knock-out lines lacking CYP5080H1 showed an increased and decreased metabolization rate of cyprodinil, respectively (Figure S1 and S2A). Competitive ABPP labelling supported the cyprodinil detoxification capabilities of CYP5080H1 in *Z. tritici*. Cyprodinil was the best AP fungicide able to supress labelling of CYP5080H1 by DB088, indicating that cyprodinil actively blocks the active site of CYP5080H1 and could be a direct substrate of CYP5080H1.

Unfortunately, due to different probe specificities, we could not block DB088 labelling of CYP5078B1 as we previously appreciated that its reactivity was far less quick and strong than with CYP5080H1 (Figure 7 and 8). Furthermore, we detected that DB088 labelling of CYP5078B1 was always far weaker, even if probe labelling concentration was increased (Figure 7B, first panel). We hypothesise that this could be because activated DB088 diffuses out of CYP507B1 before getting covalently attached to the enzyme. Therefore, when using competitive ABPP to study no-covalent CYP450 substrates such are fungicides, we recommend the use of more reactive CYP450 probes as longer incubation times saturate all CYP450 active sites by covalent probe attachments. As DB086 showed a faster reactivity profile to CYP5078B1, DB086 will be a better probe to study fungicide metabolism by CYP5078B1.

Furthermore, our data agrees with previous cyprodinil metabolism data from Syngenta, observing a more rapidly oxidation of cyprodinil in CYP5080H1 overexpressing strains. Therefore, our protocol can now be adapted to study the role of CYP450s in fungicide metabolism and, potentially, to herbicide or insecticides studies. However, application of competitive CYP450 labelling may require additional optimisation such as the finding of the best and quickest CYP450 probe to study a particular CYP450.

Phylogenetic analysis revealed orthologs of CYP5080H1 in *B. cinerea, M. oryzae*, *F. graminearum* and *U. maydis*. Multiple fungicide resistance is a real threat for the control of *B. cinerea* infections in the field as there have been many reported field strains containing multiple fungicide resistance, which confers a major threat to the chemical control of *B. cinerea* (Rupp *et al.*, 2017). Therefore, it will be particularly interesting to study if the identified orthologs of CYP5080H1 in other species have the same capacity of cyprodinil metabolism. Bcin02g01260 is the likely ortholog of *Z. tritici* CYP5080H1. We could not find

any evidence of the upregulation of this gene in cyprodinil-resistant or cyprodinil-exposed *B. cinereal* strains. However, four other *Bc*CYP450 genes were transcriptionally upregulated after a persistent cyprodinil exposure (Wang *et al.*, 2018). Additional functional studies using CYP450 overexpression and competitive CYP450 labelling and performing metabolism characterisation by using overexpressing and deletion strain are required to confirm this hypothesis.

Materials and Methods

Chemical probes and chemicals

The synthesis and chemical characterisation of the CYP450 probes will be reported in the D. Phil Thesis of Daniel Brown (DB). CYP450 probes DB080, DB086, DB088, DB089, DB096 and DB143 were resynthesised by Daniel Brown with some modifications (Wright *et al.*, 2009; Wright and Cravatt, 2007).

The CYP450 inhibitor 1-ABT (A3940-50MG) and fungicides cyprodinil (34389-100MG), mepanipyrim (33970-50MG), pyrimethanil (31577-250MG) and fenpropimorph (36772-100MG) were purchased from Sigma-Aldrich. NADPH was purchased from MELFORD (N20140-0.1).

Biologic materials and growth conditions

Zymoseptoria tritici strain IPO323 were grown in YPD agar media (20 g/L peptone, 10 g/L yeast extract, 20 g/L glucose, 20 g/L agar) at 24 °C for 5 days. Spores were harvested by the addition of 10 ml of sterile destilled water and the use of an L-shaped plastic spreader. Suspension spores were filtered through a muslin cloth and a starting inoculation of 1×10^6 spores was added to 1 L of YPD media (20 g/L peptone, 10 g/L yeast extract, 20 g/L glucose). Liquid cultures were incubated at 24 °C, 140 rpm, for approximately 72 h. For the cyprodinil treatment, 48-hours-old *Z. tritici* liquid culture was treated with 1 part per million (ppm) cyprodinil, or an equal volume of DMSO, for 4 hours previous to cell collection and microsomal fraction isolation. *Nicotiana benthamiana* plants were grown on soil at 21 °C under long day conditions (16/8 h light/dark regime) in a greenhouse.

Cloning

Golden Gate Modular Cloning kit (Weber *et al.*, 2011) and Golden Gate Modular Cloning Toolbox for plants (Engler *et al.*, 2014) were used for cloning. Used and generated plasmids are summarised in Table S1. The primers used for sequence amplification are summarised in Table S2. The binary vector pJK268c containing the P19 silencing inhibitor (pL1V2-P19-F2) was used as binary vector.

The sequences encoding *Z. tritici* CYP450s (CYP5078B1, CYP5080H1, CYP52R1 and CYP539A6) were amplified from *Z. tritici* complementary DNA (cDNA) using the forward and reverse primer pairs

summarised in Table S2. Using BsaI restriction sites, PCR products were combined with GG1-55, GG1-57, GG1-70 or GG1-78 to assemble the corresponding expression plasmids.

Generated expression plasmids were transformed into *E. coli* for their amplification and sequencing. Afterwards, plasmids were transformed into *Agrobacterium* (*Agrobacterium tumefaciens*) strain GV3101, carrying the pMP90 helper plasmid. *Agrobacterium* transformants were selected on LB plates (10 g/L NaCl, 10 g/L Tryptone, 5 g/L yeast extract, 15 g/L agar) containing 50 μM gentamycin, 25 μM rifampicin and 50 μM kanamycin. Single colonies were picked and grown in liquid LB (10 g/L NaCl, 10 g/L Tryptone, 5 g/L yeast extract) containing the same antibiotic used before. Glycerol stocks of the selected transformants were prepared mixing *Agrobacterium* cultures with 50% sterile glycerol in a 1:1 ratio.

Agroinfiltration

N. benthamiana plants were grown on soil at greenhouse conditions described before. *Agrobacterium* GV3101-pMP90 carrying the CYP450-encoding plasmids (pJK268c, plasmid containing a CYP450 sequence plus P19) were grown overnight (approximately 18 h) at 28 °C with agitation in LB media containing 50 μM gentamycin, 25 μM rifampicin and 50 μM kanamycin. Bacteria cells were collected by centrifugation at 1000 g for 10 min at room temperature (RT), washed with infiltration buffer (10 mM MES, 10 mM $MgCl_2$, pH 5.6 and 100 μM acetosyringone) to OD_{600}= 0.5. *Agrobacterium* were incubated at 28 °C for 2 h and afterwards, the two new fully-expanded leaves of *N. benthamiana* plants (4-5 weeks old) were hand-infiltrated with the *Agrobacterium* suspensions with the help of a needle-less 10 ml syringe.

Protein extraction and microsomal fraction isolation preparation

Z. tritici liquid cultures were harvest by centrifugation and washed in TEK buffer (50 mM Tris-HCL pH 7.5, 1 mM EDTA, 100 mM KCl). Hyphae were resuspended in ice-cold TESB + DTT buffer (50 mM Tris-HCL pH 7.5, 1 mM EDTA, 600 mM D-Sorbitol, 30 mM DTT) and incubated for 10 min at RT. Afterwards, *Z. tritici* hyphae were centrifuged at 5,000 g, resuspended in ice-cold TESB (50 mM Tris-HCL pH 7.5, 600 mM D-Sorbitol) and ground using 0.5 mm glass beads and a bead mill homogenizer (BioSpec BeadBeater 1107900-105). Cell extract was filtered through a nylon cloth and centrifuged at 16,000 g for 10 min. Supernatant containing soluble proteins was ultra-centrifuged at 100,000 g for 1h. Pellet containing the microsomal membranes were resuspended in TEG buffer (50 mM Tris-HCL pH 7.5, 1 mM EDTA, 20% glycerol) and protein concentration was adjusted to 2 mg/ml by Bradford protein assay. Microsomes were kept at -80 °C until used.

Agroinfiltrated *N. benthamiana* leaf tissue was collected at 4 days post-infiltration (dpi). Leaf tissue was frozen in liquid nitrogen and ground to fine powder with a mortar and pestle. Total proteins were

extracted in cold homogenization buffer (100 mM potassium phosphate buffer pH 7.5, 400 mM sucrose, 1% (w/v) polyvinylpolypyrrolidone (PVPP) and 4 mM β-mercaptoethanol). The extracts were left for 20 min rotating at 4 °C for complete homogenization and centrifuged at 5,000 g for 20 min at 4 °C. Supernatant containing soluble proteins was filtered through a layer of miracloth filter and ultra-centrifuged at 100,000 g for 1h. Pellet containing the microsomal membranes was resuspended in resuspension buffer (100 mM potassium phosphate buffer pH 7.5 containing 20% glycerol).

Total protein concentration was determined by DC protein assay Kit (Bio-Rad) with bovine serum albumin standards, protein concentration was adjusted to 0.75 mg/ml for each sample and the resulting samples were used for labelling without freeze thawing.

Activity-based protein profiling and click chemistry

All probes were prepared at 0.5–2 mM stock solutions in dimethyl sulfoxide (DMSO). Protein preparation samples of 50 µl were incubated with or without the indicated probes in the presence or absence of NADPH at the indicated probe concentration (usually 5-10 µM) for the indicated amount of time (usually 1h). For inhibition experiments, 50 µl extracts were pre-incubated with the corresponding amount of fungicide (2-200 µM) for 10 min before labelling with 5 µM DB088 for 5 min. Labelling reactions were stopped by adding 1:4 (v/v) cold acetone and precipitated by 3 min centrifugation at maximum speed using a benchtop centrifuge. Protein pellets were resuspended in 44.5 µl of PBS-SDS buffer (phosphate-buffered saline (PBS) pH 7.4 with 1% (w/v) sodium dodecyl sulfate (SDS)) and heated for 5 min at 90 °C. For click chemistry, 44.5 µl of labelled proteins were treated with 2 µM Cy5 Picolyl Azide (Click Chemistry Tools, 50 µM stock in DMSO) or Fluorescein Picolyl Azide (Click Chemistry Tools, 50 µM stock in DMSO) and a premixture of 100 µM tris((1-benzyl-1H-1,2,3-triazol-4-yl) methyl)amine (TBTA; 3.4 mM stock in DMSO:*t*-butanol 1:4), 2 mM tris(2-carboxyethyl)phosphine hydrochloride (TCEP; 100 mM stock in water) and 1 mM copper(II) sulfate ($CuSO_4$; 50 mM stock in water). Samples were incubated for 1h at RT in the dark and quenched by acetone precipitation. Protein pellets were resuspended in 50 µl of 2x gel loading buffer (100 mM Tris-HCl pH 6.8, 200 mM dithiotreitol, 4% SDS, 20% glycerol and 0.02% bromophenol blue) and heated for 5 min at 90 °C.

In-gel fluorescence scanning and Western Blot

Labelled proteins were loaded and separated on 10-12% SDS-PAGE acrylamide gels at 150V. Fluorescence scanning of acrylamide gels was performed on an Amersham Typhoon 5 scanner (GE Healthcare Life Sciences). Scanned gels were stained with Coomassie Brilliant Blue G-250. Image J was used for the quantification of the detected labelled proteins.

For Western Blot, proteins separated in SDS-PAGE gels were transferred to a PVDF membrane using Trans-Blot Turbo Transfer System (Bio-Rad). Membranes were blocked in 5% (w/v) milk in TBS-T (50 mM Tris-HCl pH 7.6, 150 mM NaCl and 0.1% Tween-20) overnight at 4 °C, incubated in 1:5,000 anti-GFP-HRP (Abcam, ab6663) for 1.5 h at RT and washed in TBS-T for 5 times for 5 min and in TBS for the last wash. Clarity Western ECL substrate (Bio-Rad) was used for chemiluminescent protein detection. For streptavidin-HRP protein blots, samples were processed the same way except that membranes were blocked in 1% (w/v) BSA in TBS-T and incubated in 1:1,000 streptavidin-HRP (Sigma, S2438).

Filter-aided sample preparation for Mass spectrometry

Z. tritici microsomes were diluted to 1 mg/ml protein concentration. YM-10 microcon centrifugal filters (Millipore) were prewashed by adding 200 μl of 0.1% trifluoroacetic acid (TFA) in 50% acetonitrile (ACN) and centrifuged at 15,000 g for 15min at RT. Filters were pre-equilibrated with 200 μl of 8 M urea in 100 mM triethylammonium bicarbonate (TEAB) pH 8.5 and centrifuged at 15,000 g for 15 min at RT. Afterwards, an equivalent of 200 μg total protein were mixed with 200 μl of 8 M urea in 100 mM TEAB, pH 8.5 in the pre-treated filters. Filters were centrifuged at 15,000 g for 40 min at RT and retained proteins were washed with 200 μl of 8 M urea in 100 mM TEAB a total of 4 times. Protein reduction and alkylation were achieved by sequential incubation of the concentrates in 200 μl of 8 M urea in 100 mM TEAB containing tris(2-carboxyethyl) phosphine hydrochloride (TCEP; 10 mM final concentration, 30 min incubation at RT) and 2-chloroacetamide (CA, 50 mM final concentration, 30 min incubation at RT in the dark) followed by centrifugation. The concentrates were washed with 6 M urea in 50 mM TEAB a total of 2 times and subjected to proteolytic digestion with 2.5 μg of lysyl endopeptidase (Lys-C from FUJIFILM Wako, in 50 mM Tris-HCL pH 8, 4 hours incubation at 37 °C) and 5 μg of trypsin (Trypsin Gold from Promega, in 50 mM TEAB pH 8.5, overnight incubation at 37 °C). Digested peptides were collected by centrifugation, and the filters were washed with 150 μl 0.1% TFA and 150 μl 0.1% TFA in 50% ACN. The combined filtrates were dried by vacuum centrifugation and submitted for MS analysis.

Large-scale labelling, affinity purification

1.5 ml of microsomal fraction extracts (0.75 mg/ml protein concentration) were incubated with or without the indicated probes (30 μM) in the presence or absence of 1 mM NADPH for 1h. Labelling reactions were stopped by methanol/chloroform precipitation (addition of 4 volumes of ice-cold methanol, 1 volume of ice-cold chloroform and 3 volumes of water) and precipitated by 40 min centrifugation at 4,000 g at 4 °C. Protein pellets were resuspended in 1ml of PBS-SDS buffer by bath sonication and heated at 90 °C for 10 min. Labelled proteins were biotinylated with 30 μM Azide-PEG3-biotin (Sigma-Aldrich, 2 mM stock in DMSO) using click chemistry as described in the previous section

"Activity-based protein profiling and click chemistry". Samples were incubated for 1 h at RT in the dark, quenched by the addition of 10 mM ethylenediaminetetraacetic acid (EDTA) and precipitated via the methanol/chloroform method. Protein pellets were resuspended in 1.5 ml of 1.2% (w/v) SDS dissolved in PBS by bath sonication and diluted by adding 7.5 ml of PBS. The resulting solution was incubated with 100 µl of pre-equilibrated Pierce High Capacity Streptavidin Agarose beads (Thermo Fisher Scientific) for 2h at RT. Agarose beads containing the labelled proteins were collected by centrifugation at 1,000 g for 5 min at RT. Agarose beads were washed successively three times with 10ml of PBS-SDS buffer, three times with PBS and a final wash with 10 ml of water.

On-bead trypsin and Lys-C digestion

For on-bead digestion, the captured agarose beads containing the labelled proteins were treated with 500 µl 6 M urea dissolved in PBS and 10mM TCEP (200 mM stock in water) for 15 min at 65 °C. A final concentration of 20 mM CA (400 mM stock in water) was added and left incubated for 30 min at 35 °C in the dark. Reaction was diluted by the addition of 950 µl of PBS and the supernatant was removed by centrifuging the beads at 500 g for 2 min. 100 µl of Lys-C digestion solution (Walko, 5 µg of Lys-C were reconstituted in 200 µl 1 M urea/ 50 mM Tris-HCl buffer pH 8) was added to the beads and left incubating at 37 °C for 3 h. 100 µl of trypsin digestion solution (Promega, 5 µl of reconstituted trypsin were dissolved in 100 µl 50 mM Tris-HCl buffer pH 8) was added to the beads and left incubating at 37 °C overnight. The supernatant containing the digested peptides was dried by vacuum centrifugation and submitted for MS analysis.

LC-MS/MS and peptide identification

MS samples from Figure 3 and 4 were run and processed at Syngenta by John Sinclair. Briefly, the acidified tryptic peptides were resuspended in 0.1% FA solution and analysed in DDA mode on a QExactive Plus instrument (ThermoFisher) coupled to an Ultimate 3000 liquid chromatography system (Thermo Fisher Scientific). Samples were separated on an EasySpray 50 cm, ID 75 µm (PepMap RSLC, C18, 100 Å, 2 µm particles) column. A linear gradient of 5-40% acetonitrile at a flow rate of 300 nL/min over 60 min, maintained at 50°C, was used to separate peptide samples. The spray voltage was set to 2.2 kV, S-lens RF level at 50, and heated capillary at 275°C. Full MS resolution was set to 70,000 at m/z 200 and a full MS AGC target at 3E6 with an injection time of 50 ms. The mass range was set to 375-1800 m/z. A top10 MS2 method was defined with an AGC target value for MS2 spectra set at 2E5 ions with a resolution of 17,500, and injection time of 100 ms. An intensity threshold was set at 1E4, isolation width of 1.6 m/z, fixed first mass of 100 m/z, and normalized collision energy set at 28%. MS spectra were acquired over 90 min.

RAW spectra were submitted to an Andromeda search in MaxQuant (version 1.5.3.30) using the default settings (Cox *et al.*, 2011; Cox and Mann, 2008). Label-free quantification and match between-runs were activated (Cox *et al.*, 2014). The MS/MS spectra data were searched against the UniProt *Zymoseptoria tritici* reference database (Downloaded 180423, 10,972 entries). All searches included a contaminants database (as implemented in MaxQuant, 245 entries). Enzyme specificity was set to 'Trypsin/P' and the MS/MS match tolerance was set to ±0.5 Da. The peptide spectrum match FDR and the protein FDR were set to 0.01 (based on target-decoy approach) and the minimum peptide length was seven amino acids. For protein quantification, unique and razor peptides were allowed. Modified peptides were allowed for quantification with a minimum score of 40. Relative quantification of proteins between different MS runs is based exclusively on the label-free quantifications as calculated by the software MaxQuant, using the "MaxLFQ" algorithm (Cox *et al.*, 2014).

MS samples from Figure 6, 9, and 10 were run and processed at Syngenta by John Sinclair using data-independent acquisition mass spectrometry (DIA-MS) and the database search was performed by Spectronaut. Briefly, the acidified tryptic peptides were resuspended in 0.1% FA solution and analysed on a Fusion Lumos instrument (ThermoFisher) coupled to an Ultimate 3000 liquid chromatography system (Thermo Fisher Scientific). Samples were separated on an EasySpray 50 cm, ID 75 μm (PepMap RSLC, C18, 100 Å, 2 μm particles) column. A linear gradient of 8-40% acetonitrile at a flow rate of 300 nl/min over 120 min, maintained at 50 °C, was used to separate peptide samples. FAIMS (ThermoFisher) was applied throughout the acquisition at a CV of -40. A spray voltage set at 2.2 kV, S-lens RF level at 30, and heated capillary at 300°C. The full MS resolution was set to 120,000 at m/z 200 and full MS AGC target set to 5E5 with an injection time of 20 ms. The mass range was set to 350-1650 m/z. An AGC target value for fragment spectra was set to 1E6. A total of 40 variable windows were employed with a resolution set to 30,000, an injection time set to 60 ms, and a normalised collision energy set at 30%. All scan events were acquired in profile mode over 150 min. DIA raw files were processed in Spectronaut with the default settings for direct DIA, data filtering by Qvalue, and no run normalization applied. A FungiDB for *Z. tritici* IP0323 release 48 (downloaded 06112020, 11,839 entries) and Zt CYP450newsome2013 DB were used for database searching.

Filtering of results was done in Perseus version 1.6.13.0 (Tyanova *et al.*, 2016). Briefly, data was filtered against contaminants and only those proteins found in at least one group in all three replicates were considered. Further analysis and graphs were performed using the Qfeatures and ggplot R packages (Gatto, 2021). Imputed values were generated using a missing not at random (MNAR) and missing at random (MAR) mixed imputation over the whole matrix, and the fold change and adjusted P values (adj. P Val) were calculated using the fdr method over the three biological replicates. The correct

clustering of the biological replicates by categorical groups was evaluated using principal component analysis (PCA) plots.

Image quantification and statistical analysis

ImageJ (U.S. National Institutes of Health) was used for the quantification of the fluorescence CYP5080H1 labelling. To quantify fluorescence signals from protein gels, scanned images (.gel format) were used. The intensity of the defined signal area was quantified using the Analyse -> Measure tool. The integrated density (IntDen) was used to compare intensities signal of the same dimensions (area) measurements within the same protein gel. Fluorescence quantifications were subjected to statistical analysis using RStudio software. P-values were calculated using one-way analysis of variance (on-way ANOVA). All values shown are mean values, and the error intervals represent the standard deviation (sd).

Bioinformatics

CYP450s amino acid sequences were retrieved from Ensemble Fungi using the BioMart tool and the cytochrome P450 Pfam entry (PF00067). Peptides sequences were aligned using the software PROMAL3D (Pei *et al.*, 2008) and the phylogenetic tree was build using the Maximum Likelihood method in MEGA X (Kumar *et al.*, 2018). Number of bootstrap replications was set to 500 and other parameters were obtained automatically by default in MegaX (Model/Method: LG model; Rates among Sites: Uniform Rates; Gap/Missing Data Treatment: use all sites; ML Heuristic Methods: Nearest-neighbour-Interchange (NNI); Initial tree for ML: Default – NJ/BioNJ.

Supplemental data

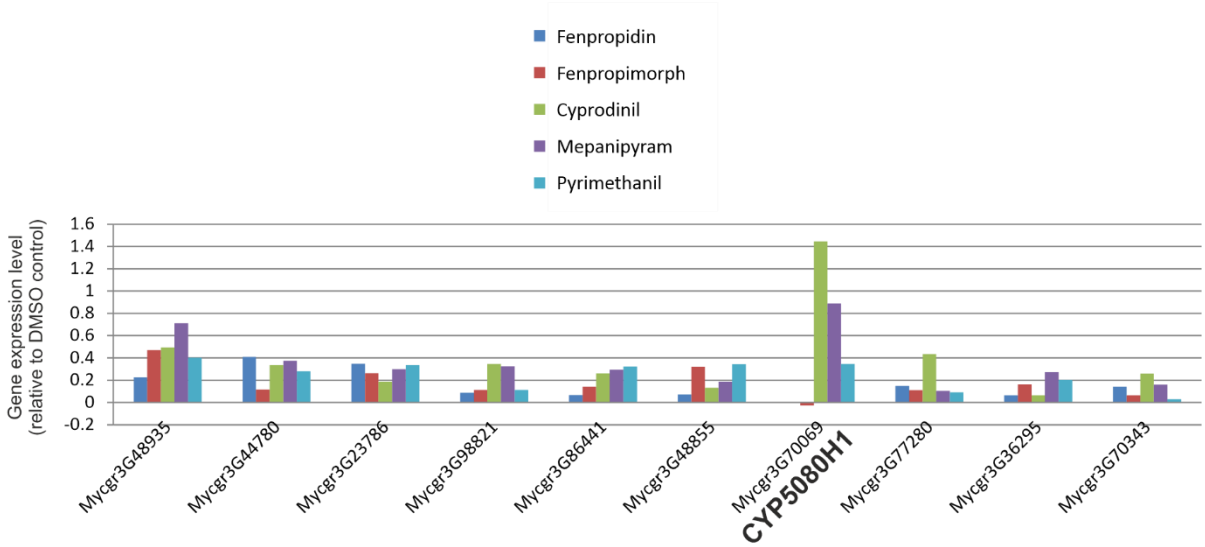


Figure S1. CYP5080H1 is identified as the main *Z. tritici* CYP450 transcriptionally responsive to cyprodinil and mepanipyrim treatments. RNA-seq gene expression values of cyprodinil-treated *Z. tritici* cell cultures

relative to the DMSO-only treated control. Three-day-old *Z. tritici* cell culture was treated with 1 ppm (part per million) of each indicated fungicide, or an equal amount of DMSO, for two hours.

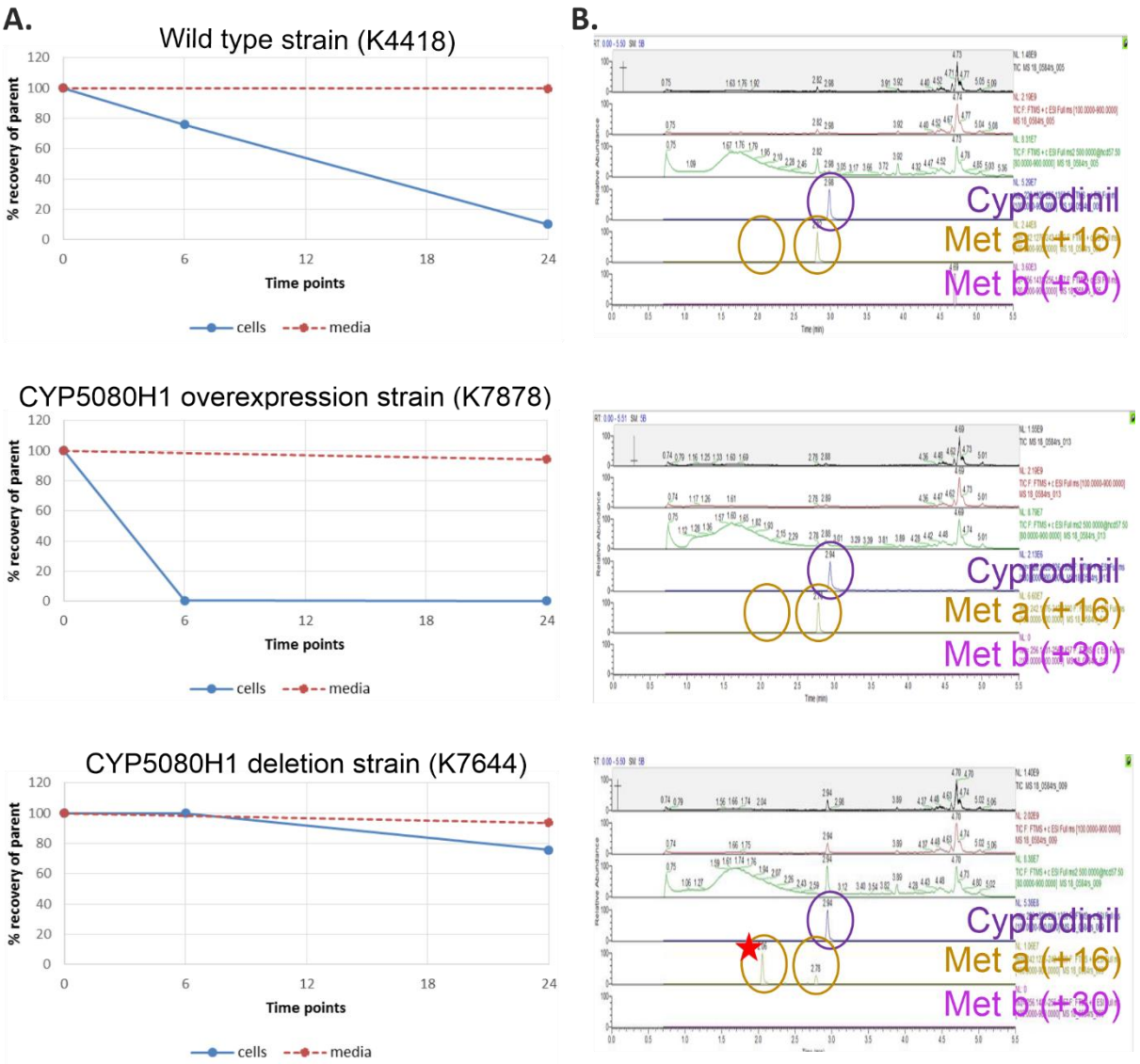


Figure S2. Characterisation of cyprodinil degradation by CYP5080H1. **A**, Cyprodinil is faster metabolised in CYP5080H1 overexpression strain and less in CYP5080H1 deletion strain. *Z. tritici* wild type and CYP5080H1 overexpression or deletion strain were incubated with media containing cyprodinil. Cyprodinil concentration remaining in the media or uptooked by *Z. tritici* cells was measured 6, 12, 18 and 24h after treatment. **B**, CYP5080H1 deletion strain has a different metabolite a (+16) profile in comparison to wild type *Z. tritici* strain. *Z. tritici* wild type, overexpression or deletion strains were incubated with cyprodinil. Metabolites were extracted and analysed via LC-MS. LC-MS chromatograms are shown.

Table S4. Plasmids

Golden Gate Modules	
Lab number	**Description**
pJK268c	pL1V2-P19-F2, Binary vector.
GG1-01	pL0V-SC1-15456, Level 0 Cloning vector, Golden Gate original vector, EC15456.
GG1-55	pL0M-T-35S-1-41414, Level 0 Module, 35S terminator, Golden Gate plant kit, pICH41414.
GG1-57	pL0M-PU-35S-TMV-3-51288, Level 0 Module, 2 x 35S promoter + TMV Ω (0.8 kb), Golden Gate plant kit, pICH51288.
GG1-78	pL0M-C2-eGFP-15095, Level 0 Module, eGFP for C terminal fusion. EC15095. ENSA consortium https://www.ensa.ac.uk/
Golden Gate binary vectors in *Agrobacterium tumefaciens* GV3101	
Lab number	**Description**
pMF330	pL2M-P19-kan-2x35S::CYP12-GFP (CYP5078B1)
pMF331	pL2M-P19-kan-2x35S::CYP51-GFP (CYP5080H1)
pMF348	pL2M-P19-kan-2x35S::CYP29-GFP (CYP52R1)
pMF349	pL2M-P19-kan-2x35S::CYP30-GFP (CYP539A6)

Table S5. Nucleotide sequences of the primers used for cloning and mutagenesis. The BsaI restriction sites for Golden Gate cloning are underlined.

Name	**Sequence**
FW_CYP12	TTGGTCTCAAATGGCTTTACCAGCACTTCTC
RV_CYP12	TTGGTCTCACACCGCAAGATCGCTCTCTG
FW_CYP51	TTGGTCTCAAATGTCGCTACTGACGG
RV_CYP51	TTGGTCTCACACCTACCCTTGGGCTCAC
FW1_CYP29	TTGGTCTCAAATGCATAACGTCGCTCTG
FW2_CYP29	TTGGTCTCAGAAACCGGTATCGATTATTCTG
RV1_CYP29	TTGGTCTCATTTCCGCAGGGATGAAGATAG
RV2_CYP29	TTGGTCTCACACCCTCCGCCTCGTGCAAC
FW1_CYP30	TTGGTCTCAAATGCTCGTCGCCCTTATC
FW2_CYP30	TTGGTCTCAGAAACCCTCCGGCTTTACC
RV1_CYP30	TTGGTCTCATTTCATTCATTGTATGTGTGAGG
RV2_CYP30	TTGGTCTCACACCTGACCTGCTTGCCTTC

*FW, forward; RV, reverse.

Chapter 4: Photoaffinity profiling of Glutathione transferases in plants

Maria Font Farre[1], Daniel Brown[2], Maurice Koning[1], Farnusch Kaschani[3], Richard Dale[4], Samantha Hall[4], Melloney Morris[4], Markus Kaiser[3], Aaron Wright[5], Jonathan Burton[2] and Renier A.L. van der Hoorn[1]

[1] The Plant Chemetics Laboratory, Department of Plant Sciences, University of Oxford, Oxford, UK.

[2] The Burton Group, Department of Chemistry, University of Oxford, Oxford, UK.

[3] Chemische Biologie, Zentrum für Medizinische Biotechnologie, Fakultät für Biologie, Universität Duisburg-Essen, Universitätsstr. 2, 45117 Essen, Germany.

[4] Bioscience, Syngenta, Jealott's Hill International Research Centre, Bracknell, UK.

[5] Chemical Biology & Exposure Sciences, Pacific Northwest National Laboratory, Richland WA USA; The Gene and Linda Voiland College of Chemical Engineering and Bioengineering, Washington State University, Pullman WA USA.

Abstract

The glutathione transferase (GST) family is a multigenic gene family involved in multiple stress response in plants. The phi (F) and tau (U) GST classes are plant-specific and abundant in plants, and are induced following exposure of plants to agrochemicals and biotic/abiotic stresses. Due to their distinct functions and catalysing mechanisms, various subcellular localizations and complex regulation, many efforts have been taken to identify the selectivity of these enzymes and understand their biological function. Here we validated the use of the GST-G, a glutathione-based photoaffinity probe designed to target the glutathione-binding (G-site) of GSTs, to target the GSTF and GSTU classes of glutathione transferases in plants. We characterised the labelling profile, identified the labelled proteins and confirmed their inhibition by well-known GST inhibitors. Furthermore, we extended GST labelling in a broad range of plant species including liverworts, bryophytes, monocots and dicots species. We also showed the use of GST-G to detect changes in GST activities after abiotic- and biotic-related chemical treatments, and identified the main GSTs activated after BION treatment of Arabidopsis plants.

Introduction

Glutathione transferases (GSTs), also referred as glutathione S-transferases, form a large and diverse multigenic enzyme family that commonly conjugate tripeptide glutathione (γGlu-Cys-Gly) to a broad range of substrates (Sylvestre-Gonon *et al.*, 2019). In plants, GSTs play important roles in biosynthetic pathways, agrochemical detoxification, plant defence and oxidative stress (Basantani and Srivastava, 2007). The vast majority of plant GSTs are cytosolic and have a conserved three-dimensional structure, containing two conserved pockets: a glutathione-binding site (G-site) and a hydrophobic substrate-binding site (H-site) (Ding *et al.*, 2017). The G-site is conserved among all GST classes, stressing the importance of the correct binding and orientation of glutathione for their correct function. The H-site is a more variable region, responsible for the promiscuous binding of diverse substrates.

Originally, the Arabidopsis (*Arabidopsis thaliana*) GST family was subdivided into seven main soluble classes: phi (GSTF), tau (GSTU), theta (GSTT), zeta (GSTZ), lambda (GSTL), dehydroascorbate reductase (DHAR) and tetrachloro-phydroquinone dehydrogenase-related (TCHQD) (Dixon *et al.*, 2002a) (Figure 1). Later, a membrane-associated GST (At1g65820), which is phylogenetically related to membrane associated proteins in eicosanoid and glutathione metabolism (MAPEG), was added as a GST member, due to their known GSH-dependent activity (Dixon and Edwards, 2010; Kammerscheit *et al.*, 2019). More recently, three new GST-like classes of have been described in Arabidopsis: the glutathionyl hydroquinone reductase (GHR), the microsomal prostaglandin E-synthase type 2 (mPGES-2) and the eukaryotic translation elongation factor 1B- γ subunit (EF1Bγ) (Lallement *et al.*, 2014). Most GSTs are dimeric proteins, with the exception of DHARs and GSTLs (Dixon *et al.*, 2002b).

GSTs are also classified depending on the composition of their catalytic centre. On one hand, Ser-GSTs contain a conserved serine residue in their catalytic site which is essential for their main ability to conjugate glutathione onto substrates. Ser-GSTs are also known to have peroxidase activities and therefore are known to play a role in agrochemical detoxification and stress responses (Sylvestre-Gonon *et al.*, 2019). Ser-GSTs include GSTU, GSTF, GSTZ, GSTT and TCHQD classes. GSTU and GSTF classes are plant-specific and the most abundant cytosolic GSTs in plants. Furthermore, GSTU and GSTF classes are highly induced following exposure of plants to agrochemicals and biotic/abiotic stresses (Cummins *et al.*, 2011). GSTZ and GSTT classes are soluble GSTs also present in other eukaryotes (Dixon *et al.*, 2002b). GSTZ1 is a cytosolic isomerase mostly related to the cell metabolism functions of tyrosine degradation and GSTTs are mainly associated with glutathione-dependent peroxidase activities and oxidative stress, although they have also some detoxification activities (Dixon *et al.*, 2009; Dixon and Edwards, 2010). TCHQD is located in the plasma membrane and has been described as an agrochemical

detoxifying enzyme for its ability to metabolise chlorinated xenobiotics (Dixon *et al.*, 2009; Dixon and Edwards, 2010).

On the other hand, Cys-GSTs contain a conserved cysteine residue in their catalytic site and are incapable of catalysing GST conjugations. Instead, Cys-GSTs are able to catalyse deglutathionylation and dehydroascorbate reductions (Lallement *et al.*, 2014; Sylvestre-Gonon *et al.*, 2019). The Ser to Cys catalytic substitution promotes the formation of mixed disulfides between the regulatory Cys and the monothiol reductant GSH (Danon, 2002; Dixon *et al.*, 2002b). In this group we find GTSL, DHAR, GHR and mPGES-2 classes. DHARs and GSTL are both plant-specific classes and reside in both the cytosol and subcellular organelles (Dixon, *et al.*, 2002b). Both classes, together with GHRs, are known to have thioltransferase activities and undergo glutathionylation, and hence they provide oxidative stress protection (Gao *et al.*, 2009; Lallement *et al.*, 2014). Furthermore, DHARs are essential in the ascorbate-glutathione cycle due to their main catalytic activity as dehydroascorbate reductases, and GSTLs are likely to be responsible for the reduction of small molecules (Dixon and Edwards, 2010).

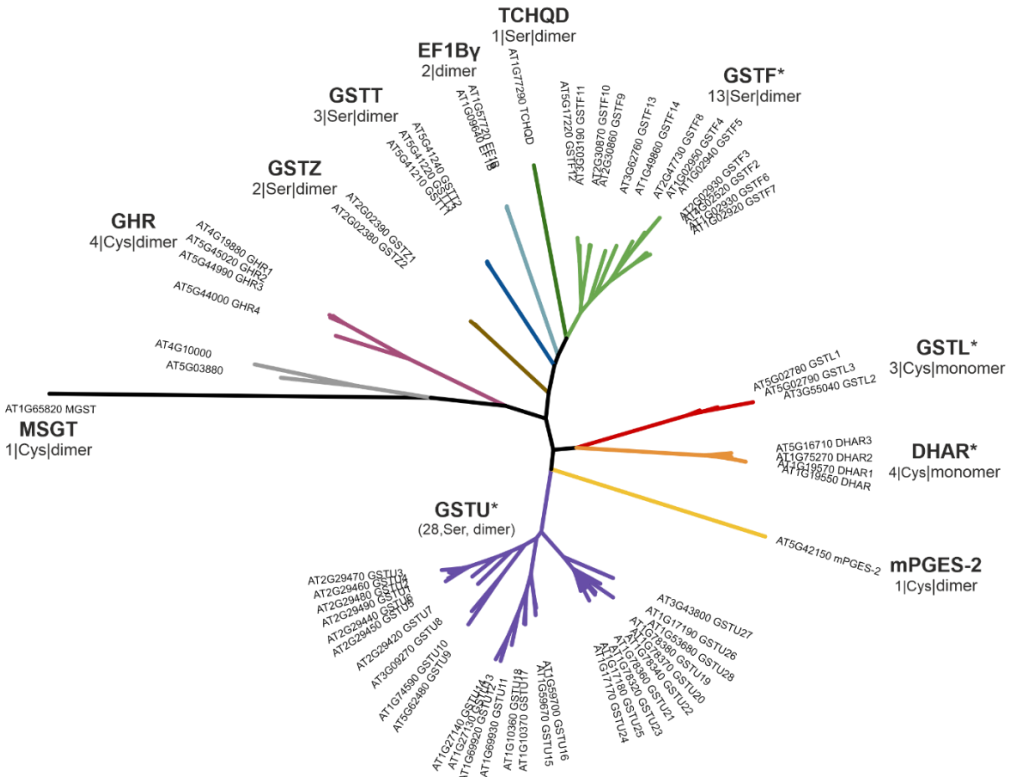


Figure 1. Classification of Arabidopsis glutathione transferases (GSTs) based on amino acid sequence identity. The sequences used were retrieved from Arabidopsis TAIR10 and aligned using PROMAL3D. The unrooted phylogenetic tree was constructed using the Maximum Likelihood method (1000 bootstraps) and edited with iTOL. GST classes are indicated in bold. Plant-specific GST classes are indicated with an asterisk (*). For each class, the number of Arabidopsis GSTs, the conservation of a serine or a cysteine in their catalytic site (Ser|Cys) and their monomeric or dimeric composition are indicated (monomer|dimer).

GSTs have a main role in the modification of exogenous compounds (xenobiotics) and their detoxification (Cummins *et al.*, 2011). In agrochemical detoxification, GSTs are responsible for conjugating glutathione to agrochemicals, converting herbicides into hydrophilic compounds with limited mobility and reduced toxicity. Metabolic herbicide resistance in weeds is associated with elevated levels of herbicide-metabolising enzymes, including GSTs. In blackgrass (*Alopecurus myosuroides*) and ryegrasses (*Lolium* spp.), the upregulation of several GST has been associated with multiple-herbicide resistant in resistant field populations, being *Am*GSTF1 a commonly upregulated GST in multiple-resistance blackgrass populations (Cummins *et al.*, 2013; Dücker *et al.*, 2019, 2020; Tétard-Jones *et al.*, 2018). Other examples are the high constitutive expression of GSTF2, which is was associated with atrazine resistance in two waterhemp (*Amaranthus tuberculatus*) populations and the high levels of GST activities in the resistant populations of American sloughgrass (*Beckmannia syzigachne*) (Evans *et al.*, 2017; Pan *et al.*, 2016; Wang *et al.*, 2020). In addition, safener applications can also enhance the expression of GSTs in many plant species such as Arabidopsis, rice, wheat and maize (Cataneo *et al.*, 2013; Deng and Hatzios, 2002; Li *et al.*, 2017; Skipsey *et al.*, 2011). Safeners are chemicals used in agriculture to protect cereal crops without compromising herbicide efficacy in weed control. Safeners improve herbicide tolerance in crops by selectively inducing herbicide metabolising activities in cereal crops but not in weeds (Hatzios and Burgos, 2004; Jablonkai, 2013). For instance, in maize the safener isoxadifen-ethyl reduces crop injury caused by the herbicide nicosulfuron through the induction of GSTs (Sun *et al.*, 2017). Similarly, fenclorim and metcamifen application protected rice against injury by pretilachlor and clodinafop herbicides, respectively, associated with the induction of several detoxification genes, including GSTs (Brazier-Hicks *et al.*, 2020; Hu *et al.*, 2020, 2021; Taylor *et al.*, 2013).

GSTs are also known to play a role in plant defence and to be stress-inducible. GSTs are induced after pathogen infections and provide pathogen resistance in multiple plant species (Gullner *et al.*, 2018; Nianiou-Obeidat *et al.*, 2017). A study on maize observed a high genetic correlation between a GST gene and a multiple disease resistance (MDR) trait providing resistance to three independent fungal leaf diseases (Wisser *et al.*, 2011). Another example is an increased susceptibility of *Nicotiana benthamiana* plants to *Colletotrichum* infections upon silencing of *Nb*GSTF1 (Dean *et al.*, 2005).

Furthermore, GSTs are commonly induced during priming responses. Priming is a physiological mechanism that allow plants to respond more rapidly and strongly to subsequent stress situations due to a more efficient perception and activation of the defence response (Aranega-Bou *et al.*, 2014). Treatment of plants with salicylic acid (SA) or functional analogues of SA (e.g. acibenzolar-S-methyl or benzothiadiazole (BTH)) are commonly used to protect plant crops against biotrophic pathogens (Aranega-Bou *et al.*, 2014). More recently, the treatment of plants with natural compounds (e.g. vitamins

or volatile organic compounds) and bioagents (e.g. beneficial microbes or pathgens) has been shown to provide protection against pathogen attacks (Abbasi *et al.*, 2020; González-Bosch, 2018). Previous studies identified GSTs as SA-inducible genes. For example, treatment of Arabidopsis with salicylic acid induced the expression of phi and thau class-specific GSTs (Sappl, Heazlewood, *et al.*, 2004). Similarly, the pre-treatment of tomato plants with salicylic acid induced the expression of GST in tomato plants, and consequently increased the salt tolerance of pre-treated tomato plants (Csiszár *et al.*, 2014).

In summary, the GST family is a multigenic gene family involved in multiple stress response in plants. Due to their distinct functions and catalysing mechanisms, various subcellular localizations and complex regulation, many efforts have been taken in order to identify the selectivity of these enzymes and understand their biological function (Sappl *et al.*, 2009). Nonetheless, just a few GSTs have been identified as the actual cause of the decreased efficacy of agrochemicals and little is known about the specific role and mechanisms by which these enzymes contribute to plant immunity. Activity-based protein profiling (ABPP) is a distinct and powerful tool used in many biological systems to monitor, identify and characterise the activity of different enzymes within complex proteomes (Kovács and van der Hoorn, 2016). ABPP aims to selectively label the active site of enzymes using bifunctional chemical, which contain a reactive warhead responsible for enzyme specificity and a reporter tag responsible for its detection. Previously, two chemical probes were designed for the chemical proteomic studies of mammalian GSTs (Stoddard *et al.*, 2017). One was a mechanism-based probe targeting the GST H-site and is based on an irreversible inhibitor of mammalian GSTs. The other was a photoaffinity-based probe targeting the GST G-site and is designed based on a glutathione molecule. Both GST probes successfully labelled a recombinant human GST and several GSTs from mouse liver and lung cytosolic extracts and were applied for studying the differential activation of GSTs in diet induced obese mice. Here we validated the use of the glutathione-based photoaffinity probe designed to target the glutathione-binding (G-site) of GSTs, GST-G probe, to target GSTs in plants.

Results

Glutathione transferases are the main target of GST-G in Arabidopsis

To apply the use of GST probes in plants, we studied the chemical reactivity of the glutathione-based photoaffinity probe, GST-G. GST-G consists of three parts: (1) a glutathione moiety (green) directs it toward the glutathione binding site, termed as the G-site; (2) a benzophenone group that facilitates the irreversible binding of the probe to a neighbouring C-H bond of an amino acid upon UV irradiation; and (3) an alkyne tag that allows the coupling of the probe to a fluorescent or affinity tag (Figure 2A).

To test for GST-G labelling, Arabidopsis leaf extracts were incubated with or without 5 μM GST-G, irradiated with UV and coupled to a fluorophore via click-chemistry. GST-G labelled two distinct bands at approximately 25 kDa molecular mass of GST (Figure 2B, arrow). GST-G labelling was UV and click-chemistry dependent as no 25 kDa signal was observed in the absence of UV irradiation or click-chemistry. Furthermore, we observed that when the Arabidopsis leaf proteome was subjected to click-chemistry a strong background signal, which presumably corresponds to rubisco, was observed at around 55 kDa (Figure 2B, asterisk).

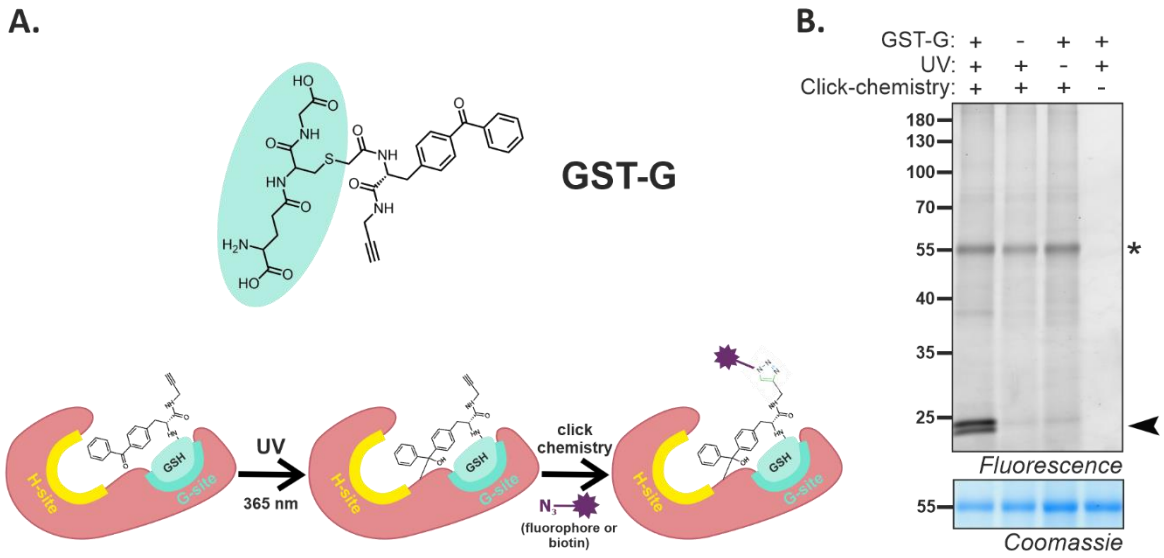


Figure 2. GST-G probe structure and activity profile in Arabidopsis leaf extracts. A, Structure and photoaffinity labelling of the glutathione-based affinity probe, GST-G, targeting the "G site" of glutathione S-transferases. GST-G contains a glutathione moiety (green), a UV-reactive benzophenone group and an alkyne chemical handle for click chemistry coupling to fluorophores and/or biotin. **B,** GST-G labels two distinct bands at approximately 25 kDa (arrow) and its labelling is UV and click chemistry dependent. (*) rubisco background signal, <, distinct GST labelling bands. Arabidopsis leaf proteome was labelled with and without 5 μM GST-G, irradiated with UV and coupled to a fluorophore via click-chemistry. Labelled proteins were coupled to a fluorophore and visualised by in-gel fluorescence scanning. Coomassie staining is shown as loading control. Similar results were obtained in two additional independent replicates. Black arrow, GSTs.

To characterise GST-G labelling further, we evaluated the concentration, UV exposure time and pH dependency labelling of GST-G in Arabidopsis leaf extracts. GST-G was tested with increasing probe concentrations and UV radiation exposures in Arabidopsis leaf extract. GST-G labelling reached saturation with 5 μM probe (Figure 3A). UV treatment of 30 min was sufficient to detect GST-G labelling, but signals increased further after 60 min of UV irradiation (Figure 3B). GST-G labelling was strongly pH dependent, with increase labelling at higher pH (Figure 3C). Therefore, the remaining experiments were performed with 5 μM GST-G, 45 min UV irradiation and a pH of 7.5.

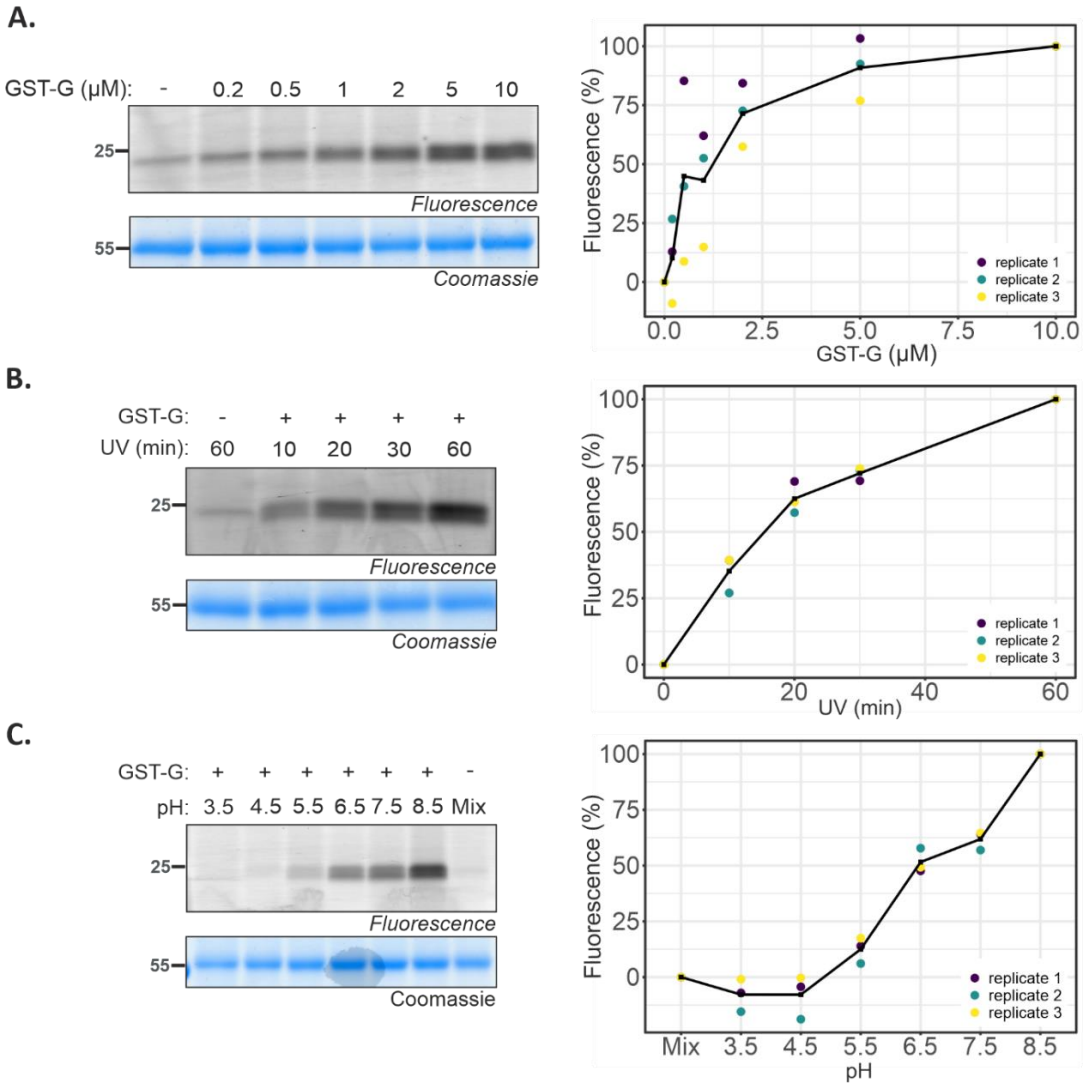
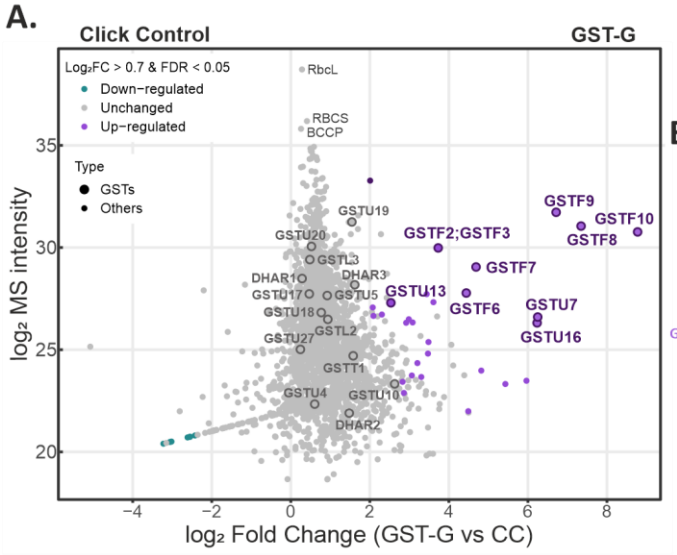


Figure 3. Concentration, UV exposure time and pH dependency labelling of GST-G. A, GST-G concentration course and signal intensity quantification. Arabidopsis leaf proteome was labelled with GST-G and UV-radiated for 30 min. **B,** GST-G UV time exposure course and signal intensity quantification. Arabidopsis leaf proteome was labelled with 5 μM GST-G and UV radiated for different amount of time. **C**, pH dependence course labelling and signal intensity quantification. Arabidopsis leaf proteome was extracted in water and buffered to different pH. Labelling was performed by adding 5 μM GST-G to the buffered samples and samples were UV-radiated for 30 min. Arabidopsis leaf proteome was labelled with GST-G and labelled proteins were processed and detected as described in Figure 2. SDS-PAGE gel is the representative of three replicates and Coomassie staining is used as loading control. Fluorescence (%) was calculated when compared to the strongest signal intensity and subtracting the background of the no-probe control (-) in each gel. The quantification graphs represent the percentage of fluorescence from the three replicates.

To identify the targets of the GST-G probe, Arabidopsis leaf extracts were incubated with 5 μM GST-G and labelled proteins were coupled to a biotin affinity tag for subsequent enrichment on streptavidin beads. Purified proteins were on-bead digested with Lys-C and trypsin, and digested peptides were identified by liquid chromatography tandem mass spectrometry (LC-MS/MS). The pull-down was performed three times for the GST-G labelled samples and three times for the click control samples.

After removing contaminants and filtering proteins to retain Arabidopsis proteins found in at least one group in all three replicates, a total of 2205 proteins were detected. After further statistical analysis, we detected nine GSTs from two different classes (Phi, F; and Tau, U) among the 29 proteins significantly enriched in the GST-G samples (Figure 4A, purple dots, and 4B). Three members of the phi class (GSTF10, GSTF9, GSTF8) and two members of the tau class (GSTU16, GSTU7) were enriched with a $\log_2$ FC higher than 6 and detected with high MS intensities. We also detected GSTF7, GSTF6, GSTF2, GSTF3 and GSTU13 with high MS intensities but a lower $\log_2$ FC enrichment ($2 < \log_2 \text{FC} > 6$). All significantly enriched GSTs were detected with several unique peptides and had good sequence coverage (50 - 85%) and a predicted molecular weight (MW) of around 25 kDa (Figure 4B). The majority of the proteins detected in the pull-down were unchanged between the GST-G and click control (Figure 4A, grey dots) and include endogenous biotinylated proteins such as BCCP, MCCA and ACC1 as well as the abundant large Rubisco subunit RbcL (Figure 4A, top signals). We consider them click chemistry contaminants and it correlates with the high background that click chemistry can give when attaching a tag to labelled proteome (Figure 2B and Figure S1). We also detected 14 GSTs among these not significantly GST-G enriched proteins (Figure 4A, grey dots encircled). The majority of these GSTs were tau class members but GSTs from the lambda, theta and DHAR classes were also detected. The rest of the proteins found significantly enriched in the GST-G sample have a molecular weight that did not correspond to the 25 kDa band signal observed in the GST-G fluorescent gels (Figure 1B).

A.



B.

	Click Control			GST-G			log₂FC
	r1	r2	r3	r1	r2	r3	
GSTF10	9.19E+07	9.01E+07	7.98E+07	4.12E+10	3.56E+10	3.79E+10	8.78
GSTF8	1.38E+08	2.55E+08	1.50E+08	2.96E+10	2.96E+10	2.60E+10	7.35
GSTF9	2.12E+08	4.69E+08	4.17E+08	4.17E+10	3.42E+10	3.37E+10	6.71
GSTU7	NA	3.95E+06	NA	3.10E+08	3.19E+08	2.74E+08	6.25
GSTU16	8.18E+06	6.50E+06	NA	7.18E+08	5.03E+08	4.57E+08	6.23
GSTF7	1.23E+08	9.86E+07	1.08E+08	3.07E+09	3.93E+09	1.86E+09	4.69
GSTF6	5.83E+07	5.09E+07	4.03E+07	9.63E+08	1.32E+09	9.60E+08	4.44
GSTF2;GSTF3	2.40E+08	3.15E+08	3.26E+08	4.27E+09	4.36E+09	3.09E+09	3.73
GSTU10	4.05E+06	3.37E+06	5.57E+06	2.48E+07	5.07E+07	1.43E+07	2.63
GSTU13	6.89E+07	7.40E+07	6.30E+07	3.92E+08	3.92E+08	4.05E+08	2.53

C.

	Name	Protein IDs	log2FC	MS intensity	adj.P.Val	u. pep.	r. pep.	SC [%]	MW [kDa]	FDR
1	GSTF10	P42761	8.78	30.76	0.00004	12	2	75.3	24.23	FDR 0.001
2	GSTF8	Q96266	7.35	31.05	0.00069	12	0	67.7	29.23	FDR 0.001
3	GSTF9	O80852	6.71	31.72	0.00243	9	0	56.7	24.15	FDR 0.01
4	GSTU7	Q9ZW24	6.25	26.60	0.01428	12	0	54.6	26.11	FDR 0.05
5	GSTU16	Q9XIF8	6.23	26.54	0.00489	7	0	50.4	26.51	FDR 0.01
6	At5g24490	Q94K97	5.96	23.48	0.03169	4	0	15.6	34.86	FDR 0.05
7	SAD2	F4IRR2	5.43	23.32	0.00531	10	0	13.8	119.25	FDR 0.01
8	rpl14	P56792	4.82	23.98	0.01249	5	0	52.5	13.58	FDR 0.05
9	GSTF7	Q9SRY5	4.69	29.05	0.00531	8	11	82.3	23.60	FDR 0.01
10	NUP50A	Q9C829	4.49	21.99	0.02683	8	0	18.2	46.59	FDR 0.05
11	GSTF6	P42760	4.44	27.77	0.00424	7	0	85.1	23.49	FDR 0.01
12	GSTF2;GSTF3	P46422;Q9SLM6	3.73	29.98	0.00531	11	1	81.6	24.13	FDR 0.01
13	T28K15.4;At1g12230	Q9FWX0;F4IC59	3.61	27.33	0.00489	11	0	40.7	43.99	FDR 0.01
14	OVA5	Q9LJE2	3.48	25.38	0.00489	9	0	25.1	67.59	FDR 0.01
15	At2g41950	O23684	3.47	24.81	0.01428	5	0	30.8	30.02	FDR 0.05
16	LTP1	Q42589	3.44	27.72	0.01061	4	0	33.1	11.76	FDR 0.05
17	unknown	Q9LVV5	3.30	23.67	0.01296	3	0	25.1	24.57	FDR 0.05
18	MLP28	Q9SSK9;A8MR61;B3H4F3;A8MRH3	3.20	24.35	0.01609	3	1	21.2	37.61	FDR 0.05
19	MFP2	Q9ZPI5	3.08	26.33	0.01352	17	0	38.9	78.84	FDR 0.05
20	CPK11	Q39016	3.06	23.74	0.01387	4	5	21.4	55.92	FDR 0.05
21	At1g09130;CLPR3	F4HZE0;Q8L770	2.99	26.49	0.04105	7	0	23.2	40.92	FDR 0.05
22	At4g39280	F4JVC5;Q9T034	2.92	26.32	0.04664	12	0	36.1	55.78	FDR 0.05
23	APX6	Q8GY91	2.86	22.88	0.03501	3	0	10.9	36.24	FDR 0.05
24	RPT2A;RPT2B	Q9SZD4;Q9SL67	2.83	23.43	0.01979	6	0	26.9	49.37	FDR 0.05
25	GSTU13	Q9FUS6	2.53	27.30	0.01113	9	0	54.6	25.13	FDR 0.05
26	unknown	Q9SKI0	2.30	26.72	0.04277	5	0	23.4	29.65	FDR 0.05
27	unknown	Q9FKA5	2.09	26.65	0.04105	16	0	48.3	43.53	FDR 0.05
28	PETE	A0A1P8APR2;P11490	2.07	27.07	0.02640	1	0	11.6	21.87	FDR 0.05
29	unknown	P46283	2.01	33.27	0.02948	18	0	53.2	42.41	FDR 0.05

Figure 4. Phi (GSTF) and tau (GSTU) are the main classes of GSTs labelled by GST-G. **A**, Representation of the detected proteins in the GST-G pull-down. Arabidopsis leaf extracts were labelled with and without 5 μM GST-G, coupled to a biotin affinity tag via click chemistry and enriched on streptavidin beads. On-bead digested proteins were analysed by MS. Graph represent the MS intensities (log_2 MS intensities) over the enrichment of GST-G samples in comparison to click control samples (log_2 Fold Change). In purple, GST-G enriched proteins; in grey, unchanged proteins; in blue, click chemistry (CC) enriched proteins. All GST proteins detected are encircled. **B**, MS spectral intensities of the GSTs labelled by GST-G of three independent replicates per treatment (r1, replicate 1; r2, replicate 2; r3, replicate 3). **C**, Description of the GST-G enriched proteins. Table includes: Name, Protein IDs, log_2 Fold Change (log_2FC), log_2 MS intensity (MS intensity), adjusted P. value (adj.P.Val), unique peptides (u.pep.), razor peptides (r. pep.), sequence coverage (SC [%]), molecular weight (MW [kDa]), FDR significance (FDR).

Next, we wanted to compare the correlation between the detected GSTs and their gene expression in Arabidopsis leaf tissues. For that, we retrieved gene expression data from Arabidopsis eFP Browser 2.0 (Figure 5). The GSTs we find with higher MS intensities correlate with those found to be highly expressed in Arabidopsis rosette leaves (> 500 RPKM). However, we could not detect the significant enrichment of GSTU20, GSTU19, DHAR1, DHAR3 and GSTL3 by GST-G, although all of them were detected and expressed in Arabidopsis leaf tissues. On the other hand, we did detect the enrichment upon labelling of several other GSTs that have a low expression in Arabidopsis leaves, such as GSTU10, GSTU16 and GSTU7, indicating a possible differential selectivity of GST-G for individual GSTs. No members of the lambda, theta, zeta, DHAR and TCHQD classes were found to be enriched upon labelling, but these GSTs are not highly expressed in Arabidopsis leaf (and root) tissues.

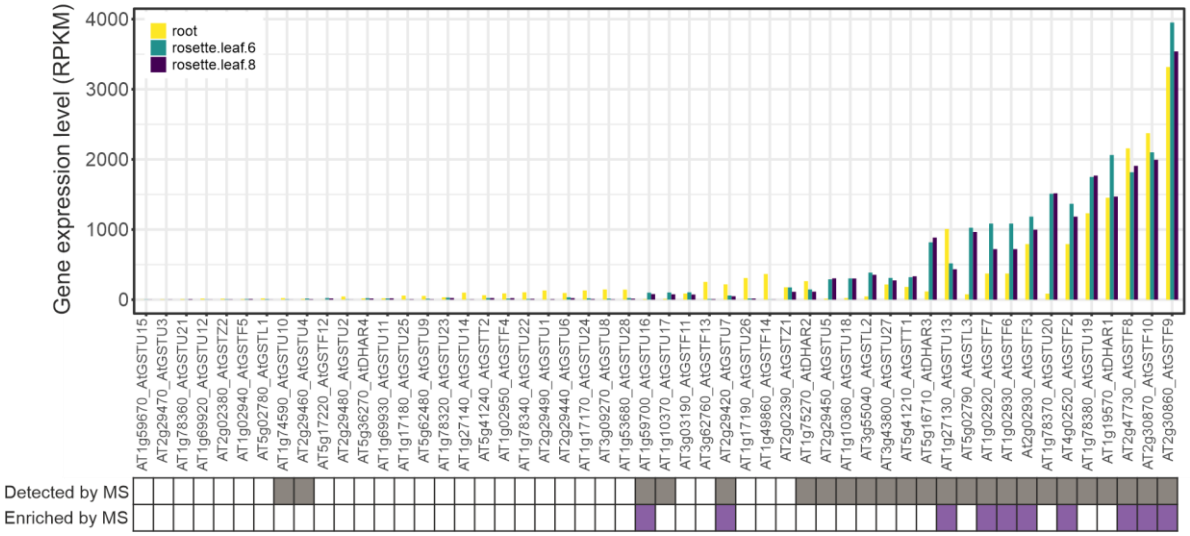


Figure 5. Gene expression level of all members of the GST family in two Arabidopsis tissues (roots and leaves, rosette leaf 6 and 8). Data retrieved from Arabidopsis eFP Browser 2.0. In grey, detected GSTs in the GST-G pull-down. In purple, enriched GSTs in the GST-G pull-down.

We next confirmed labelling of GSTs by competing GST-G labelling by known GST inhibitors. We tested S-hexylglutathione (SHG), a glutathione analogue competing for the G-site of GSTs, and ethacrynic acid (EA), a substrate/inhibitor for the H-site of GSTs (Allocati *et al.*, 2018). Pre-incubation of Arabidopsis leaf extract with SHG partially suppressed the two distinct GST-G labelled bands, inhibiting more strongly the top band (Figure 6, top arrow). By contrast, EA also partially suppressed the labelling of the two GST-G bands, inhibiting more strongly the bottom band (Figure 6, bottom arrow).

In conclusion, although the GST-G pull-down had a high click chemistry background, we confirmed the labelling of several GSTs by GST-G, including GSTs of the two highly expressed GST classes in Arabidopsis leaf tissues.

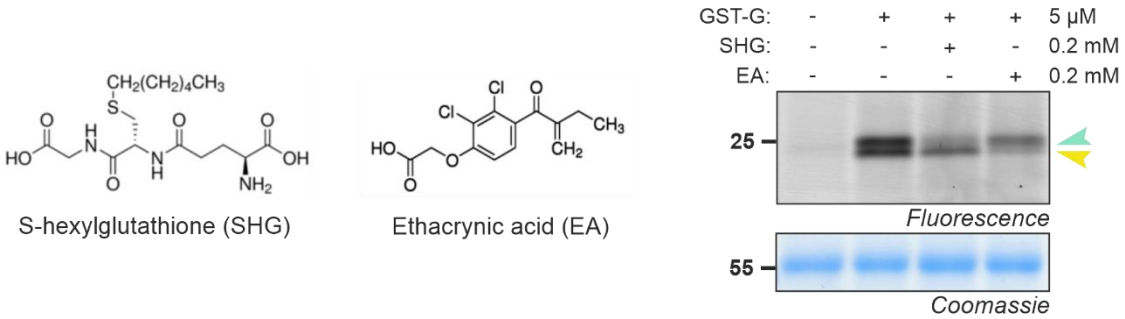


Figure 6. G-site and H-site GST inhibitors partially suppress GST-G labelling. GST-G inhibition by two known GST inhibitors: S-hexylglutathione (SHG) and ethacrynic acid (EA). Arabidopsis leaf extract at pH 7.5 was pre-incubated with or without 0.2 mM SHG or EA for 20 min and then labelled with 5 µM GST-G and UV-radiated for 45 min. Labelled proteins were processed and detected as described in Figure 2. Coomassie staining is shown as loading control. This experiment was performed three times with similar results.

GST-G has different affinities within GST classes

To validate the labelling of GSTs by GST-G, we heterologously expressed six GSTs in *Escherichia coli* (*E. coli*). We selected five Arabidopsis GSTs from the two main GST classes detected in the pull-down, as well as *Sj*GST, a well-characterised GST from *Schistosoma japonicum* commonly used as a fusion protein for protein purification and protein immobilization (Esposito and Chatterjee, 2006; Kolodziej *et al.*, 2011; Zhou *et al.*, 2014). GSTF6, GSTF8 and GSTF9 were selected as they are well-expressed GSTs in Arabidopsis leaves and were found enriched by GST-G. GSTU19 and GSTU20 were included as they are GSTs highly expressed in Arabidopsis leave tissue but were not found significantly enriched by GST-G. *Sj*GST is a good positive control as it has a well-described affinity for glutathione. We expressed SjGST from the pGEX-4T1 vector (GE Healthcare) and cloned Arabidopsis GSTs into pET-STRP3 (Novagen). Obtained plasmids were checked and transformed into *E. coli* cells. All six GST constructs were successfully expressed in *E. coli* cells as we detected an increased abundance of a single band around 25 kDa in IPTG-induced (I) samples (Figure 7A, arrow).

Next, we incubated induced *E. coli* cell extracts with GST-G and we observed an increased fluorescence in the GST-G sample for all the expressed GSTs except for GSTU20 (Figure 7B, asterisk). We observed differences in labelling intensities between GSTs accumulating at similar concentrations. For example, GSTF9 was labelled more intensely than GSTF6, although both GSTs were detected at similar concentrations by Coomassie staining (Figure 7B). Surprisingly, we also detected differences in the labelling of two closely related tau GSTs. GST-G successfully labelled GSTU19 but not GSTU20, even though GSTU20 accumulates to similar levels than GSTU19 (Figure 7B). We also observed a high MW around 55 kDa band in GSTU19 samples, which could correspond to the known homodimers GSTs form in nature that might not have been dissociated during SDS-PAGE (Sylvestre-Gonon *et al.*, 2019). Noteworthy, although *Sj*GST was used as a positive control, we observed a more efficient labelling of GSTF8 and GSTU19.

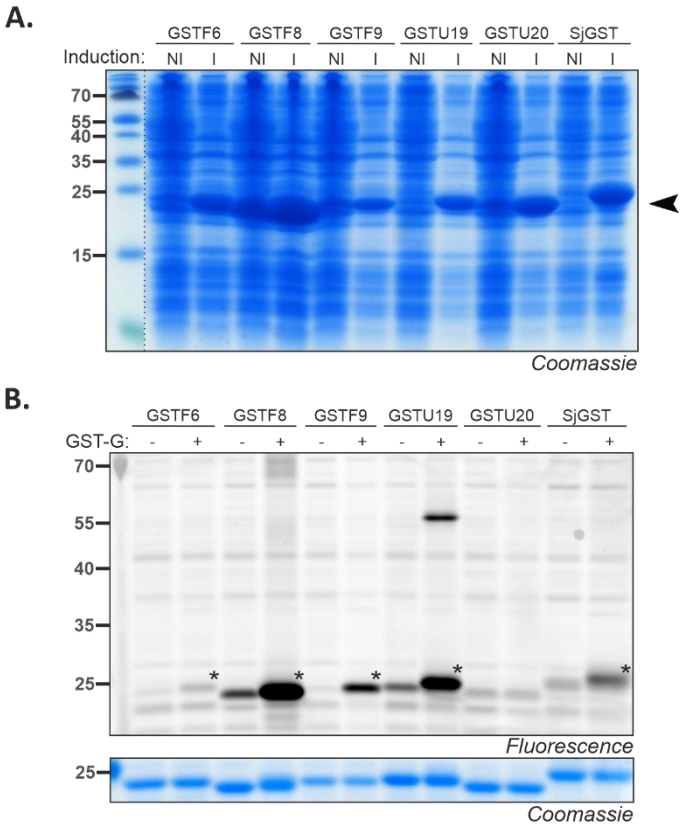


Figure 7. GSTs are main the target of GST-G in *E. coli*. **A**, Expression of five Arabidopsis (F6/F8/F9/U20/U19) and a *Schistosoma japonicum* (SjGST) GSTs. Total protein extract from non-induced (NI) and induced (I) *E. coli* cell extracts were loaded into SDS-PAGE gels and detected by Coomassie staining. **B**, GST-G labels recombinant Arabidopsis GSTs and SjGST expressed in *E. coli*. Extracts were labelled with 5 μM GST-G and UV-radiated for 45 min. Labelled proteins were coupled to a fluorophore and visualised by in-gel fluorescence scanning. Coomassie staining is shown as loading control. Similar results were obtained in an additional independent experiment.

We next studied GSTF9 and GSTU19 in more detail. We observed that inactivation by heat denaturation prevented GST-G labelling of GSTF9 and GSTU19, indicating that the correct folding and conformation of GSTs is important for GST-G labelling (Figure 8A). Moreover, GSTF9 and GSTU19 activity was evaluated by measuring 1-Chloro-2,4-dinitrobenzene (CDNB) conjugation to glutathione by detecting increased absorbance at 340 nm. Active GSTF9 and GSTU19 successfully conjugated the thiol group of GSH to CDNB as we detected an increase in absorbance at 340 nm (Figure 8B, red line). Heat denatured GSTs were unable to perform the conjugation reaction, supporting the inability of inactive GSTs to conjugate CDNB (Figure 8B, blue line).

Taken together, these data demonstrate that GSTs are the main target of the glutathione-based probe GST-G but that not all GSTs are labelled by GST-G, for example GSTU20. GST-G can be used for detecting and profiling the activity of several GSTs in Arabidopsis and its labelling can be supressed by H-site and G-site competitors.

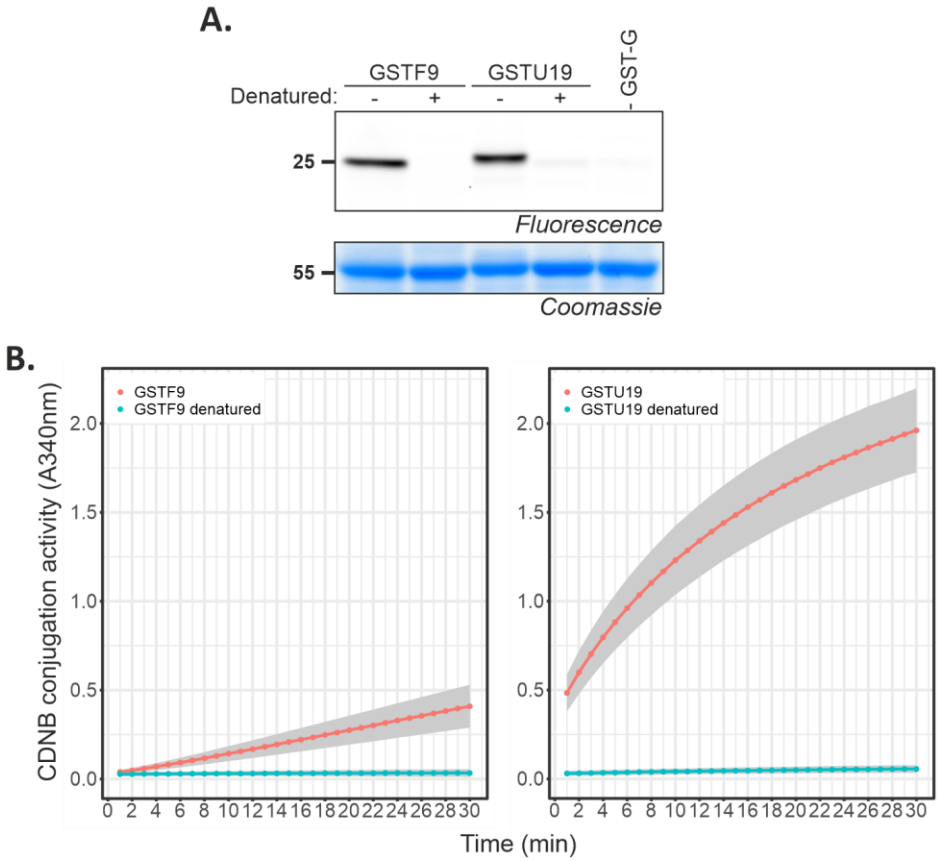


Figure 8. Heat denaturation of *At*GSTF6 and *At*GSTU19 affects GST-G labelling and CDNB conjugation. **A**, GST-G labelling is prevented by heat denaturation. *At*GSTF9 and *At*GSTU19 *E. coli* cell extracts were denatured (85 °C for 10 min) or not, labelled and detected as described in Figure 2. Coomassie staining is shown as loading control. Similar results were obtained in an additional experiment. **B**, CDNB conjugation activity assay. CDNB-SG formation was monitored by measuring absorbance at 340 nm (A340nm) for 30 min using active GSTF9 and GSTU19 (red) and their heat denatured inactive versions (blue). Grey zone represents the SD of n= 4 measurements.

GST profiling can be applied to other plant species

To profile GSTs in other plants, we performed several GST-G labelling experiments on leaf extracts of *N. benthamiana* and other plant species, but only weak signals were detected in contrast to Arabidopsis (data not shown). Crude *N. benthamiana* leaf extracts usually turn into a brown solution, instead of the usual light green of Arabidopsis leaf extracts, indicating the possible oxidation of many enzymes in the extract upon cell disruption (Figure 9B). The addition of the antioxidant β-met to the Tris-HCl buffer prevents the change in colour of the *N. benthamiana* plant extract, possibly by maintaining a similar reducing environment as in intact cells and preventing inter and intramolecular disulfide-bond formations (Cumming *et al.*, 2004). We then realised that addition of the reducing agent *β*-mercaptoethanol *(β-met)* during protein extraction was essential for the labelling of GSTs in *N. benthamiana* but did not influence the labelling of Arabidopsis GSTs (Figure 9A). Proteins are in a reducing environment within cells; however, when extracted in buffer, they are exposed to a more oxidising environment.

We next tested whether GST-G could also label GSTs in other plant species using *β-met* in buffer. We produced leaf extracts from two nonvascular plants (the liverwort *Marchantia polymorpha* and the moss *Physcomitrella patens*) and five angiosperms (the monocot *Zea mays* and four dicots: *Arabidopsis thaliana, Nicotiana benthamiana, Nicotiana tabacum and Solanum lycopersicum*). GST-G incubation in leaf extracts of all these plant species resulted in several fluorescent signals at approximately 25 kDa, consistent with the MW of GSTs (Figure 9C, bracket). Altogether, these results indicate that GST-G labels GSTs throughout the plant kingdom and can be used to monitor GSTs in other plant species.

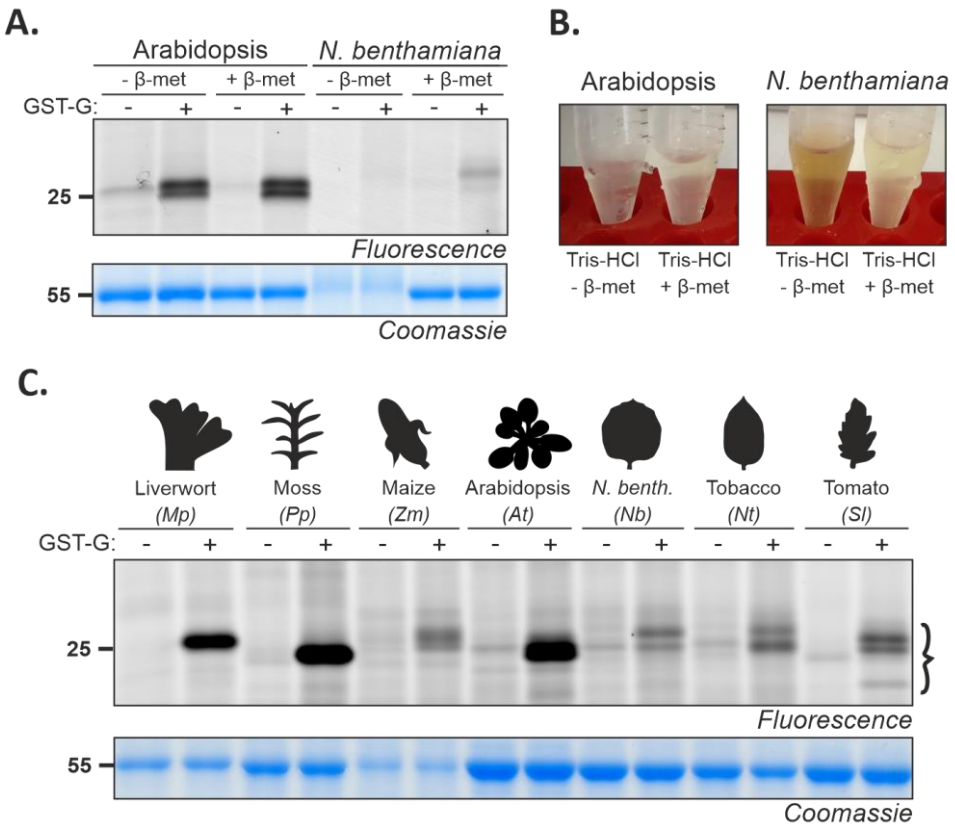


Figure 9. GSTs labelling in other plant species. Leaf extracts from various plants species were labelled with and without 5 μM and UV-radiated for 45 min and labelled protein were processed and detected as described in Figure 2. **A,** GSTs labelling in *N. benthamiana* requires a reducing agent (*β*-mercaptoethanol, *β-met)* in the extraction buffer. Similar results were obtained in an independent experiment. **B,** Profiling of GSTs in leaf extracts from various plant species: *Mp, Marchantia polymorpha; Pp, Physcomitrella patens; Ta, Triticum aestivum; Zm, Zea mays; At, Arabidopsis thaliana; Nb, Nicotiana benthamiana; Nt, Nicotiana tabacum; Sl, Solanum lycopersicum.* Similar results were obtained in an independent experiment.

Profiling of GSTs in the context of agrochemical detoxification

Fenoxaprop-P-ethyl is an extensively used post-emergence herbicide against grass weeds in wheat crops, usually applied in combination with safeners such as mefenpyr-diethyl (Figure 10A) (Taylor *et al.*, 2013). As GSTs form part of agrochemical detoxification machinery, we used GST-G to test whether the application of a safener, mefenpyr-diethyl, and its partner herbicide, fenoxaprop-P-ethyl, influences the labelling of GSTs in wheat seedlings. Wheat seedlings were germinated on Murashige and Skoog agar plates. Four days after germination, seedlings were transferred into liquid medium with and without 100 μM mefenpyr-diethyl, fenoxaprop-P-ethyl or both (Figure 10B). Total seedling extracts were generated after 24 h incubation, and labelled with GST-G. We detected two distinct bands at approximately 25 kDa, a MW consistent with being from GSTs (Figure 10C). Samples treated with the safener (S) alone or the combination of the safener and herbicide (S+H) showed increased labelling intensities than the control treatment (C) or the herbicide alone (H) (Figure 10C). In all treatments, no signals bands were observed in the absence of GST-G (Figure 10C). GST signal quantification over 3 replicates confirmed the significant difference between control and the safener or the safener + herbicide treatments (Figure 10D, S and S+H). However, no significant difference was found between the control treatment and the herbicide application (Figure 10D, H). Interestingly, we observed a possible synergistic effect of S+H combination as GST intensity signals from the combined safener and herbicide treatment were higher than when the safener was applied alone; however, this difference was not significant.

This experiment illustrates the application of GST-G profiling to study the activation of GST in the context of safener postemergence application and agrochemical detoxification in general.

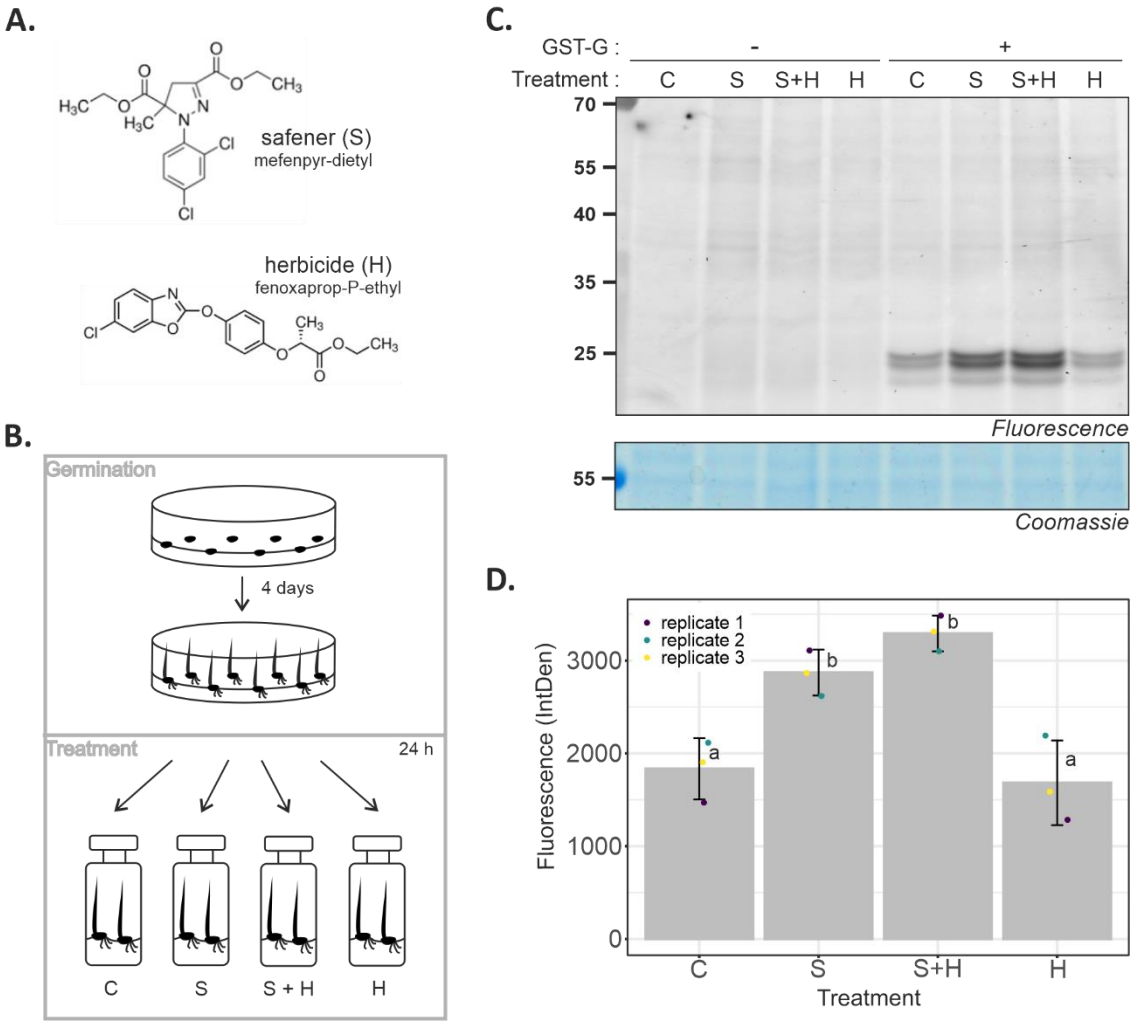


Figure 10. Increased GST labelling upon postemergence safener treatment in wheat seedlings. **A**, Structures of the safener mefenpyr-diethyl (S) and the herbicide fenoxaprop-P-ethyl (H) used in this study. **B**, Treatment procedure. Wheat seedlings were germinated in solid Murashige and Skoog media and just after postemergence transferred into liquid Murashige and Skoog media containing the safener mefenpyr-diethyl (S), the herbicide fenoxaprop-P-ethyl (H), their combination (S+H) or DMSO control (C). Seedlings were collected after 24h and frozen till further analysis. **C**, Seedlings extracts from the different treatments were extracted and labelled with or without GST-G as described in Figure 2. Shown is a representative of three independent experiments. Coomassie staining is shown as loading control. **D**, Quantified GST-G signal intensities from section C (n=3 biological repeats). ANOVA test (a, not significant; b, $P < 0.05$).

Profiling of GSTs in the context of plant immunity

GSTs also play a role in plant defence. BION®, which contains the SA analogue acid acibenzolar-S-methyl, is used as a plant activator for its known activity to induce plant defences via systemic acquired resistance (SAR) (Faize and Faize, 2018; Walters *et al.*, 2013). The priming of plants is used as a protective tool against a broad range of plant pathogens as it results in high level of defence-related gene expression and long-lasting activation of multigenic basal resistance (Buswell *et al.*, 2018; Westman *et al.*, 2019).

We used GST-G activity profiling to investigate the dynamics of GSTs upon BION treatment of Arabidopsis. BION treatment of Arabidopsis plants for 3 days did not have phenotypic effects on Arabidopsis growth (Figure 11A). BION-treated Arabidopsis accumulated the pathogenesis-related protein 2 (PR-2), indicating the successful induction of SAR by BION treatment (Figure 11B). GST-G profiling showed an increase in GST labelling upon BION treatment as GST labelling was significantly stronger in BION (B) treated samples in comparison to water (W) treated samples (Figure 11B and 11C).

We next used fluorescent GST-G labelling combined with IEF 2D gel scanning to closer investigate the changes in GST activities upon BION treatment. For the IEF 2D gel experiment, extracts from BION- and water-treated plants were labelled with GST-G and different fluorophores were attached to samples treated with either water (Cy2) or BION (Cy5). These two samples were mixed, separated on an IEF 2D gel and analysed by in-gel fluorescence scanning. Interestingly, we observed 25 kDa spots at the pI range between 5 and 6, consistent with the predicted isoelectric point (pI) of the majority of GSTs (Figure 12). When comparing GST-G labelling of water (Cy2, blue) or BION (Cy5, red) Arabidopsis treated samples, we first observed a GST-G labelling shift towards higher pI in a 2D gel (Figure 12A, Overlay). However, these results were not maintained when we swap fluorophores between water- and BION-treated samples, indicating that the pI shift is caused due to the different fluorophore attachment (Figure 12B, Overlay).

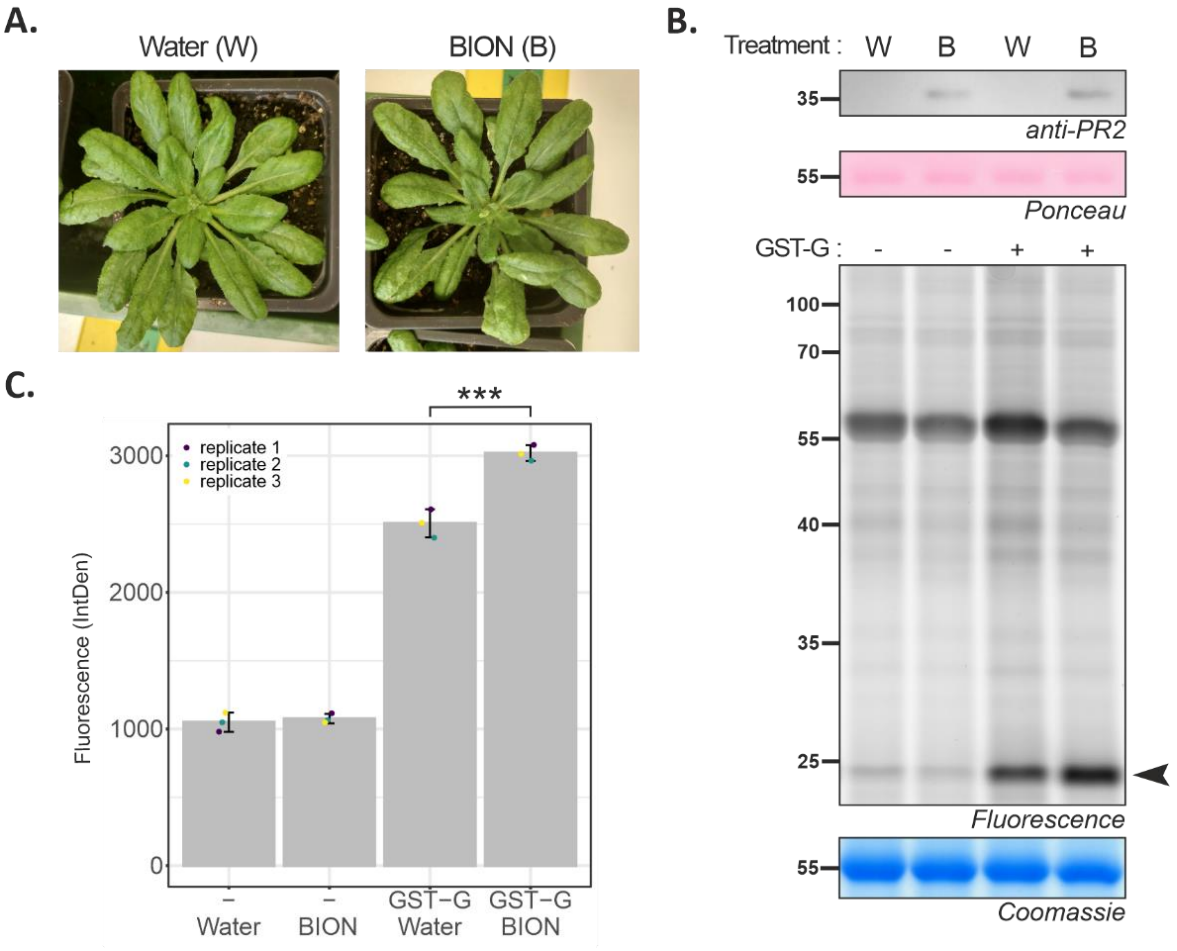


Figure 11. Differential glutathione transferase labelling upon BION treatment. **A**, No phenotypical effect of BION treatment in Arabidopsis leaves. **B**, Arabidopsis leaf extracts from BION treated and no treated plants were extracted and labelled with or without GST-G as described in Figure 2. Shown is a representative of three independent experiments. Coomassie and Ponceau staining are shown as loading controls of the fluorescence gel and western blot, respectively. This is a representation image of 3 independent biological replicates. **C**, Quantified GST-G signal intensities from section B (n=3 biological repeats). ANOVA test (***, $P < 0.001$).

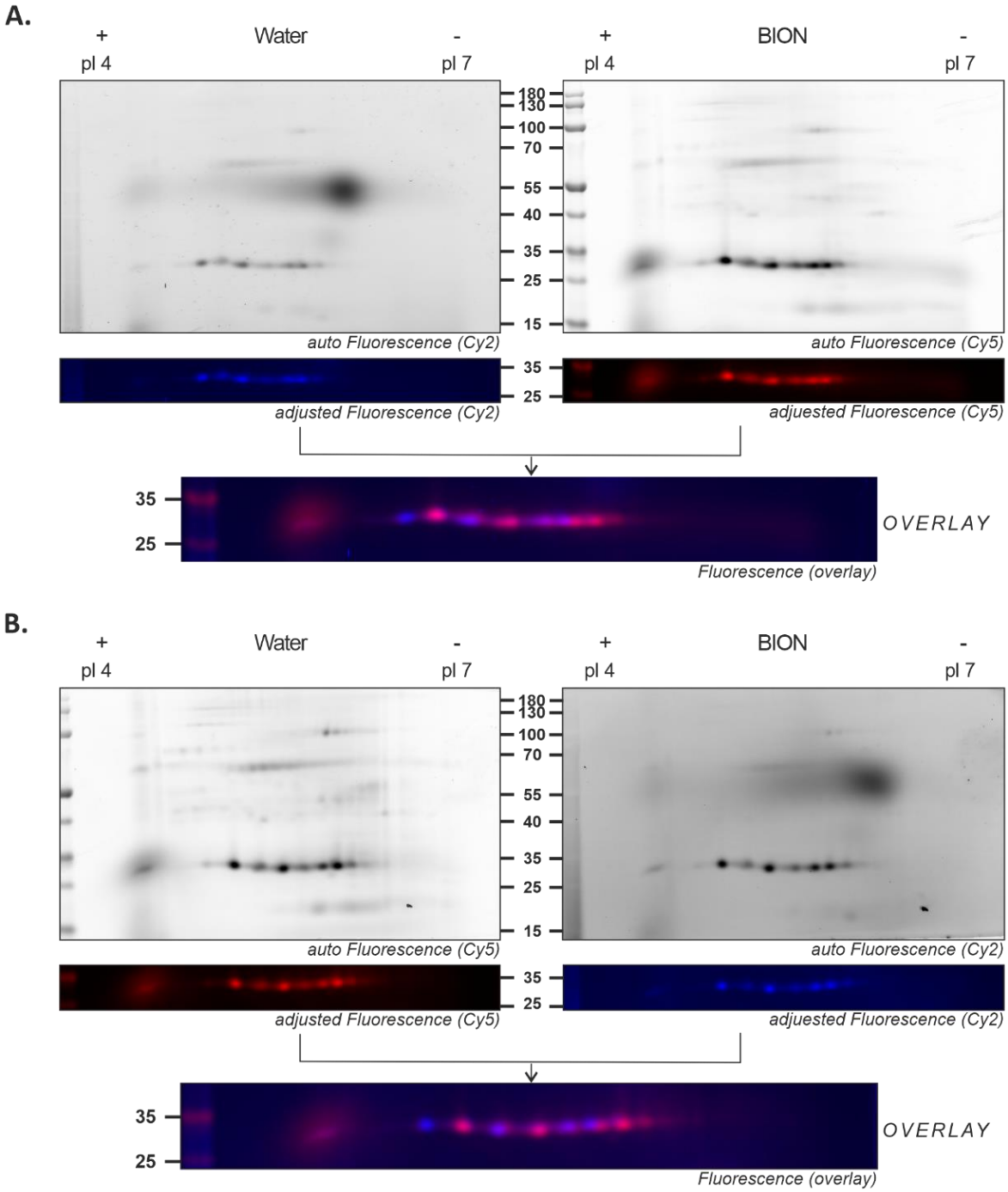


Figure 12. The attachment of a different fluorophore (Cy2 or Cy5) shifts GSTs labelling towards higher pI when comparing GST-G labelling of water or BION Arabidopsis treated samples in 2D gels. Arabidopsis plants were watered with or without BION and leaf extracts were labelled with 5 μM GST-G. **A**, Fluorophores were attached to samples treated with either water (Cy2) or BION (Cy5) via click chemistry. **B**, Fluorophores were attached to samples treated with either water (Cy5) or BION (Cy2) via click chemistry. Samples were mixed, separated on an IEF 2D gel and analysed by in-gel fluorescence scanning. The bottom gel shows the overlay of GST-G labelled water treatment in blue and BION treatment in red.

To identify the GSTs that are differentially active upon chemical induction of pathogen resistance, we performed GST-G labelling of the proteomes of water- and BION- treated Arabidopsis plants, followed by biotin tag coupling and enrichment on streptavidin beads. Purified proteins were on-bead digested with Lys-C and trypsin, and digested peptides were identified by liquid chromatography tandem mass spectrometry (LC-MS/MS). The pull-down was performed using three biological replicates of the water GST-G labelled and BION GST-G labelled samples, water click chemistry samples were included as pull-down control. As expected, samples clustered by treatment and GST-G labelling in principle component analysis (PCA) plots (Figure 13).

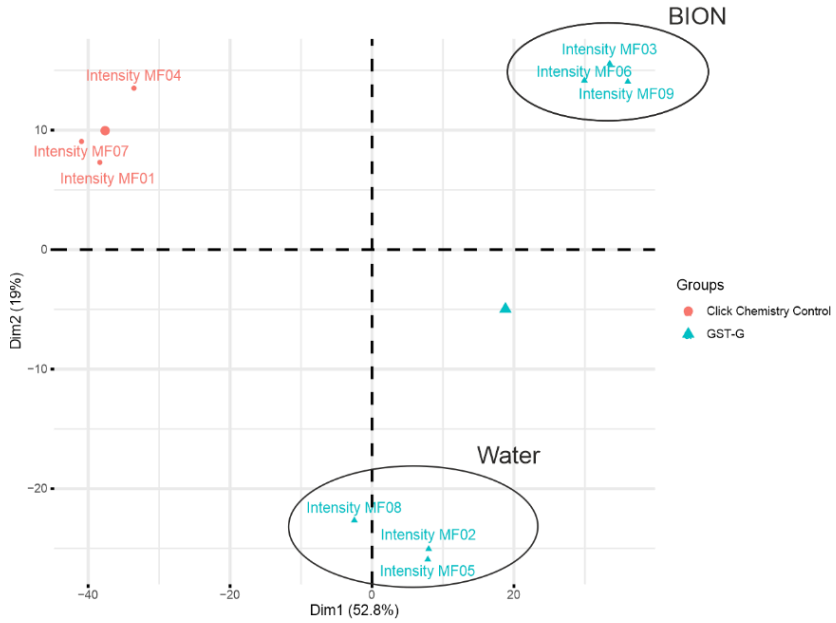
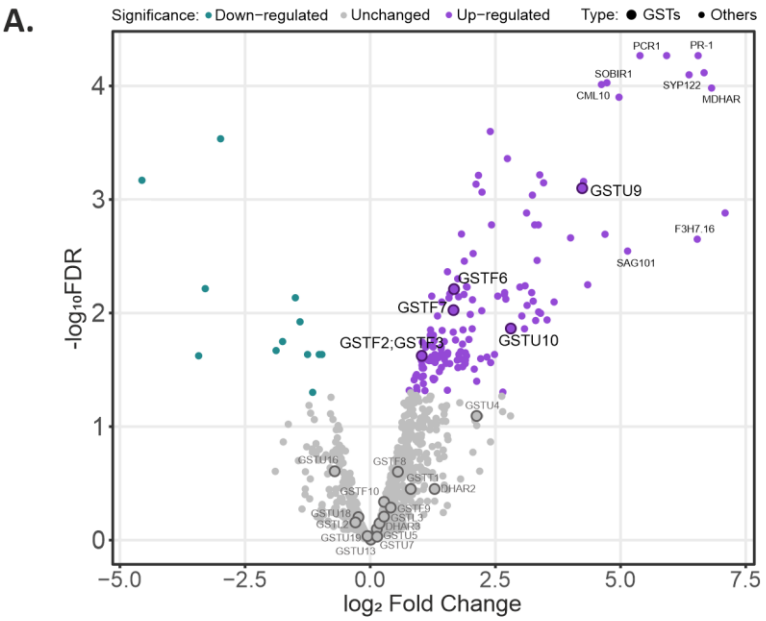


Figure 13. Principal component analysis (PCA) plot of the GST-G pull-down of water and BION treated Arabidopsis. Scatter plot of the click chemistry control samples (orange) and the GST-G labelled samples (blue) represented by the two major component axes. Samples correctly cluster by the presence or not of the probe and the water or BION treatment.

When comparing water and BION GST-G labelled samples, we detected a total of 152 proteins upregulated in the BION-treated sample (Figure 14A, purple dots). Five GSTs were detected with high intensity and were significantly up-regulated in the BION treated samples, including GSTU9, GSTU10, GSTF6, GSTF7 and GSTF2/F3 (Figure 14A, purple dots encircled). We also detected labelling of another 14 GSTs in water and BION samples, although these were not statistically significant between treatments (Figure 14A, grey dots encircled). GSTU9 and GSTU10 were the ones found with a highest fold change increase, followed by GSTF6, GSTF7 and GSTF2/3 (Figure 14B). GSTU4 and DHAR2 had a similar log2FC increases, but this increase was not significant. Surprisingly, we detected an enrichment of many other proteins that did not belong to the GST family in our GST-G pull-down (Table S1). Interestingly, the top enriched proteins with higher log2FC correspond with proteins related to pathogenesis, including SYP122, PR-1, SOBR1 and SAG101 (Figure 14A, purple dots).

A.



B.

	Names	Protein IDs	log2FC	MS intensity	adj.P.Val	u. pep.	r. pep.	SC [%]	MW [kDa]	FDR	Significance
1	**GSTU9**	Q9FUT0;A0A1P8B9C1	4.23	21.00	0.0008	3	0	28.3	27.611	FDR 0.001	Up-regulated
2	**GSTU10**	Q9CA57	2.81	24.06	0.0137	10	0	50.4	26.804	FDR 0.05	Up-regulated
3	GSTU4	Q9ZW27	2.12	22.57	0.0806	3	0	18.8	25.839	Not significant	Unchanged
4	**GSTF6**	P42760	1.67	29.07	0.0062	7	0	85.1	23.486	FDR 0.01	Up-regulated
5	**GSTF7**	Q9SRY5	1.66	30.38	0.0094	8	11	82.3	23.598	FDR 0.01	Up-regulated
6	DHAR2	Q9FRL8	1.29	22.60	0.3545	2	0	11.3	23.407	Not significant	Unchanged
7	**GSTF2;GSTF3**	P46422;Q9SLM6	1.03	30.95	0.0238	11	1	81.6	24.128	FDR 0.05	Up-regulated
8	GSTT1	Q9ZRT5	0.81	25.28	0.3545	7	0	37.6	27.653	Not significant	Unchanged
9	GSTF8	Q96266	0.55	32.46	0.2498	12	0	67.7	29.231	Not significant	Unchanged
10	GSTF9	O80852	0.41	32.98	0.5168	9	0	56.7	24.146	Not significant	Unchanged
11	GSTF10	P42761	0.27	32.32	0.4602	12	2	75.3	24.23	Not significant	Unchanged
12	GSTL3	Q9LZ06	0.27	29.42	0.6207	13	1	73.6	27.09	Not significant	Unchanged
13	DHAR3	Q8LE52	0.19	28.51	0.7120	10	0	46.9	28.514	Not significant	Unchanged
14	GSTU7	Q9ZW24	0.13	27.32	0.7984	12	0	54.6	26.112	Not significant	Unchanged
15	GSTU5	P46421	0.07	27.93	0.9107	9	0	60.3	26	Not significant	Unchanged
16	GSTU13	Q9FUS6	0.01	27.72	0.9889	9	0	54.6	25.131	Not significant	Unchanged
17	GSTU19	Q9ZRW8	-0.06	31.49	0.9215	12	2	61.2	25.65	Not significant	Unchanged
18	GSTU18	Q9FUS9	-0.24	26.89	0.6269	6	0	38.8	25.911	Not significant	Unchanged
19	GSTL2	Q9M2W2	-0.30	26.57	0.6981	7	1	36.3	33.057	Not significant	Unchanged
20	GSTU16	Q9XIF8	-0.71	27.21	0.2474	7	0	50.4	26.506	Not significant	Unchanged

Figure 14. Comparative GST-G profiling of BION and water treatments of Arabidopsis. A, Leaf extracts from water and BION treated Arabidopsis plants were labelled with GST-G in triplicate. Labelled proteins were attached to a biotin affinity tag via click chemistry and enriched on streptavidin beads. On-bead digested proteins were analysed by MS. Enrichment is represented by volcano plots where the log_2FC (BION/water) is plotted against their significance (-log_{10}FDR) using three biological replicates. The colour of the dots means whether proteins (dots) were BION GST-G enriched (purple), unchanged (grey) or water GST-G enriched (blue). All GSTs detected are represented encircled. Significance: log_2FC > 0.7 and FDR < 0.05. **B**, Description of all GSTs detected in the GST-G pull-down. Table includes: Name, Protein IDs, log_2 Fold Change (log_2FC), log_2 MS intensity (MS intensity), adjusted P. value (adj.P.Val), unique peptides (u.pep.), razor peptides (r. pep.), sequence coverage (SC [%]), molecular weight (MW [kDa]), FDR significance (FDR), Significance.

We next wanted to compare the detected GST proteins upon BION treatment with their transcriptional upregulation upon pathogen infections. For that, we retrieved gene expression data from Arabidopsis eFP Browser 2.0. All the six GSTs we find upregulated upon BION treatment of Arabidopsis via GST-G profiling are also found to be upregulated upon infection of Arabidopsis by *Phytophthora infestans*

(Figure 15A). During *Pseudomonas syringae* pv. *tomato* DC3000 infections, we also observed a high transcriptional upregulation of GSTU10, but not of the other detected GSTs upon BION treatment (Figure 15B). In both Arabidopsis infections, GSTL1 was one of the most transcriptionally upregulated GSTs upon infection. However, we did not observe more labelling of this GST upon BION treatment.

Taken together, these data indicate the activation of tau and phi GSTs upon BION treatment and challenge by *P. infestans* and *P. syringae*. However, BION treatment did not induce a MW change or a pI shift of GSTs visible in fluorescent gels.

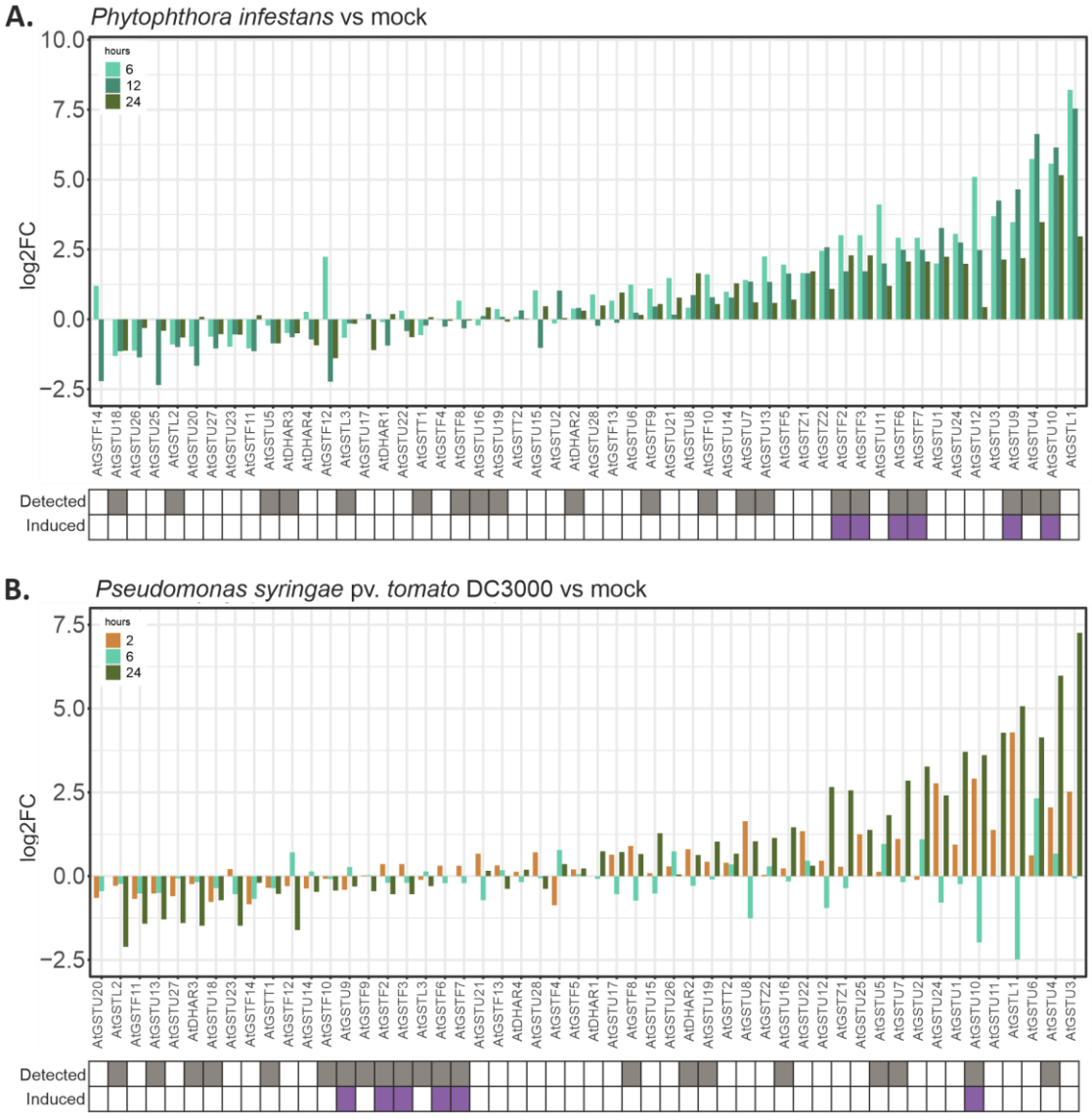


Figure 15. Differential expression of all members of the GST family upon two pathogens infection. Data retrieved from Arabidopsis eFP Browser 2.0. **A**, Differential expression of GSTs during *Pseudomonas syringae* pv. *tomato* DC3000 infection of Arabidopsis at 2, 6 and 24h time points. **B**, Differential expression of GSTs during *Phytophthora infestans* infection of Arabidopsis at 6, 12 and 24h time points. In grey, detected GSTs in the water vs BION GST-G pull-down. In purple, enriched GSTs in the BION GST-G pull-down.

Role of GSTU10, GSTF2 and GSTF6 in plant defence against biotrophic and hemibiotrophic plant pathogens

To further investigate the role of the BION-activated GSTs, we cloned the top BION-induced GSTs into a golden gate vector compatible for *Agrobacterium tumefaciens*-mediated transient transformations (agroinfiltrations) of *Nicotiana benthamiana* (*Nb*) plants. Four of the six enriched GSTs (GSTF2, GSTF6, GSTF7 and GSTU10), together with GSTU4, were amplified from Arabidopsis cDNA and fused C-terminally to HIS or GFP tags. The coding sequence was flanked by a 35S promoter and terminator and the T-DNA also encodes the silencing suppressor P19. Western blot analysis of total leaf extract taken at 4 days upon agroinfiltration revealed a successful expression of all GST constructs (Figure 16, *anti*-His and *anti*-GFP).

For the His-tagged GSTs, a clear labelling was observed for the GSTU10-H constructs, as its labelling intensity and molecular weight was higher than the endogenous *Nb*GST labelled (Figure 16A, black arrow). GSTU4-H accumulation was weakly detected and its labelling signal was not clear enough to be distinguished from the labelling of endogenous *Nb*GSTs (Figure 16A, white arrow). However, GSTF2-H, GSTF6-H and GSTF7-H fluorescent signal was more intense than GSTU-4 labelling signal, indicating that extra fluorescent signal intensity is likely to come from the overexpressed GSTs (Figure 16A, asterisk).

For the GFP-tagged GSTs, the addition of the GFP tag (27 kDa) to GST shifted the fluorescence GST-G labelling signal to approximately 50 kDa and we could clearly differentiate the labelling of GSTU10-G, GSTF6-G and GSTF7-G at approximately 50 kDa (Figure 16B, asterisk). GSTF2-G and GSTU4-G labelling was not clearly observed, most likely because of their weaker accumulation in *N. benthamiana* leaves. Labelling of endogenous *Nb*GSTs was clearly observed at 25 KDa (Figure 16B, white arrow).

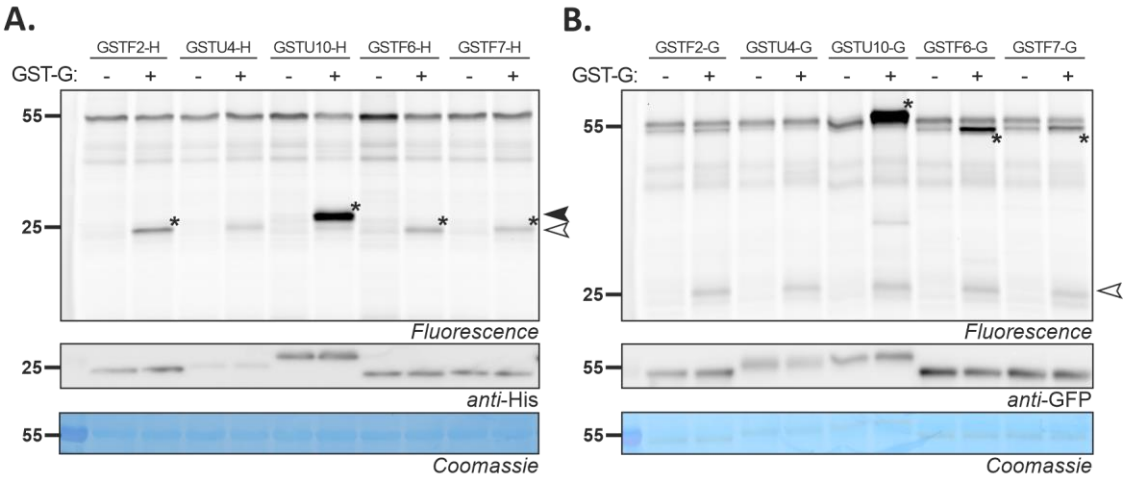


Figure 16. GST-G labelling of transiently expressed Arabidopsis GSTs in *N. benthamiana.* Arabidopsis GSTs were fused to a C-terminal His (-H) or GFP (-G) tag and expressed in *N. benthamiana* by agroinfiltration. *N. benthamiana* leaf extracts taken at 4 days upon agroinfiltration were labelled with or without 5 μM GST-G, coupled to a fluorophore via click chemistry and visualised by in-gel fluorescence scanning. Anti-His/GFP western blot and Coomassie are shown as protein expression and loading control respectively. Similar results were obtained in another experimental replicate. Asterisk, recombinant GSTs labelling. White arrow, endogenous *Nb*GSTs labelling.

Next, we wanted to evaluate the level of resistance given by BION-inducible GSTs during a plant-pathogen interaction. For that, we transiently overexpressed GSTU10-G, GSTF2-G, GSTF6-G and an empty vector (EV) in *N. benthamiana* plants. Three days after agroinfiltration we spray-inoculated *P. syringae* pv. *tomato* DC3000 (*Pto*DC3000) or drop inoculated *P. infestans* spores. For *PtoDC3000* infection assays, leaf discs were collected three days after the infection, homogenised and plated as dilution series onto selective LB plates for counting colony forming units (CFU). For *P. infestans* infection assay, *P. infestans* growth was measured by the size of its lesion at 7 days post infection (Figure 17A). Unfortunately, we did not observe any direct impact on the reduction of *Pto*DC3000 growth when GSTU10-G, GSTF2-G and GSTF6-G where transiently overexpressed, in comparison to the EV (Figure 17B). By contrast, overexpression of the well-known immune receptor flagellin-sensing 3 (FLS3) from tomato decreased bacterial growth of *Pto*DC3000 (Figure 17B). Similarly, we did not observe any difference in *P. infestans* growth between the transiently overexpressed GSTs and the EV control (Figure 17C). Meanwhile, the successful overexpression of the GST constructs was observed by the detection of the GFP fluorescence (Figure 18C, ex488/em520). Noteworthy, we observed a tendency towards the reduction of *P. infestans* growth in the presence of GSTU10-G in the first replicate (Figure 17C, purple dots). However, this result was not seen in the second replicate and lead to no significant overall differences in *P. infestans* growth between the EV and the GSTU10-G construct (Figure 17C, yellow dots).

In conclusion, these results indicate that the overexpression of the Arabidopsis GSTs (GSTU10, GSTF2 and GSTF6) do not enhance *Pto*DC3000 and *P. infestans* resistance when transiently overexpressed in *N. benthamiana*. However, it could be that the GST we identified in Arabidopsis immune responses play an indirect role in immunity that was not captured with these infection assays.

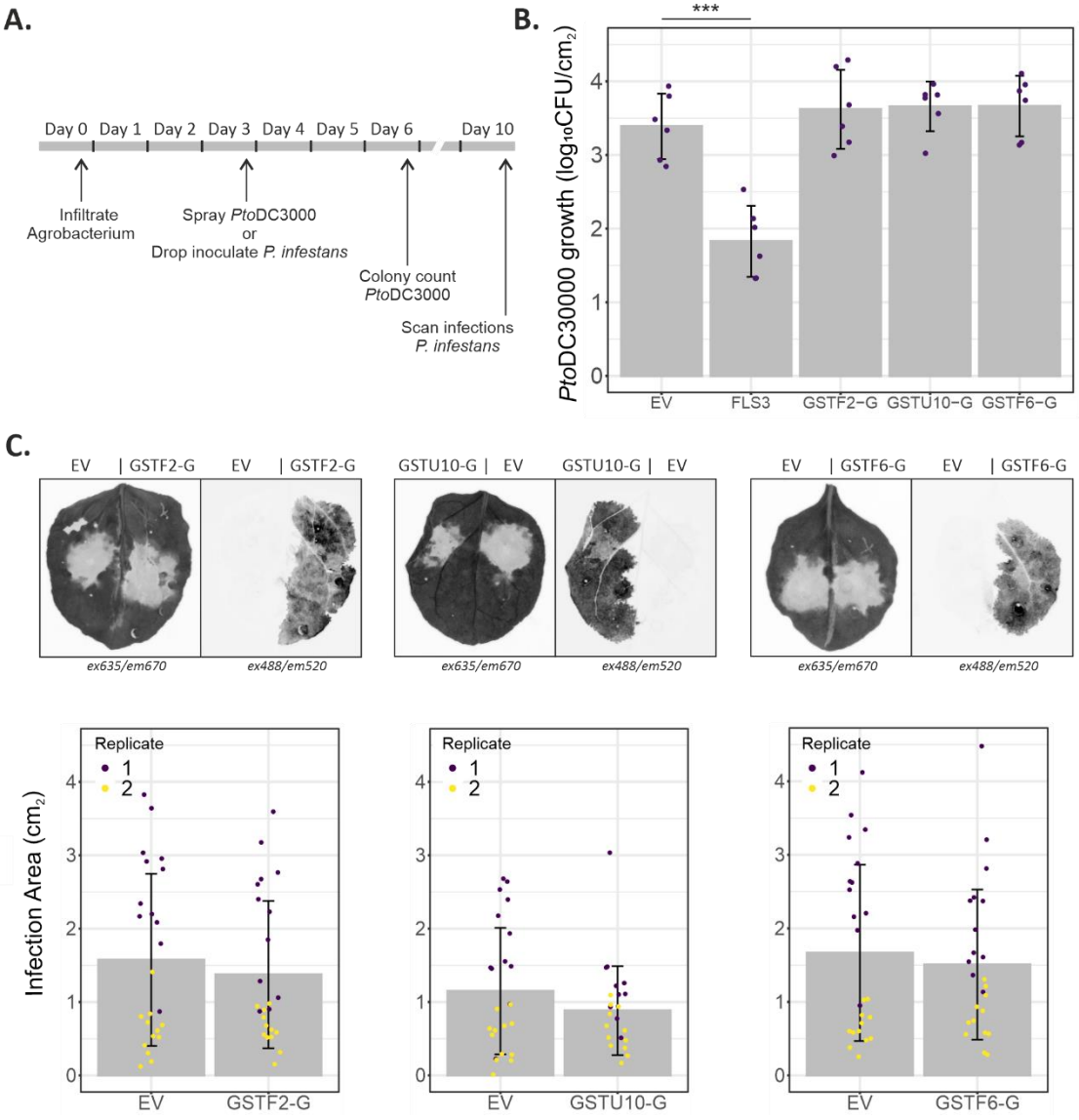


Figure 17. Transient overexpression of GSTU10, GSTF2 and GSTF6 in *N. benthamiana* does not enhance *Pto*DC3000 and *P. infestans* resistance. **A**, Experimental procedure for studying the role of overexpressed GSTs in *N. benthamiana* agroinfiltrated leaves. Three days agroinfiltration, agroinfiltrated leaves are infected with *Pto*DC3000 (spray infection) or *P. infestans* (drop inoculation). Bacterial growth is measured by colony counts at 3 days after *Pto*DC3000 infection. *P. infestans* growth is measured by the quantification of the lesion size at 7 days after infection. **B**, Transient expression of GSTs does not impact *Pto*DC3000 growth. Agroinfiltrated leaves expressing EV, FLS3, GSTF2-G, GSTU10-G and GSTF6-G were spray-inoculated with *Pto*DC3000 (at an OD_{600}=1). Bacterial growth was measured three days post infection by the selection of *Pto*DC3000 colonies on CFC selection plates. Error bars represent sd of n = 6 biological replicates. ANOVA test (***, $P < 0.001$). **C,** Transient expression of GSTs does not impact *P. infestans* growth. *N. benthamiana* leaves expressing the empty vector (EV) or the GFP-tagged GSTs (GSTF2-G, GSTU10-G, GSTF6) on either leaf half, were drop-inoculated with *P. infestans* spores (at 50,000 spores/ml). *P. infestans* growth was calculated by measuring the size of the infection lesion seven days post-infection.

Discussion

We have validated the use of photoaffinity labelling for studying GSTs in plants. GST-G can be used for the labelling and detection of GSTs in Arabidopsis and its labelling can be suppressed by H-site and G-site competitors. GST-G mainly targets phi and tau GST classes, but not all their class members are labelled by GST-G, being GSTU20 an example. Further work confirmed the use of GST-G for the identification of inducible GSTs upon agrochemical treatments, revealing the specific activation of tau and phi GSTs upon BION treatment.

GST-G labelling: targets and selectivity

GSTs are the main target of GST-G in Arabidopsis as: i) we confirmed the distinct labelling of two GST bands at 25 kDa, ii) GSTs were top enriched proteins in probe pull-downs and iii) G-site and H-site GST inhibitors partially suppress GST-G labelling (Figure 2, 4 and 6). Overall, we successfully detected the labelling of 12 different GSTs by different analyses. First, we significantly enriched GSTF10, GSTF9, GSTF8, GSTF7, GSTF6, GSTF3, GSTF2, GSTU16, GSTU13, GSTU6 in a GST-G pull-down of Arabidopsis leaf extracts (Figure 4). Further experiments confirmed the labelling of Arabidopsis GSTU19, by *E. coli* protein overexpression, and Arabidopsis GSTU10 and GSTU9 by MS analysis of BION-treated Arabidopsis plants, adding three more GSTs being labelled by GST-G (Figure 7 and 14). All labelled GSTs are from the plant-specific GSTU and GSTF classes. However, this is not surprising, as GSTU and GSTF are the two most abundant cytosolic classes of GSTs in plants (Cummins *et al.*, 2011). Furthermore, our data is consistent with previous research where when using glutathione- and S-hexylglutathione-based affinity chromatography to retain GSTs from Arabidopsis root cultures, mainly tau and phi class GSTs were purified (Dixon and Edwards, 2009; Sappl, Oñate-Sánchez, *et al.*, 2004). This data is in line with the main labelling of GSTU and GSTF class GSTs when using GST-G, a glutathione-based photoaffinity probe.

Previously, GST-G was used to successfully label and enrich nine mammalian GSTs from various GST classes (alpha, GSTA; mu, GSTM; pi, GSTP; kappa, GSTK; theta, GSTT; zeta, GSTZ and EEF1G classes)(Stoddard *et al.*, 2017). As GSTT and GSTZ are common classes between plants and mammals, we suspect that GST-G could also possibly label these classes of GSTs in plants. GSTLs and DHARs are plant-specific GSTs not present in mammals; therefore, we do not know from literature if GST-G could target these classes of GSTs. Although DHAR1, DHAR3 and GSTL1 are well expressed GSTs in Arabidopsis leaf tissue (Figure 5) and GSTL1 and GSTZ1 are transcriptionally induced after biotic stresses (Figure 16), we could not detect any enrichment of these GSTs in our MS experiments. It will be interesting to confirm the labelling of these other GST classes by protein overexpression. Additionally, a better comparison for the expression of GSTs in Arabidopsis tissues will be to perform

global proteomic analysis of the input extracts of GST-G pull-downs. Checking the initial abundance of GSTs by MS analysis will help us to further understand if there is a correlation between protein abundance and degree of labelling. It is likely that there is an association between the GSTs we find with higher MS intensities and those found to be highly expressed in Arabidopsis rosette leaves (Figure 5, > 500 RPKM), suggesting that GSTs with high expression are more likely to be detected by GST-G labelling. However, this was not the case for GSTU13, GSTU16 and GSTU7, which are low expressed GSTs in Arabidopsis leaves but significantly enriched by GST-G (Figure 4 and 5).

We have seen striking differences in the labelling of two closely related Arabidopsis GSTs, GSTU19 and GSTU20. In accordance with our phylogenetic analysis, these two tau GSTs are very closely related (Figure 1). However, when overexpressed heterologously in *E. coli*, we just observed the labelling of GSTU19 but not GSTU20 (Figure 7). This finding suggests that, although GST-G targets tau and phi GSTs, GST-G does not target all GSTs expressed, indicating a possible differential selectivity and affinity of GST-G. Intriguingly, we found that GSTU19 was labelled when overexpressed in *E. coli* but not when we performed GST-G pull-downs in Arabidopsis leaf extracts, although GSTU19 was found among the proteins not significantly GST-G enriched proteins (Figure 4, grey dots). Therefore, it will be interesting to investigate if GSTU19 activity is blocked in leaf extracts but not when expressed in *E. coli* as it is possible that GSTU19 is inhibited by an endogenous ligand in leaf extracts.

Glutathione transferases inducibility after agrochemical treatment

GSTs are transcriptionally up-regulated in response to herbicide and safener, indicating the major role of this enzyme family in agrochemical plant responses (Cummins *et al.*, 2011).

Using photoaffinity profiling of GSTs we observed that samples treated with the safener (S) alone or the combination of the safener and herbicide (S+H) showed increased GST-G labelling intensities (Figure 10). Based on the literature, we predict the potential use of GST-G for the identification of induced GSTs after safener treatments as the GSTU class is the main class of GSTs found to be induced after safener treatment of different plant species. For example, five members (GSTU25, GSTU24, GSTU19, GSTU4 and GSTU3,) were transcriptionally highly upregulated after Arabidopsis treatment with the safener fenclorim (Skipsey *et al.*, 2011). Furthermore, other proteomic analysis also identified GSTU19 as the main GST upregulated upon safener treatments (Deridder *et al.*, 2002; Smith *et al.*, 2004).

Interestingly, we also observed a possible synergistic effect of S+H combination as GST intensity signals from the combined safener and herbicide treatments were higher than when the safener was applied alone; however, this difference was not found to be significant. Although this phenomenon is less studied in plants, the synergistic and antagonistic effects of simultaneous drug applications on drug metabolising enzymes have been extensively studied before (Borisy *et al.*, 2003; Roell *et al.*, 2017;

Tallarida, 2001). Therefore, further MS analysis on safener and safener + herbicide treatments could confirm the synergistic up-regulation of specific GSTs upon mefenpyr-diethyl + fenoxaprop-P-ethyl treatment in wheat. This study could also be extended by including a common weed species that affects wheat crops to further identify molecular differences of herbicide selectivity in crops and weeds.

Another main application of ABPP is the use of chemical probes for interrogating specific inhibition of enzyme activities by small-molecules or substrates (Buscaill *et al.*, 2019; H. Xu *et al.*, 2015). We used two known GST inhibitors, SHG and EA, to compete Arabidopsis GSTs labelling by GST-G. Our data suggests that competitive labelling of GSTs could be used to discover xenobiotic substrates of GSTs as GST-G was able to be outcompeted by a H-site substrate.

Glutathione transferases inducibility after BION treatment

GSTs also play a role in plant defence (Gullner *et al.*, 2018). We used BION to induce plant defences and identified six GSTs (GSTF3/2, GSTF6, GSTF7, GSTU9, GSTU10) upregulated upon BION treatment of Arabidopsis via GST-G profiling (Figure 14). Increased GST labelling upon BION treatment was also observed in SDS-PAGE gels scanned for fluorescence (Figure 11). From literature, we could not find any studies reporting the activation of GSTs upon BION treatment, but we did find studies reporting the induction of nine GSTs upon SA treatment of Arabidopsis plants (Sappl *et al.*, 2009). Surprisingly, just GSTF2 and GSTF6 are common between these two studies. This divergence could be due to the duration of the treatment (24 hours vs 4 days) and the plant defence activators used (SA vs BION). Nonetheless, our data compares with *P. infestans* infections, where we find all the BION-induced GSTs also being transcriptionally upregulated (Figure 15). Arabidopsis GSTU10 is also transcriptionally up-regulated more than 100-fold upon *Pst*DC3000 avrRpt2 and *Alternaria brassicicola* infections (Gullner *et al.*, 2018). GSTF2, GSTF3 and GSTF7 were more than 5-fold up-regulated in *A. brassicicola* fungal infection (Gullner *et al.*, 2018). By contrast, GSTL1 and DHAR2 are common stress-inducible GSTs (Chan and Lam, 2014; Dixon *et al.*, 2002b; Yoshida *et al.*, 2006) that we did not detect among the BION-inducible GSTs. Therefore, more research is needed to study the possible limitations of GST-G for detecting the induction of other classes of GSTs, apart from GSTU and GSTF.

In 2D gel analysis, GSTs were detected at a molecular weight of approximately 25 kDa and a pI value between 5 and 6.5, same as reported by Sappl and co-workers (Figure 12) (Sappl *et al.*, 2009). Although we first observed that GSTs had a negative pI shift after BION treatment, we later found that the pI shift was due to the different attached fluorophores and not a possible post-translational modification caused by the BION treatment (Figure 12). Consequently, we would not recommend the use of Cy2 and Cy5 fluorophore combination for the detection of protein inductions in 2D gel analysis. Alternatively, other fluorophores such as Cy3, Cy5 or TAMRA should be first assessed.

We also evaluated the level of resistance given by BION-inducible GSTs during *Pto*DC3000 and *P. infestans* infections. Unfortunately, we could not detect an enhanced protection in consequence of GSTU10, GSTF2 and GSTF6 overexpression. We hypothesise that these GSTs could play an indirect role in plant immunity that is not captured in infection assays. For instance, GSTs are redox related genes that could contribute to minimise the damage made by reactive oxygen species (ROS) or have protecting functions upon biotic stress by conjugating pathogen or endogenous toxic metabolites produced as a consequence of the defence response (Dixon and Edwards, 2018). Nonetheless, future experiments should focus on stuying the possible enhanced biotic protection when similtaneously overexpressing the three identified GSTs together.

Materials and Methods

Chemical probes, inhibitors and agrochemicals

GST inhibitors and agrochemicals were purchased from Sigma-Aldrich: ethacrynic acid (Sigma-Aldrich, SML1083), S-hexylglutathione (Sigma-Aldrich, H6886), mefenpyr-diethyl (Supelco, 46302) and fenoxaprop-P-ethyl (Supelco, 36851). GST-G probe was resynthesized by Daniel Brown as described before (Stoddard *et al.*, 2017).

Plant materials, growth conditions and agrochemical treatments

Arabidopsis (*Arabidopsis thaliana*) ecotype Columbia plants were grown on soil at 25 °C at short day conditions (8/16 h light/dark regime) in a growth chamber. *N. benthamiana* (*Nicotiana benthamiana*), Maize (*Zea maize*), tobacco (*Nicotiana tabacum*) and tomato (*Solanum lycopersicum*) were grown in soil at standard greenhouse conditions. Liverwort (*Marchantia polymorpha)* and moss (*Physcomitrella patens*) were grown under sterile conditions as described in Thamm *et al.*, 2020 and Moody *et al.*, 2021, respectively. For the BION treatment, 5-week-old Arabidopsis plants were grown on soil in a controlled environment (short day conditions, 25 °C). BION granules (Syngenta) were dissolved in water to a final concentration of 1 μM acibenzolar-S-methyl and Arabidopsis plants were watered with or without BION over three consecutive days. Arabidopsis leaf tissue was harvested on day four and frozen in liquid nitrogen till further use. Winter wheat (*Triticum aestivum*) seeds were sterilised with 30% ethanol for 5 min, 30% bleach for 10 min and rinsed six times with sterile water. Sterilised seeds were plated in Murashige and Skoog agar plates (half strength Murashige and Skoog basal [Duchefa-Biochemie, M0222] salt mixture containing 0.8% agar) and stratified at 4 °C for 1 day. For germination, seeds were placed at 25 °C under long day conditions (16/8 h light/dark regime). After 4 days, germinated wheat seedlings were transferred into Hoagland's liquid medium (half strength Hoagland's No.2 Basal Salt Mixture [Sigma-Aldrich, H2395]). After one day adaptation, seedlings were treated with 100 μM

mefenpyr-diethyl, 100 μM fenoxaprop-P-ethyl, 100 μM mefenpyr-diethyl + 100 μM fenoxaprop-P-ethyl or an equal amount of DMSO solvent. Seedling tissue was harvested 24h after treatment and frozen in liquid nitrogen until used.

Cloning

Used and generated plasmids are summarised in Table S2. The primers used for sequence amplification are summarised in Table S3. For heterologous expression in *E. coli*, constructs pMF84 to pMF91 were provided by Christian Gu. For *in planta* expression, Golden Gate Modular Cloning kit (Weber *et al.*, 2011) and Golden Gate Modular Cloning Toolbox for plants (Engler *et al.*, 2014) were used for cloning. The binary vector pJK268c containing the P19 silencing inhibitor (pL1V2-P19-F2) was used as binary vector. The sequences encoding Arabidopsis GSTs (GSTF2, GSTU4, GSTU10, GSTF6 and GSTF7) were amplified from Arabidopsis complementary DNA (cDNA) using the forward and reverse primer pairs summarised in table 3. Using BsaI restriction sites, PCR products were combined with GG1-55, GG1-57, GG1-70 or GG1-78 to assemble the corresponding expression constructs. Using BpiI restriction sites, PCR products were first cloned into the level 0 module GG1-01 and later transferred to pJK268c together with GG1-55, GG1-57, GG1-70 or GG1-78 in a BsaI ligation reaction. Generated expression constructs were transformed into *E. coli* for their amplification and sequencing. Afterwards, constructs were transformed into *Agrobacterium* (*Agrobacterium tumefaciens*) strain GV3101, carrying the pMP90 helper plasmids. *Agrobacterium* transformants were selected on Lysogeny Broth (LB) agar plates (10 g/L NaCl, 10 g/L Tryptone, 5 g/L yeast extract, 15 g/L agar) containing 50 μM gentamycin, 25 μM rifampicin and 50 μM kanamycin. Single colonies were picked and grown in liquid LB (10 g/L NaCl, 10 g/L Tryptone, 5 g/L yeast extract) containing the same antibiotic used before. Glycerol stocks of the selected transformants were prepared mixing Agrobacterium cultures with 50% sterile glycerol in a 1:1 ratio. Agrobacterium carrying the FLS3 expression construct was kindly provided by Pierre Buscaill (Buscaill *et al.*, 2021).

Agroinfiltrations

N. benthamiana plants were grown on soil at greenhouse conditions described before. *A. tumefaciens* GV3101-pMP90 carrying the desired expression constructs were grown overnight (approximately 18 h) at 28 °C with agitation in LB media containing 50 μM gentamycin, 25 μM rifampicin and 50 μM kanamycin. Bacterial cells were collected by centrifugation at 1000 g for 10 min at room temperature (RT), washed with infiltration buffer (10 mM MES, 10 mM $MgCl_2$, pH 5.6 and 150 μM acetosyringone), diluted to an optical density at 600 nm (OD_{600}) of 0.5. Bacteria were incubated at 28 °C for 2 h and afterwards, the two new fully-expanded leaves of 4-5 weeks old *N. benthamiana* plants were hand-infiltrated with the bacterial suspensions with the help of a needle-less 10 ml syringe. Agroinfiltrated

N. benthamiana leaf tissue was collected at 4 days post-infiltration (dpi) or used for infections assays. For *P. infestans* infection assays, *N. benthamiana* leaves were half infiltered with the EV (control) and half infiltrated with the construct of interest (GST expressing construct).

Heterologous expression in *E. coli*

E. coli expression vectors pMF84/85/86/87/88/89 and pMF91 were grown in liquid LB medium containing 50 μM kanamycin or 100 μM carbenicillin, respectively, at 37 °C until OD_{600} = 0.5. *E. coli* induction was performed by the addition of 0.5 mM final concentration of isopropyl b-D-1-thiogalactopyranoside (IPTG) and cultures were incubated at 28 °C for 6-8h. *E. coli* cultures were centrifuged at 5, 000 g for 10 min, washed one time with sterile water and used for protein extraction.

Protein extraction

Leaf tissue from various plant species was frozen in liquid nitrogen and ground to fine powder with a mortar and pestle. Arabidopsis total proteins were extracted in cold homogenization buffer (100 mM Tris-HCl pH 7.4) in a 1:3 weight-to-volume ratio. For the other plant species, total proteins were extracted in cold Tris-HCl buffer containing 3 mM β-mercaptoethanol (β-met). The extracts were incubated for 20 min rotating at 4 °C for complete homogenization and centrifuged at 5,000 g for 20 min at 4 °C. Supernatants containing soluble proteins were filtered through a layer of miracloth filter and centrifuged again at 5,000 g for 20 min at 4 °C. Frozen wheat seedlings were ground to fine powder with the help of a tissue lyser (QIAGEN, TissueLyser II) in 1.5 ml safe-lock Eppendorf tubs containing three 2.4 mm metal beads. Next, total proteins were extracted in cold Tris-HCl homogenization buffer in a 1:3 weight-to-volume ratio and cleared by centrifugation at 10,000 g for 10 min at 4 °C. *E. coli* cell pellets were resuspended in cold Tris-HCl homogenization buffer and sonicated 5s x 12 times at 8 Hz until the homogenate was no longer cloudy. The extracts were centrifuged at 5,000 g for 10 min and the supernatant was kept. For all extractions, total protein concentration was determined by DC protein assay Kit (Bio-Rad, 5000116) with bovine serum albumin (BSA) standards. Protein concentration was adjusted to 0.5 mg/ml for each sample and the resulting samples were used for labelling without freeze thawing.

Activity-based protein profiling and click chemistry

GST-G probe was prepared at 50 - 1000 μM stock solutions in dimethyl sulfoxide (DMSO). Samples of 50 μl were incubated with or without GST-G at the indicated probe concentration (usually 5 μM) and left 20 min incubating before UV radiation (365 nm, in microtiter plates on ice) for the indicated amount of time (usually 45 min). Equal volumes of DMSO were added to no-probe controls. Heat denaturation of GSTF9 and GSTU19 was performed by incubating protein extracts at 85 °C for 10 min and chilling them to RT before labelling. For inhibition experiments, 50 μl extracts were pre-incubated

with competitor molecules, 0.2 mM of S-hexylglutathione (SHG) or ethacrynic acid (EA), for 15 min before GST-G labelling. Labelling reactions were stopped by adding 1:4 (v/v) cold acetone and precipitated by 3 min centrifugation at maximum speed using a benchtop centrifuge. Protein pellets were resuspended in 44.5 μl of PBS-SDS buffer (phosphate-buffered saline (PBS) pH 7.4 with 1% (w/v) sodium dodecyl sulfate (SDS)) and heated for 3 min at 90 °C. For click chemistry, 44.5 μl of labelled proteins were treated with 2 μM Cy5 Picolyl Azide (Click Chemistry Tools, 50 μM stock in DMSO) or Fluorescein Picolyl Azide (Click Chemistry Tools, 50 μM stock in DMSO) and a premixture of 100 μM tris((1-benzyl-1H-1,2,3-triazol-4-yl) methyl)amine (TBTA; 3.4 mM stock in DMSO:*t*-butanol 1:4), 2 mM tris(2-carboxyethyl)phosphine hydrochloride (TCEP; 100 mM stock in water) and 1 mM copper(II) sulfate ($CuSO_4$; 50 mM stock in water). Samples were incubated for 1 h at RT in the dark and quenched by acetone precipitation. Protein pellets were resuspended in 50 μl of 2x gel loading buffer (100 mM Tris-HCl pH 6.8, 200 mM dithiotreitol, 4% SDS, 20% glycerol and 0.02% bromophenol blue) and heated for 5 min at 90 °C.

CDNB assay

CDNB assay was performed using the Glutathione S-transferase (GST) Assay Kit (Sigma-Aldrich, CS0410) and following the manufacture's instruction for the assay in 96-well plate. Briefly, GSTF9 and GSTU19 overexpressing *E. coli* cell extracts were adjusted to 0.5 mg/ml protein concentration. The substrate solution was prepared by adding reduced glutathione and CDNB substrate at a final concentration of 2 mM and 1 mM, respectively. A total of 4 μl of 0.5 mg/ml GST extract was added into a 96 well plate, followed by the addition of 196ul of the substrate solution. The increase in absorbance was measured in an Infinite M200 plate reader (Tecan) at 340 nm at an interval of one 1min for a total of 30 min. A total of 4 independent biological replicates were used for the assay and CDNB conjugation activity is expressed by the increase of A340nm absorbance over time.

IEF 2D SDS-PAGE

Plant extracts (100 μl) were labelled with GST-G at and clicked to different fluorophores (usually Cy2 and Cy5) as described in 'Activity-based protein profiling and click chemistry'. Protein samples were cleaned with the 2D clean-up kit (Cytiva, GE80-6484-51) according to the manufacture's protocol and resuspended in 65 μl rehydration buffer (4% CHAPS (w/v), 2 M thiourea, 7 M urea, 65 mM DTT). Samples to be compared by 2D analysis were mixed and a total concentration of 2% (v/v) ampholytes IPG buffer pH 4-7 (Cytiva, GE17-6000-86) and 0.002% bromophenol blue were added and incubated for 30 min at RT. Sample were isoelectrically focused on 7 cm immobilised pH gradient (IPG) pH 4-7 strips (Cytiva, GE17-6001-10) using IPGphor IEF system (Amersham Biosciences) with the following focusing conditions: Current: 50 μA/strip; 20 V for 15 h active rehydration; 300 V for 30 min, Step-and-Hold;

1000 V for 30 min, Gradient; 5000V for 1.5 h Gradient; 5000 V for 1h Step-and-Hold; 20 V Step-and-Hold. After focusing, IPG strips were equilibrated in equilibration buffer (4 M urea, 320 mM thiourea, 2 % (w/v) SDS, 30% (v/v) glycerol, 0.002 % bromophenol blue, 2 % DTT in 50 mM Tris-HCl pH 6.8). The second-dimension electrophoresis was run on 4 to 12% Bis-Tris gels (Invitrogen, NP0326BOX).

In-gel fluorescence scanning and Western Blot

Labelled proteins were loaded and separated on 10-12% SDS-PAGE acrylamide gels at 150 V. Fluorescence scanning of acrylamide gels was performed on an Amersham Typhoon 5 scanner (GE Healthcare Life Sciences) using excitation and emission wavelengths of ex488/em520 and ex635/em670 for Cy2 and Cy5 scanning, respectively. Scanned gels were stained with Coomassie Brilliant Blue G-250. For Western Blot, proteins separated in SDS-PAGE gels were transferred to a PVDF membrane using Trans-Blot Turbo Transfer System (Bio-Rad). For anti-His and anti-GFP blots, membranes were blocked in 5% (w/v) milk in TBS-T (50 mM Tris-HCl pH 7.6, 150 mM NaCl and 0.1% Tween-20) overnight at 4 °C and incubated in 1:5000 anti-GFP-HRP (Abcam, ab6663) or anti-6xHis-HRP (Invitrogen, #R931-25) in TBS-T/milk 5% for 1.5 h at RT. For anti-PR2 blots, membranes were blocked in TBS-T/milk 5% overnight at 4 °C and incubated in 1:2000 anti-PR2 (Agrisera, AS122366) in TBS-T/milk 5% for 1.5h at RT. Membranes were washed 3 times for 5 min in TBS-T at RT and incubated in 1:10000 secondary anti-Rabbit-HRP (Invitrogen, #31460) in TBS-T/Milk 5% for 1 h at RT. For streptavidin blots, membranes were blocked in 1% (w/v) BSA in PBS-T (1x PBS with 0.05% Tween-20) overnight at 4 °C. Membranes were washed with 2 times for 5 min in PBS-T and incubated in 1:2000 streptavidin-HRP (Sigma-Aldrich, S2438) in PBS-T for 1.5 h at RT. Before scanning, all blots were washed 6 times for 5 min in TBS-T/PBS-T and a last wash for 5 min in TBS/PBS. Clarity Western ECL substrate (Bio-Rad) was used for chemiluminescent protein detection.

Large-scale labelling, affinity purification

A volume of 1 ml protein extracts (0.5 mg/ml protein concentration) were incubated with or without 5 μM GST-G as described in "Activity-based protein profiling and click chemistry". Labelling reactions were stopped by methanol/chloroform precipitation (addition of 4 volumes of ice-cold methanol, 1 volume of ice-cold chloroform and 3 volumes of water) and precipitated by 40 min centrifugation at 4,000 g at 4 °C. Protein pellets were resuspended in 1ml of PBS-SDS buffer by bath sonication and heated at 90 °C for 5 min. Labelled proteins were biotinylated with 20 μM azide-PEG3-biotin (Sigma-Aldrich, 2 mM stock in DMSO) using click chemistry as described in "Activity-based protein profiling and click chemistry". Samples were incubated for 1 h at RT in the dark, quenched by the addition of 10 mM ethylenediaminetetraacetic acid (EDTA) and precipitated via the methanol/chloroform method. Protein pellets were resuspended in 1.5 ml of 1.2% (w/v) SDS dissolved in PBS by bath sonication and

diluted by adding 7.5 ml of PBS. The resulting solution was incubated with 100 µl of pre-equilibrated Pierce High Capacity Streptavidin Agarose beads (Thermo Fisher Scientific, 10302384) for 2h at RT. Agarose beads containing the labelled proteins were collected by centrifugation at 1,000 g for 5 min at RT. Agarose beads were washed successively three times with 10 ml of PBS- 1% SDS buffer, three times with PBS and a final wash with 10 ml of water.

On-bead trypsin and Lys-C digestion

For on-bead digestion, the captured agarose beads containing the labelled proteins were treated with 500 µl 6 M urea dissolved in PBS and 10mM TCEP (200 mM stock in water) for 15 min at 65 °C. A final concentration of 20 mM 2-chloroacetamide (CA, 400 mM stock in water) was added and the sample incubated for 30 min at 35 °C in the dark. The reaction was diluted by the addition of 950 µl of PBS and the supernatant was removed by centrifuging the beads at 500 g for 2 min. 100 µl of Lys-C digestion solution (Walko, 5 µg of Lys-C were reconstituted in 100 µl 1 M urea/ 50 mM Tris-HCl buffer pH 8) was added to the beads and left incubating at 37 °C for 3 h. 100 µl of trypsin digestion solution (Promega, 5 µl of reconstituted trypsin were dissolved in 100 µl 50 mM Tris-HCl buffer pH 8) was added to the beads and left incubating at 37 °C overnight. The supernatant containing the digested peptides was dried by vacuum centrifugation and submitted for MS analysis.

LC-MS/MS and peptide identification using MaxQuant

MS samples were analysed as described in Morimoto et. al., 2019. Briefly, the acidified tryptic peptides were desalted using C18 Tips (Thermo Fisher Scientific, 10 µL bed, 87782) and peptide samples were resuspended in 0.1% FA solution and analysed on an Orbitrap Elite instrument (ThermoFisher Scientific) (Michalski *et al.*, 2012) attached to an EASY-nLC 1000 liquid chromatography system (Thermo Fisher Scientific). Samples were separated on an analytical column based on a fused silica capillary with an integrated PicoFrit emitter (New Objective) with Reprosil-Pur 120 C18-AQ 1.9 µm resin. Peptides were next separated using 140 min gradient of solvent and analysed with Orbitrap analyser (using Fourier Transform MS) at a resolution of 60,000 with the internal lock-mass option switched on (Olsen *et al.*, 2005).

RAW spectra were submitted to an Andromeda search in MaxQuant (version 1.5.3.30) using the default settings (Cox *et al.*, 2011; Cox and Mann, 2008). Label-free quantification and match between-runs were activated (Cox *et al.*, 2014). The MS/MS spectra data were searched against the UniProt *Mus musculus* reference database (55,412 entries) and the UniProt *Arabidopsis thaliana* reference database (39,359 entries). All searches included a contaminants database (as implemented in MaxQuant, 245 entries). Enzyme specificity was set to 'Trypsin/P' and the MS/MS match tolerance was set to ±0.5 Da. The peptide spectrum match FDR and the protein FDR were set to 0.01 (based on target-decoy approach)

and the minimum peptide length was seven amino acids. For protein quantification, unique and razor peptides were allowed. Modified peptides were allowed for quantification with a minimum score of 40. Relative quantification of proteins between different MS runs is based exclusively on the label-free quantifications as calculated by the software MaxQuant, using the "MaxLFQ" algorithm (Cox *et al.*, 2014). Filtering of results was done in Perseus version 1.6.13.0 (Tyanova *et al.*, 2016). Briefly, data was filtered against contaminants and only those proteins found in at least one group in all three replicates were considered. Further analysis and graphs were performed using the Qfeatures and ggplot R packages (Gatto, 2021). Imputed values were generated using a missing not at random (MNAR) and missing at random (MAR) mixed imputation over the whole matrix, and the fold change and adjusted P values (adj. P Val) were calculated using the fdr method over the three biological replicates. The correct clustering of the biological replicates by categorical groups was evaluated using principal component analysis (PCA) plots.

*Pto*DC3000 and *P. infestans* infections

*Pto*DC3000 infections were performed as described in Buscaill et al (2020) with some modifications. Briefly, *Pto*DC3000 was grown from glycerol in LB containing 25 ug/ml rifampicin overnight. Overnight culture was centrifugated at 1500 g for 10 min at RT, washed one time with sterile water and resuspended to a density of OD_{600}=1. Bacterial suspension was sprayed on the adaxial leaf surface of *N. benthamiana* agroinfiltrated leaves. Previous to bacterial infection, plants were covered with a humidity dome for a day. Once sprayed, *N. benthamiana* plants were re-covered with the humidity dome and left for 3 days at 21 °C under long day conditions (16/8 h light/dark regime) in a growth chamber. For bacterial growth calculations, three leaf discs (1 cm diameter) per plant were excised from the treated leaves and surface sterilised in 15% H_2O_2 for 2 min. Leaf disc were rinsed twice with sterile water and dried under sterile conditions. Leaf discs were ground in 1 ml sterile water with the help of a tissue lyser (QIAGEN, TissueLyser II) using 1.5 ml safe-lock Eppendorf tubs containing three 2.4 mm metal beads. A serial dilution of the leaf homogenate was plated onto LB agar plates containing cetrimide, fucidin and cephaloridine (CFC supplement, OXOID, OXSR0103E) for selection of *P. syringae* but not *A. tumefaciens* colonies. Plates were incubated at 28 °C for 3 days and *Pto*DC3000 colonies where counted using the best dilution plated. *Pto*DC3000 bacterial growth is expressed in the log10 transformation of the number of colony-forming unit (CFU) per cm^2 of leaf tissue ($log_{10}CFU/cm^2$). *P. infestans* (strain 88069) infections were performed as described in Song et al (2009) with some modifications. Briefly, *P. infestans* was grown on rye sucrose agar medium at 18 °C under dark conditions for 2 weeks. Zoospores were collected by the addition of cold sterile water into the plates and its incubation at 4 °C for a minimum of 4 h. Spore concentration was measured with the help of a haemocytometer and was adjusted to $1x10^5$ zoospores/ml. Three days after agroinfiltrations, *N.*

benthamiana leaves were detached and infected by drop-inoculation of 10 µl of the zoospores culture on the abaxial leaf surface. Infected leaves were incubated in moist trays at 18 °C for 7 days. The size of the infection area was measured by scanning the leaves at ex635/em670 and measuring the lesion area by ImageJ quantification. The successful expression of the GFP-tagged GST expression construct was detected by scanning the leaves at ex488/em520.

Image quantification and statistical analysis

ImageJ (U.S. National Institutes of Health) was used for the quantification of the fluorescence of the labelled proteins and *P. infestans* lesions. To quantify fluorescence signals from protein gels, scanned images (.gel format) were used. The intensity of the defined signal area was quantified using the Analyse -> Measure tool. The integrated density (IntDen) was used to compare intensities signal of the same dimensions (area) measurements within the same protein gel. To quantify *P. infestans* infection lesions, leaf scans were calibrated using the Analyse -> Set scale tool, using a ruler scan for calibration. All images to be compared were set to the same format (8-bit jpg) and an automatic threshold was applied (Image -> Adjust -> Threshold). Set areas applied by the threshold were measured using the Analyse -> Measure tool. The area measured in cm^2 was used to compare lesion sizes between GST expressing constructs and the EV control. All disease score data and fluorescence quantifications were subjected to statistical analysis using RStudio software. P-values were calculated using one-way analysis of variance (on-way ANOVA). All values shown are mean values, and the error intervals represent the standard deviation (sd).

Bioinformatics

Gene expression levels were extracted from Arabidopsis eFP Browser 2.0 (https://bar.utoronto.ca/efp/cgi-bin/efpWeb.cgi). GST amino acid sequences were retrieved from Ensemble Plants (Arabidopsis thaliana genes TAIR10 database, using the BioMart tool and the glutathione S-transferase N-terminal (PF02798, PF13409, PF13417) and C-terminal (PF00043) (https://plants.ensembl.org). At1g65820 (MGST) was included as it is described as microsomal glutathione s-transferase, however, has not been annotated as containing C-terminal and N-terminal glutathione S-transferase domains. Peptides sequences were aligned using the software PROMAL3D (Pei *et al.*, 2008) and the phylogenetic tree was build using the Maximum Likelihood method in MEGA X (Kumar *et al.*, 2018). Number of bootstrap replications was set to 1000 and other parameters were obtained automatically by default in MegaX (Model/Method: LG model; Rates among Sites: Uniform Rates; Gap/Missing Data Treatment: use all sites; ML Heuristic Methods: Nearest-neighbour-Interchange (NNI); Initial tree for ML: Default – NJ/BioNJ.

Supplemental data

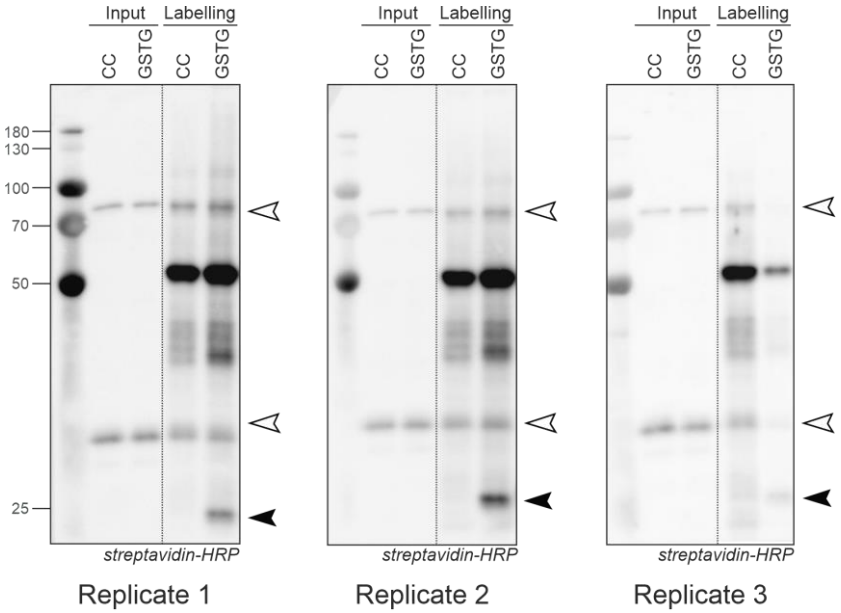


Figure S1. GST-G attached to biotin tag via click chemistry gives high click chemistry background. Arabidopsis leaf proteome was labelled with and without 5 μM GST-G, UV treatment or submitted to a click-chemistry reaction. Labelled proteins were coupled to a biotin tag and visualised by streptavidin protein blot. These is the summary of the 3 pull-down replicates analysed of the pull-down samples analysed by mass spectrometry in Figure 4. Black arrow, GSTs. White arrow, endogenous biotinylated proteins.

Table S1. Description of all proteins differentially detected in the GST-G pull-down of water and BION treated Arabidopsis. Table includes: Name, Protein IDs, log_2 Fold Change (log_2FC), log_2 MS intensity (MS intensity), adjusted P. value (adj.P.Val), unique peptides (u.pep.), razor peptides (r. pep.), Sequence coverage (SC [%]), Molecular weight (MW [kDa]), FDR significance (FDR) and Significance.

	Name	Protein IDs	log_2FC	MS intensity	adj.P.Val	u. + r. pep.	u. pep.	SC [%]	MW [kDa]	FDR	Significance
1	unknown	P33154	7.09	22.36	0.0013	4	4	46.6	17.7	FDR 0.01	Up-regulated
2	MDHAR	B3H5M0;Q9SR59	6.82	21.47	0.0001	5	5	18.2	47.6	FDR 0.001	Up-regulated
3	CWINV6;cwINV6	Q8W4S6;F4JZE3;A0A178UGU8	6.67	21.38	0.0001	7	7	18.4	62.1	FDR 0.001	Up-regulated
4	At5g42830	Q9FMN6	6.55	21.34	0.0001	4	4	11.1	50.5	FDR 0.001	Up-regulated
5	F3H7.16	Q9ZSA8	6.53	23.73	0.0022	17	17	85.4	39.2	FDR 0.01	Up-regulated
6	SYP122	Q9SVC2	6.37	21.28	0.0001	3	3	10.9	37.8	FDR 0.001	Up-regulated
7	PCR1	Q9LQU2	5.92	21.13	0.0001	3	3	20.5	16.5	FDR 0.001	Up-regulated
8	F11B9.23	Q9C768	5.39	20.95	0.0001	4	4	16.1	50.7	FDR 0.001	Up-regulated
9	SAG101	Q4F883	5.14	21.91	0.0028	4	4	8.9	62.1	FDR 0.01	Up-regulated
10	At2g32090	Q9SKZ0;F4ISS2	4.97	20.81	0.0001	3	3	37.8	15.0	FDR 0.001	Up-regulated
11	SOBIR1	Q9SKB2	4.73	20.73	0.0001	2	2	3.9	71.1	FDR 0.001	Up-regulated
12	BG2	A0A1I9LMG6; P33157	4.69	29.01	0.0020	13	13	48.5	39.4	FDR 0.01	Up-regulated
13	CML10	P30187	4.62	20.70	0.0001	1	1	6.8	21.7	FDR 0.001	Up-regulated
14	CHI	O24603	4.34	25.72	0.0056	11	11	62.1	29.8	FDR 0.01	Up-regulated
15	T8B10_80	Q9M217	4.26	22.93	0.0007	3	3	18.1	30.4	FDR 0.001	Up-regulated
16	GSTU9	Q9FUT0;A0A1P8B9C1	4.23	21.00	0.0008	3	3	28.3	27.6	FDR 0.001	Up-regulated
17	ALAAT2	Q9LDV4	4.00	23.80	0.0022	6	6	33.1	59.5	FDR 0.01	Up-regulated
18	F1N13_10	Q9LFT3	3.67	23.04	0.0080	11	11	31.1	82.9	FDR 0.01	Up-regulated
19	NUDT6	Q9SJC4	3.53	25.17	0.0115	10	10	45.9	31.9	FDR 0.05	Up-regulated
20	K18P6.6	Q9FLV0	3.46	25.51	0.0007	11	11	41.6	39.4	FDR 0.001	Up-regulated
21	T30N20_30	Q9LEW3	3.40	26.23	0.0101	10	10	39.2	49.5	FDR 0.05	Up-regulated
22	WAK1	Q39191	3.38	22.46	0.0006	4	4	8.6	81.2	FDR 0.001	Up-regulated
23	T22P22_70	Q9LYG2	3.36	21.56	0.0098	3	3	30	23.1	FDR 0.01	Up-regulated
24	DHNAT1	Q9SX65	3.36	23.67	0.0017	5	5	50	16.7	FDR 0.01	Up-regulated
25	TET8	Q8S8Q6	3.33	23.28	0.0034	3	3	11	30.7	FDR 0.01	Up-regulated

26	PUX2	A0A1P8AXE7;Q9ZU93	3.30	21.50	0.0116	2	2	5.7	42.8	FDR 0.05	Up-regulated
27	CLPP2	Q9FN42	3.28	22.54	0.0017	3	3	21.6	26.3	FDR 0.01	Up-regulated
28	NHL3	Q9FNH6	3.25	23.61	0.0079	2	2	11.3	25.9	FDR 0.01	Up-regulated
29	unknown	P28493	3.24	27.77	0.0009	11	11	66.1	25.3	FDR 0.001	Up-regulated
30	PAD4	Q9S745	3.22	25.61	0.0066	9	9	27.2	61.0	FDR 0.01	Up-regulated
31	PLDGAMMA1;PLDGAMMA2	Q9T053;A0A1P8B5J2; A0A1P8B5I3;Q9T051	3.13	21.03	0.0086	3	3	5.2	95.6	FDR 0.01	Up-regulated
32	UGT73B2	Q94C57;F4JKK6	3.12	22.24	0.0013	4	4	13.7	54.2	FDR 0.01	Up-regulated
33	FLOT1	Q501E6	3.09	22.10	0.0058	5	5	14.3	52.3	FDR 0.01	Up-regulated
34	MED37D	P22954	3.08	25.38	0.0138	13	13	62.5	71.4	FDR 0.05	Up-regulated
35	At5g43910	A0A1P8BG22;F4K7C7;F4K7C8; Q84JM3;A0A1P8BG16	3.03	21.18	0.0106	2	2	11.4	34.8	FDR 0.05	Up-regulated
36	SDR3a	O80713	2.99	25.43	0.0059	10	10	62.3	26.9	FDR 0.01	Up-regulated
37	GSTU10	Q9CA57	2.81	24.06	0.0137	10	10	50.4	26.8	FDR 0.05	Up-regulated
38	CRT3	O04153;F4HW30; F4HW29	2.74	28.35	0.0004	20	20	56.4	49.8	FDR 0.001	Up-regulated
39	AIG1	A0A1P8AUC4;P54120	2.71	23.63	0.0075	8	8	24.7	42.9	FDR 0.01	Up-regulated
40	UGT87A2	O64733	2.68	25.62	0.0066	13	13	36.5	51.7	FDR 0.01	Up-regulated
41	T26J12.10	O49304	2.68	22.78	0.0069	4	4	28.8	17.9	FDR 0.01	Up-regulated
42	PLP2	O48723	2.65	21.32	0.0497	4	4	26.8	44.2	FDR 0.05	Up-regulated
43	EGC2	Q9ZV52	2.55	22.11	0.0071	1	1	8.5	14.5	FDR 0.01	Up-regulated
44	CAD1	Q9CAI3	2.48	25.13	0.0232	11	11	41.7	38.7	FDR 0.05	Up-regulated
45	EDS1	Q9SU72	2.42	26.65	0.0017	21	21	47	71.7	FDR 0.01	Up-regulated
46	MPK3	Q39023	2.40	23.02	0.0273	6	6	30.3	42.7	FDR 0.05	Up-regulated
47	REP	Q8LLD4	2.40	21.65	0.0003	4	4	11.5	61.5	FDR 0.001	Up-regulated
48	At5g52810	Q9FLY0	2.33	25.60	0.0244	9	9	56.9	35.2	FDR 0.05	Up-regulated
49	unknown	F4J5M9	2.23	24.05	0.0009	5	4	24.4	29.2	FDR 0.001	Up-regulated
50	TRX5	Q39241	2.23	26.73	0.0095	6	6	56.8	13.1	FDR 0.01	Up-regulated
51	PMAT1	Q940Z5	2.21	23.35	0.0252	6	6	21.7	51.8	FDR 0.05	Up-regulated
52	BG3	F4J270	2.16	28.16	0.0006	16	16	75.4	37.6	FDR 0.001	Up-regulated
53	PP2AB2	Q39247	2.13	21.37	0.0399	2	2	5	56.3	FDR 0.05	Up-regulated
54	SHD	F4JQ55;Q9STX5	2.11	28.68	0.0007	28	27	38	94.1	FDR 0.001	Up-regulated
55	AP1M1;AP1M2	Q9SAC9;O22715	2.08	21.14	0.0312	2	2	4.9	49.2	FDR 0.05	Up-regulated
56	PDIL1-2	Q9SRG3	2.05	27.76	0.0030	18	17	58.7	56.4	FDR 0.01	Up-regulated
57	PDIL2-3	O48773	2.04	23.22	0.0076	4	4	13.4	47.8	FDR 0.01	Up-regulated
58	MED37B	Q8H1B3	2.04	19.33	0.0138	1	1	4.1	75.1	FDR 0.05	Up-regulated
59	At5g24260	Q9FNF6;A0A1R7T3L2	2.00	21.62	0.0103	4	4	9.9	83.9	FDR 0.05	Up-regulated
60	SAG13	Q9ZW18	1.97	25.09	0.0171	7	6	35.7	28.8	FDR 0.05	Up-regulated
61	NIFU4;NFU4	Q9LIG6;F4IWC5	1.93	23.59	0.0059	4	2	20.8	30.5	FDR 0.01	Up-regulated
62	UGT92A1	Q9LXV0	1.92	24.26	0.0238	7	7	20.1	54.9	FDR 0.05	Up-regulated
63	PA200	F4JC97	1.92	25.91	0.0059	26	26	22.6	202.9	FDR 0.01	Up-regulated
64	At5g04885	Q0WNW0;A0A1P8B9U3	1.90	22.72	0.0260	4	4	8.9	72.3	FDR 0.05	Up-regulated
65	BGLU25	O82772	1.90	21.70	0.0224	4	4	9	59.8	FDR 0.05	Up-regulated
66	unknown	Q9M069;A0A1P8B4U8;A0A1P8B4V2	1.90	25.83	0.0279	8	8	28.6	53.1	FDR 0.05	Up-regulated
67	TCH3;CML12	A0A1P8B183;F4IJ45;F4IJ44;P25071	1.88	21.48	0.0035	1	1	7.6	16.4	FDR 0.01	Up-regulated
68	At3g19010	Q9LJ65;F4J9Y9;F4J9Z1	1.87	26.63	0.0069	15	15	53.6	40.7	FDR 0.01	Up-regulated
69	TENA_E	Q9ASY9	1.85	23.26	0.0141	4	4	19.9	25.1	FDR 0.05	Up-regulated
70	PER34	Q9SMU8	1.85	25.18	0.0297	8	8	37.4	38.8	FDR 0.05	Up-regulated
71	T15B16.17a:T15B16.17b	Q94K85	1.84	28.27	0.0188	6	6	24	39.4	FDR 0.05	Up-regulated
72	GLN1-1	Q56WN1	1.82	28.57	0.0020	9	7	62.4	39.1	FDR 0.01	Up-regulated
73	RPN9A;At5g45620	Q8RWF0;F4KEK8	1.82	23.67	0.0255	5	2	17.4	44.2	FDR 0.05	Up-regulated
74	PPDK	O23404	1.81	27.20	0.0218	29	29	50.1	105.1	FDR 0.05	Up-regulated
75	T12E18_110	Q9M2U5	1.77	24.42	0.0232	4	4	17.9	29.4	FDR 0.05	Up-regulated
76	unknown	O04420	1.76	25.43	0.0072	10	10	47.6	34.9	FDR 0.01	Up-regulated
77	SGT1A	Q9SUR9	1.75	25.08	0.0302	7	7	28	39.2	FDR 0.05	Up-regulated
78	NUDT7	Q9SU14;A0A1P8B842;A0A1P8B846; F4JRE7	1.75	26.67	0.0050	5	5	28.4	31.9	FDR 0.01	Up-regulated
79	unknown	Q8RX69;A0A1P8ARL4	1.74	22.83	0.0260	5	5	11.6	63.7	FDR 0.05	Up-regulated
80	PUB1	Q9LF41	1.70	22.68	0.0173	11	11	17.6	117.5	FDR 0.05	Up-regulated
81	GSTF6	P42760	1.67	29.07	0.0062	7	7	85.1	23.5	FDR 0.01	Up-regulated
82	GSTF7	Q9SRY5	1.66	30.38	0.0094	19	8	82.3	23.6	FDR 0.01	Up-regulated
83	F24M12.40	Q9SD45	1.66	24.05	0.0147	5	5	23.5	36.7	FDR 0.05	Up-regulated
84	URE	Q9SR52	1.59	25.18	0.0068	15	15	28.4	91.0	FDR 0.01	Up-regulated
85	MED37A	Q9LKR3	1.59	22.50	0.0279	2	1	48.4	73.6	FDR 0.05	Up-regulated
86	ALDH2C4	Q56YU0	1.57	30.42	0.0074	33	33	81.2	54.4	FDR 0.01	Up-regulated
87	ARP7	Q8L4Y5	1.55	23.32	0.0224	4	4	20.7	39.9	FDR 0.05	Up-regulated
88	PDIL1-1	Q9XI01;F4HZN9	1.54	29.74	0.0043	33	28	68.1	55.6	FDR 0.01	Up-regulated
89	DIR20;DIR22	Q9C891;Q66GI2	1.54	24.74	0.0232	2	2	13.4	20.6	FDR 0.05	Up-regulated
90	T20H2.2	Q8W456	1.54	22.50	0.0478	3	3	22.3	26.1	FDR 0.05	Up-regulated
91	CAM5;CAM3;CAM2; CAM6;CAM7	F4IVN6;Q682T9;P0DH98;P0DH97; F4IJ46;A0A1I9LPJ2;Q03509;P59220; A0A1I9LPJ1	1.51	29.08	0.0278	10	3	70.2	20.6	FDR 0.05	Up-regulated
92	F10K1.25	Q9LMJ7	1.50	24.28	0.0232	6	6	16.4	40.6	FDR 0.05	Up-regulated
93	T11I11.160	Q9SW43	1.48	23.86	0.0255	5	5	16	36.4	FDR 0.05	Up-regulated

94	CINV1	Q9LQF2;F4HZY9	1.48	26.57	0.0178	17	13	46.8	62.8	FDR 0.05	Up-regulated
95	unknown	Q9SID0	1.44	25.25	0.0142	9	8	41.5	35.3	FDR 0.05	Up-regulated
96	PHOS34	Q8L4N1	1.43	21.58	0.0080	2	2	5.8	28.1	FDR 0.01	Up-regulated
97	CID6	Q6NQH9	1.42	23.48	0.0302	1	1	7.4	19.3	FDR 0.05	Up-regulated
98	SLY1	Q9SL48	1.42	22.78	0.0199	4	4	10.2	69.2	FDR 0.05	Up-regulated
99	At4g36195;At4g36190	Q683F9;Q94CC6;A4VCL8	1.42	25.92	0.0207	10	10	25.2	53.7	FDR 0.05	Up-regulated
100	MUR1	P93031	1.41	25.02	0.0232	9	9	35.4	42.0	FDR 0.05	Up-regulated
101	NHO1;GLPK	F4HS76;Q9M8L4	1.38	26.84	0.0328	9	9	26.8	52.5	FDR 0.05	Up-regulated
102	GLCNAC1PUT2	O64765	1.35	24.41	0.0249	8	5	29.5	55.8	FDR 0.05	Up-regulated
103	DJ1E	Q9ZV19	1.34	26.37	0.0106	9	9	25.6	42.7	FDR 0.05	Up-regulated
104	F22M8.11	Q9LPC3	1.29	24.97	0.0272	2	2	4.8	60.1	FDR 0.05	Up-regulated
105	PYD1	Q9LVI9	1.29	27.23	0.0232	15	15	48.8	46.8	FDR 0.05	Up-regulated
106	At2g40600	Q8H114	1.29	26.57	0.0379	5	5	36.2	27.5	FDR 0.05	Up-regulated
107	APP1	A0A1P8B665;F4JQH3;A0A1P8B667	1.28	27.46	0.0175	17	17	42.4	71.7	FDR 0.05	Up-regulated
108	LPD2	Q9M5K2	1.27	28.23	0.0387	12	12	65.1	54.0	FDR 0.05	Up-regulated
109	unknown	O80763	1.26	26.69	0.0156	15	15	32.5	65.2	FDR 0.05	Up-regulated
110	MPK4	Q39024	1.26	26.97	0.0199	11	10	39.6	42.9	FDR 0.05	Up-regulated
111	LRR-RLK	Q8GZ99	1.25	25.46	0.0376	9	9	15.7	104.7	FDR 0.05	Up-regulated
112	PED1	Q56WD9	1.23	28.06	0.0263	13	13	42	48.6	FDR 0.05	Up-regulated
113	MED37F;BIP2	Q39043;A0A1P8BF32;F4K007	1.23	29.69	0.0071	26	3	50	73.6	FDR 0.01	Up-regulated
114	PHS1;PYRR	F4JBI5;Q9STY4	1.22	23.18	0.0243	5	5	12.6	65.1	FDR 0.05	Up-regulated
115	UGE1	Q42605	1.20	24.96	0.0141	12	11	46.7	39.2	FDR 0.05	Up-regulated
116	AGAL3	Q8VXZ7	1.20	26.43	0.0156	7	7	28.8	48.4	FDR 0.05	Up-regulated
117	unknown	Q9ASZ9	1.20	22.32	0.0259	2	2	11.6	37.9	FDR 0.05	Up-regulated
118	PAP1	Q9LMX4	1.19	25.52	0.0262	8	8	19.6	68.2	FDR 0.05	Up-regulated
119	MPK6	Q39026	1.18	25.88	0.0263	7	6	31.9	45.1	FDR 0.05	Up-regulated
120	ECH2	Q8VYI3	1.15	24.54	0.0192	5	5	31.7	34.1	FDR 0.05	Up-regulated
121	ASP2	P46645	1.15	27.90	0.0259	16	13	60.5	44.3	FDR 0.05	Up-regulated
122	TPP2	F4JVN6	1.10	29.34	0.0201	49	49	52.6	152.4	FDR 0.05	Up-regulated
123	ACG12	Q9FJI5	1.09	23.94	0.0482	7	7	26	59.1	FDR 0.05	Up-regulated
124	F18E5.200;At4g21580	O65423;A8MRW5;B9DGL1	1.06	27.56	0.0305	14	14	64.6	34.5	FDR 0.05	Up-regulated
125	unknown	Q8LG92	1.06	25.61	0.0418	4	4	51.8	12.2	FDR 0.05	Up-regulated
126	CRT2	Q38858	1.06	29.13	0.0359	18	11	52.4	48.2	FDR 0.05	Up-regulated
127	unknown	Q9SJT9	1.04	25.45	0.0181	16	9	22.2	136.5	FDR 0.05	Up-regulated
128	unknown	Q0WW26	1.04	27.03	0.0305	23	23	36.1	98.5	FDR 0.05	Up-regulated
129	CPK5	Q38871	1.03	26.04	0.0288	11	7	29.5	62.1	FDR 0.05	Up-regulated
130	GSTF2;GSTF3	P46422;Q9SLM6	1.03	30.95	0.0238	12	11	81.6	24.1	FDR 0.05	Up-regulated
131	CSY3	Q9SJH7	1.02	26.47	0.0263	11	6	26.7	56.2	FDR 0.05	Up-regulated
132	GDH1	Q43314	1.02	27.73	0.0367	14	10	51.1	44.5	FDR 0.05	Up-regulated
133	CYP19-1	Q38900	0.93	30.13	0.0482	6	6	68.8	18.5	FDR 0.05	Up-regulated
134	PPC1	Q9MAH0	0.93	28.74	0.0481	30	18	63.9	110.3	FDR 0.05	Up-regulated
135	HACL	Q9LF46	0.93	26.82	0.0452	14	14	32.2	61.5	FDR 0.05	Up-regulated
136	CYP20-1	Q9SP02	0.93	27.43	0.0348	6	5	52.9	22.0	FDR 0.05	Up-regulated
137	At5g65750	Q9FLH2	0.92	26.04	0.0358	14	14	34.5	116.4	FDR 0.05	Up-regulated
138	4CLL7	Q9M0X9	0.91	24.31	0.0359	6	6	21.3	59.8	FDR 0.05	Up-regulated
139	ORP3C	Q93Y40	0.88	27.15	0.0387	13	11	39.2	52.0	FDR 0.05	Up-regulated
140	NADP-ME2	Q9LYG3	0.78	30.05	0.0480	31	24	82.5	64.4	FDR 0.05	Up-regulated
141	F15H11.7	Q9SSL0;A0A1P8AN09	-0.97	27.28	0.0232	18	18	41.8	67.3	FDR 0.05	Down-regulated
142	PKP2	Q9FLW9	-1.02	25.80	0.0232	7	7	23.7	63.5	FDR 0.05	Down-regulated
143	AMY3	Q94A41	-1.15	26.13	0.0499	14	14	21.5	99.8	FDR 0.05	Down-regulated
144	HCF101	Q6STH5	-1.25	24.15	0.0232	3	3	7.5	57.8	FDR 0.05	Down-regulated
145	GER3	P94072	-1.40	28.48	0.0119	4	4	27	21.8	FDR 0.05	Down-regulated
146	At4g28080	F4JKH6	-1.50	25.86	0.0073	19	18	14.4	199.1	FDR 0.01	Down-regulated
147	FXG1	Q9FXE5	-1.75	21.13	0.0178	2	2	9.1	40.5	FDR 0.05	Down-regulated
148	PRMT11	Q9SU94	-1.88	23.93	0.0214	5	5	18.5	43.9	FDR 0.05	Down-regulated
149	unknown	Q9SKI0	-2.99	26.11	0.0003	5	5	23.4	29.6	FDR 0.001	Down-regulated
150	T26I12.130	Q9M3C6	-3.30	20.95	0.0061	2	2	8.3	31.2	FDR 0.01	Down-regulated
151	CP29B	Q9ZUU4	-3.43	23.12	0.0238	3	3	26.3	30.7	FDR 0.05	Down-regulated
152	F18O21_250	Q9LYL4	-4.56	20.93	0.0007	3	3	17.9	19.9	FDR 0.001	Down-regulated

Table S2. Plasmids

Golden Gate Modules	
Lab number	**Description**
pGEX-4T1	pGEX-series GST fusion. Vector with Ptac promoter, lacI repressor, amp resistance.
pET-STRp3	pET series Strep tag. Vector with T7 promoter, lacI repressor, amp resistance.
pJK268c	pL1V2-P19-F2, Binary vector.
GG1-01	pL0V-SC1-15456, Level 0 Cloning vector, Golden Gate original vector, EC15456.
GG1-55	pL0M-T-35S-1-41414, Level 0 Module, 35S terminator, Golden Gate plant kit, pICH41414.
GG1-57	pL0M-PU-35S-TMV-3-51288, Level 0 Module, 2 x 35S promoter + TMV Ω (0.8 kb), Golden Gate plant kit, pICH51288.
GG1-70	pL0M-C2-6xHis-15259, Level 0 Module, His for C-terminal fusion, EC15259. ENSA consortium https://www.ensa.ac.uk/
GG1-78	pL0M-C2-eGFP-15095, Level 0 Module, eGFP for C-terminal fusion. EC15095. ENSA consortium https://www.ensa.ac.uk/
Golden Gate binary vectors in *Agrobacterium tumefaciens* GV3101	
Lab number	**Description**
pMF84	AtGSTF5-pET-STRp3/Kanr
pMF85	AtGSTF6-pET-STRp3/Kanr
pMF86	AtGSTF8-pET-STRp3/Kanr
pMF87	AtGSTF9-pET-STRp3/Kanr
pMF88	AtGSTU19-pET-STRp3/Kanr
pMF89	AtGSTU20-pET-STRp3/Kanr
pMF91	pGEX4T-1 (SjGST)
pMF355	pL1V2-P19-F2, empty vector (EV)
pMF358	pL2M-P19-kan-2x35S::AtGSTF2-HIS
pMF359	pL2M-P19-kan-2x35S::AtGSTF2-GFP
pMF360	pL2M-P19-kan-2x35S::AtGSTU4-HIS
pMF361	pL2M-P19-kan-2x35S::AtGSTU4-GFP
pMF364	pL2M-P19-kan-2x35S::AtGSTU10-HIS
pMF365	pL2M-P19-kan-2x35S::AtGSTU10-GFP
pMF366	pL2M-P19-kan-2x35S::AtGSTF6-HIS
pMF367	pL2M-P19-kan-2x35S::AtGSTF6-GFP
pMF368	pL2M-P19-kan-2x35S::AtGSTF7-HIS
pMF369	pL2M-P19-kan-2x35S::AtGSTF7-GFP
pMF381	pL2M-kan-2x35S::FLS3

Table S3. Nucleotide sequences of the primers used for cloning and mutagenesis. The BsaI restriction sites for Golden Gate cloning are underlined. The BpiI restriction sites are marked in bold.

Lab number	Name	Sequence
oMF0089	FW_GSTU10	**TTGAAGACAA**AATGGAGGAGAAGAAGAGCAAAG
oMF0090	RV_GSTU10_nostop	**TTGAAGACAA**CACCTGCATTTGCAGCCTGC
oMF0170	FW1_GSTF2	TTGGTCTCAAATGGCAGGTATCAAAGT
oMF0171	RV1_GSTF2	TTGGTCTCAGTCACCATCTTCAAAGGC
oMF0172	FW2_GSTF2	TTGGTCTCATGACCTCAAGCTCTTCGAATC
oMF0173	RV2_GSTF2	TTGGTCTCACACCCTGAACCTTCTCGGAAG
oMF0242	FW_GSTF6	TTGGTCTCAAATGGCAGGAATCAAAG
oMF0243	RV_GSTF6	TTGGTCTCACACCAAGAACCTTCTGAGCAG
oMF0244	FW_GSTF7	TTGGTCTCAAATGGCAGGAATCAAAG
oMF0245	RV_GSTF7	TTGGTCTCACACCAAGAACCTTCTTAGCAG
oMF0246	FW_GSTU8	TTGGTCTCAAATGAACCAAGAAGAGCACG
oMF0247	RV_GSTU8	TTGGTCTCACACCATTAGATGTAACACTTC

*FW, forward; RV, reverse.

Chapter 5: General Discussion and Conclusion

Cytochrome P450s (CYP450s) and Glutathione transferases (GSTs) are two main families of enzymes in prokaryotes and eukaryotes implicated in the detoxification of foreign compounds (xenobiotics) through metabolic detoxification. While a lot of research has been done in order to understand the activation of these enzyme families in the context of drug and human disease treatments, we have less knowledge about the specific treatment-dependent up-regulation, function and specificity selectivity towards their substrates in the field of plant and fungal biology. In this thesis, Activity-based protein profiling (ABPP) was introduced for the first time to study CYP450s and GSTs in plants and fungi. In the following discussion, we will discuss the great potential of CYP450 and GST profiling for studying pesticide metabolism, as well as identify their main advantages, disadvantages and important considerations for their application in plant and fungal studies.

CYP450 probes: current status and future perspectives

In chapter 2 and 3, we demonstrated the targeting of plant (*Nicotiana benthamiana* and maize) and fungi (*Zymoseptoria tritici)* CYP450s by several CYP450 probes. The following sections review the main challenges encountered during the establishment of CYP450 profiling, containing relevant guidelines for the use of these probes in plants and fungi, as well as highlighting future studies needed in order to better understand the specificity of CYP450 probes and improve their future use.

Limitations and recommendations when using CYP50 activity profiling in plants and fungi

In chapter 2, we observed the labelling of 40 of the 102 CYP450 genes products from mouse in liver microsomes by DB096 using mass spectrometry. By contrast, only 5 of the 365 CYP450 gene products of *N. benthamiana* were labelled in leaf microsomes. In chapter 3, we detected the enrichment of 13 of the 79 CYP450 gene products of *Z. tritici* in microsomes. Nonetheless, when using in-gel fluorescent scanning, we could not detect any labelling of fungal and plant CYP450s, indicating that there are some limitations when profiling CYP450s in plants and fungi.

Overall, we found three main parameters affecting the application of CYP450 labelling: i) relatively low CYP450 concentrations, ii) high click chemistry background and iii) low CYP450s reactivity towards the probes. First, we discovered that click chemistry-tagged CYP450 probes are not useful to detect labelled plant and fungi CYP450s by in-gel fluorescent scanning, partly because of the high click chemistry background and the low abundance of CYP450 in plant and fungi microsomes in comparison to mouse liver microsomes. Second, as seen in the *Z. tritici* global proteomic analysis, not all CYP450s present in the proteome are reactive to CYP450 probes and can be targeted and enriched. Therefore, we concluded that the specific CYP450 signals we aimed to detect at around the molecular size of CYP450s

might have been too weak to be detected by in-gel fluorescent scanning. We tried to understand the lower reactivity of plant and fungal CYP450s by comparing the amino acid sequences between mouse, Arabidopsis, maize and *Z. tritici* CYP450s by phylogenetic analysis. However, we clearly observe a completely different clustering of CYP450 by species more than by CYP450 families, giving little information about the reactivity of CYP450 probes towards other CYP450s in plants and fungi (Appendix 1). Therefore, due to the high diversity between CYP450 enzyme families in the three kingdoms, we cannot discard that plant and fungi CYP450s have also lower reactivity to the used probes in comparison to mammal CYP450s.

Nonetheless, when overexpressed *in planta*, mammal, plant and fungi CYP450s were successfully labelled and detected in fluorescent gels, indicating that CYP450 belonging to three different kingdoms are targeted by CYP450 probes. In all cases, in order to label endogenous or overexpressed CYP450s, the isolation of microsomal fraction was essential for the good detection and labelling of CYP450s. Therefore, for future uses of CYP450 probes we recommend: 1) the use of a good microsomal preparation as abundance of CYP450 is important for CYP450 profiling; 2) the use of CYP450 labelling in combination with mass spectrometry for the detection of endogenous CYP450s from plant and fungal microsomes; and 3) the use of CYP450 labelling using fluorescent probes on heterologously expressed CYP450s.

To circumvent the click chemistry-associated drawbacks and further improve CYP450 profiling in plants, Daniel Brown designed a biotinylated version of DB096, named DB569 (Chapter 2). DB569 reduced the click chemistry associated background observed in streptavidin protein blots. However, the bulkiness of the biotin moiety may restrict labelling of specific CYP450s as we observed poor labelling of several mouse CYP450s and the maize CYP81A9 with DB569. Nonetheless, DB569 and DB096 labelled and enriched the same *N. benthamiana* CYP450s, showing the potential use of both biotinylated and click chemistry probes for the labelling of CYP450s in *N. benthamiana* microsomes. Therefore, careful considerations have to be taken when designing and choosing CYP450 probes. On one hand, when using click chemistry CYP450 probes, the high click chemistry background at 50 kDa, which is around the molecular weight of CYP450s, has to be considered. On the other hand, when using biotinylated CYP450 probes, the likeliness of missing CYP450s with more restrictive active sites should be considered.

Next step of CYP450 profiling in plants and fungi

Although we finally managed to label and enrich several *N. benthamiana* CYP450s by MS analysis, we did not detect NADPH-dependent labelling of endogenous or overexpressed Arabidopsis CYP450s by fluorescence labelling or mass spectrometry (Chapter 2). Therefore, future research should focus on

confirming the labelling of more plant CYP450s by the probes. It will be interesting to create an *in vitro* platform of heterologous expressed plant CYP450s to discover labelling of more plant CYP450s by in-gel fluorescent scanning.

Since there are obvious differences in sequence divergence between the CYP450s of the three kingdoms studied (animals, plants and fungi), we believe that other CYP450 inhibitors and substrates could be used for the design of new, more reactive and effective probes to detect CYP450s in plants and fungi. For example, new fungicide-based probes using trizole fungicides as warheads or herbicide-based probes using urea herbicides as warheads could be designed as suicide substrate probes for fungal CYP450 labelling. However, apart from the intrinsic limitation for the application of CYP450 activity profiling in plants and fungi described above, we do think that the CYP450 labelling protocol can also be improved by refining the enrichment of CYP450 numbers in the microsomal fraction and fine-tuning the click chemistry conditions (e.g. to try new click chemistry reagents, to increase the washing stringency).

In chapter 3, we found that cyprodinil could be a direct substrate of *Zt*CYP5080H1 as cyprodinil was able to supress labelling of CYP5080H1, indicating that cyprodinil actively blocks CYP5080H1 active site. Cyprodinil is an anilino-pyrimidine (AP) fungicide highly effective for the control of many fungal plant pathogens. Some studies have reported that CYP450s can detoxify AP fungicide mepanipyrim through its hydroxylation (Schocken *et al.*, 1997; Zhu *et al.*, 2010); however, previous to our study, there was no evidence of CYP450-based detoxification of cyprodinil in any fungal plant pathogens. Therefore, our research adds new knowledge on the direct metabolism of fungicides by CYP450s in an economically relevant plant pathogen and introduces a new molecular technique for the study of fungicide-detoxification CYP450s. We believe that CYP450 competitive studies could be applied for the study of other fungal CYP450s. It will be particularly interesting to study whether the identified orthologs of *Zt*CYP5080H1 in other species (e.g. Bcin02g01260 in *Botrytis cinerea*) have the same capacity of cyprodinil metabolism. The same way we used competitive CYP450 labelling to support the cyprodinil detoxification capabilities of CYP5080H1 in *Z. tritici*, it will be interesting to create an *in vitro* platform of heterologous express plant CYP450s that could be used in pesticide research to study CYP450 substrates by competitive inhibition with the probes. We believe that the use of competitive CYP450 profiling could be a great tool to complement transcriptomic and fungicide detoxification data demonstrated by knockout and overexpression transformants.

Furthermore, now that we are confident that CYP450 probes can target plant and fungal CYP450s, we believe that CYP450 activity profiling can be used as a discovery tool for the detection of changes in activity of CYP450s and identify main players involved in herbicide and fungicide metabolism in plants

and fungal pathogens. CYP450 probes might also be used in comparative ABPP experiments to identify the differential activity of CYP450s during upon agrochemical exposures or pathogen infections.

GST-G photoaffinity profiling: current status and future perspectives

In chapter 4, we validated the use of the glutathione-based photoaffinity probe, GST-G, to target GSTs in several plant species. The following section reviews the main observations regarding GST-G photoaffinity profiling in plants, containing relevant guidelines for the use of this probes in plants, as well as our main findings observed by profiling GSTs after abiotic- and biotic-related chemical treatments.

In chapter 4, we identified the labelling of GSTF and GSTU classes of glutathione transferases in plants. However, we could not confirm labelling of other soluble classes of GSTs in Arabidopsis leaf extracts (e.g. theta (GSTT), zeta (GSTZ), lambda (GSTL), dehydroascorbate reductase (DHAR) and tetrachloro-phydroquinone dehydrogenase-related (TCHQD)). As GSTT and GSTZ are common classes between plants and mammals, and a previously GST-G was used to successfully label and enrich GSTT and GSTZ in mouse, we suspect that GST-G could also possibly label these classes of GSTs in plants. It will be interesting to confirm the labelling of other GST classes by protein overexpression.

Our study indicates that GST-G labels GSTs throughout the plant kingdom and can be used to monitor GSTs in multiple plant species, including liverworts, bryophytes, monocots and dicots species. Importantly, we found that the addition of a reducing agent (e.g. β-mercaptoethanol) in the extraction buffer is essential when using GST-G in more complex plant extracts.

We introduced the use of competitive ABPP by competing GST-G labelling by ethacrynic acid (EA), a known substrate/inhibitor of the H-site of GSTs. Therefore, we believe GST-G photoaffinity labelling could be used for the identification of herbicides that are metabolised by plant GSTs, the same way we used competitive CYP450 labelling to support the cyprodinil detoxification capabilities of CYP5080H1 in *Z. tritici*.

In chapter 4, we demonstrated the potential use of GST-G photoaffinity profiling to study the activation of GST upon safener application in wheat. Nonetheless, the time left to apply GST profiling to study the specific role of GSTs in the context of agrochemical detoxification was limited. Therefore, it will be interesting to continue our studies and perform MS analysis to identify the main GSTs activated upon safener treatments. Furthermore, although it is known that GSTs are important detoxification enzymes in mammals, insects and plants, the role of GSTs in fungicide detoxification in fungi and oomycetes has not been studied yet. There are previous studies reporting the capability of fungal GSTs (GSTFuA1 and GTT1.2) to conjugate plant-derived toxic isothiocyanates to glutathione and having peroxidase activity,

respectively (Calmes *et al.*, 2015). Furthermore, GSTs are a well-studied enzyme family in wood-degrading fungi as their life style involves the solubilization of many molecules (Morel *et al.*, 2013; Osman *et al.*, 2018). Altogether, previous data demonstrates the potential detoxification capabilities of fungal GSTs. Future work can establish and validate the profiling of GSTs in fungi and the future application of ABPP to identify and monitor the activity of GSTs upon agrochemical treatments in plant pathogens such as *Z. tritici*.

By comparative ABPP and mass spectrometry, we identified the activation of several members of GSTU and GSTF classes upon the BION treatment of Arabidopsis plants. Nevertheless, overexpression of GSTF2, GSTU10 and GSTF6 BION-inducible GSTs in *N. benthamiana* plants was not sufficient to increase resistance to *Phytophthora infestans* or *Pseudomonas syringae* pv. *tomato* DC3000. It is possible that agrobacterium-mediated transformation of GSTs in *N. benthamiana* could already alter its defence system and mask the protection given by the overexpressed GSTs. It is also possible that the identified BION-inducible GSTs have a more indirect role in protection during pathogen infections, such as being involved in the protection of cells from the oxidative stress response created during an infection. Therefore, we recommend the generation of stable Arabidopsis transformants for studying the direct or indirect protection role of the identified BION-inducible GSTs upon pathogen attack. Furthermore, one could consider to deplete the identified GSTs but this approach might be limited by redundancies among GSTs. Overall, we demonstrated the use of GST profiling to detect the activation of GSTs in the context of plant defence; however, further studies to find the implication of the identified BION-induced GSTs remain to be done.

ABPP beyond classical detoxification enzymes families

The unstudied role of sulfotransferases in xenobiotic detoxification in plants

Metabolic detoxification of agrochemicals is a complex system involving several enzyme families, in addition to the previous studied CYP450s and GSTs. Other enzyme families involved in the detoxification of agrochemicals include UDP-glycosyltransferases (UGTs), ATP-binding cassette (ABC) transporters in plants and major facilitator superfamily (MFS) transporters in fungi (Délye *et al.*, 2013; Hu and Chen, 2021). More recently, new research uncovered the involvement of sulfotransferases (SULTs or SOTs) in the modification of xenobiotics in humans (Sadeque *et al.*, 2016; Suiko *et al.*, 2017; Zhou *et al.*, 2020). Nevertheless, SOTs have never been reported as metabolising enzymes in plants and fungi.

Sulfotransferases (EC 2.8.2) are enzymes that are able to transfer the sulfonyl group from 3'-phosphoadenosine 5'-phosphosulphate (PAPS) to a wide range of substrates, from proteins and lipids

to small organic molecules such as hormones and xenobiotic compounds (Klein and Papenbrock, 2004). Sulphonated-molecules become more water soluble, thus decreasing their biological activity and facilitating their excretion (Gamage *et al.*, 2006; Hirschmann *et al.*, 2014). However, sulfonation can also lead to the bioactivation of certain drugs in humans (Gamage *et al.*, 2006). Generally, cytosolic sulfotransferases are involved in the detoxification of small molecules in eukaryotes, and are different from the membrane-bound sulfotransferases found in the Golgi that catalyse the sulfation of proteins, glycolipids and proteoglycans (Suiko *et al.*, 2017).

We identified 18 sulfotransferases in Arabidopsis using Ensemble Plants (Arabidopsis thaliana genes TAIR10 database) and the sulfotransferase (PF03567) PFAM identifier. We hypothesise that sulfotransferases could also be involved in agrochemical detoxification in plants. Indeed, microarray investigations show the transcriptional up-regulation of several SOTs in Arabidopsis (Figure 1). The SOTs up-regulated by the highest number of treatments were SOT12 and SOT15, followed by SOT16.

ABPP could be a useful tool for the study of plant SOTS. Similar to our GST-G probe, PAPS could be used as a main moiety to create a PAPS-based photoaffinity probe to target SOTs.

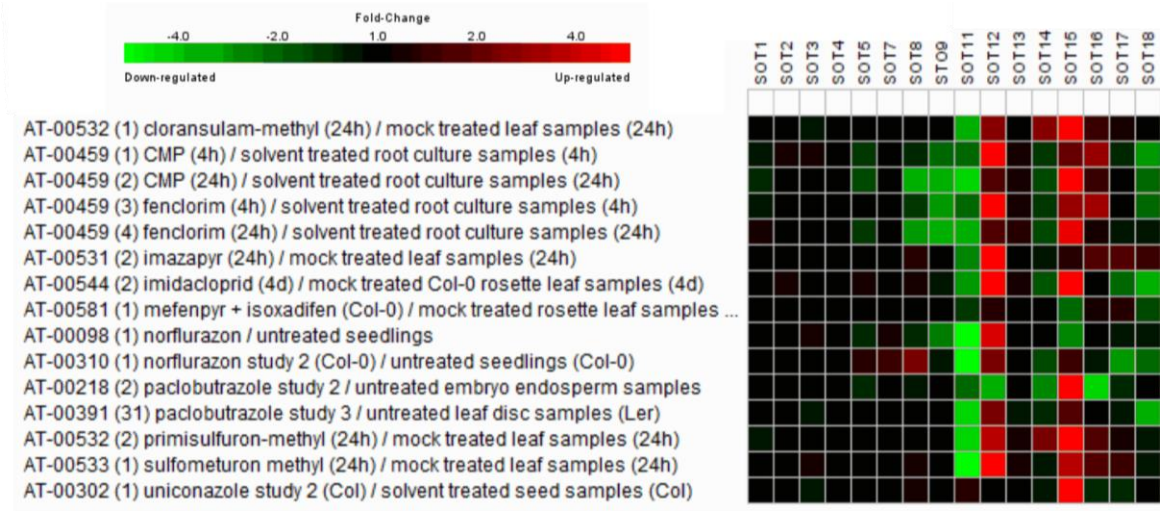


Figure 1. Heat map representing differentially expressed Arabidopsis SOTs (18) upon agrochemical treatments. Colour intensity reflects the Fold-Change perturbation between treated and control samples with red indicating up-regulation, black indicating no change and green indicating down-regulation (data obtained from Genevestigator).

ABPP for the discovery of safener receptors in cereal crops

Safeners improve herbicide tolerance in crops by selectively inducing herbicide metabolising activities in cereal crops but not in weeds (Hatzios and Burgos, 2004; Jablonkai, 2013). Many researches have

focused their study towards characterising the species-specific safener response, thus identifying key metabolising enzymes and stress protecting metabolic enzymes involved in the enhanced selective protection of cereal crops against herbicides. However, how safeners are recognised by plants and how they activate subsequent enzyme responses are unanswered questions.

In mammals, several ligand-modulated transcriptional factors that bind small molecules (e.g. drugs) and subsequently activate the xenobiotic metabolic response have been identified. Nuclear pregnane X receptor (PXR) and constitutive androstane receptor (CAR) are two of the main known families involved in drug recognition and consequent initiation of a specific detoxification response (Lemaire *et al.*, 2006; Negishi *et al.*, 2020; Wallace and Redinbo, 2013). In fungi, ligand-dependent nuclear receptors have also been identified as having regulatory functions during xenobiotic responses. For example, Pdr1p from *Saccharomyces cerevisiae* and *Candida glabrata* binds the antifungal ketoconazole and activates the up-regulation of the detoxification-related genes (Thakur *et al.*, 2008). In the fungus *Sclerotinia homoeocarpa,* a gain-of-function mutation in a putative xenobiotic detoxification regulator (ShXDR1) was able to increase the expression of CYP450s and ABC transporters, indicating the functional analogy between different families of fungal and mammalian nuclear receptors (Sang and Hulvey, 2018). However, safener receptors in plants are yet unidentified. As we do not know whether the safener interaction with their receptor will be a covalent modification, we propose the design of safener-based probes containing a small photoreactive group (e.g. diazirine group). Probes should also contain alkyne mini-tags to be able to purify and identify safener interacting proteins. Furthermore, a previous study used reactive-cysteine profiling based on a chloronitrobenzene moiety to label peroxisome proliferator-activated receptors (PPARs) and identified putative ligand inhibitors (Tsukidate *et al.*, 2020). Therefore, with these two approaches, safener-based chemical probes could be designed to identify xenobiotic receptors in plants and fungi.

Conclusion

This thesis introduces a new methodology to study CYP450s and GSTs in plants and fungi. We believe this research have demonstrated the great potential of activity-based protein profiling of CYP450s and GSTs and its use for the discovery of new enzymes involved in the metabolism of pesticides. Although we observed some limitations in the labelling of plant and fungi CYP450s and GSTs, our study is an exciting starting point for the use of ABPP as a discovery tool for the study of agrochemical-metabolising enzymes.

References

Abbasi, S., Safaie, N., Sadeghi, A., and Shamsbakhsh, M. (2020) *Tissue-specific synergistic bio-priming of pepper by two streptomyces species against phytophthora capsici*. *PLoS One*, **15**, e0230531.

Ačimovič, J., Goyal, S., Košir, R., Goličnik, M., Perše, M., Belič, A., et al. (2016) *Cytochrome P450 metabolism of the post-lanosterol intermediates explains enigmas of cholesterol synthesis*. *Sci. Rep.*, **6**, 1–15.

Agrawal, V., Choi, J.H., Giacomini, K.M., and Miller, W.L. (2010) *Substrate-specific modulation of CYP3A4 activity by genetic variants of cytochrome P450 oxidoreductase*. *Pharmacogenet. Genomics*, **20**, 611–618.

Allocati, N., Masulli, M., Di Ilio, C., and Federici, L. (2018) *Glutathione transferases: Substrates, inihibitors and pro-drugs in cancer and neurodegenerative diseases*. *Oncogenesis*, **7**, 1-15.

Aranega-Bou, P., de la O Leyva, M., Finiti, I., Garcfa-Agustfn, P., and Gonzalez-Bosch, C. (2014) *Priming of plant resistance by natural compounds. Hexanoic acid as a model*. *Front. Plant Sci.*, **5**, 488.

Avenot, H.F. and Michailides, T.J. (2010) *Progress in understanding molecular mechanisms and evolution of resistance to succinate dehydrogenase inhibiting (SDHI) fungicides in phytopathogenic fungi*. *Crop Prot.*, **29**, 643–651.

Bak, S., Beisson, F., Bishop, G., Hamberger, B., Höfer, R., Paquette, S., and Werck-Reichhart, D. (2011) *Cytochromes P450*. *Arab. B.*, **9**, e0144.

Basantani, M. and Srivastava, A. (2007) *Plant glutathione transferases — a decade falls short*. *Can. J. Bot.*, **85**, 443–456.

Beckie, H.J., Busi, R., Lopez-Ruiz, F.J., and Umina, P.A. (2021) *Herbicide resistance management strategies: how do they compare with those for insecticides, fungicides and antibiotics? Pest Manag. Sci.*, **77**, 3049–3056.

Bennett, K., Sadler, N.C., Wright, A.T., Yeager, C., and Hyman, M.R. (2016) *Activity-based protein profiling of ammonia monooxygenase in Nitrosomonas europaea*. *Appl. Environ. Microbiol.*, **82**, 2270–2279.

Benns, H.J., Wincott, C.J., Tate, E.W., and Child, M.A. (2021) *Activity- and reactivity-based proteomics: Recent technological advances and applications in drug discovery*. *Curr. Opin. Chem. Biol.*, **60**, 20–29.

Bernhardt, R. (2006) *Cytochromes P450 as versatile biocatalysts*. *J. Biotechnol.*, **124**, 128–145.

Billard, A., Fillinger, S., Leroux, P., Bach, J., Lanen, C., Lachaise, H., et al. (2011) *Fenhexamid resistance in the Botrytis species complex, responsible for grey mould disease*. *Fungicides - beneficial and harmful aspects. N. Thajuddin, ed. InTech Publisher, Rijeka, Croatia*, 61-78.

Borisy, A.A., Elliott, P.J., Hurst, N.W., Lee, M.S., Lehár, J., Price, E.R., et al. (2003) *Systematic discovery of multicomponent therapeutics*. *Proc. Natl. Acad. Sci. U. S. A.*, **100**, 7977–7982.

Brazier-Hicks, M., Gershater, M., Dixon, D., and Edwards, R. (2018) *Substrate specificity and safener inducibility of the plant UDP-glucose-dependent family 1 glycosyltransferase super-family*. *Plant Biotechnol. J.*, **16**, 337–348.

Brazier-Hicks, M., Howell, A., Cohn, J., Hawkes, T., Hall, G., McIndoe, E., and Edwards, R. (2020) *Chemically induced herbicide tolerance in rice by the safener metcamifen is associated with a phased stress response*. *J. Exp. Bot.*, **71**, 411–421.

Burton, N.R., Kim, P., and Backus, K.M. (2021) *Photoaffinity labelling strategies for mapping the small molecule–protein interactome*. *Org. Biomol. Chem.*, **19**, 7792–7809.

Buscaill, P., Chandrasekar, B., Sanguankiattichai, N., Kourelis, J., Kaschani, F., Thomas, E.L., et al. (2019) *Glycosidase and glycan polymorphism control hydrolytic release of immunogenic flagellin peptides*. *Science*, **364** (6436).

Buscaill, P., Sanguankiattichai, N., Lee, Y.J., Kourelis, J., Preston, G., and van der Hoorn, R.A.L. (2021) *Agromonas: a rapid disease assay for Pseudomonas syringae growth in agroinfiltrated leaves*. *Plant J.*, **105**, 831–840.

Buswell, W., Schwarzenbacher, R.E., Luna, E., Sellwood, M., Chen, B., Flors, V., et al. (2018) *Chemical priming of immunity without costs to plant growth*. *New Phytol.*, **218**, 1205–1216.

Calmes, B., Morel-Rouhier, M., Bataillé-Simoneau, N., Gelhaye, E., Guillemette, T., and Simoneau, P. (2015) *Characterization of glutathione transferases involved in the pathogenicity of Alternaria brassicicola*. *BMC Microbiol.*, **15**, 1–10.

Cataneo, A.C., Ferreira, L.C., Mischan, M.M., Velini, E.D., Corniani, N., and Cerdeira, A.L. (2013) *Mefenpyr-diethyl action on fenoxaprop-p-ethyl detoxification in wheat varieties*. *Planta Daninha*, **31**, 387–393.

Chan, C. and Lam, H.M. (2014) *A putative lambda class glutathione S-transferase enhances plant survival under salinity stress*. *Plant Cell Physiol.*, **55**, 570–579.

Chen, W., Lee, M.K., Jefcoate, C., Kim, S.C., Chen, F., and Yu, J.H. (2014) *Fungal cytochrome P450 monooxygenases: Their distribution, structure, functions, family expansion, and evolutionary origin*. *Genome Biol. Evol.*, **6**, 1620–1634.

Cheval, P., Siah, A., Bomble, M., Popper, A.D., Reignault, P., and Halama, P. (2017) *Evolution of QoI resistance of the wheat pathogen Zymoseptoria tritici in Northern France*. *Crop Prot.*, **92**, 131–133.

Cho, B., Kim, S., In, S., and Choe, S. (2017) *Simultaneous determination of bentazone and its metabolites in postmortem whole blood using liquid chromatography–tandem mass spectrometry*. *Forensic Sci. Int.*, **278**, 304–312.

Cools, H.J. and Fraaije, B.A. (2013) *Update on mechanisms of azole resistance in Mycosphaerella graminicola and implications for future control*. *Pest Manag. Sci.*, **69**, 150–155.

Cox, J., Hein, M.Y., Luber, C.A., Paron, I., Nagaraj, N., and Mann, M. (2014) *Accurate proteome-wide label-free quantification by delayed normalization and maximal peptide ratio extraction, termed MaxLFQ*. *Mol. Cell. Proteomics*, **13**, 2513–2526.

Cox, J. and Mann, M. (2008) *MaxQuant enables high peptide identification rates, individualized p.p.b.-range mass accuracies and proteome-wide protein quantification*. *Nat. Biotechnol.*, **26**, 1367–1372.

Cox, J., Neuhauser, N., Michalski, A., Scheltema, R.A., Olsen, J. V., and Mann, M. (2011) *Andromeda: A peptide search engine integrated into the MaxQuant environment*. *J. Proteome Res.*, **10**, 1794–1805.

Csiszár, J., Horváth, E., Váry, Z., Gallé, Á., Bela, K., Brunner, S., and Tari, I. (2014) *Glutathione transferase supergene family in tomato: Salt stress-regulated expression of representative genes from distinct GST classes in plants primed with salicylic acid*. *Plant Physiol. Biochem.*, **78**, 15–26.

Cumming, R.C., Andon, N.L., Haynes, P.A., Park, M., Fischer, W.H., and Schubert, D. (2004) *Protein disulfide bond formation in the cytoplasm during oxidative stress*. *J. Biol. Chem.*, **279**, 21749–

21758.

Cummins, I., Dixon, D.P., Freitag-Pohl, S., Skipsey, M., and Edwards, R. (2011) *Multiple roles for plant glutathione transferases in xenobiotic detoxification*. *Drug Metab. Rev.*, **43**, 266–280.

Cummins, I., Wortley, D.J., Sabbadin, F., He, Z., Coxon, C.R., Straker, H.E., et al. (2013) *Key role for a glutathione transferase in multiple-herbicide resistance in grass weeds*. *Proc. Natl. Acad. Sci. U. S. A.*, **110**, 5812–5817.

Dalazen, G., Markus, C., Kaspary, T.E., Pisoni, A., Gallon, M., Queiroz, A.R.S. de, et al. (2016) *Occurrence and importane of herbicide resistance caused by degradation enhancement for weed management*. *Rev. Bras. Herbic.*, **15**, 26–28.

Danon, A. (2002) *Redox reactions of regulatory proteins: Do kinetics promote specificity? Trends Biochem. Sci.*, **27**, 197–203.

Das, M., Reichman, J.R., Haberer, G., Welzl, G., Aceituno, F.F., Mader, M.T., et al. (2010) *A composite transcriptional signature differentiates responses towards closely related herbicides in Arabidopsis thaliana and Brassica napus*. *Plant Mol. Biol.*, **72**, 545–556.

Dean, J.D., Goodwin, P.H., and Hsiang, T. (2005) *Induction of glutathione S-transferase genes of Nicotiana benthamiana following infection by Colletotrichum destructivum and C. orbiculare and involvement of one in resistance*. *J. Exp. Bot.*, **56**, 1525–1533.

Dean, R., Van Kan, J.A.L., Pretorius, Z.A., Hammond-Kosack, K.E., Di Pietro, A., Spanu, P.D., et al. (2012) *The Top 10 fungal pathogens in molecular plant pathology*. *Mol. Plant Pathol.*, **13**, 414–430.

Deising, H.B., Reimann, S., and Pascholati, S.F. (2008) *Mechanisms and significance of fungicide resistance*. *Brazilian J. Microbiol.*, **39**, 286–295.

Délye, C. (2013) *Unravelling the genetic bases of non-target-site-based resistance (NTSR) to herbicides: A major challenge for weed science in the forthcoming decade*. *Pest Manag. Sci.*, **69**, 176–187.

Délye, C., Jasieniuk, M., and Le Corre, V. (2013) *Deciphering the evolution of herbicide resistance in weeds*. *Trends Genet.*, **29**, 649–658.

Deng, F. and Hatzios, K.K. (2002) *Characterization and safener induction of multiple glutathione S-transferases in three genetic lines of rice*. *Pestic. Biochem. Physiol.*, **72**, 24–39.

Deponte, M. (2013) *Glutathione catalysis and the reaction mechanisms of glutathione-dependent enzymes*. *Biochim. Biophys. Acta - Gen. Subj.*, **1830**, 3217–3266.

Deridder, B.P., Dixon, D.P., Beussman, D.J., Edwards, R., and Goldsbrough, P.B. (2002) *Induction of glutathione S-transferases in* Arabidopsis *by herbicide safeners*. *Plant Physiol.*, **130**, 1497–1505.

Didierjean, L., Gondet, L., Perkins, R., Lau, S.M.C., Schaller, H., O'Keefe, D.P., and Werck-Reichhart, D. (2002) *Engineering herbicide metabolism in tobacco and Arabidopsis with CYP76B1, a cytochrome P450 enzyme from Jerusalem artichoke*. *Plant Physiol.*, **130**, 179–189.

Ding, N., Wang, A., Zhang, X., Wu, Y., Wang, R., Cui, H., et al. (2017) *Identification and analysis of glutathione S-transferase gene family in sweet potato reveal divergent GST-mediated networks in aboveground and underground tissues in response to abiotic stresses*. *BMC Plant Biol.*, **17**, 1–15.

Dixon, David P., Davis, B.G., and Edwards, R. (2002b) *Functional divergence in the glutathione transferase superfamily in plants: Identification of two classes with putative functions in redox homeostasis in Arabidopsis thaliana*. *J. Biol. Chem.*, **277**, 30859–30869.

Dixon, D.P. and Edwards, R. (2010) *Glutathione Transferases*. *Arabidopsis. Book*, **8**, e0131.

Dixon, D.P. and Edwards, R. (2018) *Protein-ligand fishing in planta for biologically active natural products using glutathione transferases*. *Front. Plant Sci.*, **871**, 1–9.

Dixon, D.P. and Edwards, R. (2009) *Selective binding of glutathione conjugates of fatty acid derivatives by plant glutathione transferases*. *J. Biol. Chem.*, **284**, 21249–21256.

Dixon, D.P., Hawkins, T., Hussey, P.J., and Edwards, R. (2009) *Enzyme activities and subcellular localization of members of the arabidopsis glutathione transferase superfamily*. *J. Exp. Bot.*, **60**, 1207–1218.

Dixon, David P, Lapthorn, A., and Edwards, R. (2002a) *Plant glutathione transferases*. *Genome Biol* **3,** 1–10.

Dooley, H., Shaw, M.W., Mehenni-Ciz, J., Spink, J., and Kildea, S. (2016) *Detection of Zymoseptoria tritici SDHI-insensitive field isolates carrying the SdhC-H152R and SdhD-R47W substitutions*. *Pest Manag. Sci.*, **72**, 2203–2207.

Dücker, R., Parcharidou, E., and Beffa, R. (2020) *Flufenacet activity is affected by GST inhibitors in blackgrass (Alopecurus myosuroides) populations with reduced flufenacet sensitivity and higher expression levels of GSTs*. *Weed Sci.*, **68**, 451–459.

Dücker, R., Zöllner, P., Lümmen, P., Ries, S., Collavo, A., and Beffa, R. (2019) *Glutathione transferase plays a major role in flufenacet resistance of ryegrass (Lolium spp.) field populations*. *Pest Manag. Sci.*, **75**, 3084–3092.

Duhoux, A., Carrère, S., Gouzy, J., Bonin, L., and Délye, C. (2015) *RNA-Seq analysis of rye-grass transcriptomic response to an herbicide inhibiting acetolactate-synthase identifies transcripts linked to non-target-site-based resistance*. *Plant Mol. Biol.*, **87**, 473–487.

Durairaj, P., Hur, J.S., and Yun, H. (2016) *Versatile biocatalysis of fungal cytochrome P450 monooxygenases*. *Microb. Cell Fact.*, **15**, 1–16.

Edwards, R., Del Buono, D., Fordham, M., Skipsey, M., Brazier, M., Dixon, D.P., and Cummins, I. (2005) *Differential induction of glutathione transferases and glucosyltransferases in wheat, maize and Arabidopsis thaliana by herbicide safeners*. *Zeitschrift fur Naturforsch. - Sect. C J. Biosci.*, **60**, 307–316.

Edwards, R. and Dixon, D.P. (2005) *Plant glutathione transferases*. *Methods Enzymol.*, **401**, 169–186.

Elmore, M.T., Brosnan, J.T., Armel, G.R., Kopsell, D.A., Best, M.D., Mueller, T.C., and Sorochan, J.C. (2015) *Cytochrome P450 inhibitors reduce creeping bentgrass (Agrostis stolonifera) tolerance to topramezone*. *PLoS One*, **10**, 1–10.

Engler, C., Youles, M., Gruetzner, R., Ehnert, T.M., Werner, S., Jones, J.D.G., et al. (2014) *A Golden Gate modular cloning toolbox for plants*. *ACS Synth. Biol.*, **3**, 839–843.

Esposito, D. and Chatterjee, D.K. (2006) *Enhancement of soluble protein expression through the use of fusion tags*. *Curr. Opin. Biotechnol.*, **17**, 353–358.

Evans, A.F., O'Brien, S.R., Ma, R., Hager, A.G., Riggins, C.W., Lambert, K.N., and Riechers, D.E. (2017) *Biochemical characterization of metabolism-based atrazine resistance in Amaranthus tuberculatus and identification of an expressed GST associated with resistance*. *Plant Biotechnol. J.*, **15**, 1238–1249.

Faize, L. and Faize, M. (2018) *Functional analogues of salicylic acid and their use in crop protection*. *Agronomy*, **8**, 5.

Fedoryshchak, R.O., Ocasio, C.A., Strutton, B., Mattocks, J., Corran, A.J., and Tate, E.W. (2020) *Wheat pathogen Zymoseptoria tritici N -myristoyltransferase inhibitors: on-target antifungal activity and an unusual metabolic defense mechanism* . *RSC Chem. Biol.*, **1**, 68–78.

Feyereisen, R. (2015) *Insect P450 inhibitors and insecticides: Challenges and opportunities*. *Pest Manag. Sci.*, **71**, 793–800.

Fones, H. and Gurr, S. (2015) *The impact of Septoria tritici Blotch disease on wheat: An EU perspective*. *Fungal Genet. Biol.*, **79**, 3–7.

Forman, H.J., Zhang, H., and Rinna, A. (2009) *Glutathione: Overview of its protective roles, measurement, and biosynthesis*. *Mol. Aspects Med.*, **30**, 1–12.

Fraaije, B.A., Cools, H.J., Fountaine, J., Lovell, D.J., Motteram, J., West, J.S., and Lucas, J.A. (2005) *Role of ascospores in further spread of QoI-resistant cytochrome b alleles (G143A) in field populations of Mycosphaerella graminicola*. *Phytopathology*, **95**, 933–941.

Fujiyama, K., Hino, T., Kanadani, M., Watanabe, B., Jae Lee, H., Mizutani, M., and Nagano, S. (2019) *Structural insights into a key step of brassinosteroid biosynthesis and its inhibition*. *Nat. Plants*, **5**, 589–594.

Gaines, T.A., Duke, S.O., Morran, S., Rigon, C.A.G., Tranel, P.J., Anita Küpper, and Dayan, F.E. (2020) *Mechanisms of evolved herbicide resistance*. *J. Biol. Chem.*, **295**, 10307–10330.

Gaines, T.A., Lorentz, L., Figge, A., Herrmann, J., Maiwald, F., Ott, M.C., et al. (2014) *RNA-Seq transcriptome analysis to identify genes involved in metabolism-based diclofop resistance in Lolium rigidum*. *Plant J.*, **78**, 865–876.

Gamage, N., Barnett, A., Hempel, N., Duggleby, R.G., Windmill, K.F., Martin, J.L., and McManus, M.E. (2006) *Human sulfotransferases and their role in chemical metabolism*. *Toxicol. Sci.*, **90**, 5–22.

Gao, X.H., Bedhomme, M., Veyel, D., Zaffagnini, M., and Lemaire, S.D. (2009) *Methods for analysis of protein glutathionylation and their application to photosynthetic organisms*. *Mol. Plant*, **2**, 218–235.

Garnault, M., Duplaix, C., Leroux, P., Couleaud, G., Carpentier, F., David, O., and Walker, A.S. (2019) *Spatiotemporal dynamics of fungicide resistance in the wheat pathogen Zymoseptoria tritici in France*. *Pest Manag. Sci.*, **75**, 1794–1807.

Gatto L (2021). *RforProteomcs: Companion package to the 'Using R and Bioconductor for proteomics data analysis' publication*. *R package version 1.30.1.*

Giannakopoulos, G., Dittgen, J., Schulte, W., Zoellner, P., Helmke, H., Lagojda, A., and Edwards, R. (2020) *Safening activity and metabolism of the safener cyprosulfamide in maize and wheat*. *Pest Manag. Sci.*, **76**, 3413-3422.

Girvan, H.M. and Munro, A.W. (2016) *Applications of microbial cytochrome P450 enzymes in biotechnology and synthetic biology*. *Curr. Opin. Chem. Biol.*, **31**, 136–145.

González-Bosch, C. (2018) *Priming plant resistance by activation of redox-sensitive genes*. *Free Radic. Biol. Med.*, **122**, 171–180.

Green, R., Sang, H., Im, J., and Jung, G. (2018) *Chlorothalonil biotransformation by cytochrome P450 monooxygenases in Sclerotinia homoeocarpa*. *FEMS Microbiol. Lett.*, **365**, 1–6.

Guengerich, F.P. (2007) *Mechanisms of cytochrome P450 substrate oxidation: MiniReview*. *J. Biochem. Mol. Toxicol.*, **21**, 163–168.

Guengerich, F.P., Martin, M. V., Sohl, C.D., and Cheng, Q. (2009) *Measurement of cytochrome P450 and NADPH-cytochrome P450 reductase*. *Nat. Protoc.*, **4**, 1245–1251.

Gullner, G., Komives, T., Király, L., and Schröder, P. (2018) *Glutathione S-transferase enzymes in plant-pathogen interactions*. *Front. Plant Sci.*, **871**, 1–19.

Guo, F., Iwakami, S., Yamaguchi, T., Uchino, A., Sunohara, Y., and Matsumoto, H. (2019) *Role of CYP81A cytochrome P450s in clomazone metabolism in Echinochloa phyllopogon*. *Plant Sci.*, **283**, 321–328.

Hannemann, F., Bichet, A., Ewen, K.M., and Bernhardt, R. (2007) *Cytochrome P450 systems-biological variations of electron transport chains*. *Biochim. Biophys. Acta - Gen. Subj.*, **1770**, 330–344.

Hatzios, K.K. and Burgos, N. (2004) *Metabolism-based herbicide resistance: regulationby safeners*. *Weed Sci.*, **52**, 454–467.

Hayes, L.E., Sackett, K.E., Mundt, C.C., Anderson, N.P., and Flowers, M.D. (2016) *Evidence of selection for fungicide resistance in Zymoseptoria tritici populations on wheat in Western Oregon*. *Plant Dis.*, **100**, 483–489.

Heick, T.M., Justesen, A.F., and Jørgensen, L.N. (2017) *Anti-resistance strategies for fungicides against wheat pathogen Zymoseptoria tritici with focus on DMI fungicides*. *Crop Prot.*, **99**, 108–117.

Hernández Estévez, I. and Rodríguez Hernández, M. (2020) *Plant Glutathione S-transferases: An overview. Plant Gene*, **23**, 100233.

Hirschmann, F., Krause, F., and Papenbrock, J. (2014) *The multi-protein family of sulfotransferases in plants: Composition, occurrence, substrate specificity, and functions*. *Front. Plant Sci.*, **5**, 1–13.

Hossain, M.A., Mostofa, M.G., Diaz-Vivancos, P., Burritt, D.J., Fujita, M., and Tran, L.S.P. (2017) *Glutathione in plant growth, development, and stress tolerance*. *Springer International Publishing.*

Hrycay, E.G. and Bandiera, S.M. (2015) *Monooxygenase, peroxidase and peroxygenase properties and mechanisms of cytochrome P450. Adv. Exp. Med. Biol.*, **851**, 1-61.

Hu, L., Huang, Y., Ding, B., Cai, R., and Bai, L. (2021) *Selective Action Mechanism of Fenclorim on Rice and Echinochloa crusgalli Is Associated with the Inducibility of Detoxifying Enzyme Activities and Antioxidative Defense*. *J. Agric. Food Chem.*, **69**, 5830–5839.

Hu, L., Yao, Y., Cai, R., Pan, L., Liu, K., and Bai, L. (2020) *Effects of fenclorim on rice physiology, gene transcription and pretilachlor detoxification ability*. *BMC Plant Biol.*, **20**, 1–12.

Hu, M. and Chen, S. (2021) *Non-target site mechanisms of fungicide resistance in crop pathogens: A review*. *Microorganisms*, **9**, 1–19.

Hu, Z., He, B., Ma, L., Sun, Y., Niu, Y., and Zeng, B. (2017) *Recent Advances in Ergosterol Biosynthesis and Regulation Mechanisms in Saccharomyces cerevisiae*. *Indian J. Microbiol.*, **57**, 270–277.

Ismail, H.M., O'Neill, P.M., Hong, D.W., Finn, R.D., Henderson, C.J., Wright, A.T., et al. (2013) *Pyrethroid activity-based probes for profiling cytochrome P450 activities associated with insecticide interactions*. *Proc. Natl. Acad. Sci.*, **110**, 19766–19771.

Iwakami, S., Endo, M., Saika, H., Okuno, J., Nakamura, N., Yokoyama, M., et al. (2014) *Cytochrome P450 CYP81A12 and CYP81A21 are associated with resistance to two acetolactate synthase inhibitors in Echinochloa phyllopogon*. *Plant Physiol.*, **165**, 618–629.

Iyanagi, T. (2007) *Molecular Mechanism of Phase I and Phase II Drug-Metabolizing Enzymes:*

Implications for Detoxification. *Int. Rev. Cytol.*, **260**, 35–112.

Jablonkai, I. (2013) *Herbicide Safeners: Effective Tools to Improve Herbicide Selectivity*. *Herbicides-current research and case studies in use*. IntechOpen.

Jeffreys, L.N., Poddar, H., Golovanova, M., Levy, C.W., Girvan, H.M., McLean, K.J., et al. (2019) *Novel insights into P450 BM3 interactions with FDA-approved antifungal azole drugs*. *Sci. Rep.*, **9**, 1–12.

Jensen, N.B., Zagrobelny, M., Hjernø, K., Olsen, C.E., Houghton-Larsen, J., Borch, J., et al. (2011) *Convergent evolution in biosynthesis of cyanogenic defence compounds in plants and insects*. *Nat. Commun.*, **2**, 1-9.

Jiu, S., Xu, Y., Wang, J., Wang, L., Liu, X., Sun, W., et al. (2020) *The cytochrome P450 monooxygenase inventory of grapevine (Vitis vinifera L.): genome-wide identification, evolutionary characterization and expression analysis*. *Front. Genet.*, **11**, 1–19.

Jugulam, M. and Shyam, C. (2019) *Non-target-site resistance to herbicides: Recent developments*. *Plants*, **8**, 417.

Kammerscheit, X., Chauvat, F., and Cassier-Chauvat, C. (2019) *From cyanobacteria to human, MAPEG-type glutathione-S-transferases operate in cell tolerance to heat, cold, and lipid peroxidation*. *Front. Microbiol.*, **10**, 1–14.

Karadag, H. and Ozhan, F. (2015) *Effect of cyprodinil and fludioxonil pesticides on bovine liver catalase activity*. *Biotechnol. Biotechnol. Equip.*, **29**, 40–44.

Kelly, S.L. and Kelly, D.E. (2013) *Microbial cytochromes P450: Biodiversity and biotechnology. Where do cytochromes P450 come from, what do they do and what can they do for US? Philos. Trans. R. Soc. B Biol. Sci.*, **368**.

Kelly, S.L., Lamb, D.C., Corran, A.J., Baldwin, B.C., Parks, L.W., and Kelly, D.E. (1995) *Purification and reconstitution of activity of Saccharomyces cerevisiae P450 61, a sterol Δ22-desaturase*. *FEBS Lett.*, **377**, 217–220.

Kettles, G.J. and Kanyuka, K. (2016) *Dissecting the molecular interactions between wheat and the fungal pathogen Zymoseptoria tritici*. *Front. Plant Sci.*, **7**, 1–7.

Klein, M. and Papenbrock, J. (2004) *The multi-protein family of Arabidopsis sulphotransferases and their relatives in other plant species*. *J. Exp. Bot.*, **55**, 1809–1820.

Kolodziej, C.M., Chang, C.W., and Maynard, H.D. (2011) *Glutathione S-transferase as a general and reversible tag for surface immobilization of proteins*. *J. Mater. Chem.*, **21**, 1457–1461.

Korovesis, D., Beard, H.A., Mérillat, C., and Verhelst, S.H.L. (2021) *Probes for Photoaffinity Labelling of Kinases*. *ChemBioChem*, **22**, 2206–2218.

Kovács, J. and van der Hoorn, R.A.L. (2016) *Twelve ways to confirm targets of activity-based probes in plants*. *Bioorganic Med. Chem.*, **24**, 3304–3311.

Kumar, S. (2010) *Engineering cytochrome P450 biocatalysts for biotechnology, medicine and bioremediation*. *Expert Opin. Drug Metab. Toxicol.*, **6**, 115–131.

Kumar, S., Stecher, G., Li, M., Knyaz, C., and Tamura, K. (2018) *MEGA X: Molecular evolutionary genetics analysis across computing platforms*. *Mol. Biol. Evol.*, **35**, 1547–1549.

Kumar, S. and Trivedi, P.K. (2018) *Glutathione S-transferases: Role in combating abiotic stresses including arsenic detoxification in plants*. *Front. Plant Sci.*, **9**, 1–9.

Lah, L., Podobnik, B., Novak, M., Korošec, B., Berne, S., Vogelsang, M., et al. (2011) *The versatility of*

the fungal cytochrome P450 monooxygenase system is instrumental in xenobiotic detoxification. *Mol. Microbiol.*, **81**, 1374–1389.

Lallement, P.A., Brouwer, B., Keech, O., Hecker, A., and Rouhier, N. (2014) *The still mysterious roles of cysteine-containing glutathione transferases in plants*. *Front. Pharmacol.*, **5**, 192.

Lamb, D.C. and Waterman, M.R. (2013) *Unusual properties of the cytochrome P450 superfamily*. *Philos. Trans. R. Soc. B Biol. Sci.*, **368**, 20120434.

Lee, D.S., Nioche, P., Hamberg, M., and Raman, C.S. (2008) *Structural insights into the evolutionary paths of oxylipin biosynthetic enzymes*. *Nature*, **455**, 363–368.

Lemaire, G., Mnif, W., Pascussi, J.M., Pillon, A., Rabenoelina, F., Fenet, H., et al. (2006) *Identification of new human pregnane X receptor ligands among pesticides using a stable reporter cell system*. *Toxicol. Sci.*, **91**, 501–509.

Lepesheva, G.I., Friggeri, L., and Waterman, M.R. (2018) *CYP51 as drug targets for fungi and protozoan parasites: Past, present and future*. *Parasitology*, **145**, 1820–1836.

Li, D., Xu, L., Pang, S., Liu, Z., Wang, K., and Wang, C. (2017) *Variable levels of Glutathione S-Transferases are responsible for the differential tolerance to metolachlor between Maize (Zea mays) shoots & roots*. *J. Agric. Food Chem.*, **65**, 39–44.

Li, J., Yu, H., Zhang, F., Lin, C., Gao, J., Fang, J., et al. (2013) *A built-in strategy to mitigate transgene spreading from genetically modified corn*. *PLoS One*, **8**, 1–8.

Li, X., Baudry, J., Berenbaum, M.R., and Schuler, M.A. (2004) *Structural and functional divergence of insect CYP6B proteins: From specialist to generalist cytochrome P450*. *Proc. Natl. Acad. Sci. U. S. A.*, **101**, 2939–2944.

Li, X., Schuler, M.A., and Berenbaum, M.R. (2007) *Molecular mechanisms of metabolic resistance to synthetic and natural xenobiotics*. *Annu. Rev. Entomol.*, **52**, 231–253.

Li, Z., Jiang, Y., Guengerich, F.P., Ma, L., Li, S., and Zhang, W. (2020) *Engineering cytochrome P450 enzyme systems for biomedical and biotechnological applications*. *J. Biol. Chem.*, **295**, 833–849.

Liu, C., Liu, S., Wang, F., Wang, Y., and Liu, K. (2012) *Expression of a rice CYP81A6 gene confers tolerance to bentazon and sulfonylurea herbicides in both Arabidopsis and tobacco*. *Plant Cell. Tissue Organ Cult.*, **109**, 419–428.

Liu, P. (2017) *The future of food and agriculture: Trends and challenges. FAO Annual Report*, **296**.

Liu, W., Bai, S., Zhao, N., Jia, S., Li, W., Zhang, L., and Wang, J. (2018) *Non-target site-based resistance to tribenuron-methyl and essential involved genes in Myosoton aquaticum (L.)*. *BMC Plant Biol.*, **18**, 1–14.

Liu, X., Bi, B., Xu, X., Li, B., Tian, S., Wang, J., et al. (2019) *Rapid identification of a candidate nicosulfuron sensitivity gene (Nss) in maize (Zea mays L.) via combining bulked segregant analysis and RNA-seq*. *Theor. Appl. Genet.*, **132**, 1351–1361.

Lu, K., Song, Y., and Zeng, R. (2021) *The role of cytochrome P450-mediated detoxification in insect adaptation to xenobiotics*. *Curr. Opin. Insect Sci.*, **43**, 103–107.

Lucas, J.A., Hawkins, N.J., and Fraaije, B.A. (2015) *The Evolution of Fungicide Resistance*. *Adv. Appl. Microbiol.*, **90**, 29-92.

Martell, J. and Weerapana, E. (2014) *Applications of copper-catalyzed click chemistry in activity-based protein profiling*. *Molecules*, **19**, 1378–1393.

McDonald, M.C., Renkin, M., Spackman, M., Orchard, B., Croll, D., Solomon, P.S., and Milgate, A. (2019) *Rapid parallel evolution of azole fungicide resistance in Australian populations of the Wheat Pathogen Zymoseptoria tritici*. *Appl. Environ. Microbiol.*, **85**, 1–14.

McFadyen, M.C.E., Melvin, W.T., and Murray, G.I. (2004) *Cytochrome P450 enzymes: Novel options for cancer therapeutics*. *Mol. Cancer Ther.*, **3**, 363–371.

Michalski, A., Damoc, E., Lange, O., Denisov, E., Nolting, D., Müller, M., et al. (2012) *Ultra high resolution linear ion trap orbitrap mass spectrometer (orbitrap elite) facilitates top down LC MS/MS and versatile peptide fragmentation modes*. *Mol. Cell. Proteomics*, **11**, 1–11.

Mikaberidze, A. and McDonald, B.A. (2015) *Fitness Cost of Resistance: Impact on Management*. In: *Fungicide Resistance in Plant Pathogens* (Ishii,H. and Hollomon,D.W., eds), 77–89. Tokyo: Springer Japan.

Mnguni, F.C., Padayachee, T., Chen, W., Gront, D., Yu, J.H., Nelson, D.R., and Syed, K. (2020) *More p450s are involved in secondary metabolite biosynthesis in streptomyces compared to bacillus, cyanobacteria, and mycobacterium*. *Int. J. Mol. Sci.*, **21**, 1–21.

Moellering, R.E. and Cravatt, B.F. (2012) *How chemoproteomics can enable drug discovery and development*. *Chem. Biol.*, **19**, 11–22.

Mooij, W. J. (2018) *Chemical probes to probe the metabolism of fungicides. Doctor of Philosophy (PhD). Imperial College London.*

Montellano, P.R.O. de (2018) *1-Aminobenzotriazole: A Mechanism-Based Cytochrome P450 Inhibitor and Probe of Cytochrome P450 Biology*. *Med. Chem.*, **8**, 38–65.

Moody, L.A., Kelly, S., Clayton, R., Weeks, Z., Emms, D.M., and Langdale, J.A. (2021) *NO GAMETOPHORES 2 Is a Novel Regulator of the 2D to 3D Growth Transition in the Moss Physcomitrella patens*. *Curr. Biol.*, **31**, 555-563.e4.

Morel, M., Meux, E., Mathieu, Y., Thuillier, A., Chibani, K., Harvengt, L., et al. (2013) *Xenomic networks variability and adaptation traits in wood decaying fungi*. *Microb. Biotechnol.*, **6**, 248–263.

Morimoto, K. and van der Hoorn, R.A.L. (2016) *The increasing impact of activity-based protein profiling in plant science*. *Plant Cell Physiol.*, **57**, 446–461.

Mosbach, A., Edel, D., Farmer, A.D., Widdison, S., Barchietto, T., Dietrich, R.A., et al. (2017) *Anilinopyrimidine resistance in Botrytis cinerea is linked to mitochondrial function*. *Front. Microbiol.*, **8**, 2361.

Mullins, J.G.L., Parker, J.E., Cools, H.J., Togawa, R.C., Lucas, J.A., Fraaije, B.A., et al. (2011) *Molecular modelling of the emergence of azole resistance in Mycosphaerella graminicola*. *PLoS One*, **6**, e20973.

Nebert, D.W., Wikvall, K., and Miller, W.L. (2013) *Human cytochromes P450 in health and disease*. *Philos. Trans. R. Soc. B Biol. Sci.*, **368**, 20120431.

Negishi, M., Kobayashi, K., Sakuma, T., and Sueyoshi, T. (2020) *Nuclear receptor phosphorylation in xenobiotic signal transduction*. *J. Biol. Chem.*, **295**, 15210–15225.

Nelson, D.R. (2009) *The cytochrome P450 homepage*. *Hum. Genomics*, **4**, 59–65.

Nelson, D.R., and Werck-Reichhart, D. (2011) *A P450-centric view of plant evolution*. *Plant J.*, **66**, 194–211.

Nelson, D.R., Schuler, M. A., Paquette, S. M., Werck-Reichhart, D., and Bak, S. (2004) *Comparative*

Genomics of Rice and Arabidopsis. Analysis of 727 Cytochrome P450 Genes and Pseudogenes from a Monocot and a Dicot. *Plant Physiol.*, **135**, 756–772.

Nelson, D.R., and Nebert, D.W. (2018) *Cytochrome P450 (CYP) Gene Superfamily . eLS*, **450**, 1–19.

Newsome, A.W., Nelson, D., Corran, A., Kelly, S.L., and Kelly, D.E. (2013) *The cytochrome P450 complement (CYPome) of Mycosphaerella graminicola*. *Biotechnol. Appl. Biochem.*, **60**, 52–64.

Nianiou-Obeidat, I., Madesis, P., Kissoudis, C., Voulgari, G., Chronopoulou, E., Tsaftaris, A., and Labrou, N.E. (2017) *Plant glutathione transferase-mediated stress tolerance: functions and biotechnological applications*. *Plant Cell Rep.*, **36**, 791–805.

Oakley, A. (2011) *Glutathione transferases: A structural perspective*. *Drug Metab. Rev.*, **43**, 138–151.

Ohk, S.O., Park, H.G., Lee, H., Kwon, Y.J., Kim, B.J., Kim, D., and Chun, Y.J. (2015) *Heterologous expression and characterization of CYP61A1 from dandruff-causing Malassezia globosa*. *Protein Expr. Purif.*, **114**, 89–94.

Olsen, J. V., de Godoy, L.M.F., Li, G., Macek, B., Mortensen, P., Pesch, R., et al. (2005) *Parts per million mass accuracy on an orbitrap mass spectrometer via lock mass injection into a C-trap*. *Mol. Cell. Proteomics*, **4**, 2010–2021.

Omrane, S., Audéon, C., Ignace, A., Duplaix, C., Aouini, L., Kema, G., et al. (2017) *Plasticity of the MFS1 Promoter Leads to Multidrug Resistance in the Wheat Pathogen Zymoseptoria tritici*. *MSphere*, **2**, e00393-17.

Omrane, S., Sghyer, H., Audéon, C., Lanen, C., Duplaix, C., Walker, A.S., and Fillinger, S. (2015) *Fungicide efflux and the MgMFS1 transporter contribute to the multidrug resistance phenotype in Zymoseptoria tritici field isolates*. *Environ. Microbiol.*, **17**, 2805–2823.

Omura, T. (2010) *Structural diversity of cytochrome P450 enzyme system*. *J. Biochem.*, **147**, 297–306.

Osman, W.H.W., Lin, M.I., Kondo, K., Nagata, T., and Katahira, M. (2018) *Characterization of the glutathione S-transferases that belong to the GSTFuA class in Ceriporiopsis subvermispora: Implications in intracellular detoxification and metabolism of wood-derived compounds*. *Int. J. Biol. Macromol.*, **113**, 1158–1166.

Özdemir, E., İnak, E., Evlice, E., Yüksel, E., Delialioğlu, R.A., and Susurluk, I.A. (2021) *Effects of insecticides and synergistic chemicals on the efficacy of the entomopathogenic nematode Steinernema feltiae (Rhabditida: Steinernematidae) against Leptinotarsa decemlineata (Coleoptera: Chrysomelidae)*. *Crop Prot.*, **144**, 105605.

Pan, G., Zhang, X., Liu, K., Zhang, J., Wu, X., Zhu, J., and Tu, J. (2006) *Map-based cloning of a novel rice cytochrome P450 gene CYP81A6 that confers resistance to two different classes of herbicides*. *Plant Mol. Biol.*, **61**, 933–943.

Pan, L., Gao, H., Xia, W., Zhang, T., and Dong, L. (2016) *Establishing a herbicide-metabolizing enzyme library in Beckmannia syzigachne to identify genes associated with metabolic resistance*. *J. Exp. Bot.*, **67**, 1745–1757.

Parker, J.E., Warrilow, A.G.S., Price, C.L., Mullins, J.G.L., Kelly, D.E., and Kelly, S.L. (2014) *Resistance to antifungals that target CYP51*. *J. Chem. Biol.*, **7**, 143–161.

Pataky, J.K., Meyer, M.D., Bollman, J.D., Boerboom, C.M., and Williams, M.M. (2008) *Genetic basis for varied levels of injury to sweet corn hybrids from three cytochrome P450-metabolized herbicides*. *J. Am. Soc. Hortic. Sci.*, **133**, 438–447.

Pei, J., Kim, B.H., and Grishin, N. V. (2008) *PROMALS3D: A tool for multiple protein sequence and*

structure alignments. *Nucleic Acids Res.*, **36**, 2295–2300.

Persans, M.W., Wang, J., and Schuler, M.A. (2001) *Characterization of maize cytochrome P450 monooxygenases induced in response to safeners and bacterial pathogens*. *Plant Physiol.*, **125**, 1126–1138.

Peters, B. and Strek, H.J. (2017) *Herbicide discovery in light of rapidly spreading resistance and ever increasing regulatory hurdles*. *Pest Manag. Sci., **74**,* 2211-2215.

Pikuleva, I.A. and Waterman, M.R. (2013) *Cytochromes P450: Roles in diseases*. *J. Biol. Chem.*, **288**, 17091–17098.

Ponomarenko, A., Goodwin, S. B., & Kema, G. H. J. (2011). *Septoria tritici blotch (STB) of wheat. Plant Health.*

Poulos, T.L., Finzel, B.C., and Howard, A.J. (1987) *High-resolution crystal structure of cytochrome P450cam*. *J. Mol. Biol.*, **195**, 687–700.

Powles, S.B. and Yu, Q. (2010) *Evolution in action: Plants resistant to herbicides*. *Annu. Rev. Plant Biol.*, **61**, 317-347.

Rajniak, J., Barco, B., Clay, N.K., and Sattely, E.S. (2015) *A new cyanogenic metabolite in Arabidopsis required for inducible pathogen defence*. *Nature*, **525**, 376–379.

Rehfus, A., Strobel, D., Bryson, R., and Stammler, G. (2018) *Mutations in sdh genes in field isolates of Zymoseptoria tritici and impact on the sensitivity to various succinate dehydrogenase inhibitors*. *Plant Pathol.*, **67**, 175–180.

Rettie, A.E. and Thummel, K.E. (2014) *Cytochrome P450 polymorphisms of clinical importance*. In *Fifty Years of Cytochrome P450 Research*, 371-401. Springer, Tokyo.

Roell, K.R., Reif, D.M., and Motsinger-Reif, A.A. (2017) *An introduction to terminology and methodology of chemical synergy-perspectives from across disciplines*. *Front. Pharmacol.*, **8**, 158.

Roohparvar, R., De Waard, M.A., Kema, G.H.J., and Zwiers, L.H. (2007) *MgMfs1, a major facilitator superfamily transporter from the fungal wheat pathogen Mycosphaerella graminicola, is a strong protectant against natural toxic compounds and fungicides*. *Fungal Genet. Biol.*, **44**, 378–388.

Rupp, S., Weber, R.W.S., Rieger, D., Detzel, P., and Hahn, M. (2017) *Spread of botrytis cinerea strains with multiple fungicide resistance in german horticulture*. *Front. Microbiol.*, **7**, 2075.

Sadeque, A.J.M., Palamar, S., Usmani, K.A., Chen, C., Cerny, M.A., and Chen, W.G. (2016) *Identification of human sulfotransferases involved in lorcaserin n-sulfamate formation*. *Drug Metab. Dispos.*, **44**, 570–575.

Saika, H., Horita, J., Taguchi-Shiobara, F., Nonaka, S., Nishizawa-Yokoi, A., Iwakami, S., et al. (2014) *A novel rice cytochrome P450 gene, CYP72A31, confers tolerance to acetolactate synthase-inhibiting herbicides in rice and arabidopsis*. *Plant Physiol.*, **166**, 1232–1240.

Sang, H. and Hulvey, J.P. (2018) *A xenobiotic detoxification pathway through transcriptional regulation in filamentous fungi. MBio*, **9**, e00457-18.

Sappl, P.G., Carroll, A.J., Clifton, R., Lister, R., Whelan, J., Harvey Millar, A., and Singh, K.B. (2009) *The Arabidopsis glutathione transferase gene family displays complex stress regulation and co-silencing multiple genes results in altered metabolic sensitivity to oxidative stress*. *Plant J.*, **58**, 53–68.

Sappl, P.G., Heazlewood, J.L., and Millar, A.H. (2004) *Untangling multi-gene families in plants by*

integrating proteomics into functional genomics. *Phytochemistry*, **65**, 1517–1530.

Sappl, P.G., Oñate-Sánchez, L., Singh, K.B., and Millar, A.H. (2004) *Proteomic analysis of glutathione S-transferases of Arabidopsis thaliana reveals differential salicylic acid-induced expression of the plant-specific phi and tau classes*. *Plant Mol. Biol.*, **54**, 205–219.

Schocken, M.J., Mao, J., and Schabacker, D.J. (1997) *Microbial Transformations of the Fungicide Cyprodinil (CGA-219417)*. *J. Agric. Food Chem.*, **45**, 3647–3651.

Schuler, M.A., Duan, H., Bilgin, M., and Ali, S. (2006) *Arabidopsis cytochrome P450s through the looking glass: A window on plant biochemistry*. *Phytochem. Rev.*, **5**, 205–237.

Schuler, M.A. and Werck-Reichhart, D. (2003) *Functional genomics of P450s. Annu. Rev. Plant Biol.*, **54**, 629–667.

Shi, Y., Wang, H., Liu, Z., Wu, S., Yang, Y., Feyereisen, R., et al. (2018) *Phylogenetic and functional characterization of ten P450 genes from the CYP6AE subfamily of Helicoverpa armigera involved in xenobiotic metabolism*. *Insect Biochem. Mol. Biol.*, **93**, 79–91.

Shin, J., Kim, J.E., Lee, Y.W., and Son, H. (2018) *Fungal cytochrome P450s and the P450 complement (Cypome) of Fusarium graminearum*. *Toxins.*, **10**, 76–91.

Sierotzki, H. and Scalliet, G. (2013) *A review of current knowledge of resistance aspects for the next-generation succinate dehydrogenase inhibitor fungicides*. *Phytopathology*, **103**, 880–887.

Siminszky, B. (2006) *Plant cytochrome P450-mediated herbicide metabolism*. *Phytochem. Rev.*, **5**, 445–458.

Singh, R.R. and Reindl, K.M. (2021) *Glutathione S-Transferases in Cancer*. *Antioxidants*, **10**, 701.

Skipsey, M., Knight, K.M., Brazier-Hicks, M., Dixon, D.P., Steel, P.G., and Edwards, R. (2011) *Xenobiotic responsiveness of Arabidopsis thaliana to a chemical series derived from a herbicide safener*. *J. Biol. Chem.*, **286**, 32268–32276.

Smith, A.P., DeRidder, B.P., Guo, W.J., Seeley, E.H., Regnier, F.E., and Goldsbrough, P.B. (2004) *Proteomic analysis of Arabidopsis glutathione S-transferases from benoxacor- and copper-treated seedlings*. *J. Biol. Chem.*, **279**, 26098–26104.

Smith, E. and Collins, I. (2015) *Photoaffinity labeling in target-and binding-site identification*. *Future Med. Chem.*, **7**, 159–183.

Soanes, D.M., Alam, I., Cornell, M., Wong, H.M., Hedeler, C., Paton, N.W., et al. (2008) *Comparative genome analysis of filamentous fungi reveals gene family expansions associated with fungal pathogenesis*. *PLoS One*, **3**.

Šrejber, M., Navrátilová, V., Paloncýová, M., Bazgier, V., Berka, K., Anzenbacher, P., and Otyepka, M. (2018) *Membrane-attached mammalian cytochromes P450: An overview of the membrane's effects on structure, drug binding, and interactions with redox partners*. *J. Inorg. Biochem.*, **183**, 117–136.

Stoddard, E.G., Killinger, B.J., Nair, R.N., Sadler, N.C., Volk, R.F., Purvine, S.O., et al. (2017) *Activity-Based Probes for Isoenzyme- and Site-Specific Functional Characterization of Glutathione S-Transferases*. *J. Am. Chem. Soc.*, **139**, 16032–16035.

Suiko, M., Kurogi, K., Hashiguchi, T., Sakakibara, Y., and Liu, M.C. (2017) *Updated perspectives on the cytosolic sulfotransferases (SULTs) and SULT-mediated sulfation*. *Biosci. Biotechnol. Biochem.*, **81**, 63–72.

Sun, L., Wu, R., Su, W., Gao, Z., and Lu, C. (2017) *Physiological basis for isoxadifen-ethyl induction of nicosulfuron detoxification in maize hybrids*. *PLoS One*, **12**, e0173502.

Sylvestre-Gonon, E., Law, S.R., Schwartz, M., Robe, K., Keech, O., Didierjean, C., et al. (2019) *Functional, structural and biochemical features of plant serinyl-glutathione transferases*. *Front. Plant Sci.*, **10**, 608.

Tallarida, R.J. (2001) *Drug synergism: Its detection and applications*. *J. Pharmacol. Exp. Ther.*, **298**, 865–872.

Tanaka, E. (1998) *Clinically important pharmacokinetic drug-drug interactions: Role of cytochrome P450 enzymes*. *J. Clin. Pharm. Ther.*, **23**, 403–416.

Taylor, V.L., Cummins, I., Brazier-Hicks, M., and Edwards, R. (2013) *Protective responses induced by herbicide safeners in wheat*. *Environ. Exp. Bot.*, **88**, 93–99.

Tétard-Jones, C., Sabbadin, F., Moss, S., Hull, R., Neve, P., and Edwards, R. (2018) *Changes in the proteome of the problem weed blackgrass correlating with multiple-herbicide resistance*. *Plant J.*, **94**, 709–720.

Thakur, J.K., Arthanari, H., Yang, F., Pan, S.J., Fan, X., Breger, J., et al. (2008) *A nuclear receptor-like pathway regulating multidrug resistance in fungi*. *Nature*, **452**, 604–609.

Thamm, A., Saunders, T.E., and Dolan, L. (2020) *MpFEW RHIZOIDS1 miRNA-Mediated Lateral Inhibition Controls Rhizoid Cell Patterning in Marchantia polymorpha*. *Curr. Biol.*, **30**, 1905-1915.

Todd, O.E., Figueiredo, M.R.A., Morran, S., Soni, N., Preston, C., Kubeš, M.F., et al. (2020) *Synthetic auxin herbicides: finding the lock and key to weed resistance*. *Plant Sci.*, **300**, 110631.

Torriani, S.F.F., Melichar, J.P.E., Mills, C., Pain, N., Sierotzki, H., and Courbot, M. (2015) *Zymoseptoria tritici: A major threat to wheat production, integrated approaches to control*. *Fungal Genet. Biol.*, **79**, 8–12.

Tsukidate, T., Li, Q., and Hang, H.C. (2020) *Nuclear Receptor Chemical Reporter Enables Domain-Specific Analysis of Ligands in Mammalian Cells*. *ACS Chem. Biol.*, **15**, 2324–2330.

Tyanova, S., Temu, T., Sinitcyn, P., Carlson, A., Hein, M.Y., Geiger, T., et al. (2016) *The Perseus computational platform for comprehensive analysis of (prote)omics data*. *Nat. Methods*, **13**, 731–740.

Urlacher, V.B. and Girhard, M. (2019) *Cytochrome P450 Monooxygenases in Biotechnology and Synthetic Biology*. *Trends Biotechnol.*, **37**, 882–897.

Wallace, B.D. and Redinbo, M.R. (2013) *Xenobiotic-sensing nuclear receptors involved in drug metabolism: A structural perspective*. *Drug Metab. Rev.*, **45**, 79–100.

Walters, D.R., Ratsep, J., and Havis, N.D. (2013) *Controlling crop diseases using induced resistance: Challenges for the future*. *J. Exp. Bot.*, **64**, 1263–1280.

Wang, J., Chen, J., Li, X., Li, D., Li, Z., and Cui, H. (2020) *Pro-197-Ser Mutation in ALS and High-Level GST Activities: Multiple Resistance to ALS and ACCase Inhibitors in Beckmannia syzigachne*. *Front. Plant Sci.*, **11**, 1496.

Wang, J., Chen, Q., Shan, Y., Pan, X., and Zhang, J. (2019) *Activity-based proteomic profiling: The application of photoaffinity probes in the target identification of bioactive molecules*. *TrAC - Trends Anal. Chem.*, **115**, 110–120.

Wang, W., Yang, J., Edin, M.L., Wang, Y., Luo, Y., Wan, D., et al. (2019) *Targeted metabolomics*

identifies the cytochrome P450 monooxygenase eicosanoid pathway as a novel therapeutic target of colon tumorigenesis. *Cancer Res.*, **79**, 1822–1830.

Wang, X., Gong, C., Zhao, Y., and Shen, L. (2018) *Transcriptome and resistance-related genes analysis of Botrytis cinerea B05.10 strain to different selective pressures of cyprodinil and fenhexamid*. *Front. Microbiol.*, **9**, 2591.

Weber, E., Engler, C., Gruetzner, R., Werner, S., and Marillonnet, S. (2011) *A modular cloning system for standardized assembly of multigene constructs*. *PLoS One*, **6**, e16765.

Wei, K. and Chen, H. (2018) *Global identification, structural analysis and expression characterization of cytochrome P450 monooxygenase superfamily in rice*. *BMC Genomics*, **19**, 1–18.

Westman, S.M., Kloth, K.J., Hanson, J., Ohlsson, A.B., and Albrectsen, B.R. (2019) *Defence priming in Arabidopsis – a Meta-Analysis*. *Sci. Rep.*, **9**, 1–13.

Willems, L.I., Overkleeft, H.S., and Kasteren, S.I. Van (2014) *Current Developments in Activity-Based Protein Profiling*. *Bioconjug. Chem.*, **25**, 1181-1191.

Wisser, R.J., Kolkman, J.M., Patzoldt, M.E., Holland, J.B., Yu, J., Krakowsky, M., et al. (2011) *Multivariate analysis of maize disease resistances suggests a pleiotropic genetic basis and implicates a GST gene*. *Proc. Natl. Acad. Sci. U. S. A.*, **108**, 7339–7344.

Wong, N.K., Zhong, S., Li, W., Zhou, F., Deng, Z., and Zhou, Y. (2020) *Selective profiling of steviol-catalyzing UDP-glycosyltransferases with a metabolically synthesized probe*. *Chem. Commun.*, **56**, 12387–12390.

Wright, A.T. and Cravatt, B.F. (2007) *Chemical Proteomic Probes for Profiling Cytochrome P450 Activities and Drug Interactions In Vivo*. *Chem. Biol.*, **14**, 1043–1051.

Wright, A.T., Song, J.D., and Cravatt, B.F. (2009) *A suite of activity-based probes for human cytochrome P450 enzymes*. *J. Am. Chem. Soc.*, **131**, 10692–10700.

Wright, M.H. (2018) *Chemical Proteomics of Host–Microbe Interactions*. *Proteomics*, **18**, 1700333.

Wright, M.H. and Sieber, S.A. (2016) *Chemical proteomics approaches for identifying the cellular targets of natural products*. *Nat. Prod. Rep.*, **33**, 681–708.

Wu, B. and Dong, D. (2012) *Human cytosolic glutathione transferases: Structure, function, and drug discovery*. *Trends Pharmacol. Sci.*, **33**, 656–668.

Wu, L., Zhang, Z.F., Yu, Z., Yu, R., Ma, E., Fan, Y.L., et al. (2020) *Both LmCYP4G genes function in decreasing cuticular penetration of insecticides in Locusta migratoria*. *Pest Manag. Sci.*, **76**, 3541–3550.

Xu, C., Li, C.Y.-T., and Kong, A.-N.T. (2005) *Induction of phase I, II and III drug metabolism/t... [Arch Pharm Res. 2005] - PubMed result*. *Arch. Pharm. Res.*, **28**, 249–68.

Xu, H., Majmudar, J.D., Davda, D., Ghanakota, P., Kim, K.H., Carlson, H.A., et al. (2015) *Substrate-competitive activity-based profiling of ester prodrug activating enzymes*. *Mol. Pharm.*, **12**, 3399–3407.

Xu, J., Wang, X.Y., and Guo, W.Z. (2015) *The cytochrome P450 superfamily: Key players in plant development and defense*. *J. Integr. Agric.*, **14**, 1673–1686.

Yanniccari, M., Gigón, R., and Larsen, A. (2020) *Cytochrome P450 herbicide metabolism as the main mechanism of cross-resistance to ACCase- and ALS- inhibitors in Lolium spp. populations from Argentina: a molecular approach in characterization and detection*. *Front. Plant Sci.*, **11**, 600301.

Yin, Q., Qian, L., Song, P., Jian, T., and Han, Z.J. (2019) *Molecular mechanisms conferring asymmetrical cross-resistance between tebufenozide and abamectin in Plutella xylostella*. *J. Asia. Pac. Entomol.*, **22**, 189–193.

Yoshida, S., Tamaoki, M., Shikano, T., Nakajima, N., Ogawa, D., Ioki, M., et al. (2006) *Cytosolic dehydroascorbate reductase is important for ozone tolerance in Arabidopsis thaliana*. *Plant Cell Physiol.*, **47**, 304–308.

Yu, Q. and Powles, S. (2014) *Metabolism-based herbicide resistance and cross-resistance in crop weeds: a threat to herbicide sustainability and global crop production*. *Plant Physiol.*, **166**, 1106–1118.

Yuan, J.S., Tranel, P.J., and Stewart, C.N. (2007) *Non-target-site herbicide resistance: a family business*. *Trends Plant Sci.*, **12**, 6–13.

Yun, C.H., Kim, K.H., Kim, D.H., Jung, H.C., and Pan, J.G. (2007) *The bacterial P450 BM3: a prototype for a biocatalyst with human P450 activities*. *Trends Biotechnol.*, **25**, 289–298.

Zanger, U.M. and Schwab, M. (2013) *Cytochrome P450 enzymes in drug metabolism: Regulation of gene expression, enzyme activities, and impact of genetic variation*. *Pharmacol. Ther.*, **138**, 103–141.

Zanger, U.M., Turpeinen, M., Klein, K., and Schwab, M. (2008) *Functional pharmacogenetics/genomics of human cytochromes P450 involved in drug biotransformation*. *Anal. Bioanal. Chem.*, **392**, 1093–1108.

Zhang, C., Meng, D., Wang, W., Dai, T., Wang, J., Guan, A., et al. (2020) *Overexpression of three P450 genes is responsible for resistance to novel pyrimidine amines in Magnaporthe oryzae*. *Pest Manag. Sci.*, **76**, 4268–4277.

Zhang, J., Li, L., Lv, Q., Yan, L., Wang, Y., and Jiang, Y. (2019) *The fungal CYP51s: Their functions, structures, related drug resistance, and inhibitors*. *Front. Microbiol.*, **10**, 691.

Zhang, T., Cao, Q., Li, N., Liu, D., and Yuan, Y. (2020) *Transcriptome analysis of fungicide-responsive gene expression profiles in two Penicillium italicum strains with different response to the sterol demethylation inhibitor (DMI) fungicide prochloraz*. *BMC Genomics*, **21**, 1–16.

Zheng, Y.G., Wu, X.Q., Su, J., Jiang, P., Xu, L., Gao, J., et al. (2017) *Design and synthesis of a novel photoaffinity probe for labelling EGF receptor tyrosine kinases*. *J. Enzyme Inhib. Med. Chem.*, **32**, 954–959.

Zhou, S., Li, Wei, Tian, M., Zhang, N., Yang, X., Li, Weiwei, et al. (2020) *Metabolic Activation of Pirfenidone Mediated by Cytochrome P450s and Sulfotransferases*. *J. Med. Chem.*, **63**, 8059–8068.

Zhou, Y., Guo, T., Tang, G., Wu, H., Wong, N.K., and Pan, Z. (2014) *Site-selective protein immobilization by covalent modification of GST fusion proteins*. *Bioconjug. Chem.*, **25**, 1911–1915.

Zhu, Y.Z., Keum, Y.S., Yang, L., Lee, H., Park, H., and Kim, J.H. (2010) *Metabolism of a fungicide mepanipyrim by soil fungus Cunninghamella elegans ATCC36112*. *J. Agric. Food Chem.*, **58**, 12379–12384.

Zwiers, L.H., Stergiopoulos, I., Gielkens, M.M.C., Goodall, S.D., and De Waard, M.A. (2003) *ABC transporters of the wheat pathogen Mycosphaerella graminicola function as protectants against biotic and xenobiotic toxic compounds*. *Mol. Genet. Genomics*, **269**, 499–507.

Appendix

Electronic supplementary information included with this thesis:

Appendix 1. Phylogenetic analysis of cytochrome P450 proteins from mouse, Arabidopsis, maize and *Zymoseptoria tritici.*